THE DEVELOPMENT AND VERIFICATION OF A PAVEMENT RESPONSE AND PERFORMANCE MODEL FOR UNBOUND GRANULAR PAVEMENTS

A thesis

submitted in partial fulfilment

of the requirements for the Degree

of

Doctor of Philosophy

in the

University of Canterbury

by

Bruce Daniel Steven

University of Canterbury

2005

This page is intentionally left blank.

Copyright

Abstract

The research presented in this thesis covers the development, calibration and verification of two thin surfaced unbound granular pavement models: one model to predict the response of a pavement to loading by the monotonic application of a single load event (Response model) and the other model to predict the accumulation of permanent deformation of the pavement when it is subjected to a large number of load applications (Performance model). The response model was developed using the finite element method and used an anisotropic stress dependent stiffness model to represent the granular and subgrade materials. The models were verified with an extensive set of stress, strain and surface deflection measurements collected at the CAPTIF facility. The calibrated models were able to predict the subsurface response of the pavement to a range of dual tyre and FWD load levels (23-72 kN). It was found that the measured stress and strain response of the pavement was different under the two loading mechanisms. It was also found that a particular response at a point in the pavement was linear with respect to load. The performance model was based on similarities observed in the performance of granular materials in both laboratory and full-scale experiments. When the specimen or pavement was showing a steady state response, it was found that the rate of accumulation of permanent deformation was related to the resilient strain. This relationship was then used to predict the deformation of CAPTIF pavements based on the outputs from the response model. The application of laboratory derived models required the use of shift functions to be able to be successfully used in replicating field measurements, this was expected given the differences in boundary conditions and loading mechanisms for the laboratory and field systems.

Acknowledgements

I would like to thank all the people who gave me support and encouragement over the duration of the research, especially:

Iona, Briana and Angus who gave up so much to allow me to complete this research.

Bryan Pidwerbesky and John de Pont for providing the opportunity and encouragement to start this research.

Industrial Research Limited and Transport Engineering Research New Zealand Limited for providing the funding for this research.

Land Transport New Zealand, David Alabaster and Greg Arnold at Transit New Zealand for allowing me to use the data collected at CAPTIF in this thesis.

Alan Fussell, Frank Adams and Frank Greenslade for their work in developing the instrumentation systems and collecting all the extra data that I requested.

Andy Buchanan, Rob Davis, Rob Douglas, Bryan Pidwerbesky and Sabine Werkmeister who helped review my ideas and work.

Dedication

This thesis is dedicated to my parents, Dan and Helen, who provided me with an enriching childhood and who always supported and encouraged my endeavours as I grew up.

Table of Contents

List of Figures

List of Tables

Chapter 1 Introduction

The current mechanistic pavement design method in New Zealand uses Multi-Layer Linear Elastic Theory (MLLET) to calculate the elastic response of the pavement. The use of MLLET to predict pavement responses has proven to be satisfactory for pavement structures containing asphalt concrete layers that have a thickness greater than 80 mm. Until recently, most of the overseas research into pavement materials and models was concentrated on asphalt concrete and structural asphalt pavements. In these types of pavements, the response of the granular pavement layers was less critical than the response of the asphalt layer. However, pavements of this type are relatively uncommon in New Zealand, and are typically only used on urban motorways carrying high volumes of traffic. In New Zealand, the majority of roads are constructed using unbound granular materials and are usually surfaced with a sprayed bitumen and sealing chip layer.

Researchers used Finite Element Method (FEM) models in the late 1960's to model multi layer pavements using non-linear materials (Duncan et al. 1968). However, the material models that were used in the FEM models tended to be somewhat simple and were based on parameters that could be measured at the time in the laboratory. Pavement models based on the FEM have remained predominately in the realm of research, initially due to the computational power required and more recently as the computational power available increased, due to the continued difficulty in obtaining the required material parameters for: a) determining the stress dependent stiffness; and b) the effect of repeated loading on the long term performance of the material.

This has meant that engineers involved in the mechanistic design of pavements are still reliant on pavement models based on MLLET and parameters derived from empirical or historical design methods. When this type of model (MLLET) has been used to model thin surfaced unbound granular pavements that have been tested at the Canterbury Accelerated Pavement Testing Indoor Facility (CAPTIF), the measured strains have ranged between two to ten times the corresponding computed strains (Steven et al. 1998).

In thin surfaced unbound granular pavements, the response of the granular pavement layers is critical to the satisfactory performance of the pavement structure. Only in the last 10 years has a significant effort been made to understand the complex non-linear behaviour of granular materials. There is now a wide range of material models available that are able to predict the response of materials subjected to Repeated Load Triaxial (RLT) testing loading in a laboratory environment. The most recently developed pavement models are based on three-dimensional FEM models, and these models can now be run on readily available computer systems.

One of the outcomes of this thesis research is an enhanced method of using the MLLET model that has been verified with the results from the FEM model. This research combines international pavement material and model research with measured field data that is directly applicable to New Zealand conditions, resulting in a pavement model that is able to predict the response of a thin surfaced granular pavement.

1.1 Objective

The objective of the work reported in this thesis was to develop pavement response and pavement performance models that are able to account for the stress dependent properties of unbound granular materials, to be verified with an extensive set of data collected from thin surfaced unbound granular pavements.

1.2 Scope of Research

This research has been developed using pavement designs and materials that would meet the requirements for use in New Zealand's state highway network. The materials were well compacted and drained and not subjected to extreme environmental conditions. The underlying philosophy was that if the models could accurately predict the performance of "well-behaved" pavements in controlled conditions, then the models presented could either be extended or replaced within the framework to use characterisation parameters from either wet and/or poorly compacted materials as well as accounting for seasonal variations.

The work described in this thesis regarding the collection and post-processing of some of the data (Chapters 3 and 4) was related to experimental work performed by the author for third parties (Transit New Zealand and Land Transport New Zealand, formerly Transfund New Zealand).

The description of the equipment and systems are included in this thesis to provide completeness and to allow the methodologies to be examined to ensure the robustness of this research. The subsequent analysis of the measured data is solely the work of the author and was undertaken as independent and original doctoral research.

1.3 Thesis Outline

Chapter 2 provides a review of the relevant literature and theory relating to the materials and models required to represent unbound granular pavement systems.

Chapter 3 describes the CAPTIF setup and the projects undertaken at CAPTIF from which the field data was collected. The laboratory test setup and tests undertaken are also described in this chapter.

Chapter 4 presents the data collected from tests at CAPTIF and in the laboratory. The data includes the resilient vertical stress and strain response of the pavement to loading by the Falling Weight Deflectometer (FWD) and a dual tyre assembly at various loads. Data such as the resilient vertical strains and rut depth measurements relating to the long-term performance of the pavement are also presented. The laboratory data includes the results of tests where triaxial specimens were subjected to large numbers of load cycles at various levels of stress.

Chapter 5 outlines the development of the non-linear MLLET and FEM pavement response models required to predict the pavement response when the pavement is subjected to loading by a dual tyre assembly. The calculated responses from the models are then compared to the measured pavement responses when the pavement was subjected to loading by the FWD and a rolling wheel.

Chapter 6 details the development of a pavement performance model (permanent deformation/rutting). Similar relationships between the level of the resilient strain

and rate of plastic strain accumulation were observed for both the laboratory and field data when the specimens/pavements were responding in a “steady-state”: the response of the pavement structure could be expected to remain the same over a large number of load applications. The model was initially developed using the data from the laboratory tests and this relationship was used to predict the performance of the pavement.

Chapter 7 provides the conclusions and recommendations for further research.

Chapter 2 Review of Literature and Theory

2.1 Introduction

This chapter is a review of the literature and theory that contribute to the design and modelling of pavement structures. The basis of the current design process in New Zealand is presented and this is followed by an explanation of the different modelling theories that can be used to model pavement structures. The different types of laboratory equipment that is used to characterise pavement materials are covered and then some of the different factors that affect the response of granular materials are reviewed. Numerous models have been proposed by different researchers to predict either the stiffness or the permanent deformation of granular materials and some of the more prominent models are presented in this chapter. Finally, a range of instrumented full-scale field trials that had similar pavement structures to New Zealand pavements are reviewed, along with a selection of pavement models that have been developed with the Finite Element Method (FEM).

As the pavement design methodology develops over time from an empirical to a mechanistic based process, the components of the process can become either out of date or not relevant. There are four main factors that make the modelling of pavement structures complex;

1) Non-linear stress strain relationship and or time dependent properties of some pavement materials

2) Inability of unbound granular materials to sustain tensile stresses

3) Anisotropic material behaviour

4) The use of a static modelling technique to model a load that is varying in both magnitude and spatial position.

The first three factors can be accounted for by adopting a numerical rather than an analytical approach. In 1968 Duncan et. al. (1968) was the first to use the then recently developed FEM to account for the first point above. The second point can be accounted for by: recognising any residual or locked in stresses due to the

deposition or construction processes; applying a failure criterion to the material; or redistributing the stresses to eliminate the tensile stresses. The third point can be accounted for by using an appropriate constitutive relationship between the stresses and strains. The fourth factor can be dealt with once satisfactory solutions have been found for the first three points.

2.2 Current Pavement Design in New Zealand

The current design method in New Zealand for State Highways is the AUSTROADS Pavement Design Guide (APDG) (AUSTROADS 2004a). The current version of the APDG is the second revision since it was published in 1987; the first revision was in 1992.

> *The AUSTROADS Guide is based on the philosophy that the design engineer must have a good understanding of the design process and the mechanics of pavement behaviour. The engineer is encouraged to develop the design from first principles with the use of a computer program (e.g. CIRCLY, Wardle 1980) for calculating stresses and strains in multi-layered elastic media.(Transit New Zealand 2000)*

Thus, the design guide is promoted as a mechanistic based design method, that is, the performance of the pavement structure can be determined from the application of an analytical process. The current pavement design uses an analytical process to determine the response of the pavement structure to a single load and a critical response; either the horizontal tensile strain at the bottom of a bound layer or the vertical compressive strain at the top of the subgrade layer, Figure 2.1. The strain is used as an input into a performance relationship that relates the critical response to the allowable number of design axles/traffic. Jameson (1996) documented the history of the current design method and the origins can be traced back to the Californian State Highways Department design method (Porter 1942). The performance relationship given in the APDG for unbound granular pavements is the subgrade strain criterion.

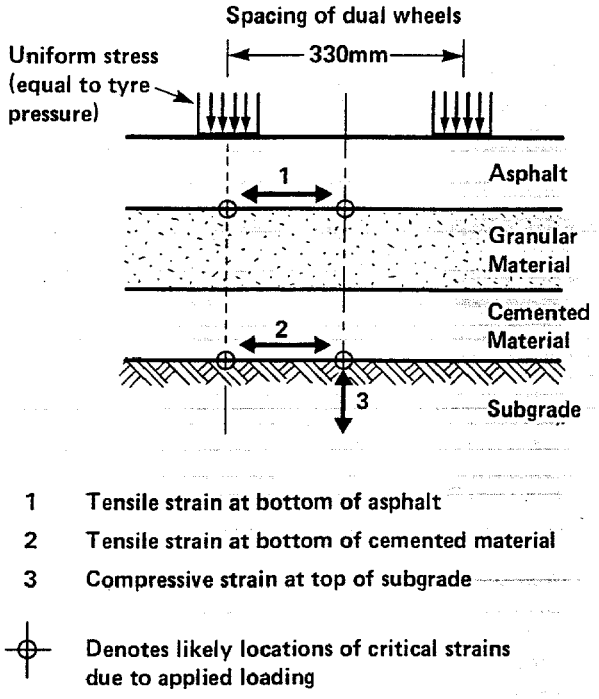

Figure 2.1 Location of critical strains in the pavement (AUSTROADS 1992).

$$N_{allowable} = \left[\frac{9300}{\varepsilon_{sg}}\right]^{7} \tag{2.1}$$

Where

$N_{allowable}$ = Allowable number of equivalent number of standard axles

ε_{sg} = Vertical compressive strain at the top of the subgrade (microstrain)

The concept of the subgrade strain (initially stress) criteria was first proposed in the pavement design method developed by the Shell Oil Company (Peattie 1962) and was also intended to apply to the compressive stress at the top of the unbound granular layers. Peattie (1962) and Dorman (1962) briefly mentioned some work that indicated if the stress criteria for the subgrade was satisfied, then the stresses in the granular layers would be below the failure level for the granular material. The initial values of the coefficients for Equation (2.1) for the Shell Design method were based on the analysis of successful pavements design in accordance with the Californian State Highways Department design method (Dormon et al. 1964). Therefore, it would appear that the original analytical pavement design method

initially had a performance requirement for the granular materials, but this was removed from the final version of the design method, as the subgrade performance was usually the critical criteria, compared to the granular criteria.

The coefficients for the 1992 version of Equation (2.1) were derived from the analysis of 25 pavements from 1979 NAASRA Design Chart (Figure 2.2) and assumptions were made for the:

- thickness of the base material (150 mm)
- modulus of the base material (350 MPa)
- thickness of sub-base layers (<150 mm)
- modular ratio between any two layers (<2)
- Poisson's ratio of all granular layers (0.35)
- subgrade modulus (10xCBR)
- subgrade Poisson's ratio (0.45)
- granular layers and subgrade were cross-anisotropic with the vertical modulus being twice the horizontal modulus
- standard axle/loading was two uniformly loaded circular areas with radii of 110 mm
- centre to centre to distance was 330 mm
- the vertical pressure was 550 kPa (Jameson 1996).

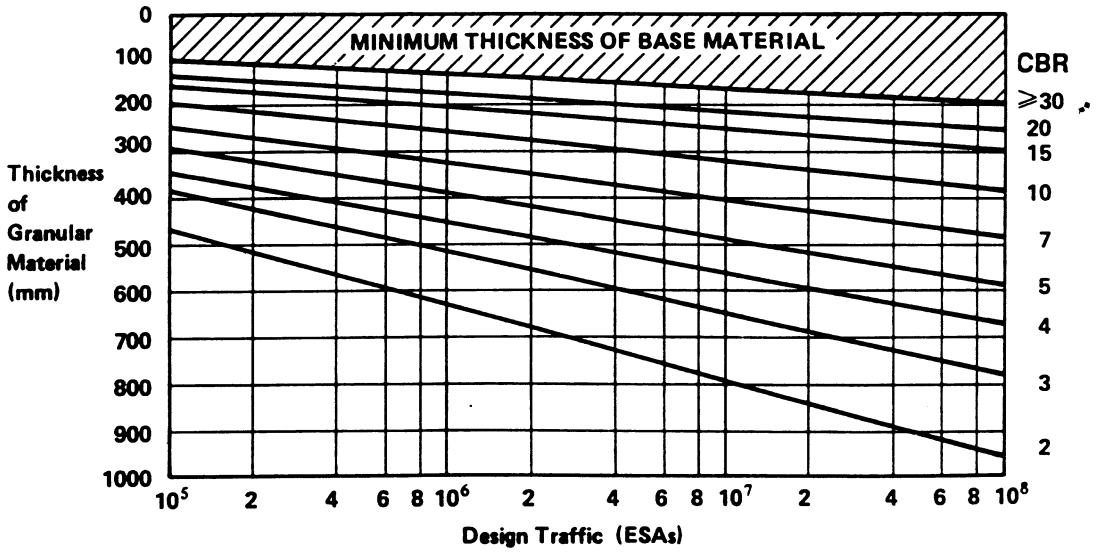

Figure 2.2 Design chart for unbound granular pavements (AUSTROADS 1992).

The coefficients for the 2004 version of Equation (2.1) have changed slightly from the 1992 version of the APDG due to the following changes in the modelling assumptions:

- a full axle is now modelled rather than a half axle
- the vertical pressure has increased from 550 kPa to 750 kPa
- the modulus of the top granular layer varies in order to account for the effect of an asphalt concrete surface (if present) (AUSTROADS 2004b).

A reduction in the number of significant figures in the coefficients (9300,7 instead of 8511,7.14) was made in order not to imply an increased level of precision in the equation. The application of the aforementioned assumptions immediately renders the mechanistic design process artificial, that is, it is impossible to compare actual pavement response measurements to the design outputs.

One of the assumed advantages of a mechanistic based design process is that new materials or pavement configurations can be used, since the analytical process should be able to calculate the critical response required for the appropriate performance relationship. A difficulty lies in the development of performance criteria for new materials, since Equation (2.1) was derived from an empirical

design chart, after many years of observations and changes had gone into the development of the base design chart. A new material will most likely only have a limited amount of performance data from laboratory and/or limited field tests.

Results from the field study of Steven (1993) and the analysis of some CAPTIF pavements (Steven et al. 1998) showed that using the assumptions outlined above to model pavement structures resulted in the calculation of vertical compressive strains that were between 0.33 and 0.10 of the measured values. These findings raise a question over robustness or applicability of the analytical part of the current design to accurately model either materials or pavement structures.

2.3 Pavement Response Models

This section provides a brief description of the subset of the field of continuum mechanics as it relates to pavement engineering and the modelling of pavement materials. The definition of a pavement response model is a model that predicts the response of a pavement structure subjected to the single application of a tyre/wheel assembly/axle/vehicle. These models calculate the distribution of the stress and strain in the pavement due to the applied load. The loading can either be: static and monotonic; static and cyclic; moving with constant amplitude; or moving with varying amplitude. The last case is the most realistic of an actual pavement structure, but the most complex to model. The models that incorporate cyclic loading are best suited to modelling materials that have either time dependent and/or non-elastic properties.

The equations that model the response of the material to an external load/traction are called the constitutive laws/equations/models. The constitutive model can be based on either physical theories or the analysis of laboratory or field measurements. In order for any proposed constitutive model to be scientifically robust, it should obey the fundamental laws of Newtonian physics, that is the conservation of mass, momentum, moment of momentum and energy and the laws of thermodynamics.

From a practical engineering viewpoint, the benefits that might be gained from the use of a complex constitutive model may not be realized if the parameters of the

model cannot be readily or easily determined. A typical pavement structure will be composed of two or more layers of different materials, with each material having its own constitutive model. If the pavement structure is modelled using these different constitutive models, the only practical and readily available way to compare the modelled pavement with the actual pavement is compare the surface deflection under an applied load. Since only one response is measured to test the validity of two or more components of the system, it is difficult to assess the accuracy or relative contribution of each component to the total system response.

There are generally two types of response models, analytical and numerical. Analytical models use established principles from the field of solid mechanics in order to model the complete system, whilst numerical models are based on an assemblage of small analytical models that are solved simultaneously to achieve an overall system equilibrium.

2.3.1 Theory of Elasticity

The theory of elasticity is the basis that most analytical solutions use for determining the response of a free body subject to an external force. In applying this theory, several assumptions are made, namely that the material is elastic, homogeneous and isotropic (Timoshenko and Goodier 1970). Materials that are used to construct pavements rarely exhibit those exact properties, however, the deviations from the first two requirements, elasticity and homogeneity, are assumed small enough that they can be ignored for most purposes. The assumption of elasticity is that there is no permanent deformation of the material once the applied load is removed. The theory of elasticity is based on the solid being able to be represented as a continuum. This approach works well when the point of interest is both large with respect to the particle size making up the continuum, but small enough with respect to the size of the model. When the size of the discrete particles becomes large enough with respect to the area of interest, the material may not be able to be accurately represented as a continuum within the classical theories that are used.

The application of the principles of solid mechanics to the solution of an external action on a free body can either be resolved in terms of a force, resulting in the

determination of the stress distribution in the free body, or in terms of a displacement, resulting in the determination of the strain distribution in the free body or a combination of forces and displacements.

Desai and Siriwardane (1984) describe two types of elasticity models, Cauchy and Green. The Cauchy model assumes that the stress is a function of strain and in the Green model the internal energy function describes the constitutive relationship of the material. Green type models are also described as hyperelastic models. A first-order (linear) Cauchy elastic model is usually described as Hooke's Law. Both the Green and Cauchy models are stress path independent. A third formulation of elastic model is the hypoelastic model. The Hypoelastic model is an incremental formulation and is stress/strain path dependent. The Cauchy, Green and Hypoelastic formulations have a strong fundamental basis and have been known to geotechnical engineers since at least 1967, but the difficulty in obtaining the required coefficients appears to have limited their use in pavement engineering (Uzan 1994).

Any Cauchy model can be reduced to

$$\varepsilon_{ij} = B_{ijkl}\sigma_{kl} \tag{2.2}$$

where

ε_{ij} = strain tensor
σ_{kl} = stress tensor
B_{ijkl} = constitutive matrix linking stress and strain

For a three dimensional system, up to 21 B_{ijkl} coefficients exist due to the symmetric nature of the constitutive matrix. For the analysis of most engineering problems, Hooke's Law is used to describe the relationship between the components of stress and strain and the number of B_{ijkl} coefficients reduces to two.

For the two dimensional case[1]:

$$E = \frac{\sigma_{11}}{\varepsilon_{11}} \tag{2.3}$$

where

E = Young's Modulus
σ_{11} = Stress applied in the direction of the 1 axis
ε_{11} = Resulting strain in the direction of 1 axis

and

$$\upsilon = \frac{-\varepsilon_{11}}{\varepsilon_{22}} \tag{2.4}$$

where

υ = Poisson's ratio
ε_{22} = strain normal to the 2 (or 33) direction

This two dimensional relationship can be expanded for the generalised three-dimensional case.

[1] the subscripts 11, 22 and 33 are used to denote the appropriate co-ordinate directions in the two or three dimensional space. The first subscript denotes the direction of the normal of the plane on which the response is calculated and the second subscript denotes the orientation of the response. The use of a single subscript denotes a principal value, that is, the axes are orientated in such a way that the applied traction can be described completely in terms of the three orthogonal directions, i.e. there are no shear components.

$$\begin{bmatrix} \varepsilon_{11} \\ \varepsilon_{22} \\ \varepsilon_{33} \\ \varepsilon_{12} \\ \varepsilon_{23} \\ \varepsilon_{31} \end{bmatrix} = \begin{bmatrix} \frac{1}{E} & \frac{-\upsilon}{E} & \frac{-\upsilon}{E} & 0 & 0 & 0 \\ \frac{-\upsilon}{E} & \frac{1}{E} & \frac{-\upsilon}{E} & 0 & 0 & 0 \\ \frac{-\upsilon}{E} & \frac{-\upsilon}{E} & \frac{1}{E} & 0 & 0 & 0 \\ 0 & 0 & 0 & \frac{1}{2G} & 0 & 0 \\ 0 & 0 & 0 & 0 & \frac{1}{2G} & 0 \\ 0 & 0 & 0 & 0 & 0 & \frac{1}{2G} \end{bmatrix} \begin{bmatrix} \sigma_{11} \\ \sigma_{22} \\ \sigma_{33} \\ \sigma_{12} \\ \sigma_{23} \\ \sigma_{31} \end{bmatrix} \tag{2.5}$$

where

$$G = \text{Shear Modulus}$$
$$= \frac{E}{2(1+\upsilon)}$$

Two specific applications or solutions utilising of the theory of elasticity that are relevant to geotechnical and pavement engineering are given below.

2.3.1.1 Semi-infinite Half Space

A solution for the application of a point load acting on the surface of an infinite, elastic half-space was given by the French mathematician Joesph Boussinesq in 1878 (Boussinesq 1878). The point load solutions can be integrated in either a cylindrical or an orthogonal three-dimensional space to give a solution for uniform pressure acting over a regular area. One advantage of a linear elastic solid is that the theory of superposition can be used to determine the effect of multiple loads on the solid. The solutions for the vertical components of stress, strain and displacement on the centreline of a uniformly loaded circular area are given below:

$$\sigma_z(r=0)=\sigma_0\left(1-\frac{1}{\left(\sqrt{1+\left(\frac{a}{z}\right)^2}\right)^3}\right) \tag{2.6}$$

$$\sigma_r(r=0)=\sigma_0\left(\frac{1+2\upsilon}{2}-\frac{1+\upsilon}{\sqrt{1+\left(\frac{a}{z}\right)^2}}+\frac{1}{2\left(\sqrt{1+\left(\frac{a}{z}\right)^2}\right)^3}\right) \tag{2.7}$$

$$\varepsilon_z=\frac{(1+\upsilon)\sigma_0}{E}\left[\frac{\frac{z}{a}}{\left(\sqrt{1+\left(\frac{z}{a}\right)^2}\right)^3}-(1-2\upsilon)\left(\frac{\frac{z}{a}}{\sqrt{1+\left(\frac{z}{a}\right)^2}}-1\right)\right] \tag{2.8}$$

$$d_z=\frac{(1+\upsilon)\sigma_0 a}{E}\left[\frac{1}{\sqrt{1+\left(\frac{z}{a}\right)^2}}+(1-2\upsilon)\left(\sqrt{1+\left(\frac{z}{a}\right)^2}-\frac{z}{a}\right)\right] \tag{2.9}$$

where

σ_0 = applied pressure
σ_z = vertical pressure
σ_r = radial pressure
ε_z = vertical strain
d_z = surface deflection of halfspace
a = radius of the loaded area
z = depth below the surface

The full set of solutions are given in Ullidtz (1998).

2.3.1.2 Semi-infinite Layered Half Space

Boussineqs's solutions were further developed by Burmister in 1943 to give a solution for a two layered system (Burmister 1943). Burmister extended the single layer solution by accounting for the thickness and stiffness of the upper layer as a ratio of the radius of the loaded area and the ratio of the stiffness of the lower layer respectively. In 1949 Odemark (1949) presented his method, the Method of Equivalent Thicknesses (MET), of accounting for a system with multiple layers. This method is based on the assumption that stresses and strains below a layer interface depend on the stiffness of that layer only. The stiffness of a layer is defined by:

$$\frac{h^3 E}{1-\upsilon^2} \tag{2.10}$$

where h = the thickness of the layer. If the thickness, modulus and Poisson's ratio of a layer are changed, but the stiffness of the layer remains unchanged, the stresses and strains below the layer interface should remain unchanged. Therefore the upper layer can be replaced by a layer that has the same modulus as the lower layer and an equivalent thickness, h_e, given by:

$$h_e = h_{upper} \sqrt[3]{\frac{E_{upper}}{E_{lower}} \times \frac{1-\upsilon_{lower}^2}{1-\upsilon_{upper}^2}} \tag{2.11}$$

Ullidtz (1998), states that while Odemark's method is not mathematically correct, reasonable answers can be obtained if the moduli are decreasing by at least 50% between successive layers with depth and that the equivalent thickness of each layer is greater than the radius of the loaded area. A major advantage of the MET approach is that it can be implemented in a computer spreadsheet and is very fast.

A large number of computer programs have been developed that use the theory of linear elasticity and superposition to provide solutions. Superposition allows the combination of responses from a number of single point/area solutions to determine the response of a layered halfspace to multiple loaded areas, such as a dual tyre assembly of a complete truck. These programs compute a numerical solution to the fourth order differential equations that form the basis of the multilayer solutions.

Four of these programs are: BISAR (Peutz et al. 1968); CIRCLY (Wardle 1977); ELSYM5 (FHWA 1987); and WESLEA (Van Cauwelaert et al. 1989). These models are all based on an internal cylindrical co-ordinate system and only allow the analysis of circular loaded areas. BISAR and CIRCLY allow the application of oblique, varying and tractive forces to the surface of the model. CIRCLY also incorporates the ability to model materials that exhibit anisotropic characteristics.

2.3.2 Finite Element Method

The FEM has been developed over the last 40 years, starting in 1956 (Turner et al. 1956) with the analysis of aircraft frames. An excellent overview of the matrix analysis methods leading up to the advent of the FEM is given in Felippa (2001). In the FEM, the model is broken into any number of small elements, each element is modelled as a complete self-contained system, usually as a linear elastic system, although any Cauchy, Green or other constitutive relationship can be used. Nodes at each corner define the simplest elements; higher order elements define nodes at other points along the edges of the elements. Adjacent elements are joined at common nodal points and the complete system is formulated as a series of equations to ensure equilibrium in terms of forces and displacements is maintained at each nodal point. FEM formulations can be expressed in one, two (planar or axisymmetric), or three dimensions. The first published FEM analysis of a pavement structure appeared in 1968 (Duncan et al. 1968), in which the authors used an axisymmetric formulation and specified the stiffness of each element in the granular layer as a function of the stresses in the element. Since 1968, pavement researchers have used the FEM to model pavement structures in three dimensions, with static and dynamic loads and with stress and time dependent material properties. A more complete description of the FEM work relating to the modelling of pavement structures is given in Section 2.14.

2.3.3 Probabilistic Analysis

Probabilistic analysis can be used in the analysis of particulate media (Harr 1977). A particulate medium is a collection of discrete particles. The particles can vary in size, shape and orientation. Upon the application of an external traction, only an approximate prediction of the internal distribution of the traction can be made. The

basis of this method of analysis is to use probability theory to predict the response of a system to an applied load(s). The distribution of particle sizes, shapes and roundness, together with the degree of packing of the particles or porosity contribute to this method of analysis. This method can be extended to three dimensions and multi-layered systems. The multi-layered approach utilizes an equivalent thickness approach similar to Odemark's method. Turnbull et. al. (1961) reported the measured stress distribution in a particulate medium as "…too large vertical and too small lateral stresses were measured in the region of the load…" when compared to the stress distribution predicted by elastic theory. Freeman and Harr (2004) report field measurements of stress and backcalculated the ratio of horizontal to vertical stress (coefficient of lateral stress), which is required to calculate the stress distribution. They calculated coefficients of lateral stress of 0.13 for crushed limestone, 0.14 for sand and 0.43 for clay.

This method of analysis still requires a constitutive relationship to relate the stresses and strains.

2.3.4 Discrete Element Method

The Discrete Element Method (DEM) was developed to model granular materials (Strack and Cundall 1978). The granular material is modelled as an assembly of distinct or discrete particles that behave independently, but interact with each other at the contact points. Rules or laws are set to allow for slippage, rotation, contact forces, particle strength/compressibility between particles. The distribution of particle sizes and shapes through the assembly is intended to reflect the actual distribution of particles in a granular structure. This method allows the modelling of actual load paths through the structure by tracing the particle-to-particle load path. The initial two-dimensional application was developed using disks, but this has been extended to angular shapes and the logical next step is the implementation of a three dimensional model. Ullidtz (1997) used the DEM to model a two dimensional representation of a granular material and reported good results when compared to the actual response of the granular material. The horizontal stresses predicted by continuum mechanics were much less than those predicted by the DEM. Zeghal (2004) also used two-dimensional DEM to model a triaxial specimen

and reported a good match with the observed behaviour. The biggest limitation to the adoption of DEM would appear to be the need for large computational capacity.

2.3.5 Summary

Initially pavement structures were modelled with analytical solutions of layered linear elastic theory, but this has recently been surpassed by the FEM, a numerical representation of a system. The use of a FEM model allows the model to accommodate the load dependant stiffness of the granular and subgrade materials, although most models still use linear elastic theory as the constitutive relationship. Other techniques for modelling pavement structures exist, such as probalistic and DEM systems, although these methods are not widely used. The DEM approach may gain popularity as computational power increases in the future.

2.4 Laboratory Measurements

Laboratory measurements are used to determine the coefficients of the constitutive equations that describe the behaviour or materials used in the modelling of pavement structures. Material properties of interest to pavement engineers are the resilient modulus, Poisson's ratio, the degree of anisotropy and the permanent deformation characteristics.

For most engineering materials the Young's modulus of the material is defined as the slope of the load – deformation curve obtained from a monotonic loading test as shown in Figure 2.3. Under normal loading conditions, pavement structures are generally not loaded to a point of material failure; instead they are subjected to a cyclic load that is usually well below the ultimate failure load of the materials.

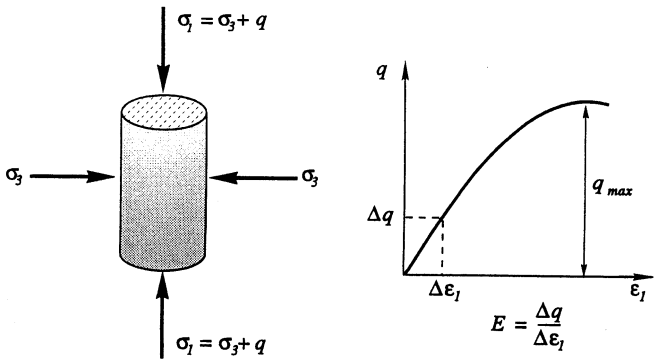

Figure 2.3 Determination of modulus from monotonic triaxial test (Davis and Selvadurai 1996).

In order to define a modulus that was more representative of the cyclic loading, Hveem (1955), proposed the definition of a resilient modulus (Figure 2.4):

$$M_r = \frac{\sigma_d}{\varepsilon_r} \tag{2.12}$$

where:

M_r = Resilient Modulus
σ_d = Cyclic or deviatoric stress
ε_r = recoverable (elastic) axial strain

The resilient modulus has become the de facto modulus definition for granular and fine-grained soils in the field of pavement engineering and is freely substituted for the Young's Modulus in constitutive relationships. Australia (Standards Australia International Limited. 1995), the United States of America (American Association of State Highway and Transportation Officials (AASHTO) 1999) and the European Union, (European Committee for Standardization CEN 2004) have published standardised test methods for the determination of the resilient modulus by using the Repeat Load Triaxial (RLT) test. In general, the specimens are subjected to a number (50-200) of load pulses at a series (typically 10-60) of various stress states and the resilient modulus is calculated for each stress state.

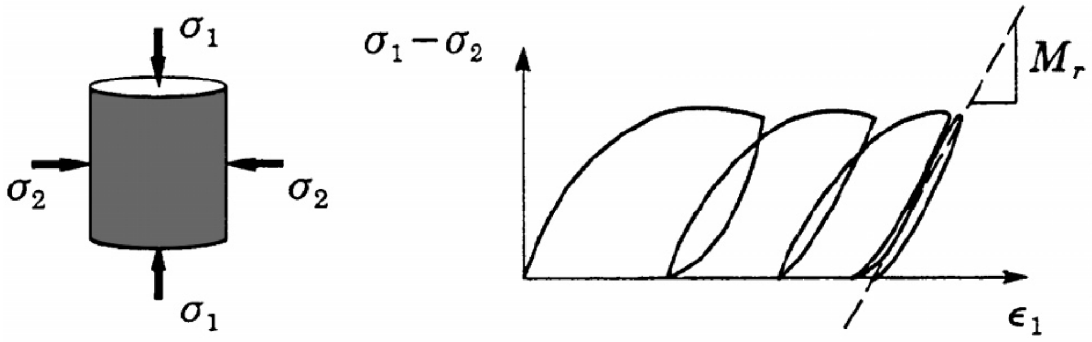

Figure 2.4 Triaxial Test and Resilient Behavior of Granular Materials (Hjelmstad and Taciroglu 2000).

2.4.1 Repeat Load Triaxial Test

The Repeat Load Triaxial (RLT) test is a cyclic version of the monotonic triaxial test widely used in geotechnical testing to determine the modulus of a soil or granular material. A typical RLT test cell is shown in Figure 2.5. A RLT test system can be configured in a number of ways:

- The loading system can be servo-hydraulic or pneumatic;
- The load control can be open or closed loop feedback;
- The loading ram and cell cap interface can either be a double linear bearing with a rolling diaphragm seal or a bronze bushing with an O-ring seal;
- The load measuring system can be external or internal to the load cell;
- Axial displacement can be measured external to the cell or mounted on the specimen;
- The confining medium can be air, water or oil;
- The measurement of radial strains is optional and;
- The confining pressure can be constant (Constant Confining Pressure (CCP)) or cycled in or out of phase with the axial load (Variable Confining Pressure (VCP)).

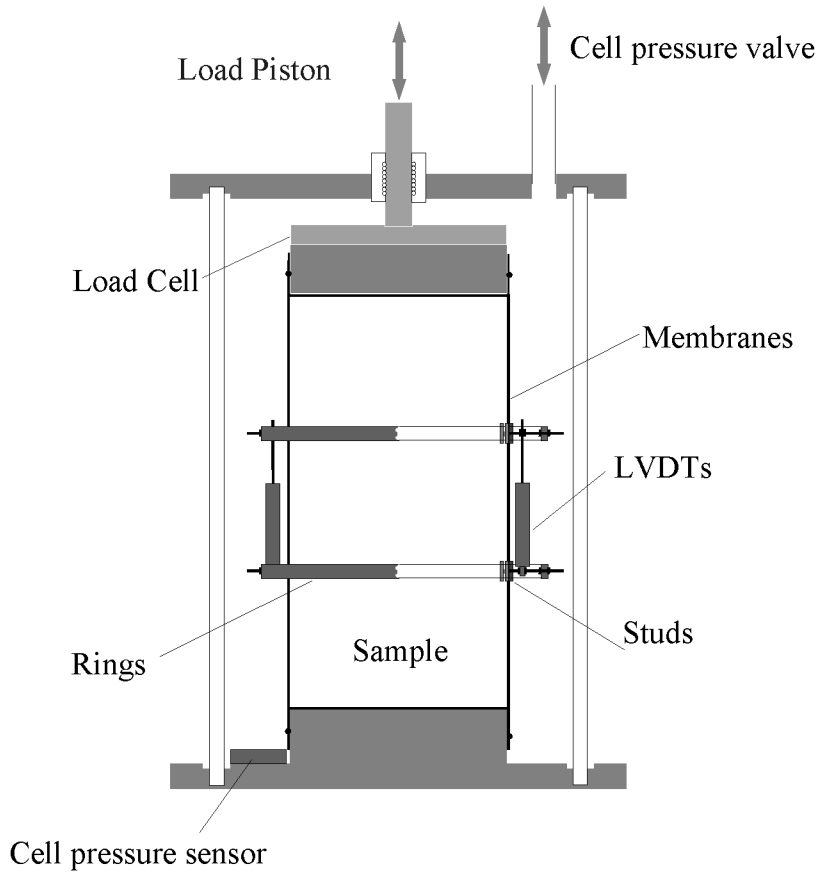

Figure 2.5 Example of triaxial cell and systems for measuring axial displacements using LVDTs (European Committee for Standardization CEN 2004).

The recommended specimen diameter and height to diameter ratio is five to six times the largest particle size and 2:1 respectively. The calculation of the resilient modulus for the VCP case is more complicated than for the CCP case. The resilient modulus is a chord modulus, that is, it represents the stiffness of the specimen as the stress state changes from one state (isotropic confining stress) to another (confining plus deviatoric stress). Assuming that the specimen behaves as an isotropic linear elastic solid, Hooke's Law (Equation (2.5)) can be rearranged to give a definition for stiffness, E:

$$E = \frac{1}{\varepsilon_1}\left(\sigma_1 - \upsilon\sigma_2 - \upsilon\sigma_3\right) \tag{2.13}$$

Since $\sigma_2 = \sigma_3$,

$$E = \frac{1}{\varepsilon_1}\left(\sigma_1 - 2\upsilon\sigma_3\right) \tag{2.14}$$

Given that the resilient modulus is defined as a function of the incremental stress condition, then in the CCP case, there is no change in the value of σ_3 and the resilient modulus definition as given in Equation (2.12) suffices. For the VCP case, both the confining and axial stresses change and Equation (2.14) should be used in the following form:

$$M_r = \frac{1}{\varepsilon_r}\left(\Delta\sigma_1 - 2\nu\Delta\sigma_3\right) \tag{2.15}$$

where:

$\Delta\sigma_1$ = total change in axial stress
$\Delta\sigma_3$ = change in confining stress

The use of this equation requires that the radial strains be measured so that the Poisson's ratio can be calculated, while the calculation of the Poisson's ratio for the CCP case is optional.

Vuong (1999) reported the results of an Australian study looking at the accuracy and source of errors in RLT testing. He concluded that: systems using a bronze bushing between the loading ram and the cell cap should use an internal load cell; water or oil was the preferred confinement medium; systems using external axial displacement measurement should (a) determine and correct for any compliance in the reaction frame system and (b) use two displacement transducers with a range of 5 mm to reduce errors due to sample bending and electrical noise. Galjaard et. al. (1996) reported the results of a European study looking at inter laboratory variation of results. The European laboratories used various types of internal measurement systems to determine the axial and radial displacements. The resilient axial displacements were all similar and lower than the external axial measurements that were measured simultaneously. There was a large scatter in the radial strain measured and this was largely attributed to the different methods employed to attach the measurement systems to the specimens. The recommended method of measuring axial displacements was three Linear Variable Displacement

Transducers (LVDT's) attached at either the third or quarter heights of the specimen. Ping and Ge (1997) measured the resilient modulus of subgrade soils using both internal and external axial strain measurement systems, and reported that the modulus values calculated from the external axial measurements were 16% lower than the values determined from the internal axial measurements. Maher et. al. (1996) reported a 20% reduction in resilient modulus values determined from external LVDT when compared with non-contact proximity sensors. Barksdale et. al. (1997) undertook a comprehensive study looking at suitable equipment and methodologies to determine resilient modulus values for the 2002 AASHTO Pavement Design Guide and they reported that internal on-specimen axial measurements (using instruments clamped between the quarter points) produced modulus values that were up to 16% higher than external measurements although the difference between the values from the two measurement systems reduced as the specimen stiffness reduced from 350 to 50 MPa. One reason put forward for this was that system compliance was a greater percentage of the total measured external displacement in the stiffer specimens, thus under-calculating the true stiffness of the specimen. In addition, the use of on-specimen transducers allows the true response of the specimen to be measured without having to consider the interaction between the specimen and loading platens.

Galjaard et. al. (1996) also reported the results of a study looking at the variation in density in relation to the height of the specimen. A nuclear density meter operating in transmission mode measured the density of four specimens compacted with single layer vibrocompression and vibrating hammer (3, 5, and 7 layers). The variation in density for the three layer specimen was 15% and the variation for the vibrocompression and seven layer specimen was 3.5%.

In summary, the European and North American test methods for determining the resilient modulus by triaxial testing recommend internal on-specimen measurement of axial displacement while the Australian method allows external displacement measurement in order to reduce the complexity and cost of the test.

2.4.2 Hollow Cylinder Apparatus

The Hollow Cylinder Apparatus (HCA) allows the application of shear stresses to a specimen unlike the triaxial test cell that can only apply principal stresses to a specimen. The HCA at the University of Nottingham is described by Thom and Dawson (1996). The specimen for the HCA is similar to a thick walled tube with an external diameter to wall thickness ratio of 10 and the diameter to height ratio is 0.5. The dimensions limit the maximum particle size to coarse sand (less than 4.75 mm). The internal and external confining pressures can be controlled independently and the top platen is serrated to ensure a positive bond with the specimen. Shear stresses are applied to the specimen by rotating the top platen about the specimen axis. Because of the complexity of the apparatus and the limits of the particle sizes, this equipment is not routinely used.

2.4.3 K-Mould

The K-Mould was developed in South Africa by the Council for Scientific and Industrial Research (CSIR) (Semmelink and de Beer 1995; Semmelink et al. 1997) as an alternative to the RLT test. The specimen has the same dimensions as a CBR specimen (diameter and height of 152.4 mm) and is subjected to either a monotonic or cyclic axial load. A steel mould that is cut into eight segments provides radial confinement and each segment reacts against two springs. As the axial load is increased, the specimen expands in a radial direction and because the stiffness and compression of the radial springs are known, the radial stress can be determined.

One potential limitation of this test is that the radial stiffness is fixed, unlike the situation in a pavement where the surrounding material resists the lateral expansion of a notional "free body" and the stiffness of the material may be stress dependent, thus continually altering the amount of radial expansion.

2.4.4 UI-FastCell

The University of Illinois, in conjunction with IPC Global, has developed a new type of triaxial testing device, the UI-FastCell, which is shown in Figure 2.6 (Tutumluer and Seyhan 2000; Seyhan and Tutumluer 2002). The UI-FastCell is based on a standard RLT apparatus but has two major differences.

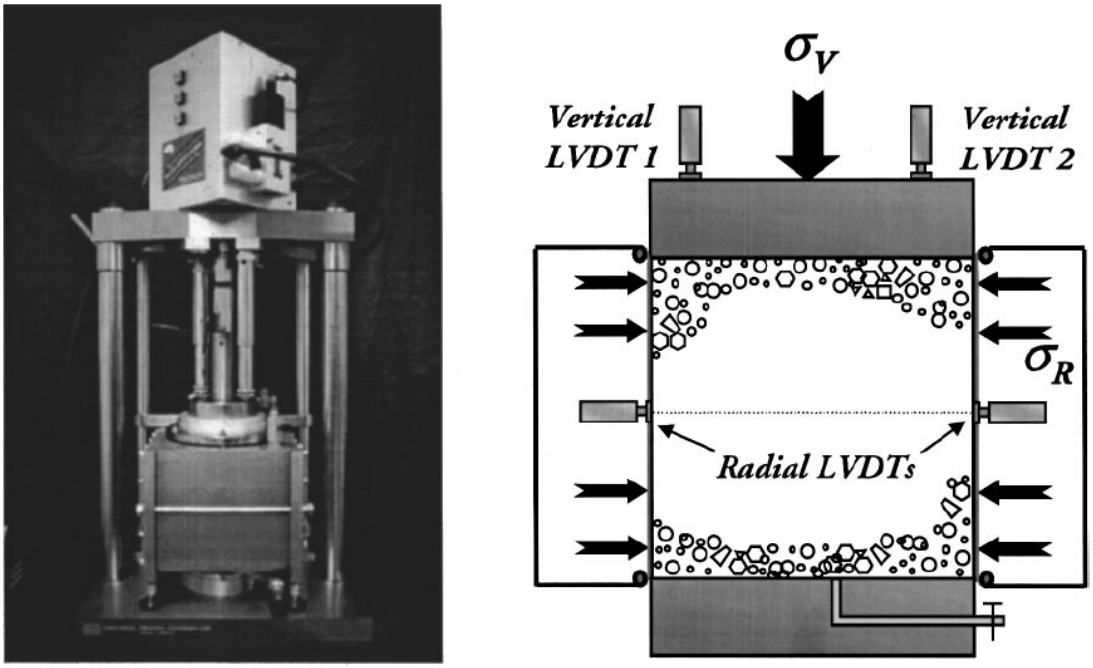

Figure 2.6 The University of Illinois FastCell (UI-FastCell) triaxial testing device (Seyhan and Tutumluer 2002).

The first difference is the height to diameter ratio of 1:1. The UI-FastCell uses a low-friction plastic paper disk between the specimen and polished end platen to reduce the end effects as much as possible, thus allowing specimens to be tested at a height to diameter ratio of 1:1. The second difference is that the confining medium is an integral part of the test cell. A rubber membrane is attached to the confining cell and this is lowered over the prepared specimen. The confining cell can use either air or oil to apply the confining pressure to the specimen. Radial strains are measured by four LVDT's mounted at mid-height inside the confining cell. The LVDT's are spring-loaded and bear directly onto the confining membranes. Axial displacements are measured by two LVDT's that are mounted on the top platen. By pulsing the radial or confining pressure only, the radial (normally defined as horizontal) modulus can be determined. However, since the end platens are rigid, the type of confinement provided to the specimen subjected to radial loading will not be the same as for conventional axial loading. Seyhan and Tutumluer (2002) report that the modulus values obtained from the UI-FastCell were in close agreement with the values obtained from conventional RLT testing, thus confirming the 1:1 aspect ratio. A major advantage of the UI-FastCell would be in not having to mount measuring equipment on the sides of the specimen.

Another advantage would be that samples could be prepared by using a gyratory compactor if desired.

2.4.5 Summary

Four laboratory techniques (RLT, HCA, K-Mould and UI-FastCell) that are used to characterise granular and cohesive pavement materials have been reviewed, of the four, the RLT is the most widely used. Some shortcomings of the RLT method are: the applied stress state does not accurately subject the specimen to the same sort of stress state that a rolling wheel does; the potential differences between reconstituted and undisturbed specimens; the complexity of the test; and the reproducibility of the results between laboratories.

2.5 Factors Affecting Material Response and Performance

Numerous studies have been undertaken to determine the effect of stress, density, moisture content, gradation or particle size distribution and stress rotation on the resilient and plastic response of granular materials. These factors are usually incorporated into models that are used to determine the resilient modulus (resilient response) or permanent deformation (plastic response). Specific models that have been developed to characterise the resilient and plastic response are described later.

2.5.1 Stress

Over 40 years ago it was recognised that the modulus of granular materials was non-linear with respect to stress level. Biarez (1961) and Seed et al (1967a) were some of the early researchers to report that the resilient modulus of unbound granular materials was a function of the mean stress level and/or confining stress. Monismith et. al. (1967) reported that an increase in the confining stress from 21 to 207 kPa resulted in a 500% increase in the resilient modulus. Sweere (1990) and Lekarp and Isacsson (2001) showed a positive linear relationship between the bulk stress and resilient modulus for crushed materials.

2.5.2 Density

Rada and Witczak (1981) summarised earlier research and found that the resilient modulus increased as the density increased, but it was a second order effect when compared with the effects of stress level and moisture content. Vuong (1992) reported that, for a given stress state, the resilient modulus increased as the density increased but there was no improvement when the density was greater than the Maximum Dry Density (MDD).

Barksdale (1972) reported that when the density of a triaxial specimen was reduced by 5%, the plastic strain increased by 185%. Allen and Thompson (1974b) reported that when the compactive effort was increased from standard Proctor to modified Proctor, the plastic strains decreased by 20% for a gravel and by 80% for a crushed limestone.

2.5.3 Moisture Content

Vuong (1992) found that the resilient modulus increased as the moisture content reduced but the increase was insignificant once the moisture content dropped below 70% of the optimum moisture content. Researchers have tended to express stress relationships in terms of total stresses, usually ignoring the effect of pore water pressures because it is difficult to determine the pore water pressure in a partially saturated material or pavement structure. Dawson et. al. (1996) found that the resilient modulus of well graded aggregates increased as the moisture content increased from dry to optimum moisture content. The increase in stiffness was attributed to the development of suction within the pore spaces. Once the moisture was greater the than the optimum value, the stiffness decreased rapidly due to excess pore water pressure. Thom and Brown (1987) postulated that the presence of moisture acted as a lubricant and therefore increased the resiliency of the aggregate assembly with the attendant effect of reducing the stiffness. They based their assumption on the evidence from a series of tests that no pore pressures were measured if the degree of saturation was less than 85%. This could also be interpreted that no pore pressures were measured because the pore pressures that were in the specimens were countering the suction already present in the specimens and it wasn't until the specimens were almost totally saturated that the suction was negated and positive pore pressures were registered by the instrumentation.

McInnes (1984), Loi et. al. (1992), Fredlund et. al. (1997), Walker (1997), Heath et. al. (2004) have all measured matric suction in either RLT or field situations and have reported suction values of at least 70 kPa for partially saturated granular materials, with suction values much higher for cohesive materials (Sauer and Monismith 1968; Walker 1997; Oloo and Fredlund 1998). Wallace (1998) measured the apparent tensile strength of a granular layer in a laboratory test and concluded that the apparent tensile strength of a high quality granular material was 15 kPa when the material was at 50% saturation. Numerical modelling of the test showed that the material had a tensile strength of 60 kPa.

2.5.4 Gradation

Thom and Brown (1988) reported the results of a study examining the effect of material grading and concluded that the type of grading (going from dense to open) had little influence (less than 13%) on the resilient and plastic response of the material. Brown and Selig (1991) and Raad et. al. (1992) both found that a uniformally graded material was only slightly stiffer than a well graded material. Sweere (1990) and Lekarp and Isacsson (2001) conducted a series of RLT tests on large scale equipment (Sweere: 400/800 mm and Lekarp: 500/1000 mm diameter/height respectively) and found that as the maximum particle sized increased, the stiffness of the specimen increased. They both concluded that unbound aggregates should be tested at their natural grading/maximum size, with the implicit requirement that large scale RLT equipment is required in order to maintain a suitable maximum particle size to specimen diameter ratio (5-6).

2.5.5 Stress Rotation

The stress state that an element of soil/aggregate is subjected to varies widely as a rolling wheel approaches and then departs. As a wheel approaches an element of soil in the pavement, initially the major stress component is a horizontal shear stress. When the wheel is directly over the element, the major stress component is the vertical stress and as the wheel travels away from the element, the major stress component becomes a horizontal shear stress with the opposite sign to the initial shear stress. This effect is shown in Figure 2.7 and Figure 2.8.

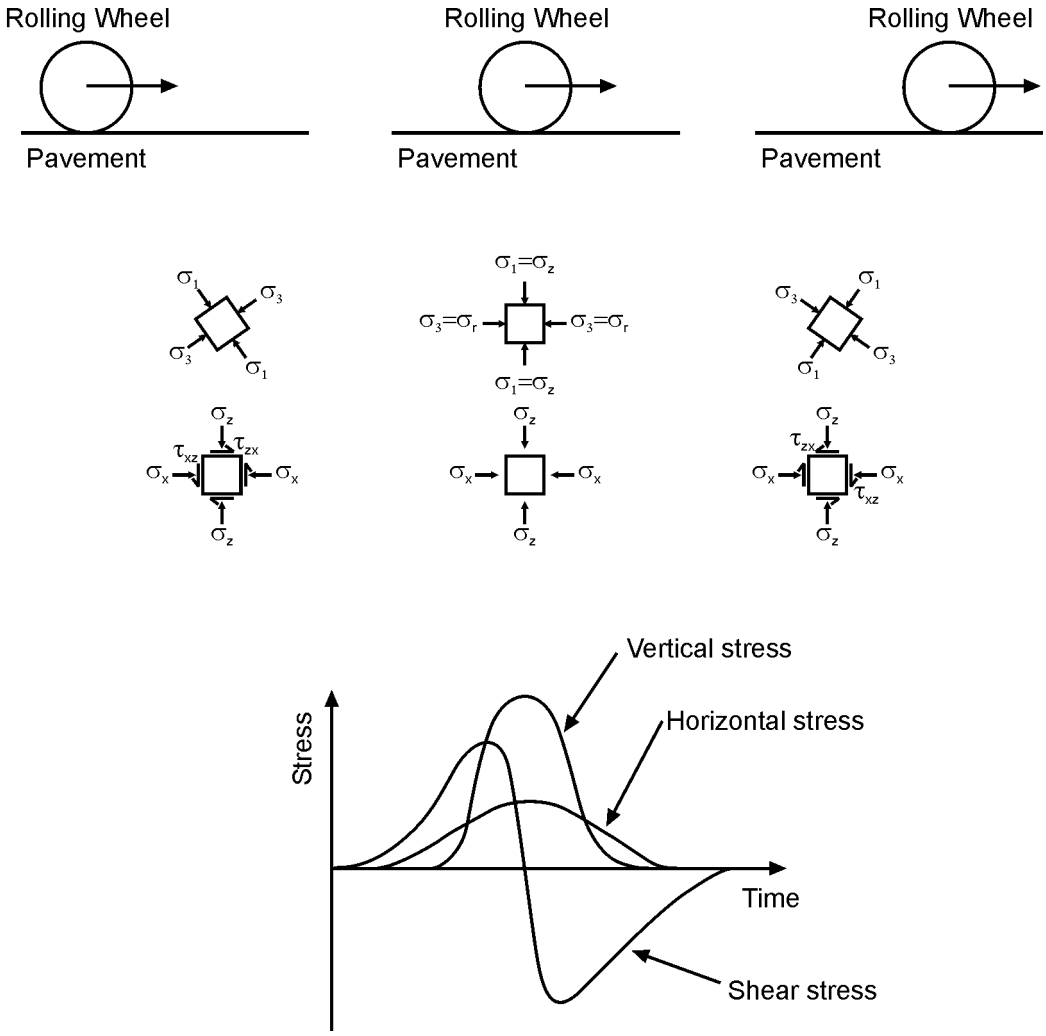

Figure 2.7 Variation of the stress state beneath a rolling wheel (adapted from Lekarp et. al. (2000a))

As it is shown in Figure 2.8, there is a major difference in the stress paths between the triaxial cell and a pavement. The implication of this is that material and constitutive models that have been developed and verified with laboratory data may not be accurate when they are compared with measurements from pavements subjected to moving loads.

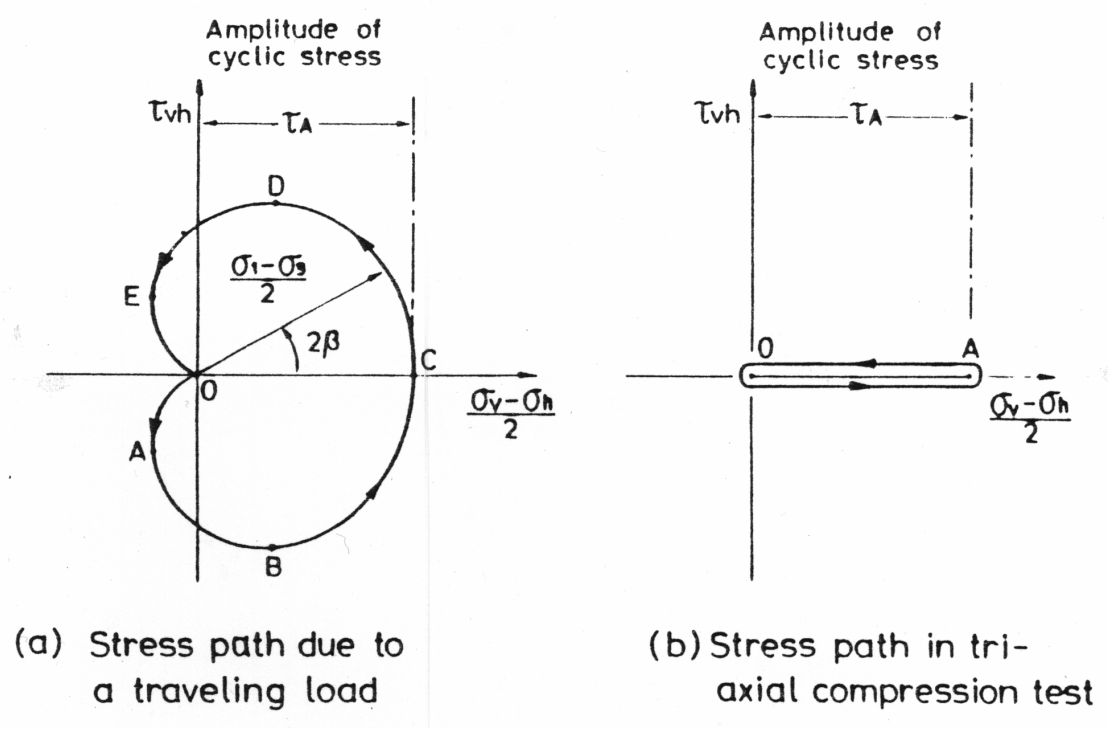

Figure 2.8 Stress path due to: a) moving wheel, and b) cyclic triaxial test (Ishihara 1983).

2.5.6 Summary

Researchers have shown that stress level, density and moisture all influence the response of granular materials. If the material is partially saturated and well compacted, stress level has the biggest influence. The effect of stress rotation on the material response is the biggest unknown and there is no readily available technique to assess this whilst maintaining the material at its full size or natural grading.

2.6 Resilient Non-linear Material Models

A large number of non-linear constitutive models have been proposed over the last 40 years, some are given in the following section. Some models only give a definition of the resilient modulus and/or Poisson's ratio, these types of models are usually based on observations from RLT test results, such as the k-theta model (Seed et al. 1967b). The resilient modulus is then used as a surrogate Elastic Modulus in Hooke's Law to define the stress-strain relationship. These models could be described as "curve-fit" models. Other models separate the stresses or

strains into the bulk and shear components and define the bulk and shear moduli, such as the Boyce Model (Boyce 1980). Lekarp et. al. (2000a) provided a state of the art summary on the resilient response of granular materials. This summary listed 18 different models. The large number of models proposed would indicate that the most appropriate model for cyclic loading of granular materials has yet to be found.

2.6.1 Unbound Granular Materials: Resilient Modulus Models

The earliest non-linear model for cyclic loading of granular materials was proposed in 1962 by Biarez (1961)

$$E = K\sigma_m^n \tag{2.16}$$

where

$$\begin{aligned} E &= \text{Secant Modulus} \\ K, n &= \text{empirical constants} \\ \sigma_m &= \text{mean normal stress} \\ &= \frac{\text{sum of principal stresses}}{3} \end{aligned}$$

This model was modified by Seed et. al. (1967b) who replaced the secant modulus with the resilient modulus and the mean normal stress with the first invariant of the stress tensor or bulk stress (θ):

$$M_r = k_1 J_1^n \tag{2.17}$$

where

$$\begin{aligned} M_r &= \text{Resilient Modulus} \\ k_1, n &= \text{constants} \\ J_1 &= \sigma_1 + \sigma_2 + \sigma_3 = \theta \end{aligned}$$

This model is known as the K-Theta model, but the model as proposed is not dimensionally correct. The bulk stress needs to be normalised by either the unit stress or atmospheric pressure to allow it to be raised to a power. Seed et. al.

(1967a) also proposed a second model where the bulk stress was replaced by confining stress:

$$M_r = k_1 \sigma_3^n \tag{2.18}$$

Allen and Thompson (1974b) undertook a non-linear FEM study to determine the sensitivity of various input factors; one of their conclusions was that if the n parameter of the K-Theta model is held at a constant value and the k_1 parameter is varied, the percentage change in the pavement response (surface deflection and subgrade strain) is much less than the percentage change in the parameter. A major shortcoming of this model is that the effect of shear stresses is not considered and that multiple stress conditions will predict the same modulus. An example of this is that low values of confining (σ_2 / σ_3) stress and high axial (σ_1) stress will have the same bulk stress value as a stress state where the confining stress is high and the axial stress is low.

Shackel (1973) proposed a three parameter model using two functions of the stress state

$$M_r = k_1 \sigma_{oct}^{k_2} \tau_{oct}^{k_3} \tag{2.19}$$

where

$$\begin{aligned} k_1, k_2, k_3 &= \text{constants} \\ \sigma_{oct} &= \text{octahedral normal stress} \\ &= \frac{\sigma_1 + \sigma_2 + \sigma_3}{3} \\ \tau_{oct} &= \text{octahedral shear stress} \\ &= \frac{1}{3}\sqrt{(\sigma_1 - \sigma_2)^2 + (\sigma_2 - \sigma_3)^2 + (\sigma_3 - \sigma_1)^2} \\ &\quad or \ \frac{\sqrt{2}}{3}\sigma_d \ \text{for two dimensional conditions} \end{aligned}$$

Uzan (1985) proposed a model of essentially the same form as Equation (2.19), but he replaced the octahedral normal stress with the bulk stress and the octahedral shear stress with the deviatoric stress. This model has been refined over time with the shear stress term reverting to the octahedral shear stress, the change to non-

dimensional power terms and finally the addition of 1 to the shear stress term to remove the singularity that occurs when the shear stress term is equal to zero (Andrei et al. 2004).

$$M_r = k_1 p_a \left(\frac{\theta}{p_a} \right)^{k_2} \left(\frac{\tau_{oct}}{p_a} + 1 \right)^{k_3} \tag{2.20}$$

where p_a = atmospheric pressure (100 kPa)

This model will be referred to as the Uzan model, as most researchers have attributed its origin to Uzan rather than Shackel.

Wellner and Gleitz (1999) proposed the "Dresden Model" to determine the modulus and Poisson's ratio from RLT tests:

$$\begin{aligned} M_r &= \left(k_1 + k_2 \sigma_3^{k_3} \right) \sigma_1^{k_4} + k_5 \\ \upsilon &= k_6 \frac{\sigma_1}{\sigma_3} + k_7 \sigma_3 + k_8 \end{aligned} \tag{2.21}$$

This model requires eight parameters, but it has the advantage of providing a nominal stiffness (k_5) when the stress levels are low. However, this value cannot be determined from RLT tests as the definition of resilient modulus does not allow for a zero stress result. The model is also not dimensionally correct in its published form.

As part of the development of the new ASSHTO 2002 Pavement Design Guide, Andrei et. al. (2004) examined a number of different log-log and semi-log formulations of two parameter models (two of: σ_d, τ_{oct}, θ, or σ_3) and up to 5 constants and concluded that the best representation of M_r in terms of accuracy, implementation and numerical stability was Equation (2.20).

One of the limitations of the models described above is that whilst they are promoted as non-linear models, they are still essentially secant moduli that are path independent. They are usually implemented into finite element models as fixed point iterative models, that is the entire load is applied in one step and the calculation is repeated until the moduli used in the solution are equal to or within a specified error of the moduli calculated from the stresses extracted from the

solution. The finite element solution is usually formulated as a first order Cauchy or Hookean stress strain problem.

2.6.2 Unbound Granular Materials: Bulk and Shear Models

This class of model was first promoted by Brown and Hyde (1975) when they showed that a better representation of the behaviour of granular materials could be obtained when the stress and strain components were separated into the volumetric and shear components. The volumetric and shear components are represented by the octahedral normal and shear definitions respectively. Brown and Hyde used isotropic, linear elastic relationships as the basis of their definition. Boyce (1980) developed a non-linear version of this model based on the K-Theta model but modified it to comply with the theorem of reciprocity, that is there is no energy loss in the loading / unloading cycle. Boyce still assumed that the granular behaviour was isotropic and elastic

$$\begin{aligned} \varepsilon_v &= \frac{1}{K_1} p^n \left(1 - \beta \frac{q^2}{p^2}\right) \\ \varepsilon_s &= \frac{1}{3G_1} p^n \frac{q}{p} \end{aligned} \tag{2.22}$$

where

$$\begin{aligned} \varepsilon_v &= \text{volumetric strain} \\ \varepsilon_s &= \text{shear strain} \\ q &= \sigma_1 - \sigma_3 \\ p &= \frac{\sigma_1 + \sigma_2 + \sigma_3}{3} \\ \beta &= \frac{K_1}{6G_1}(1-n) \\ K_1, G_1, n &= \text{constants} \end{aligned}$$

Sweere (1990) also used the Boyce Model and found a good correlation with the shear strains but a poor correlation with the volumetric strains. He concluded that this was due to the theorem of reciprocity, which linked the volumetric and shear components. Sweere uncoupled the two relationships by replacing the *n* exponent in the shear strain equation with *m* and the β term as defined by Boyce, was made

independent of G. This meant that there was a requirement to determine five constants (K_1, G_1, n, m and β) instead of three (K_1, G_1 and n). The result of this modification was that the dilation of the granular material could be accounted for, although it violated the laws pertaining to the definition of an elastic isotropic material.

Karasahin et. al. (1993) reported the work by Elhannani (1991) where Elhannani proposed an anisotropic version of the original Boyce Model

$$\begin{aligned} \varepsilon_v &= p_a^{1-B} p^B \left[\frac{1}{A} - \frac{(1-B)}{6C} \left(\frac{q}{p} \right)^2 - \frac{B}{D} \left(\frac{q}{p} \right) \right] \\ \varepsilon_s &= p_a^{1-B} p^B \left[\frac{1}{3C} \left(\frac{q}{p} \right) - \frac{1}{D} \right] \end{aligned} \tag{2.23}$$

where

$$A, B, C, D = \text{constants}$$

The constants for this model were determined using RLT results and statistical methods, thus no meaningful measure of anisotropy can be determined.

Guezouli et. al. (1996), Balay et. al. (1997), and Gomes Correia and de Almeida (1998) implemented the modified Boyce Model into the FEM programs NOEL and CESAR LCPC-2D/3D and FENLAP respectively. These implementations also incorporated the Drucker-Prager failure criterion in order to modify the material response when the failure criterion is exceeded. Hornych et. al. (1998) modified the original Boyce Model to account for anisotropic behaviour:

$$\begin{aligned} \varepsilon_v &= \frac{p^{*\,n}}{p_a^{n-1}} \left[\frac{\gamma + 2}{3K_a} + \frac{n-1}{18G_a} (\gamma + 2) \left(\frac{q^*}{p^*} \right)^2 + \frac{\gamma - 1}{3G_a} \left(\frac{q^*}{p^*} \right) \right] \\ \varepsilon_s &= \frac{2p^{*\,n}}{3p_a^{n-1}} \left[\frac{\gamma - 1}{3K_a} + \frac{n-1}{18G_a} (\gamma - 1) \left(\frac{q^*}{p^*} \right)^2 + \frac{2\gamma + 1}{6G_a} \left(\frac{q^*}{p^*} \right) \right] \end{aligned} \tag{2.24}$$

where

$$p^* = \frac{\gamma\sigma_1 + 2\sigma_3}{3}$$
$$q^* = \gamma\sigma_1 - \sigma_3$$
$$\gamma = \text{anisotropy factor}$$

Hornych et. al. (1998) implemented this model into the CESAR-LCPC FEM program. Hornych et. al. did not have access to the anisotropic properties of the granular material, instead they carried out a parametric study to determine the best fit for the model constants.

Brown and Pappin (1981) also developed a model that separated the volumetric and shear components; it was labeled a contour model and is shown in Figure 2.9. The volumetric strain was the difference between the contour values at the start and end of the stress path and was shown to be independent of the stress path. The shear strain was found to be dependent on both the stress path and the length of the stress path. The equations for the contours for the volumetric and shear strains are given by

$$\varepsilon_v = \left(\frac{p'}{A}\right)^m \left[1 - B\left(\frac{q}{p'}\right)^n\right]$$
$$\varepsilon_s = \frac{Cq}{p'+D} \qquad (2.25)$$

where

$$p' = \text{mean normal effective stress}$$
$$A, B, C, D, m, n = \text{constants}$$

The shear strain is given by

$$\varepsilon_s = C\left[\frac{q_1}{p'_1+D} - \frac{q_2}{p'_2+D}\right]\left(\frac{\sqrt{\Delta p'^2 + \Delta q^2}}{p'_m}\right)^r \qquad (2.26)$$

where

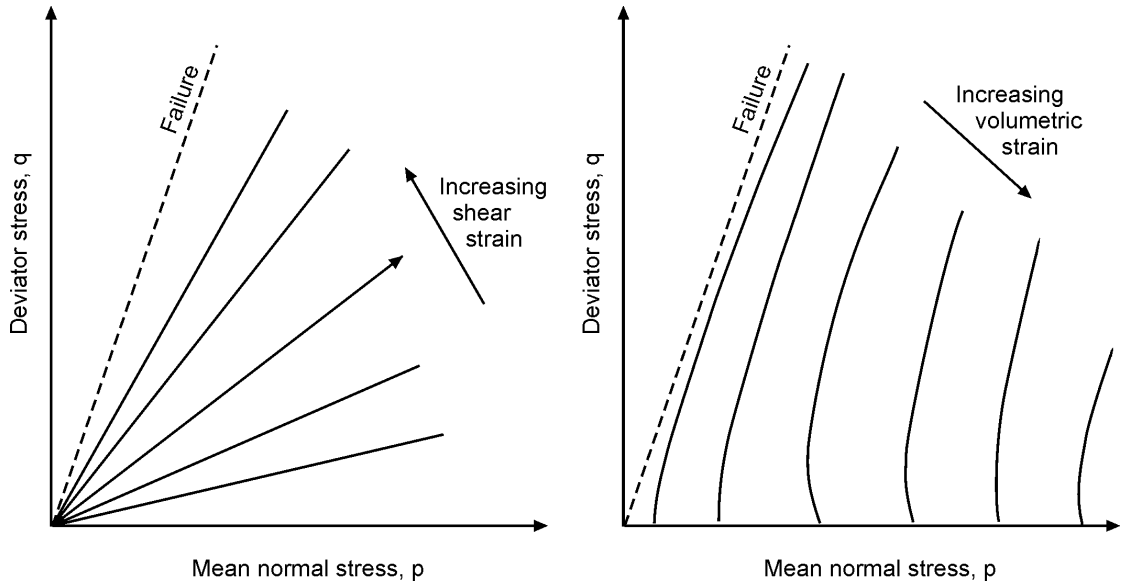

Figure 2.9 Resilient strain contours: (left) normalised shear strain and (right) volumetric strain (Brown and Pappin 1981).

$$p_1, q_1 = \text{initial stress state}$$
$$p_2, q_2 = \text{final stress state}$$
$$\Delta p' = p_2 - p_1$$
$$\Delta q = q_2 - q_1$$
$$p'_m = \frac{p_1 + p_2}{2}$$
$$r = \text{constant}$$

Mayhew (1983) used the Contour Model to predict the results from RLT testing and found that the best correlation for volumetric was Equation (2.25) but the best predictor of shear strain was Equation (2.26) with the term in the second brackets being equal to one, i.e. no dependence on the length of the stress path. Mayhew's model reduces to the same form that Sweere proposed, that is, the volumetric and shear terms are uncoupled.

For non-linear material models that are derived from laboratory tests, consideration should be given to the behaviour of the model when stress states that lie outside the range of tested stress states are used with the model. Kramer (1996) shows that there is a lower limit for the shear (deviatoric) stress or strain and below this limit the modulus is constant and is equal to the small strain linear elastic modulus. The nominal contact pressure for tyres is usually in the range from 500 to 1000 kPa. Most resilient modulus RLT testing regimes have maximum deviator stress values

in this range so the stress states calculated during the analysis of a pavement structure are unlikely to exceed the stress states achieved in the RLT test.

2.6.3 Fine Grained Cohesive Materials

The non-linear aspects of the subgrade soils have not received as much attention from pavement engineers when compared to granular materials. Seed et. al. (1962) used a bi-linear model to represent the resilient modulus as a two stage linear function of the deviator stress (Figure 2.10);

$$M_r = \begin{cases} k_2 + k_3[k_1 - (\sigma_1 - \sigma_3)], & k_1 > (\sigma_1 - \sigma_3) \\ k_2 + k_4[(\sigma_1 - \sigma_3) - k_1], & k_1 < (\sigma_1 - \sigma_3) \end{cases} \tag{2.27}$$

If the value of k_4 is positive, as indicated by Seed et. al. then this would imply that the material became stiffer as failure approached, this is clearly not the case. In this form, the value of k_4 should be negative. Kondner (1963) defined the modulus as a hyperbolic function of the form

$$M_r = \frac{a + b\sigma_d}{\sigma_d} \tag{2.28}$$

This relationship provides a continuous function that is similar to the bi-linear relationship described above. The constants for the hyperbolic relationship can be found by plotting the resilient modulus data in the σ_d-$M_r\sigma_d$ space as the data then plots on a straight line and the constant a is the intercept and b is the slope of the line.

Correia (1985) (cited in Tam and Brown (1989)) proposed the following model for use with subgrade materials

$$M_r = A\left(\frac{p_0}{q_r}\right)^B \tag{2.29}$$

where

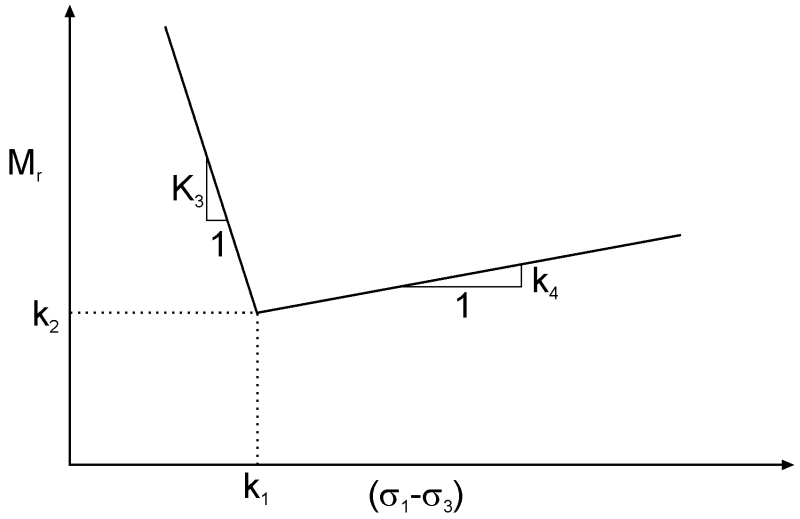

Figure 2.10 Bi-linear resilient modulus model for cohesive soils (Seed et al. 1962).

p_0 = mean stress due to overburden
q_r = deviator stress due to applied load
A, B = constants

This model was developed from RLT tests on unconfined specimens that were subjected to internal suction. Loach (1987) proposed a similar model for confined specimens,

$$M_r = A\left(\frac{p_0}{q_r}\right)^B q_r \tag{2.30}$$

The Uzan model can also be used with fine grained or cohesive soils. Dawson and Gomes Correia (1996) proposed a generalized linear relationship based on mean overburden stress, deviatoric stress and the Plastic Limit (w_p):

$$M_r = 49{,}200 + 950\,p'_0 - 370q_r - 2{,}400w_p \tag{2.31}$$

The coefficients in this relationship were based on test results for Keuper Marl, Gault, London and Kaolin clays so there could some universality in the value of the coefficients, but like all empirical relationships, the values of the coefficients would ideally be determined for the particular material and applicable environmental

conditions. Because the values of modulus for subgrade materials are usually <100 MPa, any variation or uncertainty in the values of the model coefficients is going to have a significant effect on the predicted levels of strain. If the modulus is predicted to be 50 MPa, a variation of 10 MPa in the value is going to alter the predicted strain value by 20%; a variation of 10 MPa in the laboratory determined value would not be considered a significant variation.

2.7 Anisotropy

Granular and cohesive materials tend to exhibit anisotropic characteristics, that the stiffness of the material is not the same in the vertical and horizontal directions. The anisotropic behaviour can be either inherent and/or stress induced. The inherent behaviour can come about through the action of placement and compaction or consolidation through either geologic or construction processes. The effect of anisotropy is to increase the magnitude of the stress in the planar direction for a cross-anisotropic material. The best way to measure the anisotropic characteristics is to use either: the HCA; a true cubic cell (Lade and Duncan 1973; Sture and Desai 1979) where the three normal and shear stresses can be independently and simultaneously varied; or to create/sample specimens where the plane of anisotropy is inclined at some known angle to the direction of the major principal stress (Budiman et al. 1992; Richardson et al. 1996).

Pickering (1970) described the stiffness matrix for a cross anisotropic material and the bounds of the elastic constants in order for the material to satisfy the laws of thermodynamics. For a transversely isotropic material, that is a material where the material properties are the same in the 1-3 plane, the stiffness matrix for an elastic solid is

$$\begin{bmatrix} \varepsilon_{11} \\ \varepsilon_{22} \\ \varepsilon_{33} \\ \varepsilon_{12} \\ \varepsilon_{23} \\ \varepsilon_{31} \end{bmatrix} = \begin{bmatrix} \frac{1}{E_1} & \frac{-\upsilon_{12}}{E_1} & \frac{-\upsilon_{11}}{E_1} & 0 & 0 & 0 \\ \frac{-\upsilon_{12}}{E_1} & \frac{1}{E_2} & \frac{-\upsilon_{12}}{E_1} & 0 & 0 & 0 \\ \frac{-\upsilon_{11}}{E_1} & \frac{-\upsilon_{12}}{E_1} & \frac{1}{E_1} & 0 & 0 & 0 \\ 0 & 0 & 0 & \frac{1}{G_{12}} & 0 & 0 \\ 0 & 0 & 0 & 0 & \frac{1}{G_{12}} & 0 \\ 0 & 0 & 0 & 0 & 0 & \frac{2(1+\upsilon_{11})}{E_1} \end{bmatrix} \begin{bmatrix} \sigma_{11} \\ \sigma_{22} \\ \sigma_{33} \\ \sigma_{12} \\ \sigma_{23} \\ \sigma_{31} \end{bmatrix} \tag{2.32}$$

where

E_1 = Modulus in the plane of isotropy
E_2 = Modulus normal to the plane of isotropy
υ_{12} = Poisson's ratio for strain in the 2 direction due to a strain in the 1 direction
υ_{21} = Poisson's ratio for strain in the 1 direction due to a strain in the 2 direction
υ_{11} = Poisson's ratio in the 1 direction due to a strain in the 3 direction (or vice versa)
G_{12} = Shear Modulus in the 2 plane
$\frac{E_1}{E_2} = \frac{\upsilon_{12}}{\upsilon_{21}}$

Zienkiewicz and Taylor (2000) defined two anisotropic parameters, *n* and *m*, where:

$$n = \frac{E_1}{E_2}$$
$$m = \frac{G_{12}}{E_2} \tag{2.33}$$

Gazetas (1982), and Yu and Dakoulas (1993) summarised the work of previous research and reported that measured values of *n* ranged between 0.9 and 4 for cohesive soils and the value of *n* increased as the OCR increased. They also reported *n* values as low as 0.2 for sands. Gazetas (1982) showed that the theoretical distribution of vertical and horizontal stresses was influenced by the degree of anisotropy. Graham and Houlsby (1983) showed that by modelling clay with an anisotropic model, the estimation of strains was improved by 30-40% when compared to the measured values. For stress induced anisotropy, Lo and Lee (1990) showed that for granular materials, the value of *n* decreased as the ratio of vertical to horizontal stresses increased. These researchers showed that the stiffness of a material decreases as the angle between the orientation of the major principal

stress and a vector normal to the plane of anisotropy increases from 0° to 90° as shown in Figure 2.11. Duncan and Dunlop (1969) also found similar results for a silty marine clay and they proposed a modified $\sin^2$ function:

$$E_\theta = E_v - (E_v - E_h)\left(\sin^2 \theta + 0.2 \sin 2\theta\right) \tag{2.34}$$

to describe the reduction in the modulus as the deviation of the angle of the major principal stress changed from 0° to 90°. Desai and Christian (1977) calculated the variation in modulus values as the orientation of the major principal stress was rotated through 90° for a cross anisotropic material and came up with a different relationship:

$$E_\theta = E_v - (E_v - E_h)\left(\sin^2 \theta - 0.25 \sin 2\theta\right) \tag{2.35}$$

The differences between the different relationships are shown in Figure 2.12 and the theoretically correct relationship of Desai and Christian shows an almost constant value for the first 30° of rotation whereas the Duncan and Dunlop relationship has a more rapid reduction in modulus before reaching a constant value for the last 30° of rotation. Pavement researchers have attempted to measure the anisotropic properties of granular materials using the RLT, Allen and Thompson (1974a) concluded that the granular materials exhibited anisotropic behaviour in both CCP and VCP RLT tests as the measured value of Poisson's ratio exceeded 0.5, the upper bound for an isotropic material, and therefore the material response must be anisotropic. This may not necessarily be a correct assumption, as values of Poisson's ratio that are greater than 0.5 may also indicate that the material is dilating, which is a phenomena that granular materials exhibit when the grains slide past each other as the material is subjected to external forces.

Tutumluer and Thompson (1998) developed equations for horizontal, vertical and shear resilient moduli in the Uzan form and determined relationships between the various coefficients based on previously published RLT test results.

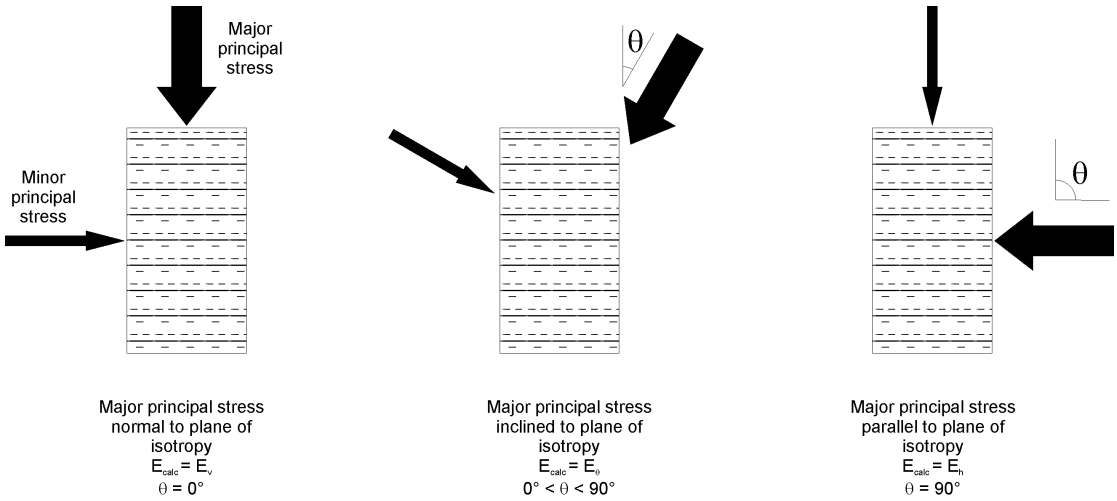

Figure 2.11 Rotation of principal stress direction relative to plane of transverse isotropy.

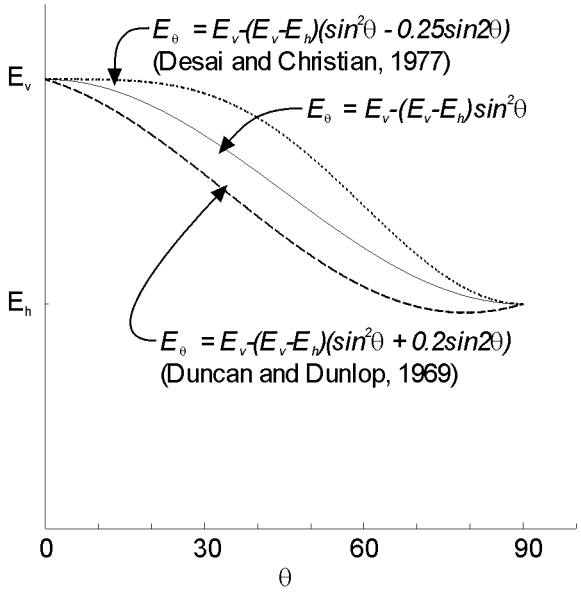

Figure 2.12 Reduction of modulus relative to the angle between the major principal stress and the direction normal to the plane of transverse isotropy.

$$M_r^H = k_1 p_a \left(\frac{\theta}{p_a}\right)^{k_2} \left(\frac{\sigma_d}{p_a}\right)^{k_3} \tag{2.36}$$

$$M_r^V = k_4 p_a \left(\frac{\theta}{p_a}\right)^{k_5} \left(\frac{\sigma_d}{p_a}\right)^{k_6} \tag{2.37}$$

$$G_r = k_7 p_a \left(\frac{\theta}{p_a}\right)^{k_8} \left(\frac{\sigma_d}{p_a}\right)^{k_9} \tag{2.38}$$

where

$$\begin{aligned} M_r^H &= \text{Horizontal Resilient Modulus} \\ &= \frac{\sigma_3}{\varepsilon_3} \\ M_r^V &= \text{Vertical Resilient Modulus} \\ G_r &= \text{Resilient Shear Modulus} \\ &= \frac{\sigma_\text{d}}{2(\varepsilon_1 - \varepsilon_3)} \\ k_{1\text{-}9} &= \text{constants} \end{aligned}$$

The definition of horizontal resilient modulus as given in Equation (2.36) does not appear to be consistent with the definition of resilient modulus elsewhere, which is: the ratio of the major cyclic stress to the recoverable strain, where the stress and strain are measured on the same axis. This definition as presented by the authors does not consider the change in the radial stress; instead, it uses the absolute value. The relationships between the various constants were formulated to give modular ratios between the horizontal and vertical moduli and the shear and vertical moduli (Tutumluer and Thompson 1998). They also made assumptions about the values for the difference between the k_8 and k_5, and k_2 and k_5 terms (2.5 and 0.2 respectively). This makes all three definitions of modulus interrelated as they derive nine constants from a test where only two parameters are varied and only two material responses are measured.

$$k_7(psi) = -90.92 + 0.27\,k_4 + 305.34\,k_5 + 158.22\,k_6$$

$$\frac{k_7}{k_4} = 0.187 + 1.079\frac{k_1}{k_4}$$

$$k_8 - k_5 = k_6 - k_9$$

$$k_2 - k_5 = k_6 - k_3$$

Tutumluer and Thompson (1997) used the above equations in a finite element program and the *n* values for the granular material ranged from 0.09 near the load to 0.15 far away from the load. The *m* values for the granular material ranged from 0.29 near the load to 0.34 far away from the load. Tutumluer and Seyhan (1999) redefined the horizontal resilient modulus as

$$M_r^h = \frac{\sigma_{3d}(1-\upsilon)}{\varepsilon_r} \tag{2.39}$$

where

$$\sigma_{3d} = \text{cyclic radial stress}$$

Their definition was based on the analysis of an elastic cylinder subjected to a radial stress and as such, there is a dependence on the Poisson's ratio. They also present results from RLT tests where only the axial or radial stress was cycled and determined values of *n* in the range of 0.4 to 0.7 for a range of granular materials. Tutumluer and Seyhan (2000) used the UI-FastCell to determine the degree of anisotropy and reported a *n* value of 0.7 for a granular material with 2% fines over a range of stress conditions. Adu-Osei et. al. (2000) used the UI-FastCell to calculate the anisotropic properties of granular materials. He used the assumption that response was linear if the change in the stress state was small (less than 10% of bulk stress). By varying the axial and/or radial stresses, the state of triaxial compression, extension or shear could be simulated and the anisotropic properties could be determined. He calculated average *n* and *m* values of approximately 0.50 and 0.33 respectively. Zamhari (1998) measured the anisotropic properties of granular materials in a true cubical tri-axial cell and reported *n* values of between 0.57 and 1.0. Karasahin and Dawson (2000) measured the anisotropy of a sand and gravel mix under cyclic isotropic consolidation and determined a range of *n* values

from 0.1 at a low cyclic cell pressure (50 kPa) to 0.7 at high cyclic cell pressure (225 kPa). They also found that the anisotropy increases with an increasing number of load cycles, possibly as the material undergoes plastic straining and the particles are reoriented during consolidation. Hornych et. al. (1998) modified the Boyce model to include anisotropy but gave no indication as to the origin of the anisotropic factor. He appeared to use an *n* value of 0.85.

Emeriault and Chang (1997) used a micro mechanical approach to determine the degree of anisotropy of glass beads and sands and they calculated *n* values of between 1.0 for low principal stress ratios (σ_{major} / σ_{minor}) and 0.7 for a principal stress ratio of 3. Masad et. al. (2004) developed a micro mechanical model that accounted for the different properties of the particles (shape, packing, gradation etc) to successfully model the anisotropic behaviour of different granular materials that were tested by Adu-Osei (2000).

The APDG recommends that the granular and subgrade materials are modelled as cross-anisotropic with a *n* value of 0.5 (AUSTROADS 1992). The use of n=0.5 can be traced back to the following statement

> *This anisotropy is regarded as a device to compensate for the absence of a lateral stress dependent mechanism for elastic modulus (Potter and Donald 1985).*

Based on the research summarised above, the assumed valued for *n* was not a bad estimate for the granular material.

In summary, the majority of the published data on the degree of anisotropy would suggest that the value of *n* is relatively constant for granular materials that have been recompacted and could be assumed equal to 0.5. The value of *n* for cohesive materials could be set to equal 2 in the absence of any specific information.

2.8 Poisson's Ratio

It is assumed that the value of Poisson's ratio is relatively constant. Allen and Thompson (1974a) conducted a series of RLT tests using constant and variable confining pressures with axial and radial strain measurements. They developed a

third order polynomial equation for Poisson's ratio based on the ratio of axial and radial stresses.

$$\upsilon_r = b_0 + b_1\left(\frac{\sigma_1}{\sigma_3}\right) + b_2\left(\frac{\sigma_1}{\sigma_3}\right)^2 + b_3\left(\frac{\sigma_1}{\sigma_3}\right)^3 \tag{2.40}$$

where

υ_r = resilient Poisson's ratio
b_{0-3} = constants

Their calculations showed that the Poisson's ratio exceeded 0.5 for the CCP tests, which indicates an increase in volume, but the Poisson's ratio calculated from VCP tests were in the range of 0.35 to 0.40 for stress ratios that varied from 2 to 7. Similar values of Poisson's ratio were found for three different granular materials. They concluded that the stress conditions in a CCP specimen were non-uniform and lead to overstated values of Poisson's ratio, assuming that the material behaves as an isotropic solid. Uzan (1992) presented an alternative method for calculating Poisson's ratio based on the work done along a closed cycle. This relationship is somewhat complex; the required coefficients are linked to the coefficients in the Uzan Model and it requires the computation of the incomplete Beta Bessel function each time the determination of the resilient modulus and Poisson's ratio is required. The relationship calculated Poisson's ratios of up to 0.7, indicating dilation of the material. This response is permitted because while the material is regarded as isotropic, it was modelled as a non-linear material and the strain energy was conserved. The contribution of the material anisotropy to the measured dilation is not considered; instead, the dilation is wholly attributed to the Poisson's ratio.

Pickering (1970) assumed that $\upsilon_{11} = \upsilon_{12}$. Bellotti et. al. (1996) measured the in-plane Poisson's ratio, υ_{11}, using seismic wave methods in a sand tank and found that $\upsilon_{11} \approx \upsilon_{21}$ for values of υ_{21} in the range of 0.07-0.19. Jiang et. al. (1997) stated that it is not possible to measure υ_{11} in a triaxial cell since the 2 planar stress values are the same. Kohata et. al. (1997) found that any calculation errors would be small if it was assumed that $\upsilon_{11} = \upsilon_{21}$ since υ_{21} was much less than unity. Zamhari (1998) used a cubical cell to measure the elastic parameters and found that $\upsilon_{11} \approx$

$0.8\upsilon_{21}$. Adu-Osei (2000) determined values of Poisson's ratio from RLT tests using compressive and tensile stress states and found that the inferred value of υ_{11} was twice the measured value of υ_{12} (0.40 vs. 0.20). The findings presented by the above researchers show that if consideration is given to the true loading mechanism, the axisymmetric loading conditions present in the RLT test cannot determine υ_{11} and based on the research presented here, the best estimate for υ_{11} is that $\upsilon_{11} = \upsilon_{21} = n$ x υ_{12} (Equation (2.32)).

2.9 Initial Stresses

The solutions proposed by Boussinesq and Burmister make no allowance for existing stress conditions in the pavement structure; the solutions provided by these equations are only in terms of the applied load. The constitutive equations described earlier are expressed as functions of the total stress state, that is, the existing hydrostatic stress applied as the confining stress plus the deviatoric stress. In order for the correct stresses to be passed to the constitutive models, the initial stress state needs to be added to the applied stress state. The initial vertical stress is the overburden stress caused by the weight of the material above the point of interest

$$\sigma_{v_0} = h\gamma g \tag{2.41}$$

where

σ_{v_0} = vertical overburden stress
h = depth below the surface
γ = unit mass of overlying material
g = acceleration due to gravity

The initial horizontal stress can be calculated from

$$\sigma_{h_0} = K_0\sigma_{v_0} \tag{2.42}$$

where

σ_{h_0} = horizontal stress due to overburden

K_0 = coefficient of earth pressure at rest

For an elastic medium

$$K_0 = \frac{\upsilon}{1-\upsilon} \tag{2.43}$$

Materials in soil deposits can be described as either normally consolidated or overconsolidated. A normally consolidated soil has only been subjected to stresses due to current overburden. Overconsolidated soils have been subjected to stresses in excess of the current overburden, either through the removal of some overburden or the use of compaction equipment. The Over Consolidation Ratio (OCR) is the ratio of the maximum stress to the current stress. For a normally consolidated clay or sand (from Barnes (1995),Table 4.1 p79)

$$K_0 = 1 - \sin\phi \tag{2.44}$$

For clay or sand materials that are overconsolidated

$$K_0 = (1 - \sin\phi) OCR^{\sin\phi} \tag{2.45}$$

A theoretical value of K_0 would be 0.35 for a granular material with a friction angle of 40°. Pearson-Kirk (1976) reported measured K_0 values of 3 for sands compacted behind a scaled down retaining wall. Duncan and Seed (1986a; 1986b) describe a technique for estimating the compaction induced lateral stresses behind retaining walls and the application of the technique to several case studies where good agreement with measured values are obtained. Their technique uses the concept of the OCR approach described earlier, but resulting in a constant value of lateral pressure regardless of depth. The measured lateral stress was approximately 15 kPa for a granular material, resulting in a K_0 value of 3 near (300 mm) the surface and reducing with depth. Stewart et. al. (1985) measured lateral stresses of up to 35 kPa in railway ballast, resulting in an apparent K_0 value of approximately 9. Selig (1987) reported the results of a two layer (sand/clay) laboratory test where the horizontal stresses were measured at the bottom of the top layer. The measured

stresses stabilized after a small number of load cycles to around 10 kPa, giving an apparent K_0 value of 2.

In summary of the above results, the initial stresses due to the overburden and compaction could be determined using Equations (2.41) and (2.42), where the value of K_0 can be assumed to be 3 for granular pavement layers, based on the published data.

2.10 Permanent Deformation Models

As with models for the prediction of resilient response, there are a large number of models that have been proposed to model the Permanent Deformation (PD) of granular materials. These models appear to be either based on: observed performance and are expressed as function of the number of load applications/cycles and/or the applied stress state or constructed from the established theory of continuum mechanics. Lekarp et. al. (2000b) presents a state of the art summary in which he listed 15 different models for determining PD. The PD for a pavement is determined from the sum of the PD for each layer within the pavement structure, so for a thin surfaced granular pavement at least two PD models are required, one for the subgrade material and the balance for the granular material/s.

2.10.1 Permanent Deformation as a Function of the Number of Load Applications

Barksdale (1972) proposed that the PD of granular material was best modelled as a log-normal function;

$$\varepsilon_p = a + b\log(N) \tag{2.46}$$

however the constants a and b were unique for different RLT test conditions. Sweere (1990) suggested that a log-log approach gave a better fit;

$$\varepsilon_p = aN^b \tag{2.47}$$

Both Barksdale and Sweere based their models on the results of large number of RLT tests. Wolff and Visser (1994) studied the results of Heavy Vehicle Simulator (HVS) tests and found that after a large number of load applications, the rate of increase in PD of the pavement became linear. They proposed that the development of PD was a linear function, with the addition of an exponential decay function to model the rapid changes of PD in the early stages of the test;

$$\varepsilon_p = (cN + a)(1 - e^{-bN}) \tag{2.48}$$

Theyse (1997) used this model along with a large collection of MDD data from the South African HVS program to determine the values of the coefficients as functions of the backcalculated stress invariants and material types. This information was then incorporated into the South African Mechanistic Design Method.

Kenis (1977) proposed a PD model as part of the VESYS Computer System model that calculated the PD for each load application as a function of resilient response and a fraction of the accumulated number of load applications to date.

$$R_p(N_j) = R_\delta(\tfrac{d}{2}) \cdot \mu_{sys} \left(N_j\right)^{-\alpha_{sys}} \tag{2.49}$$

where

$R_p(N_j)$ = Permanent deformation for a single load application after N_j load applications

$R_\delta(\frac{d}{2})$ = Total deformation response for a single load application

$\mu_{sys} = \frac{IS}{e}$

$\alpha_{sys} = 1 - S$

I = Intercept of line of best fit on a log - log plot of permanent strain vs load applications

S = Slope of line of best fit on a log - log plot of permanent strain vs load applications

e = Strain amplitude of permanent strain RLT test at the 200^{th} load application

It was assumed that whilst the incremental permanent deformation attributable to a particular load application, ($R_p(N_j)$), would decrease as the total number of load applications (N_j) increased, the total deformation ($R_\delta(d/2)$) response would remain constant over the total number of load applications. The *I*, *S* and *e* parameters are determined from a single RLT test at a stress state that is determined by the user.

Paute et. al. (1996) proposed the following model to calculate the amount of PD occurring after the first 100 load cycles:

$$\varepsilon_p^* = A\left[1 - \left(\frac{N}{100}\right)^{-B}\right] \tag{2.50}$$

where

ε_p^* = PD occuring after the first 100 load applications

$$A = \frac{\frac{q}{\left(p + p^*\right)}}{b\left(m - \frac{q}{\left(p + p^*\right)}\right)}$$

p^* = value of the intersection of the static failure line and the p axis in p - q space

m = slope of the static failure line

B, b = constants derived from PD RLT tests

The form of this model suggests that the PD will asymptotically approach the value A as N becomes large. Ignoring the PD occurring in the first 100 load cycles is a sensible approach, as this will ignore the effect of any seating/bedding-in PD that occurs. Lekarp and Dawson (1998) used Equation (2.50) to model the results of 17 PD RLT tests and found that while it provided a good fit for 12 of the tests, the remaining tests did not show a stabilisation of the PD accumulation, even after 80,000 load cycles. Also, the *A* constant showed a high degree of scatter for the same material tested at a range of stress states. To counter lack of complete agreement with Equation (2.50), Lekarp and Dawson proposed a single relationship for each material that determined the PD at a specified number of load cycles (say 20,000) as a function of the length of the stress path and the maximum stress ratio:

$$\frac{\varepsilon_p\left(N_{ref}\right)}{\frac{L}{p_0}} = a \cdot \left(\frac{q}{p}\right)_{\max}^{b} \tag{2.51}$$

where

$\varepsilon_p(N_{ref})$ = accumulated PD at N_{ref} load cycles, where $N_{ref} > 100$

L = length of stress path

p_0 = reference stress

$\left(\frac{q}{p}\right)_{\max}$ = maximum stress ratio achieved for the test series

a, b = constants

2.10.2 Hyperbolic Model

Duncan and Chang (1970) proposed a hyperbolic model for predicting plastic strains from monotonic triaxial shear tests as a function of confining and deviator stresses, cohesion, the angle of internal friction and a ratio of compressive strength to an asymptotic stress difference.

$$\varepsilon_a = \frac{(\sigma_1 - \sigma_3)}{K\sigma_3^n} \cdot \frac{1}{1 - \left[\frac{R_f(\sigma_1 - \sigma_3)(1 - \sin\phi)}{2(C\cos\phi + \sigma_3 \sin\phi)}\right]} \tag{2.52}$$

where

ε_a = plastic axial strain

C = cohesion

ϕ = angle of internal friction

R_f = a constant relating compressive strength at failure to the asymptotic value of ultimate compressive strength $(\sigma_1 - \sigma_3)$

K, n = constants

Barksdale (1972) modified this model for use with resilient loading conditions and developed a set of parameters from triaxial test results for a number of materials. Barksdale determined the parameters for the plastic axial strain after 100,000 load cycles. The agreement between the predicted and measured values for a range of stress conditions was quite good and is shown in Figure 2.13.

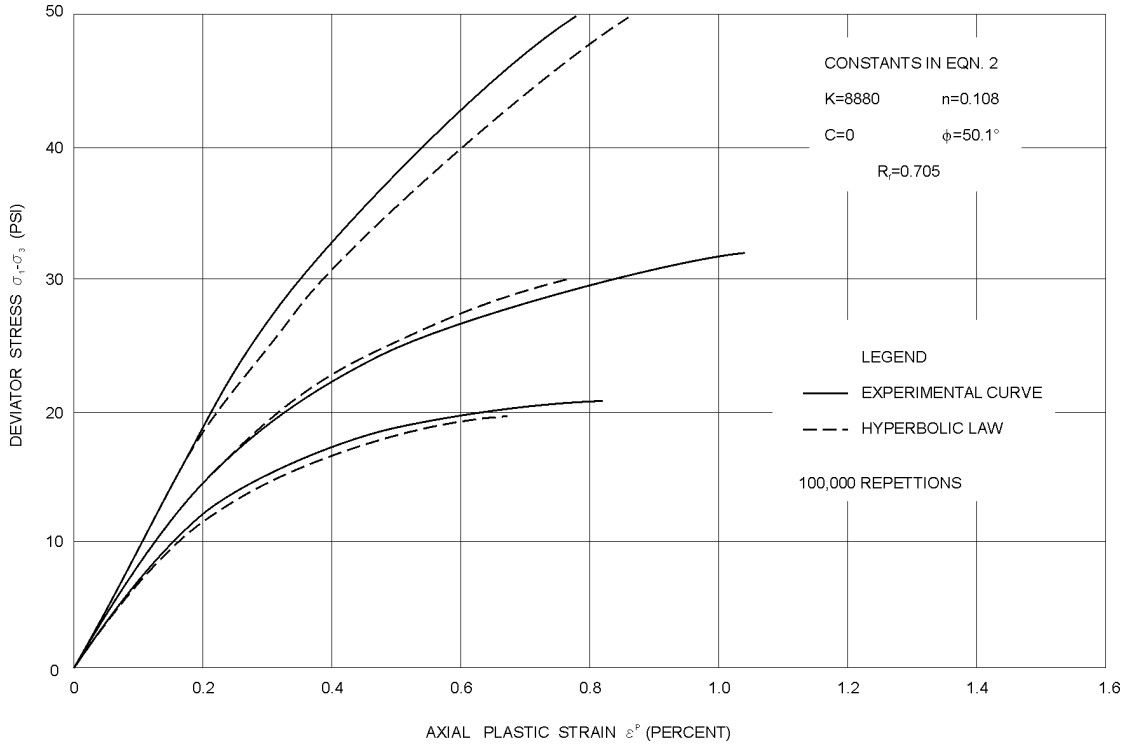

Figure 2.13 Comparison of calculated hyperbolic plastic stress-strain with experimental curves (Barksdale 1972).

2.10.3 Yield Models

Yield or elastoplastic models have two parts, an elastic phase and a plastic or yield phase. The material response is elastic up to a failure stress and if the stress continues to increase, the material yields or undergoes plastic (permanent) straining. Well-known geotechnical models of this type are the Cam-Clay (Schofield and Wroth 1968) and Drucker-Prager (Drucker and Prager 1952) models. In these models the elastic response is linear and isotropic. A limitation of these models is that they were developed from monotonic loading cases and as such, they may not realistically model the lower load levels of fast cyclic loading that a pavement experiences. Desai et. al. (1986) presented a HIerarchical Single Surface (HISS) framework for yield models that allow increasing complex features to be added to them such as anisotropic elastic behaviour, non-associative flow, strain softening and pore water pressures. Desai et. al. used functions that could be described from relatively common laboratory tests. Bonaquist and Witczak (1997) used Desai's hierarchical model with the Drucker-Prager failure surface, a non-linear elastic model and added a simplified component to allow for cyclic loading

which accounted for the previous loading and the current stress state. This was considered necessary as pavements undergo continual deformation for a constant, but repeated stress state. Classical plastic flow theory, which is based on monotonic loading, would show that the pavement would have plastic flow for the first load application and then subsequent load applications at the same load level would be within the elastic state of the model. Bonaquist and Witczak used layered elastic theory and their plastic flow model to estimate the deformation of a hypothetical pavement. Uzan (1999) compared the HISS model with one proposed by Vermeer (1982). The Vermeer model is an elastoplastic model that consists of two separate strain-hardening mechanisms, one for volumetric and the other for shear states. This model was developed for granular materials with zero cohesion and only requires four parameters that are based around the Mohr-Coulomb failure law. The HISS model was modified to include a non-linear elastic model and required eight parameters, of which not all were easily obtained. Uzan concluded that both models were of equal rank, as the HISS model was more accurate in predicting the first cycle plastic straining, but it was easier to find the parameters for the Vermeer model.

2.10.4 Mechano-Lattice Analysis

The Mechano-Lattice (ML) method of analysis (Yandell 1971), determines the elastic and plastic response of the system as a wheel rolls across the surface of the model. The pavement structure is modelled as a series of springs in a lattice framework. The observation from repeat load triaxial testing that materials have a higher secant modulus on unloading than loading is used to develop the plastic strains within the structure. Yandell (1971; 1982b; 1982a; 1983), Lim and Yandell (1997) and Yandell and Behzadi (1988) report the analysis of ALF trials from Australia and pavements design using the Shell Pavement Design method (Shell International Petroleum Company Ltd. 1978) using the ML framework. The plastic strains predicted by the ML method are comparable to the measured plastic strains/ruts. The ML method of analysis appears to have not been adopted by other researchers.

2.10.5 Theory of Shakedown

The theory of shakedown proposes that in the early life of a continuum subjected to repeated loading, the response has elastic and plastic components and after a certain number of load applications the plastic component reduces to zero and the response is purely elastic. At this point the continuum is said to have undergone "shakedown" (Werkmeister 2004). Werkmeister called this type of response Range A, she also described the behaviour where a small amount of plastic deformation occurs with each load application, but the accumulation of the plastic strain is not significant until after millions of load applications, this type of response is called Range B. A third type of response, Range C, is where large plastic strains occur with each load application and failure is rapid. The concept of the various response mechanisms is shown in Figure 2.14. For a pavement to perform satisfactorily, either Range A or B behaviour is desired. An applied load, which results in a stress state in the pavement that defines the boundary between Range A and B behaviour, is called the critical shakedown stress. Sharp and Booker (1984) used the Mohr-Coulomb theory in a linear programming framework to determine the level of load that could be applied to the pavement which would result in only Range A behaviour. Collins and Boulbibane (2000) used the classic wedge failure approach to determine the critical shakedown stress.

Werkmeister (2004) and Arnold (2004) used permanent deformation RLT tests to categorise the plastic response of different granular materials into Range A/B/C behaviour depending on the RLT stress state. In addition, Werkmeister and Arnold both used resilient non-linear FEM models to determine the stress state in various pavement structures, in order to predict the long-term behaviour of the pavement based on the RLT results.

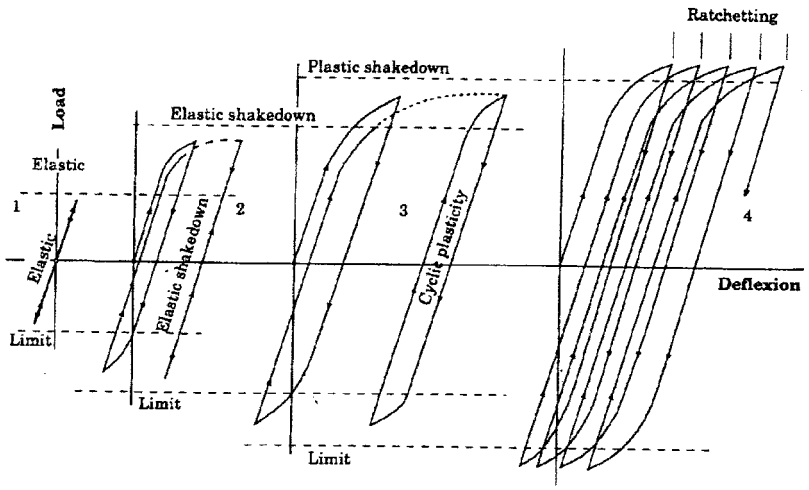

Figure 2.14 Four Types of Response of Elastic/Plastic Structure to Repeated Loading Cycles (Collins and Boulbibane 2000).

2.11 Tyre Contact Pressures

The Austroads Pavement Design Guide recommends that the contact stress used for modelling should be set to the cold inflation pressure of the tyre, which is currently 750 kPa. de Beer et. al. (1997) developed a tyre contact stress measuring system and reported that the distribution of stress under a tyre was not uniform and that vertical stress was greatest at the edges of the tyre, up to 2 times the nominal inflation pressure. However for a typical radial tyre (315/80 R22.5) operating at normal inflation pressure and tyre load (750 kPa / 20 kN) the distribution was relatively uniform. Variations in the applied stress at the pavement surface will become insignificant below a certain distance in the pavement structure; they are only a significant issue for the design and performance of the surfacing layer/material.

2.12 Backcalculation

The process of backcalculation involves the determination of the stiffness of the various layers of a pavement structure in order for the computed pavement response to a known loading condition to match the measured pavement response. One such loading mechanism is the Falling Weight Deflectometer device and the measured pavement response is the transient surface deflection. Lytton (1989) presented a

state of the art on nondestructive testing and the backcalculation of pavement layer properties. Uzan (1994) states that when using a non-linear material model, only the scalar coefficient of the model, typically the k_1 coefficient should be allowed to vary during the backcalculation process in order to provide the optimum solution. The remaining material coefficients either should be obtained from laboratory results or published material databases. Uzan also recommends the use of a static load, non-linear material method when there is either no bedrock within 6 metres of the surface or stress dependent materials are present. Linear elastic methods are suitable where there are stiff and thick AC layers. A potential problem when using static elastic methods for modelling the response of the pavement to loading by a FWD is that due to the dynamic nature of the loading, the load pulse takes a finite amount of time to reach the outer sensors. The FWD records the maximum deflection of each sensor without regard to the time of arrival of the peak value. The FWD equipment have the capability to record full time histories of the load and deflection traces, but this is not routinely done due to the increased data storage requirements. Figure 2.15 shows how the time histories are combined to create a static surface deflection bowl.

de Almeida et. al. (1994) developed a back calculation program that used layered elastic analysis and a non-linear modulus model (LEAD). This model used stresses calculated at radial offsets corresponding to the locations of the geophones to determine the material stiffness at the same offsets. These stiffness values were altered in order to match the measured and computed surface deflections. The resulting pavement response profile was a composite of several models but overcame the problem of constant modulus values in the horizontal direction. The outputs from LEAD compared favourably with those from a non-linear finite element program (FEAD). de Beer et. al. (1989) used Multidepth Deflectometers (MDD) to determine the moduli of various pavement layers in a thin surfaced granular pavement subjected to loading by the South African Heavy Vehicle Simulators (HVS). He used a layered elastic program (ELSYM5) and manually changed the layer moduli until a good match between the predicted and measured deflections at various depths was obtained. de Beer et. al. (1989) also reported a study where the computed moduli from MDD measurements were compared with

laboratory derived moduli and found that for the same stress conditions, the laboratory moduli were two to three times greater than the field values.

Scullion et. al. (1989) used MDD devices to measure the response of an unbound granular pavement surfaced with 125 mm of asphalt concrete under various FWD loads. The field moduli were calculated from the MDD readings and three backcalculation computer programs using the surface deflections measured by the FWD. The MDD moduli decreased with depth while the surface deflection moduli showed some scatter as the depth increased. These two studies show that moduli from both laboratory measurements and computer backcalculation programs can be different from values that are derived from subsurface measurements and that care should to be taken when interpreting the results from these measurement and analysis methods.

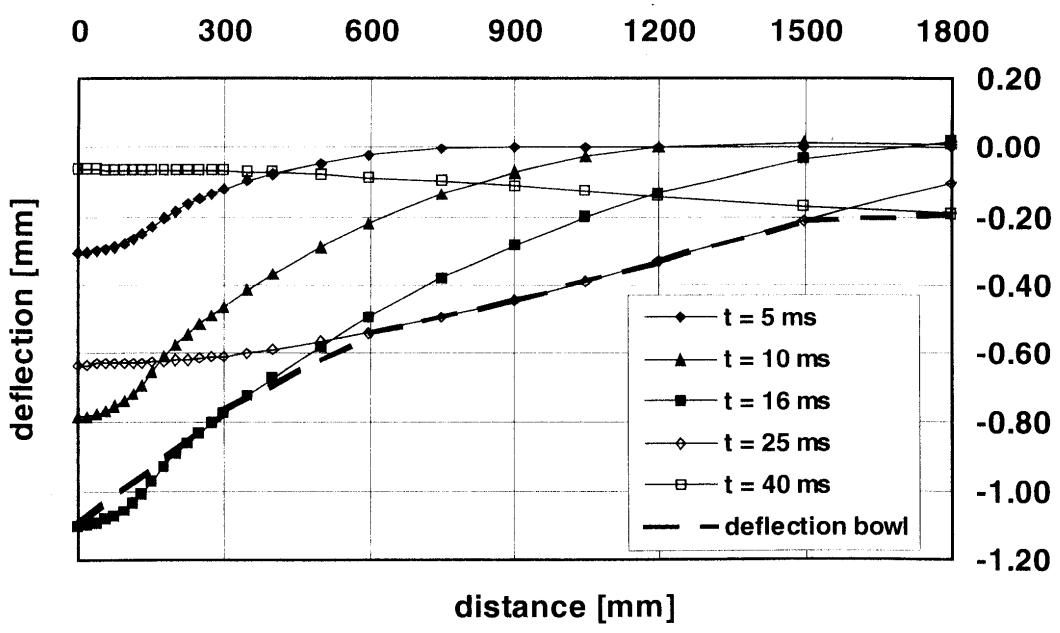

Figure 2.15 Time snapshot of surface deflection and the deflection bowl (Al-Khoury 2002).

2.13 Field Measurements

In order to measure the accuracy of the modelling process, it is preferable to get different types of pavement responses to an applied load. There are two sources of field data; full-scale Accelerated Pavement Test (APT) facilities and instrumented in-service roads. A comprehensive list of APT facilities and their capabilities can be found in Metcalf (1996) and Hugo and Epps-Martin (2004). APT facilities that have published test results that pertain to thin surfaced unbound granular pavements are the Canterbury Accelerated Pavement Testing Indoor Facility (CAPTIF), located in Christchurch, New Zealand, the Accelerated Loading Facility (ALF), located in Melbourne, Australia and the Heavy Vehicle Simulator (HVS), located in South Africa. Of these three facilities, the ALF program does not use any subsurface instrumentation, the HVS and CAPTIF programs includes extensive subsurface instrumentation to measure pavement response: the CAPTIF program uses inductive soil strain and pressure cells (described in detail in Chapter 3) and the HVS program has been mainly limited to measurements taken with the MDD device.

Akou et. al. (1999) present the results from a LCPC study of an asphalt concrete (85 mm thick) and granular (430 mm thick) pavement. The measured resilient strains were compared with those predicted with a non-linear (isotropic Boyce) FEM model (CESAR-LCPC). The computed vertical strains at the top of the granular layer and subgrade layers were 70 and 155% of the measured values.

Akram et. al. (1994) presented the results of a study looking at the MDD response of a thin surfaced (37.5 mm asphalt concrete) granular pavement (250 mm) that was loaded by a FWD and a truck. They reported a good match between measured subgrade strains induced by truck loading and those computed by a layered linear elastic program (BISAR). The moduli used in the BISAR analysis were determined from the subsurface MDD measurements under FWD loading. If only the surface deflections were used in the back-calculation process, the predicted strains were 18% less than the measured strains.

Hildebrand (2002) measured the response of an asphalt concrete pavement subjected to loading by a FWD. The pavement structure was (top to bottom): 60

mm asphalt concrete, 128 mm granular layer, 414 mm sand layer and a natural sand subgrade. Pressure cells and LVDT strain instruments were installed 50 mm above the subgrade layer and their response to various load levels and offset positions was measured. The pavement response was modelled with a number of programs/techniques, namely a Boussinesq half space, layered elastic theory, MET and 3D-FEM. The best results were obtained when non-linear material models were used. The vertical strain measurements were within 20% of the model predictions while significant differences were found for the stress measurements.

Dawson and Little (1997) used the recently developed strain (ε) Measuring Unit (εmu) soil strain system to measure the vertical strains in an unsurfaced granular pavement (350-550 mm thick) built on top of a soft clay. The transient strains in the top of the subgrade were high, ranging from 0.3 to 1.5% and likewise for the granular material (0.2-0.7%). The pavement was only subjected to 2015 vehicle passes during the experiment.

Theyse (1997) presented a large amount of MDD and PD data from the South African HVS program, however the test pavements all contained thick asphalt concrete layers (> 60 mm) and/or cemented layers.

In the AUSTROADS PDG, the criteria for pavement rutting, Equation (2.1) uses the vertical compressive strain at the top of the subgrade as the critical response, which implies rutting will only occur in the subgrade. Results from various field and accelerated test pavements have reported that a significant percentage of the deformation can be attributed to the granular layers (Pidwerbesky 1996; de Pont et al. 1999; de Pont et al. 2001; Korkiala-Tanttu et al. 2003).

2.14 Finite Element Modelling

The FEM was developed in the 1960's and the first attempt to utilize the FEM for the analysis of pavements was by Waterhouse (1967) when he outlined a method to use the FEM to calculate the linear elastic pavement response at all points in the pavement structure rather than at the centre line of an axi-symmetric analysis. Duncan et. al. (1968) used the method to model a three layer (Asphalt concrete, unbound granular layer and subgrade) pavement structure in 1967. They used an

axi-symmetric formulation and modelled the stiffness of the granular material with the k-theta model and the subgrade with the bi-linear model. Raad and Figueroa (1980), Wolff (1982) Vuong (1986), Harichandran and Yeh (1988) also published results from axi-symmetric models incorporating materials that had a stress dependent stiffness. These models had asphalt concrete layers ranging from 25 to 250 mm thick and used the k-θ model for the granular material. Wolff (1982), Vuong (1986), Harichandran and Yeh (1988), Helwany et. al. (1998) compared their FEM results with linear elastic theory while Duncan et. al. (1968) and Raad and Figueroa (1980) compared the model results to measured surface deflection bowls. Zaghloul and White (1993) achieved a good match between measured and computed surface deflections for a pavement constructed with a 100 mm thick asphalt concrete layer over a 250 mm thick granular layer using the Drucker-Prager material model in a 3D ABAQUS model. White et. al. (1997) used the Drucker-Prager elasto-plastic model in a dynamic 3D ABAQUS to model an aircraft wheel for a pavement structure with a 50 mm thick asphalt surfacing overlying a 150 mm thick granular base. They achieved good agreement with MDD measurements and surface deflections. Tutumluer and Barksdale (1995) used an axisymmetric FEM program GT-PAVE with a cross-anisotropic Uzan resilient modulus model to model a pavement with an asphalt concrete layer 89 mm thick over a granular base 203 mm thick. The predicted strains and stresses in the subgrade and granular layers were in reasonable agreement with measured values.

2.14.1 Modelling of the Falling Weight Deflectometer Loading Plate

There are two options available to model the application of an FWD load to the surface of the model. The first option is to apply the load as a uniform pressure directly to the appropriate area and the second option is to apply the load through a representation or model of all or part of the FWD load plate system. The second approach has been adopted by Boddapati and Nazarian (1994) and Scarpas et. al. (1998). Boddapati and Nazarian modelled the FWD load as a uniform pressure acting on a composite plate with a diameter of 300 mm. The composite plate comprised of an aluminum plate 25 mm thick, a PolyVinyl Chloride (PVC) plate 25 mm thick and a rubber pad 6 mm thick. The elastic stiffness and Poisson's ratio for the three materials were 70 GPa, 0.3, 7 GPa, 0.3, and 35 MPa, 0.49 respectively.

They concluded that for a flexible pavement, the most important factor was the stiffness of the rubber pad. Scarpas et. al. (1998) modelled the FWD load plate as a steel plate 19.2 mm thick, a PVC plate 22.4 mm thick and a rubber pad 6 mm thick. The elastic stiffness and Poisson's ratio for the three materials were 200 GPa, 0.2, 1 GPa, 0.3, and 5-1000 MPa, 0.49 respectively. The effect of a range of stiffness values for the rubber pad was studied and they concluded that the stiffness of the rubber pad had a negligible effect on the pavement response. The differing conclusions presented by the researchers show that this area requires further study. In addition, the use of a semi-rigid loading mechanism on a flexible pavement will result in higher stress values at the edge of the plate than the centre. The presence of the higher stresses at the edge of the plate may cause numerical instabilities in a FEM model as the stiffness of the plate increases.

2.15 Conclusions

This chapter reviewed some of the relevant literature and theory that is used to model the non-linear behaviour of thin surfaced granular pavements. Although the current pavement design process uses a mechanistic framework to determine the pavement response, the underlying assumptions are based on empirical relationships derived from years of experience. This makes the inclusion of new pavement structures or materials in the design process difficult without waiting a number of years to collect field data. Researchers have used a wide range of methods available to model the stress dependant stiffness of granular materials and pavement structures, both analytically and numerically. The number of different methods that have been presented over the last 40 years implies that the best and/or "correct" solution has yet to be found. As the complexity of the solution increases, the difficulty of obtaining the required input values increases and the "reality" or practicality of the solution decreases. There has been a very small number of published studies of field studies or tests that are both: (a) comparable to the types of pavements typically constructed in New Zealand and (b) have either stress and/or strain subsurface response measurements.

This page is intentionally left blank.

Chapter 3 Field and Laboratory Measurement Systems

3.1 Introduction

The field data used in this thesis was collected at the Canterbury Accelerated Pavement Testing Indoor Facility. This chapter describes the test facility, the loading apparatus, the different types of measurements collected, the research projects from which data was collected and the laboratory equipment and test methods used to characterise the materials used in the test pavements.

3.2 Canterbury Accelerated Pavement Testing Indoor Facility (CAPTIF)

Accelerated pavement testing has been carried out at the University of Canterbury since 1969 (Williman and Paterson 1971). In 1984 the first testing machine was replaced with the current machine (Pidwerbesky 1989). The Canterbury Accelerated Pavement Testing Indoor Facility (CAPTIF) is housed in a hexagon-shaped building that is 26 m wide and 6 m high. An annular concrete tank, 1.5 m deep and 4 m wide, confines the bottom and sides of the track (Figure 3.1), enhancing the control of moisture contents in the subsurface systems and drainage. The track has a median diameter and circumference of 18.5 m and 58.1 m respectively. The pavements were constructed using typical road construction techniques and equipment when ever possible, however the constraints of working indoors and in a short radius circular concrete tank meant that some variations from normal field practice where required. These variations mainly relate to the types of compaction equipment used; for example, plant with a small footprint but equivalent compactive effort to full size plant is used at CAPTIF. The small footprint allows vertical compaction without the loosening or screwing effect that a wide (2 m) drum roller would have on the surface when it is working on a continuous arc due to the differential velocity of the outside edges of the drums.

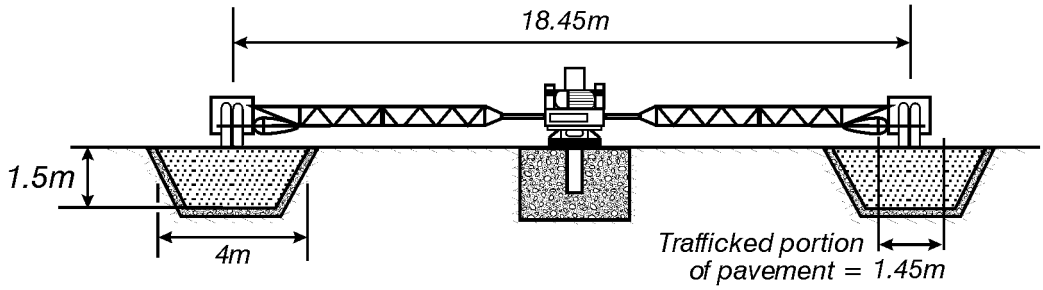

Figure 3.1 Elevation of SLAVE.

The main feature of CAPTIF is the Simulated Loading And Vehicle Emulator (SLAVE). In 1997 the facility underwent a major upgrade and the main features of the upgrade were: a Programmable Logic Controller (PLC) system was installed for controlling the rig; 2 tangential ramps were constructed to give access into the pavement tank; a new enlarged, elevated and sound insulated control room was built; extensions to the track enclosure constructed to allow safer access around the track while the machine is running or when the pavement tank is empty and improved storage and workshop facilities. A complete description of the facility can be found in Pidwerbesky (1995; 1996) and Steven et. al. (1999; 2001).

3.2.1 Simulated Loading And Vehicle Emulator (SLAVE)

SLAVE was designed for the accelerated testing and evaluation of subgrades, pavements and surfacings by replicating the effect on the pavement of actual road traffic conditions. Each vehicle consists of the axle, which is driven by a hydraulic motor, a suspension, a frame, instrumentation, and standard wheel hubs and truck tires (Figure 3.2). A sliding frame within the central platform is moved horizontally a maximum of 1 m (from stop to stop) by two hydraulic rams; this radial movement produces multiple wheel paths. The control system was designed so that the SLAVE could operate continuously without operator intervention, and if a sensor reported a level outside a preset limit, the control system would bring the SLAVE to a stop. The operational limits of the SLAVE are shown in Table 3.1.

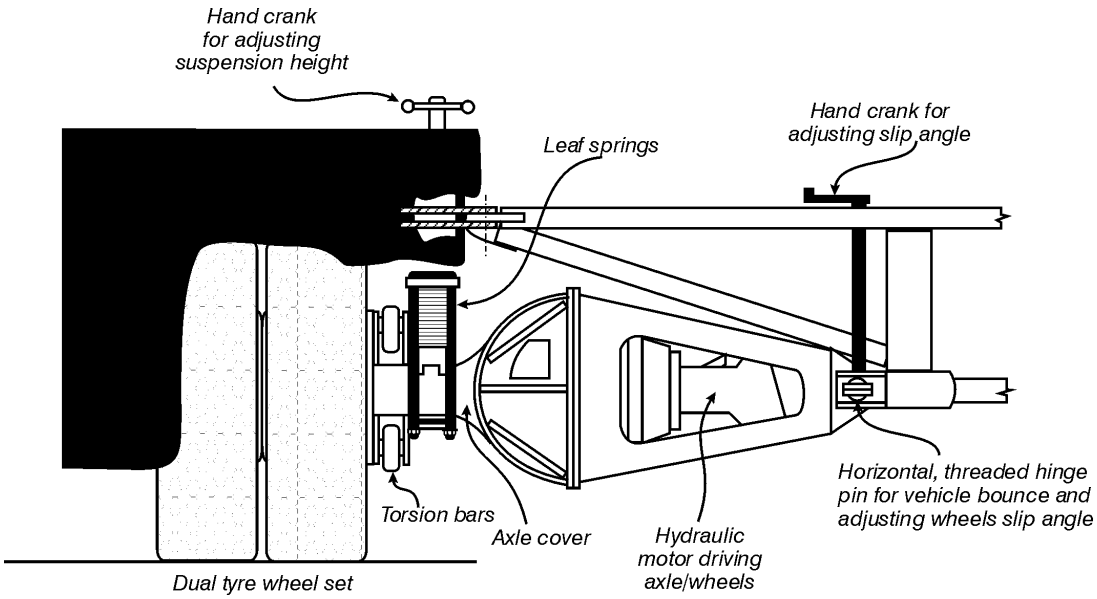

Figure 3.2 Detailed elevation of SLAVE.

3.2.2 Instrumentation and Data-acquisition

The instrumentation systems that are described below were used to collect data for this research work. No instrumentation was installed specifically for this research; instead the required information was extracted from the data collected for research programs that have been undertaken at CAPTIF. Descriptions of the research programs, pavement designs and loading histories are given below in Section 3.3.

Table 3.1 Characteristics of the Simulated Loading and Vehicle Emulator (SLAVE)

Item	Characteristic
Test Wheels	Dual- or single-tyres; standard or wide-base; bias or radial ply; tube or tubeless; maximum overall tyre diameter of 1.06 m
Mass of Each Vehicle	21 kN to 60 kN, in 2.75 kN increments
Suspension	Air bag; multi-leaf steel spring; single or double parabolic
Power drive to wheel	Controlled variable hydraulic power to axle; bi-directional
Transverse movement of wheels	1.0 m centre-to-centre; programmable for any distribution of wheel paths
Speed	0-50 km/h, programmable, accurate to 1 km/h
Radius of Travel	9.2 m

3.2.2.1 Dynamic Pavement Strain

Dynamic pavement strains in both the vertical and horizontal directions were measured using the εmu soil strain system (Dawson 1994). The soil strain measuring system determines minute strains (less than 100 μm/m) with good resolution (±50 μm/m) using Bison Coil type strain sensors. The sensors use the principle of inductance coupling between two free-floating, flat, circular wire-wound induction coils coated in epoxy, with a diameter of 50 mm. One of the two discs acts as the transmitter coil, creating an electro-magnetic field, which induces a signal in the receiving coil. The magnitude of the induced signal is inversely proportional to the spacing between the two coils. The εmu system determines the change in the induced signal as the coils move relative to each other and the variation or error function of the signal relative to the initial at-rest signal is available for measuring as a voltage. The initial or "at-rest" voltage is also available for measuring. The operation of the system is shown schematically in Figure 3.3. The gauge length or separation distance between each paired coil is a function of the initial voltage and the change or delta in the gauge length is a function of the varying voltage. Each coil pair is calibrated individually prior to installation and the coil pairs can be either orientated coaxially or co-planar. The coaxial arrangement gives a much stronger signal than the co-planar arrangement. The discs are installed during the formation of the subgrade and the overlying layers, to minimise the disturbance to the materials (Figure 3.4).

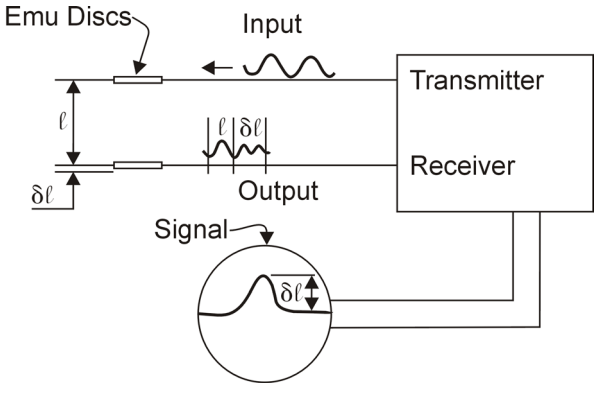

Figure 3.3 Schematic diagram of εmu system.

Figure 3.4 Installation of εmu coils.

Paterson (1972) and Janoo et. al. (1999) examined the effect of both axial misalignment and axial rotation of the coils relative to each other and they both concluded that as long as the rotation was less than 10° and the misalignment was less than 12 mm, the resultant effect on the static strain was less than 2%.The original Canterbury test track facility used a Bison Model 4101A Soil Strain Gauge (Paterson 1972). This was replaced in 1992 by an automated multi-channel system based on a modified prototype of the Saskatchewan Soil Strain/Displacement-measuring system (SSSD) developed by Saskatchewan (Canada) Highways and Transportation (Pidwerbesky 1996). In 2000 a new soil strain εmu system was purchased from the University of Nottingham to replace the SSSD system. The SSSD system was replaced because of reliability problems with the hardware and commercially manufactured coils could no longer be obtained. The new system still uses the same inductive coil principal as before, but the excitation, reading and decoding hardware is different. An unlimited number of coil pairs can now be read as each coil is connected to a multiplexor upstream of the εmu unit. The supply of coils is also guaranteed as CAPTIF personnel now manufacture them to a specification developed by the University of Nottingham. The multiplexing and

computer interface equipment are standard commercial parts and the controlling software is written using the National Instruments LabView computer program.

A typical CAPTIF installation of εmu coils for a project is up to four separate sites, with each site comprising of up to 36 coils arranged in a number of one and three-dimensional arrays. Each site comprises of a power supply, an εmu conditioning unit, a 36 channel multiplexor and an industrial computer running Microsoft WindowsXP containing a National Instruments PCI 6025E 16 channel, 12 bit Analog to Digital converter and 8 channels of digital input/output (used to control the multiplexor). This equipment is housed in a 19" rack cabinet located beside the pavement tank. For operational and safety reasons, the trackside computers are operated by remote control software (PC Anywhere) from within the control room. The use of the remote control software allows a single person to simultaneously control all four cabinets.

For a one-dimensional array, the coils are arranged in a coaxial stack with the coils spaced at 75 mm centres. This configuration is used to measure vertical strains. The three-dimensional array is an extension of the one-dimensional array, with two co-planar coils being energised from each coil in the central stack. A co-planar coil can be orientated to either measure longitudinal or transverse horizontal strains. This coil arrangement is shown in Figure 3.5. The repeatability of the SLAVE loading on the pavement over a number of laps and the high frequency of loading (one revolution every 4.5 s) was utilised to simplify the electronic systems used to monitor the εmu system. Only one coil pair is energised for each vehicle pass and the output from five vehicle passes is recorded to allow for missed triggers and other events that may influence the system. The 36 coils at each site are typically configured to produce 33 coil pairs, so each set of complete measurements will take 165 vehicle passes. The acquisition software stores the raw voltages in a tab-separated array in an ASCII text file. The project, temporal, spatial and collection parameters are also written to the same file to ensure that a complete record of the data is preserved.

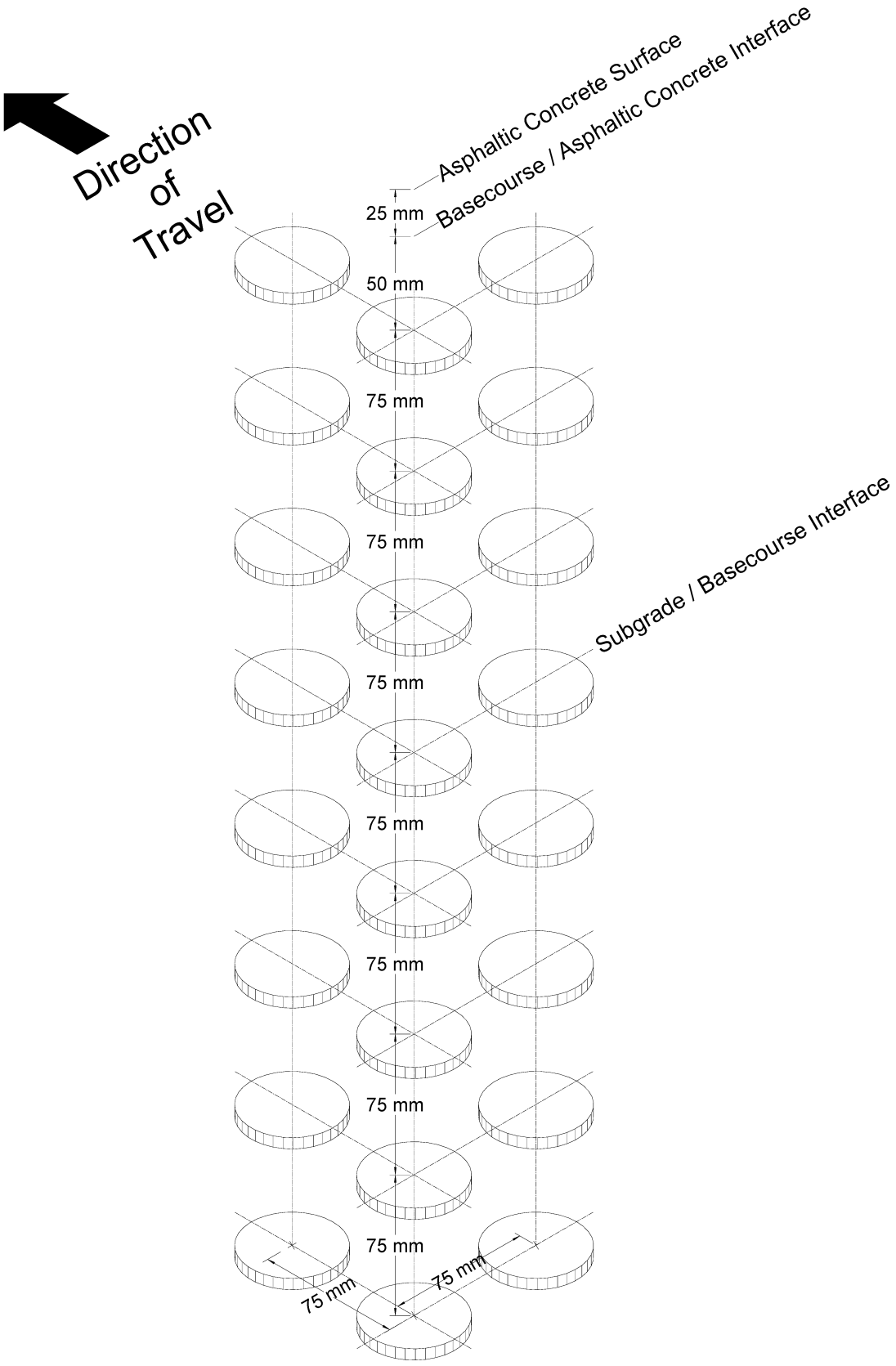

Figure 3.5 Typical CAPTIF installation of εmu coils.

Once the data has been collected, it is processed by software written in Microsoft Visual Basic for Applications (Excel). The following operations are performed on the data:

- The raw voltages are passed through a digital filter (4 pole Butterworth with a cut-off frequency of 40 Hz) to reduce the signal noise to an acceptable level.

- The filtered signal is converted to distances using the calibration factors stored in an Access database.

- The gauge length is calculated by averaging the first 100 readings and the dynamic strains are calculated. The maximum and minimum strain values are also calculated.

- All the raw voltage and calculated strain traces for each coil pair are displayed on the screen for the researcher to check/verify. At this point individual traces can be rejected.

- The surviving traces for each coil pair are averaged and the strain traces are resampled to a standard spacing of 25 mm regardless of vehicle speed.

Each trace is then written to an Access database. Each record contains the temporal and spatial data for the trace, maximum and minimum strain values for that trace, as well as the averaged maximum and minimum values for the coil pair, a flag to indicate whether that particular trace was accepted or rejected and up to 5700 mm of strain trace at a spacing of 25mm.

The resolution of the resampled trace is sufficiently good enough to enable the creation of figures suitable for publication.

3.2.2.2 Dynamic Pavement Stress

The dynamic pavement stress in the pavement was measured with Dynatest Soil Pressure Cells. These pressure cells are constructed as a hydraulic stress cell, which consists of two metal plates that are welded together around the boundary, and the internal cavity is filled with a thin layer of liquid. Changes in the applied

pressure result in a variation in the fluid pressure and this is measured by a four-way rosette foil strain gauge bonded to the lower diaphragm. Details of the stress cell are shown in Figure 3.6. The cell body is manufactured from titanium, which has a material stiffness of 68 GPa. The strain gauges are configured as a full Wheatstone bridge. The use of a full bridge inside the cells provides automatic temperature compensation. An excitation voltage of 12 V is used to energise the cell.

The applied stress is calculated according to the following formula:

$$\sigma = \frac{V_{out}}{U_{bridge} \times A \times C} \tag{3.1}$$

where

σ = stress (kPa)
V_{out} = measured voltage (mV)
U_{bridge} = bridge excitation voltage (12 V)
A = Amplification factor (1000)
C = Calibration factor (approx 200 x 10^{-5} mV/V/kPa)

The cells come in two ranges, 20–200 kPa and 100-800 kPa. Nine cells were purchased, three high range cells suitable for use in the basecourse and six low range cells suitable for use in the subgrade or for measuring horizontal stresses. The factory supplied calibration factors were used for this research.

The data was processed in a similar manner to the εmu data, except that the filter was a 25-point rolling window. The low level of noise in the raw data justified the use of a simple filter.

Brown (1977) summarised research considering aspects of cell design such as temperature, aspect ratio, cell stiffness, diaphragm thickness and the effect of tangential or lateral stresses on cell responses and concluded that for short term dynamic measurements, temperature effects are not likely to be significant and the presence of lateral stresses is likely to effect the cell registration (ratio of measured to free field stress).

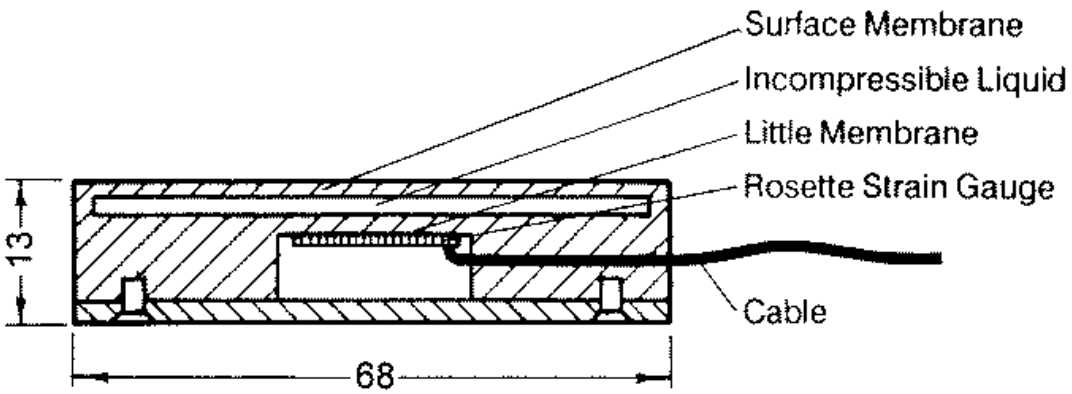

Figure 3.6 Dynatest Soil Pressure Cell (dimensions are in mm).

Ullidtz and Busch (1979) installed a number of the Dynatest pressure cells in the Danish Road Testing Machine (RTM) at differing depths in the pavement and reported difficulty in correlating the stress field integrated over a horizontal plane through the cell and the load applied to the pavement surface with a FWD. They put the error down to problems with the installation method, although the research reported by Brown (1977) suggests that the error may be due to the use of cell responses when the applied load is not directly normal to the cell diaphragm. Selig et al. (1997) reported the results of a comparison between Dynatest and Kulite pressure cells and found that while the Dynatest cells have low hysteresis and a linear response to load, the no-load cell output drifts both over time and with ambient temperature changes (-1 kPa/°C). Selig et al. also reported measurements where the cells were embedded in a chamber containing either sand or clay and subjected to cyclic three-dimensional stress states, the cell responses did not register the assumed stress condition. They attributed the differences to using an air calibration curve and unknown problems with the test design/configuration. Askegaard et al. (1998) measured the cell response when the cell was installed at various inclinations in sand and developed a calibration equation of the form

$$q = C\sigma_{33} + D(\sigma_{11} + \sigma_{22}) \tag{3.2}$$

where

$$q = \text{hydraulic stress}$$
$$\sigma_{33} = \text{normal stress}$$
$$\sigma_{11}, \sigma_{22} = \text{tangential stresses}$$
$$C, D = \text{constants}$$

If the cell response was a true response of the normal stress in the medium, C would be equal to unity and D would be equal to zero. For the Dynatest cells, D was found to be zero and C equal to 1.10.

In summary, the Dynatest pressure cells have good linearity but are susceptible to temperature and time, making their suitability for measuring long-term stresses questionable. Questions over the accuracy of the response arise when the cells are subjected to tangential or lateral stresses. This makes the use of the cells to measure either horizontal stresses or non-normal stresses somewhat doubtful.

At the completion of the research the calibration factors were checked and they were found to have changed from the factory supplied values. The calibration of the cells was checked by embedding the cells in fine sand contained in a thick walled container with a diameter and height of 150 mm. The container was placed in a loading frame inside an environmental chamber and a series of loads was applied to the container via a loading platen with a diameter of 150 mm. This calibration process is similar to that used by Hildebrand (2002).

3.2.2.3 Dynamic Wheelforces

The SLAVE vehicle at CAPTIF could almost be regarded as a "quarter truck" consisting of a sprung mass (the chassis and load) connected by a suspension to an unsprung mass (the axle and wheels), which in turn interacts with the road through its tyres (de Pont et al. 1998). The wheel forces generated by a quarter truck can be determined very simply using the following expression:

$$F = M_{unsprung} \times A_{unsprung} + M_{sprung} \times A_{sprung} \tag{3.3}$$

where

$$F = \text{Wheel force (N)}$$
$$M_{unsprung} = \text{Unsprung mass (kg)}$$
$$A_{unsprung} = \text{Unsprung acceleration } (ms^{-2})$$
$$M_{sprung} = \text{Sprung mass (kg)}$$
$$A_{sprung} = \text{Sprung acceleration } (ms^{-2})$$

By measuring the vertical accelerations of the sprung and unsprung masses using two accelerometers and knowing the two mass values, the dynamic wheel forces can be calculated.

In practice the situation is a little more complicated; rather than being a simple quarter truck with movement constrained to the vertical direction, the SLAVE vehicle is still a simple two-degree of freedom system but the degrees of freedom are two rotations, rather than two vertical displacements (Figure 3.7). The equations of motion for this system can be determined and then manipulated to give an expression for the wheel force, F, which is identical to the above except that the masses are replaced by mass factors. These depend on not only the masses of the components but also on the geometry and the distance of the accelerometers from the pivot points. For a given loading configuration these mass factors can be calculated and so the method as described above can still be applied.

For each SLAVE vehicle the wheel force measurement system consists of two accelerometers, one mounted on top of the chassis and the other mounted as far outboard as possible on the axle. Each SLAVE vehicle is also fitted with a displacement transducer (LVDT) measuring the suspension deflections. This is used for characterising the suspension response and also as a crosscheck on the accelerometer signals. A Hewlett Packard 3852S microprocessor-based unit and computer are mounted on the centre pedestal to capture the data from the accelerometers and displacement transducers. The computer is controlled by remote control software (PC Anywhere) operating over a wireless LAN, while the vehicles are running at speeds of up to 50 km/h.

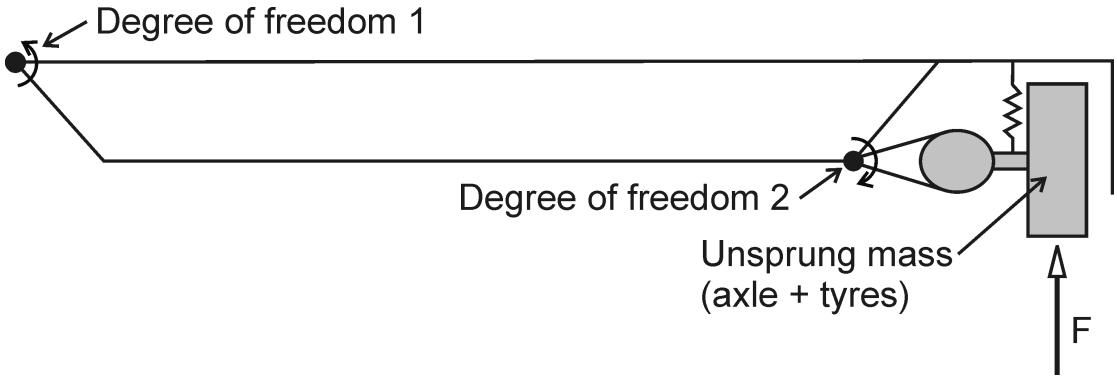

Figure 3.7 Schematic of SLAVE unit.

3.2.2.4 Surface Profiles

Transverse surface profiles are measured using the CAPTIF Profilometer (Figure 3.8). The Profilometer consists of a braced aluminium beam, 4.4 m long, supported at each end by adjustable feet. An aluminium carriage is driven along the beam by an electric motor and drive chain. The carriage holds a Linear Variable Differential Transducer (LVDT) with a jockey wheel riding along the pavement surface. Vertical displacement is recorded every 25 mm of horizontal travel of the carriage. The analog output signals from the position senor and LVDT are converted to a digital signal by electronics contained within the device, and a Psion hand-held computer captures the digital data.

During the construction process, transverse inter layer profiles are measured with a manual profilometer which consists of a 4.5 m length of aluminium channel section, a machined plastic block which slides along the channel and a 1 m steel ruler which is located in a slot in the plastic block. The ruler is lowered down to the surface being measured and the corresponding depth is measured at the edge of the block. Readings are taken every 200 mm across the track. By calculating the difference between readings taken on the surface of different materials, the layer thickness can be determined.

Figure 3.8 CAPTIF Profilometer.

Longitudinal profiles are measured with a non-contact laser and accelerometer sensor system mounted on one of the SLAVE vehicles (Figure 3.9). The system was developed by ARRB Transport Research Limited, Melbourne, Australia. Due to the double integration of the accelerometer signal to obtain a vertical displacement measurement of the vehicle, significant offsets are introduced into the signal. These offsets are removed by breaking the complete profile into six sections, each ten metres in length and then subtracting a linear correction from each section. The endpoint points of the linear correction are determined from the transverse profile measurements as these measurements are considered to be absolute values. This experience at CAPTIF with accelerometer based profile measurement devices has shown the difficulty in extracting absolute surface profiles from these types of systems.

Figure 3.9 CAPTIF longitudinal laser profiler.

3.2.2.5 Pavement Surface Deflection Bowl

The surface deflection of a pavement under a static wheel load is measured using the CAPTIF Deflectometer (Figure 3.10). The Deflectometer is a modified version of the Geobeam device developed by Tonkin and Taylor Ltd. of Auckland and resembles a Benkelman Beam. The Deflectometer probe is positioned between the tires of a dual-tyred wheel and, as the wheel is moved away, the rebound of the pavement is measured, to the nearest 0.01 mm, every 50 mm of horizontal movement. Unlike the Benkelman Beam, there are no moving parts on the device; instead an electro-magnetic gap-measuring sensor at the end of the beam measures the vertical distance between the sensor and a steel disc placed on the pavement surface. A separate, associated device measures the horizontal movement of the wheel. The output from the Deflectometer is captured in the same way as the Profilometer.

Figure 3.10 CAPTIF Deflectometer.

3.2.2.6 Falling Weight Deflectometer

The Falling Weight Deflectometer has been designed at a stationary device that can simulate the effects of a moving wheel load. This is accomplished by dropping a mass onto a loading plate resting on the pavement surface. The resulting load and surface deflections are measured by a load cell and a series of geophones (velocity sensors) at various distances from the loading plate respectively. The mass of the falling weight, the drop height and damping in the system has been designed to replicate a vehicle moving at highway speeds (Crovetti et al. 1989). The testing at CAPTIF was carried out with a Dynatest Model 8000 FWD.

3.3 CAPTIF Research Programs

In 1999 Transfund New Zealand commissioned Transit New Zealand to undertake a four year research program to investigate the effects of increasing the axle limits for heavy vehicles on the pavement structure and surfacings. This project was carried out in parallel to a similar project undertaken by ARRB Transport Research Ltd in Melbourne, Australia. This research program involved the construction of two test

pavements, each pavement was subjected to two different load levels applied concurrently, but separately in two concentric wheelpaths. For each pavement one of the load levels was fixed at 40 kN, which corresponds to a standard axle load of 80 kN or 8.2 tonnes. The other load levels were 50 kN for the first pavement and 60 kN for the second pavement. For both pavements after the completion of 1 million load applications, the 40 kN load was increased to the level of the other load (either 50 or 60 kN) and an additional 320,000 (50 kN) and 447,000 (60 kN) load applications were applied. Prior to the start of this project, a 300 mm long extension was fitted to one of the arms connecting the SLAVE vehicles. This extension allowed a greater separation between the wheelpaths formed by one SLAVE and by the other.

The pavement tank is 4 m wide and when the hydraulic rams that control the lateral position of the vehicles are in the middle of their travel, both vehicles are positioned in the centre of the tank and would thus run on the same radius of travel. The commands that control the lateral position of the vehicles are entered by and reported to the operator as a function of the position of the centre of a dual tyre wheel set on vehicle A in relation to the reference system used to describe the transverse (or radial) location on the pavement. For operational reasons, surface measurements are only done over the middle 3.5 m of the tank, so when the two vehicles are located on the same radius, in the centre of the tank, this corresponds to a transverse location of 1.75 m (half of 3.5 m). In order to operate the two vehicles in two separate wheelpaths, the lateral position of vehicle A is set to almost the minimum radial position that the rams can accommodate. This means that vehicle A will run in a wheelpath that has a transverse position of 1.35 m (the minimum possible value would be 1.25 m). Normally this would mean that the vehicle B would be located at a transverse position of 2.15 m (1.75+ (1.75-1.35)), however the inclusion of the 300 mm long extension in the arm connected to vehicle B means that the transverse location of vehicle B is now 2.45 m (2.15+ 0.30). The transverse location that corresponds to both vehicles located on the same radius is now 1.90 m (1.75 + 0.30/2).

Throughout this thesis the following terms are interchanged and mean the same. The inner wheelpath corresponds to a transverse position of 1.35 m, therefore the

terms inner wheelpath and 1.35 m mean the same and are interchangeable. Likewise the terms outer wheelpath and 2.45 m mean the same and are also interchangeable.

3.3.1 Pavement Design and Construction

The first test pavement was a single pavement design and was split into four segments, each containing a different granular base material. The second test pavement comprised of two pavement designs and was split into five segments, with three different granular base materials used in the five segments. The two pavements shall be referred to as the "PR3-0404" and "PR3-0610" pavements respectively; this nomenclature corresponds to the Tranfund NZ project numbers relating to the two tests. Two of the granular base materials were common to both pavements.

A full description of the tests, analysis and findings can be found in other sources (de Pont et al. 2001; de Pont et al. 2003; Arnold et al. 2005b; Arnold et al. 2005c; Arnold et al. 2005a). For completeness, a description of the materials used, pavement designs, instrumentation and loading history follows.

Four different granular base materials were used; three of the materials were local Canterbury aggregates and the fourth was an imported crushed rock from Melbourne, Australia. The properties of the granular materials are listed in Table 3.2. For both pavements, the same subgrade (Waikari silty clay) was used. The subgrade properties are given in Table 3.3.

The design thicknesses for the two series of pavements are shown in Table 3.4, both series were surfaced with a paver-laid 25 mm nominal thick asphalt concrete wearing course. The asphalt concrete conformed to TNZ M/10 Mix 10 specifications (Transit New Zealand 1975).

Table 3.2 Characteristics of the granular base materials.

Characteristic	TNZ M4	TNZ M4 + fines	TNZ M5	AUS Fine Crushed Rock (FCR)	Recycled Concrete
Source material	Alluvial Greywacke			Quarried Rhyolite	Unknown
Maximum particle size (mm)	40	40	40	20	40
Fines content (passing 75 μm) (%)	3	8	4	9	7
Maximum Dry Density[1] (t/m³)	2.32	2.36	2.38	2.26	2.12
Optimum Moisture Content (%)	6.0	4.8	4.2	6.0	10.5

[1] NZS 4402:1986 Test 4.1.3 – vibrating hammer compaction test (Standards New Zealand 1986b)

The layouts of the two test pavements, including the location of the Segment Codes used in Table 3.4 are shown in Figure 3.11 and Figure 3.12. Three dimensional εmu coil arrays were installed in both pavements, in three segments for the PR3-0404 pavement and in four segments for the PR3-0610 pavement.

Table 3.3 Characteristics of the subgrade material.

Characteristic	Waikari Silty Clay
Source material	Quartz and minor feldspar, with smectite and minor illite and kaolinite forming the clay mineral component.
Maximum Dry Density[1] (t/m³)	1.87
Optimum Moisture Content (%)	14
Liquid Limit (LL)	28
Plastic Limit (PL)	14
Plasticity Index (PI)	14
Fines content (passing 75 μm) (%)	72
Classification	CL (UCS) A-6 (7) (AASHTO)

[1] NZS 4402:1986 Test 4.1.1 – standard compaction test (Standards New Zealand 1986a).

Table 3.4 Designs for PR3-0404 and PR3-0610 pavements.

Segment		Pavement PR3-0404	PR3-0610
A	Material	TNZ M4	AUS FCR
	Thickness (mm)	275	275
B	Material	TNZ M4	AUS FCR
	Thickness (mm)	275	200
C	Material	AUS FCR	TNZ M4
	Thickness (mm)	275	200
D	Material	Recycled Concrete	TNZ M4
	Thickness (mm)	275	275
E	Material	-	TNZ M5
	Thickness (mm)		275

In the PR3-0404 pavement the pressure cells were distributed evenly in three segments to measure the vertical, horizontal transverse and horizontal longitudinal stresses in the top 50 mm of the subgrade. In the PR3-0610 pavement the pressure cells were concentrated on measuring the vertical stress at various depths in segment A and single cells were used to measure vertical stress at the top of the subgrade in three other segments (B, C and D). The instrument layouts are shown in Figure 3.13 and Figure 3.14. εmu soil strain coils and Dynatest Soil Pressure Transducers were installed to measure vertical, transverse horizontal and longitudinal horizontal pavement responses in the granular and subgrade layers. The as-constructed layer thicknesses, density and moisture content test results are shown in Table 3.5. The density and moisture content test results were obtained with a Troxler Nuclear Density meter operating in backscatter mode.

The measured densities pavement obtained at CAPTIF would not be acceptable in the construction of a typical field pavement as the field requirement is to reach 96% of the MDD value. Because of the difficulty in drying material in the indoor facility, the amount of water applied during the construction process is minimised. The low levels of moisture in the granular material, compared to the OMC value, result in lower density values, compared to the MDD value. In order to achieve higher levels of compaction, either more water would be required and/or compaction equipment with greater amounts of compactive would be required. The influence of the concrete tank on the Nuclear Density meter results can be

discounted, as the nuclear results are similar to the density values obtained by the sand replacement method. However, despite the low levels of density obtained at CAPTIF, the performance of the test pavements are acceptable.

FWD tests were done during and after the pavement construction, and at intervals during the pavement loading. Measurements were usually taken at each station in the inner and outer wheelpaths (58x2 = 116 readings). The target drop height was set to give a nominal plate load of 40 kN.

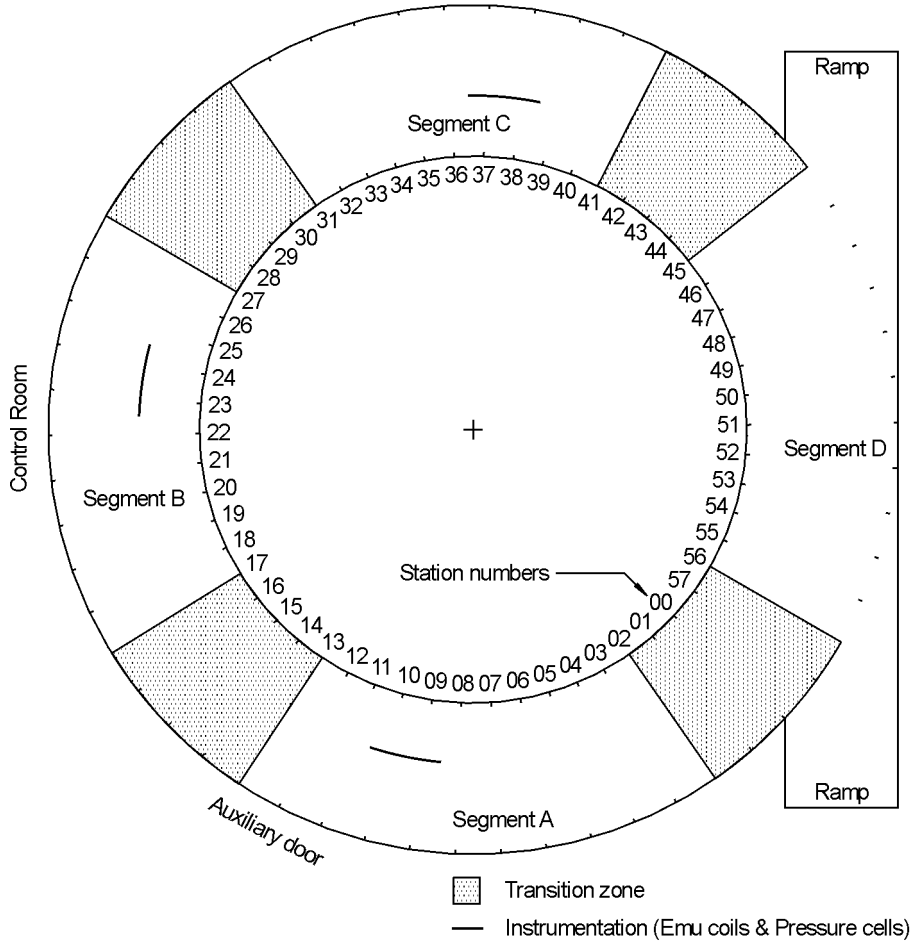

Figure 3.11 Layout for the PR3-0404 pavement.

3.3.2 Pavement Loading

The loading regime was similar for both tests; five thousand load cycles were completed with the vehicles loaded to 30 kN each, operating on a rectangular transverse distribution across the maximum trafficable width. This was done to condition the pavement and to expose any construction and/or material deficiencies. At the completion of these load applications a series of initial characterisation tests using the εmu and pressure cell instruments were completed with the vehicles at various weights and transverse locations. After the completion of the characterisation tests, the accelerated loading was started.

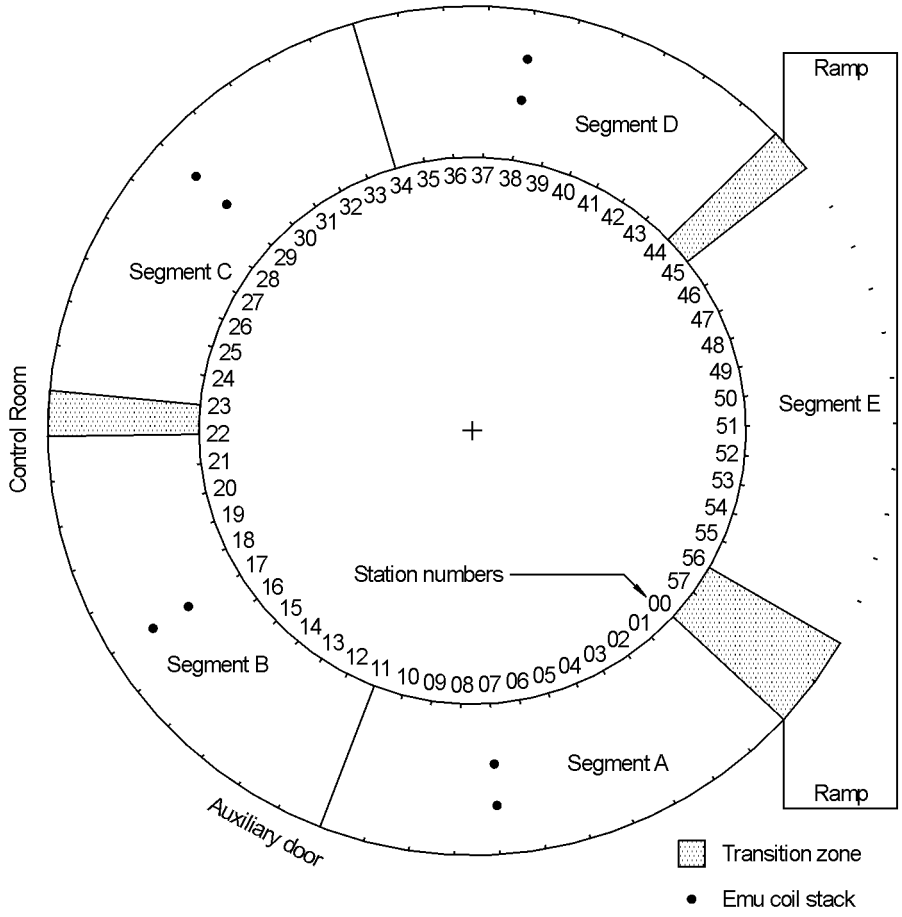

Figure 3.12 Layout for the PR3-0610 pavement.

For the accelerated loading, the transverse position of the vehicles was programmed to have a lateral wander equal to ± 100 mm. The pattern of the wander was set to a normal distribution, with the standard deviation equal to one sixth of the total wander. During the accelerated loading phase, sets of transverse and longitudinal profiles, stress, strain and wheelforce measurements were taken after the application of set loading intervals. Initially the loading intervals were short (10,000 load cycles), but as the rate of pavement change reduced, the length of the loading intervals increased to a maximum of 100,000 load cycles. After the completion of 1 million load applications the load on the standard vehicle (40 kN) was increased to match the more heavily loaded vehicle (50 or 60 kN). The loading histories for both pavements are listed in Table 3.6. At the completion of the accelerated loading phase, up to three locations were selected in each segment for a post-mortem trench, this was done to determine the percentage of the rutting attributable to the different pavement layers.

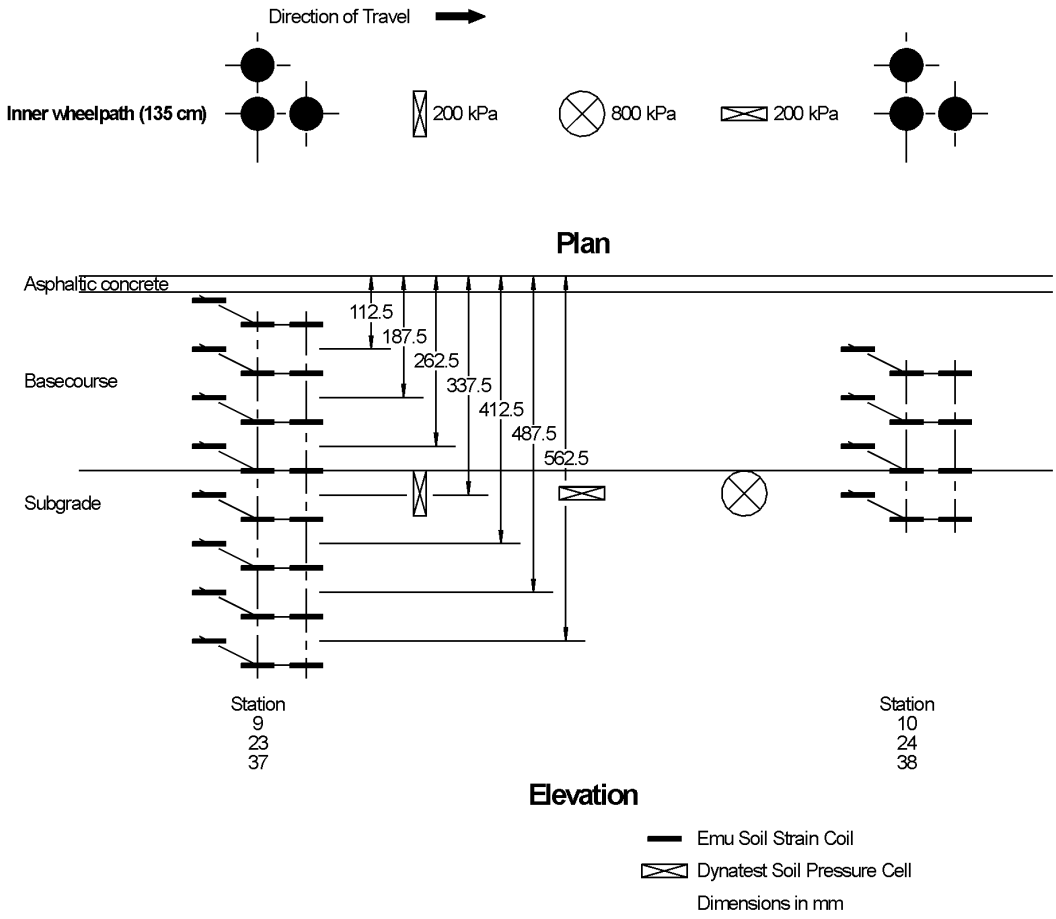

Figure 3.13 Instrument layout for the PR3-0404 pavement.

3.3.3 Calculation of Rut Depths

Rut depths in a pavement can be calculated in one of two ways, either by resting a straightedge across the rut and measuring the maximum deviation of the pavement surface beneath the straightedge or by measuring the change in profile since the pavement was constructed. The first method is known as the Straight Edge Rut Depth (SERD) and the second method is known as the Vertical Surface Deformation (VSD). In the field only the SERD method is used, as there are usually no initial profile measurements made and the SERD can be calculated with the data obtained at the current point in time. The SERD can be determined mathematically from the data obtained from the laser profile devices fitted to High Speed Survey Vehicles.

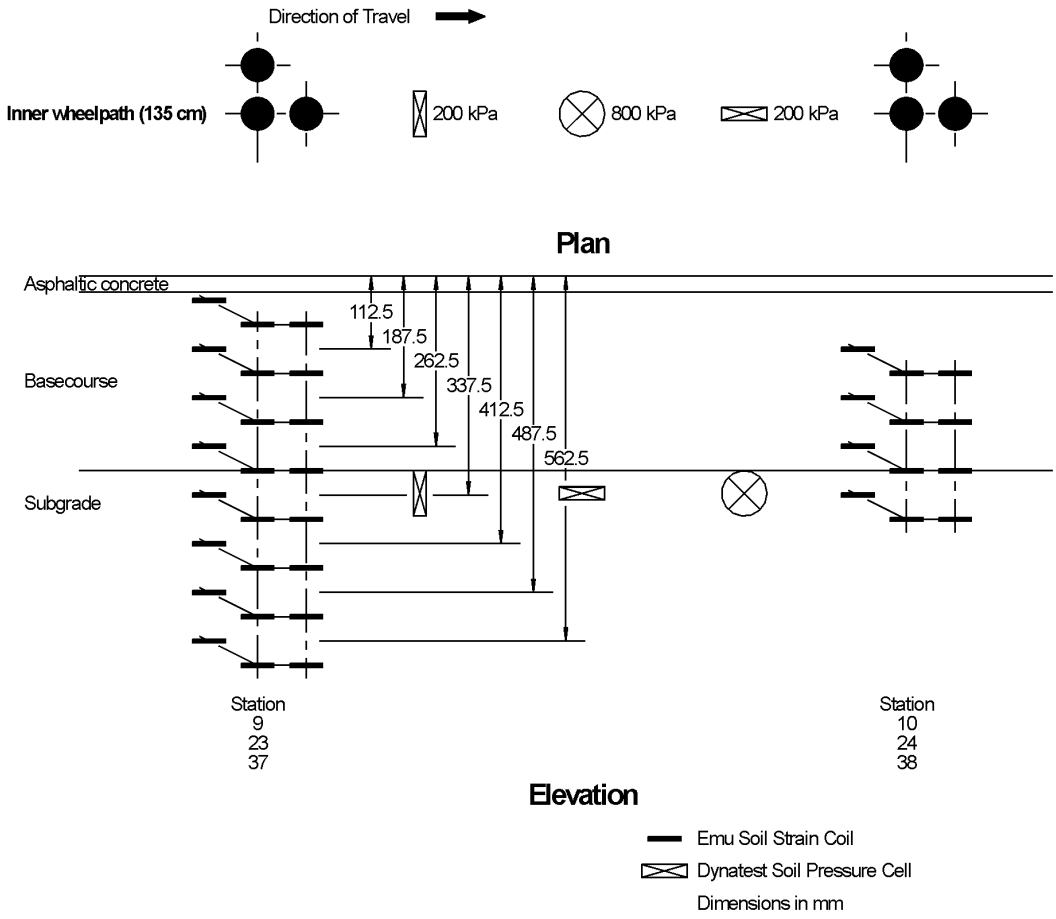

Figure 3.14 Instrument layout for the PR3-0610 pavement.

At CAPTIF all profile measurements are measured relative to the pavement tank and records are taken throughout the life of the pavement. This enables an accurate determination of the absolute vertical movement of the pavement relative to the initial profile. The maximum difference between the initial profile and the profile at the relevant point in time is the VSD. At CAPTIF the calculation of the SERD is done mathematically on the profiles obtained from the CAPTIF Profilometer using a 1.5 metre straight edge that has one end placed on the track centreline (190 cm) and the other end on the opposite side of the wheelpath being measured. The VSD is calculated as the maximum difference between the initial and current profile. The differences are determined over the trafficked width of pavement for the relevant wheelpath. It is expected that the SERD value should be greater than the VSD value as the SERD method takes into account any shoving or heaving that

occurs beside the trafficked area of the pavement. However when the SLAVE is configured to run in separate wheelpaths the VSD is usually greater than the SERD.

Table 3.5 Layer thickness, density and moisture content values for the test pavements.

Pavement	Segment	Average granular thickness (mm)	Average asphalt concrete thickness (mm)	Average density (t/m³) (% of MDD)	Average moisture content (%) (% of OMC)
PR3-0404	Subgrade	-	-	1.87 (100)	11.3 (81)
	A	280	28	2.12 (91)	2.1 (35)
	B	277	30	2.17 (92)	2.8 (58)
	C	275	27	2.14 (95)	3.4 (57)
	D	276	27	2.11 (100)	5.2 (50)
PR3-0610	Subgrade	-	-	1.84 (98)	8.5 (61)
	A	283	40	2.15 (95)	3.6 (60)
	B	214	34	2.18 (96)	4.1 (68)
	C	214	36	2.16 (93)	2.7 (45)
	D	289	28	2.16 (93)	2.8 (47)
	E	290	32	2.22 (93)	2.6 (62)

This anomaly can be attributed to the downward movement of the section of untrafficked pavement between the two wheelpaths. This effect is shown in Figure 3.15. One possible explanation for this is that the lower pavement layers are increasing in density and/or rutting as a result of trafficking due to the effect of loading spreading with depth and the granular material between the two wheelpaths in sinking as the supporting material reduces in volume. Because of this effect, the VSD values will be used in this thesis.

Table 3.6 Loading history for test pavements.

Pavement	Loading cycles	Wheelpath	
		Inner / 135 cm	Outer / 245 cm
		Vehicle load (kN)	
PR3-0404	0-1,000,000	40	50
	1,000,000-1,320,000	50	30
PR3-0610	0-1,000,000	60	40
	1,000,000-1,447,000	60	60

3.4 Laboratory Measurements

Resilient Modulus and Permanent Deformation tests were carried out on the granular and subgrade materials used in the test pavements. The tests were done using the triaxial test equipment in the Tranportation Laboratory in the Department of Civil Engineering at the University of Canterbury. The triaxial equipment comprises of a trixial cell, a custom made loading frame, a pneumatic closed loop servo controlled loading ram, and a Control and Data Acquisition System (CDAS) linked to a computer via two RS-232C communication links.

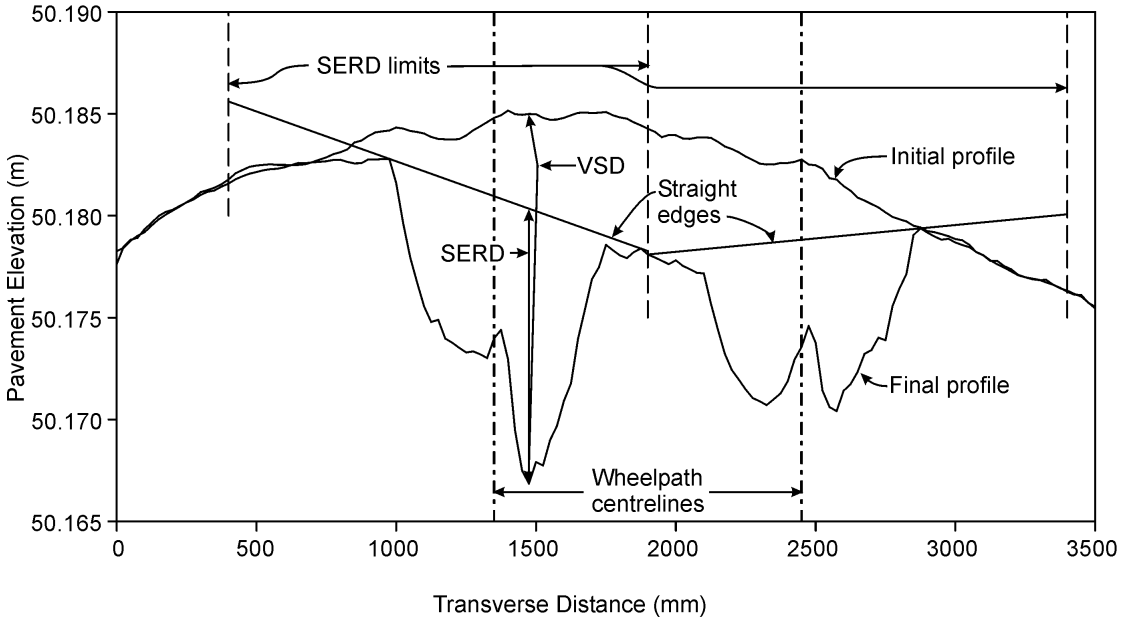

Figure 3.15 Explanation of SERD and VSD.

The loading ram, CDAS and appropriate software were supplied by IPC Global. The triaxial cell was supplied by Wykeham Farrance Limited and can test specimens with a maximum diameter of 150 mm and a height of 300 mm. The applied load was measured with an internal Wykeham Farrance 10 kN load cell, the axial deformation was measured with an externally mounted RDP Electronics (5 mm range) LVDT and the confining stress was applied using water. All the tests were done as CCP tests.

3.4.1 Sample Preparation and Testing

The resilient modulus and permanent deformation tests were carried out in accordance with AS 1289.6.8.1-1995 (Standards Australia International Limited.

1995) for the granular material and AASHTO T-307-99 (American Association of State Highway and Transportation Officials (AASHTO) 1999) for the subgrade material. Two variations from the standard test procedure for the granular material were made. The first variation was that the specimen had a height of 300 mm and a diameter of 150 mm (the standard procedure uses a specimen height of 200 mm and a diameter of 100 mm). The second variation was the compaction procedure used to prepare the specimens. The specimens were prepared using the compaction equipment described in NZS 4402: Test 4.1.3 (the standard procedure uses a falling hammer compaction device). The samples were compacted in six lifts of equal height and the compaction times were scaled to ensure that the compactive effort was the same as in NZS 4402: Test 4.1.3. The compacted specimens were allowed to stand overnight before being transferred to the triaxial cell. The specimens for the subgrade material had a diameter of 100 mm and a height of 200 mm. The specimens were compacted using the equivalent compactive effort as specified in NZS 4402: Test 4.1.1 (standard compaction). The loading conditions (wave shape, duration, stress conditions) were in accordance with the appropriate standard.

The test conditions for the permanent deformation tests were chosen to match the field stresses and strains that were measured in the PR3-0404 pavement. The procedure for determining the test conditions was carried out on the specimen used for the resilient modulus tests at the completion of the resilient modulus test. The deviator stress was fixed at the measured value and the confining pressure was adjusted so that the axial strain was equal to the measured value from the test pavement. This method resulted in confining pressures that were substantially lower than the values specified in the Australian standard for the granular material. The AASHTO standard gives no guidelines for permanent deformation testing. The loading parameters for the permanent deformation testing are given in Table 3.7.

Table 3.7 RLT permanent deformation test parameters.

	Actual		AS 1289.6.8.1 Table 2	
	Axial stress (kPa)	Confining stress (kPa)	Axial stress (kPa)	Confining stress (kPa)
TNZ M/4 aggregate	450	50	705	211
	85	10	375	26
Subgrade	80	10	NA	
	56	10		

This page is intentionally left blank.

Chapter 4 Analysis of CAPTIF Measurements

4.1 Introduction

This chapter presents the pavement response and performance data that was collected at CAPTIF, along with the resilient modulus and permanent deformation RLT test results from tests undertaken in Transportation Laboratory at the University of Canterbury. The various measurements were collected from two test pavements of similar design, construction and loading. The CAPTIF measurements include: the measurement of the tyre footprint; the response of the pavement, namely the vertical and horizontal stress and strain, to wheel loads of various weights and positions relative to the instruments; the vertical stress and strain response of the pavement to FWD loads of various magnitudes; the resilient vertical strain and the development of surface rutting over the duration of the accelerated loading phase of the projects; and the relative contribution of permanent deformation of the granular and subgrade layers to the surface rutting of the pavements.

4.2 Tyre Footprint/Contact Area

In order to determine the contact area of the tyre for use in the pavement modelling stage of this project, the actual dimensions of the tyre footprints were measured. The method used to measure the contact area is described below: a vehicle jack was used to lift the tyres clear of the ground. A section of the tyre tread was then painted with spray paint and the tyres were lowered onto a piece of poster card. The tyres were then lifted off the poster card and the card was removed. The tyre imprint was then measured. The photograph of the tyre imprint for vehicle B, loaded to 40 kN and with a cold tyre inflation pressure of 750 kPa is shown in Figure 4.1. The photograph of the tyre imprint for vehicle A, loaded to 60 kN and with a cold tyre inflation pressure of 750 kPa is shown in Figure 4.2. The dimensions of the footprints for 40, 50 and 60 kN dual tyre loads are listed in Table 4.1.

Figure 4.1 Tyre imprint for vehicle B, 11R22.5 tyres, 40 kN, 750 kPa.

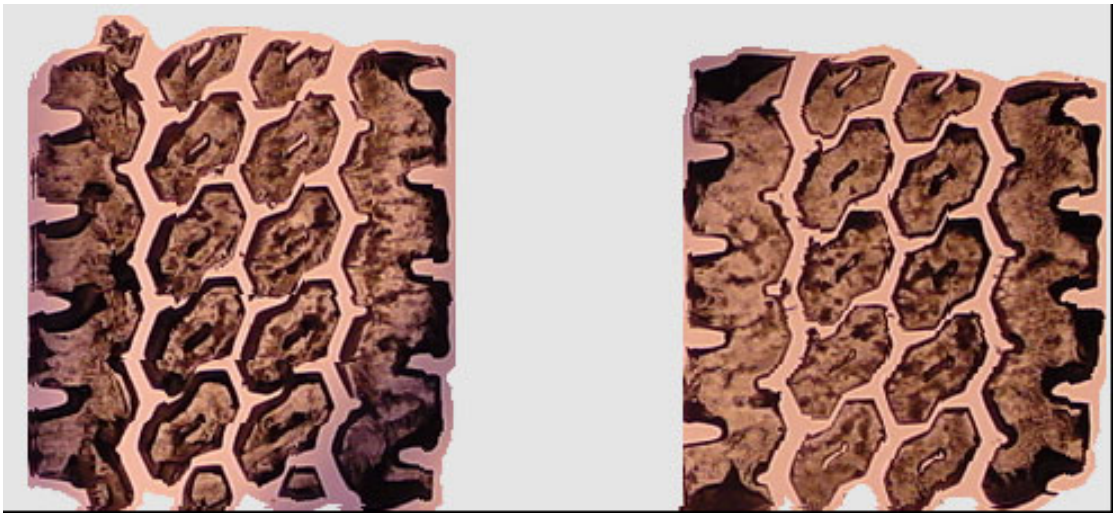

Figure 4.2 Tyre imprint for vehicle A, 11R22.5 tyres, 60 kN, 750 kPa.

The measurements show that as the load carried by the tyre increases, the length of the contact patch increases but the width remains the same. This shows that the contact patch can be modelled by either a rectangular area (for a rectangular finite element analysis) or a circular area (for an axisymmetric analysis) for typical in-service tyre loads of 20-30 kN.

Table 4.1 Tyre imprint dimensions for 11R22.5 dual tyres at various loads.

	Dual tyre load (kN) / Cold inflation pressure (kPa)		
	40/750	50/750	60/750
Single tyre width (mm)	225	225	225
Single tyre length (mm)	243	277	303
Distance between the tyres (mm)	125	125	125
Effective contact pressure (MPa) (applied load / measured area)	0.366	0.401	0.440

4.3 Stress Measurements

4.3.1 Verification of Soil Pressure Measurements

The response of the soil pressure cells can be measured and compared with the applied wheel load by calculating the vertical forces on a specified free body within the pavement structure. The shape of the free body could be an irregular cone with the tip of the cone located at the surface, at the centre of the wheel. The base of the cone is located at a depth corresponding to the depth of the soil pressure cell. The perimeter of the base of the cone is defined by the locus of points where the maximum measured vertical compressive stress drops below a percentage of the maximum measured vertical compressive stress. For this comparison, the cut off percentage was set to 5% of the maximum measured vertical compressive stress.

4.3.1.1 Limitations of the Gauges

The gauges have a factory specified range of either 20-200 kPa or 100-800 kPa. If the measured pressure is outside the specified range, the accuracy of that reading could be questionable. However, when the stresses are measured as a loaded wheel rolls over the pressure cell, the trace appears smooth and continuous below the specified lower limit of the device. Because of the continuous trace, the cut off value was set at 5% of the maximum measured vertical compressive stress. The calibration factors of the gauges were checked in the Transportation Laboratory after the PR3-0610 pavement had been excavated and for the 100-800 kPa cells, the calibration factors were found to have decreased by an average factor of 0.900

(values of 0.932, 0.893, 0.874). The calibration factors for the 20-200 kPa cells were found to have increased by an average factor of 1.273 (values of 1.391, 1.246, 1.182). The consistency of the changes and the difference between the two types of cells may have been due to the methodology used to carry out the checks. Because of the difference of the two factors, it was decided not to adjust the measured values, but to note the potential source of error in the measurements.

4.3.1.2 Measurement Process

Multiple measurements of the pressure cells were taken with the SLAVE unit at various transverse offsets from the pressure cell array. The initial measurement was taken with the centre of the dual tyre assembly over the centre of the cell array. Subsequent readings were taken with the transverse offset increasing at 50 mm intervals until the centre of the dual tyres was 550 mm away from the cell array. The SLAVE was loaded to a static weight of 40 kN, the cold tyre inflation pressure was 750 kPa and the tests were conducted at a speed of 45 km/h. The data was collected at a frequency of 3000 Hz. The data was filtered, resampled to give an interval between values of 25 mm in the longitudinal direction and then added to the project database.

4.3.1.3 Integration of the Pressure Flux.

For each gauge the pressure readings were integrated and compared with the applied wheel load. This was done by multiplying each pressure value by the area over which it acted and summing the individual values. The area over which each reading acted was 25 mm long by 50 mm wide (spacing between the longitudinal readings x spacing between the transverse readings). In order to compensate for the fact that the offset measurements were only done on one side of the array, the result for each offset was doubled before it was added to the total measurement. The values of the integrated stresses are shown in Table 4.2. The results show a high level of variability, with only four of the eight values lying within ± 20% of the static load (40 kN). Hildebrand (2002) also found large differences (12-60%, 6 cells) between the applied load (FWD loading) and the integrated response.

Table 4.2 Integrated stress values and stress bowl lengths for a static weight of 40 kN.

Station	Depth	Integrated Force	Bowl Length based on 5 kPa cutoff	Bowl Length based on 5% cutoff	Peak stress value used to determine cutoff value
	(mm)	(kN) (% of 40 kN)	(mm)	(mm)	(kPa)
7	75	35.8 (90%)	750	525	319.4
7	150	37.4 (94%)	1050	525	173.6
7	225	31.3 (78%)	1075	1075	98.0
7	300	11.6 (29%)	775	1075	37.8
7	375	14.4 (36%)	950	1300	36.7
17	225	47.2 (118%)	1150	1025	144.7
29	225	58.6 (147%)	1000	875	190.2
38	300	39.8 (100%)	1250	1300	87.0

Four possible reasons could exist for the wide range of results. First, the measured values that are outside the limits for the gauge are inaccurate, however these small values are not going to have a significant effect on the total value. Second, as the tyre moves towards the gauge, there is a continuous change of the direction of the major principal stress with respect to the pressure cell. The angle at which this pulse is acting on the cell continuously changes as the wheel moves closer to the cell. When the wheel is a long way from the gauge, the direction of the major principal stress would be greater than 45 degrees from the normal direction of the cell surface, thus resulting in a large shear stress across the surface of the cell, and the effect of a shear force on the cell is unknown. The third reason is that the dynamic load of the vehicle is varying as the wheel travels along the pavement surface and this variation is large enough to significantly change the measured stress value. Fourth, the calibration of the gauges may have altered over the life of the gauge as noted in Section 4.3.1.1. The gauges have a nominal fatigue life of $3x10^6$ cycles, so after being used in the two pavements described in this thesis the cells had been subjected to $2.76x10^6$ cycles which is approaching the design life of the cells.

4.3.2 Vertical Stress Variation With Depth

In order to examine the distribution of stress in the pavement structure with respect to depth, the width of the stress distribution at a particular depth was determined. This was calculated by measuring the distance between the two points on the rising and trailing edges of a longitudinal trace where the values were equal to 5% of the maximum value for that trace. The longitudinal trace that was used was the one closest to the centre of one tyre, equating to a transverse position of 1500 mm. The lengths of the stress bowls at different depths and stations are listed in Table 4.2 and shown in Figure 4.3.

Calculations were done to determine the approximate angle of the stress cone. The cone was defined as the line of best fit that passed through the point at each depth (where the stress was measured) where the stress was equal to 5% of the maximum value for a particular depth. The measurements were taken from the same longitudinal trace that was used to determine the length of the stress bowl (corresponding to a ram position of 1500 mm). For the purposes of determining the line of best fit, it was assumed that the width of the bowl at the surface was equal to the length of the tyre contact patch. The calculated angle of the cone was 33° to the centreline of the cone.

The variation of the maximum vertical stress values with depth is shown in Figure 4.4. It can be seen that the variation is approximately linear with depth through the granular material. The surface stress imposed by the tyre is set to the average computed stress based on the measured loaded area and the wheel load, assuming an equal distribution of the total load on both wheels.

The dimensions of the tyre footprint were approximately rectangular, 243 mm long and 225 mm wide. The weight transmitted by the tyre was 20 kN. Therefore the average contact pressure is given by

$$P = \frac{F}{A} \tag{4.1}$$

where

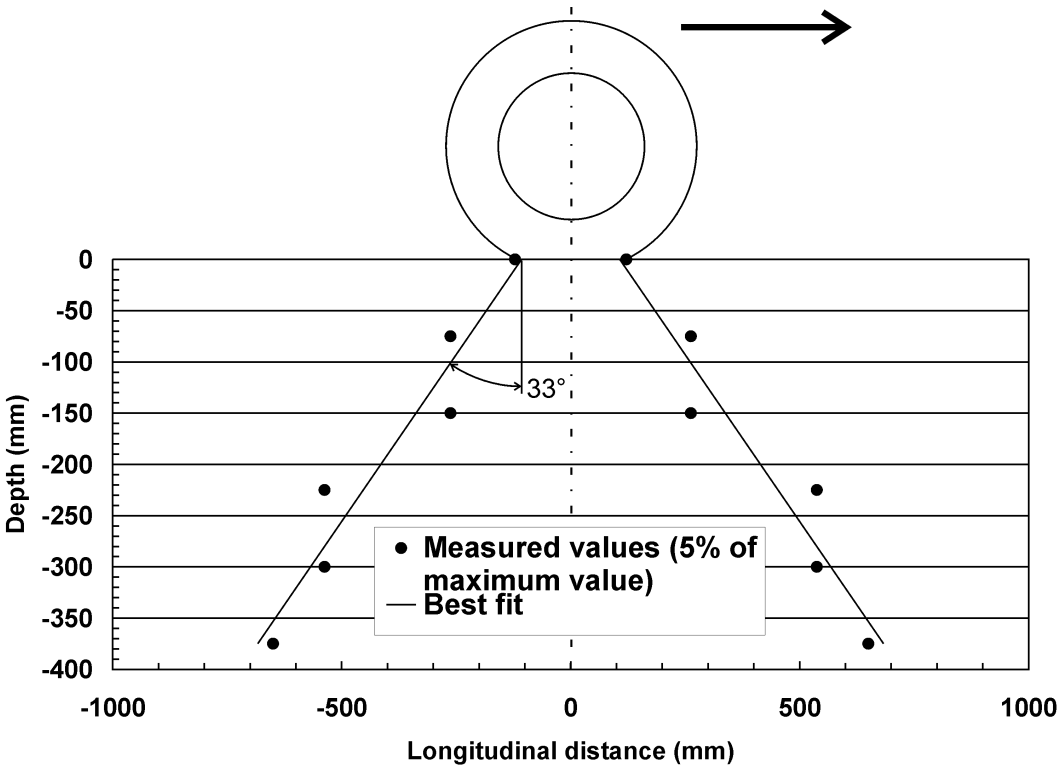

Figure 4.3 Limits of stress distribution with depth.

$$P = \text{Pressure (kPa)}$$
$$F = \text{Force (kN)}$$
$$A = \text{Area (m}^2\text{)}$$

so

$$P_{40} = \frac{20}{0.243 \times 0.225}$$
$$= 366 \text{ kPa}$$

The average contact pressures for the 50 and 60 kN dual tyre assemblies are listed in Table 4.1. These pressure values are considerably less than the inflation pressure of the tyre (750 kPa).

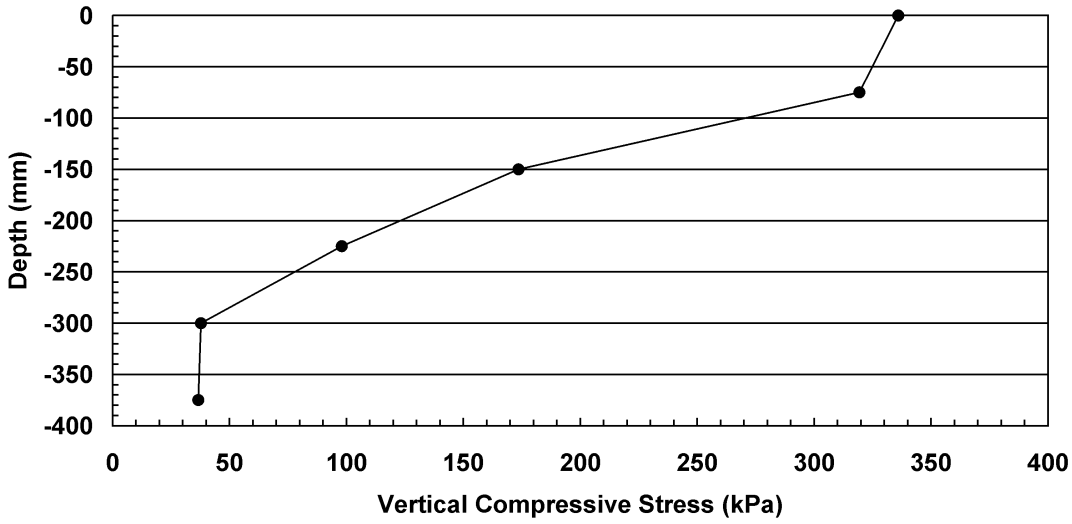

Figure 4.4 Variation of maximum stress values with depth.

4.3.3 Vertical Stress Variation in the Horizontal Plane

The maximum stress value from each of the longitudinal traces measured at various transverse offsets is plotted in Figure 4.5. From this figure, it can be seen that in the upper levels of the granular layer, the effect of the individual tyres is pronounced and the peak value is recorded beneath a tyre. As the depth increases, the combined effect of the two tyres causes the peak value to be located between the two tyres. The transverse distributions for each station at the top of the subgrade are shown in Figure 4.6. From this figure, it can be seen that at a depth of 300 mm, the distribution is smooth across the pavement and for a depth of 225 mm, the influence of the individual wheels is still visible. This would infer that the material has little influence on the shape of the stress distribution as the measurements for stations 17 and 29 (depth = 225 mm) are at the top of the subgrade while the measurement for a depth of 225 mm at station 7 is in the granular layer. The magnitude of the stiffness at a particular depth is clearly dependent on the material/pavement composition.

The set of longitudinal traces measured at various transverse offsets were plotted as contour plots to show the variation in stress values in the horizontal plane corresponding to the depth of the pressure cell. The contour plot of vertical stress at station 7, at the top of the subgrade is shown in Figure 4.7. The contour plots for the other depths/stations are shown in Appendix A.

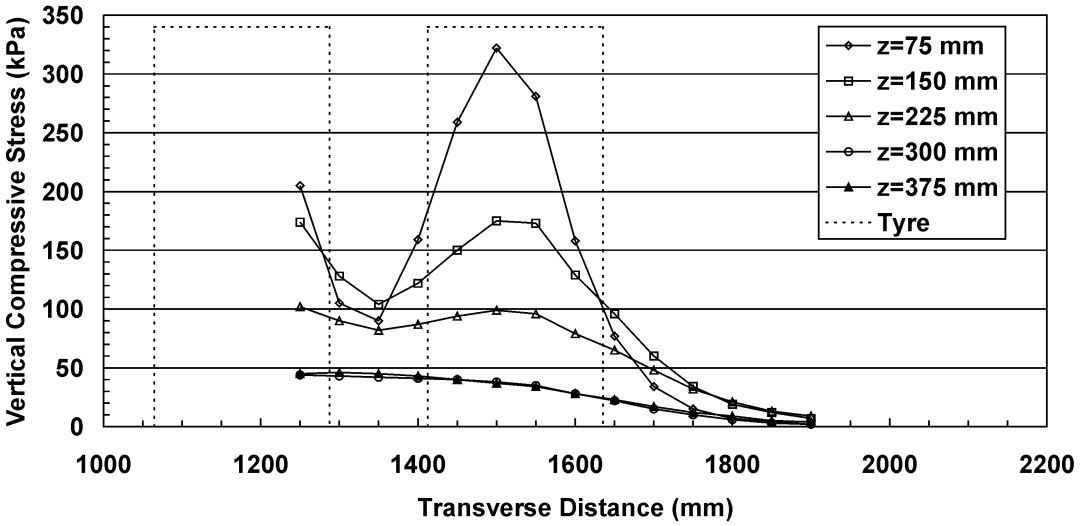

Figure 4.5 Transverse distribution of stress with depth at Station 7, PR3-0610 pavement.

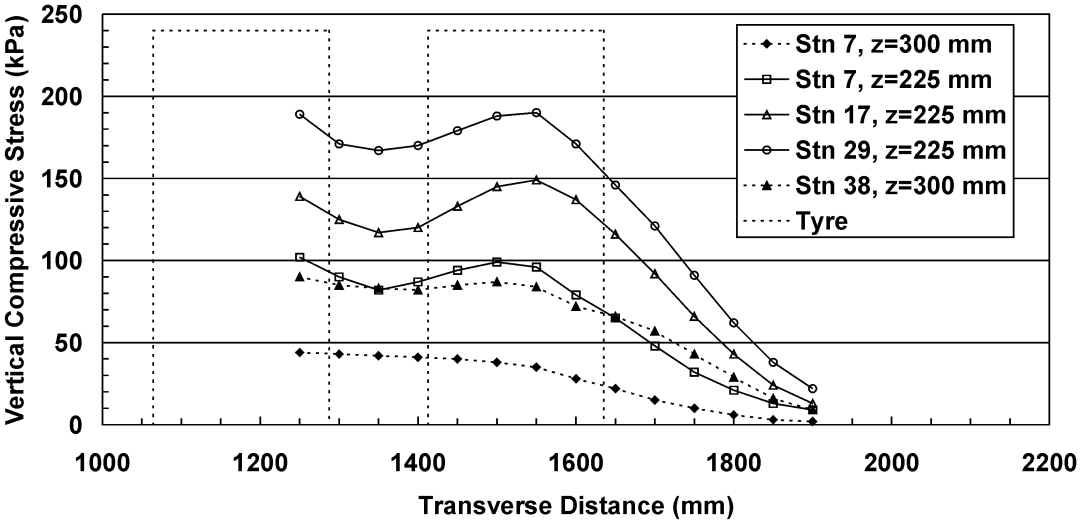

Figure 4.6 Transverse distribution of stress at the top of the subgrade/lower basecourse, PR3-0610 pavement.

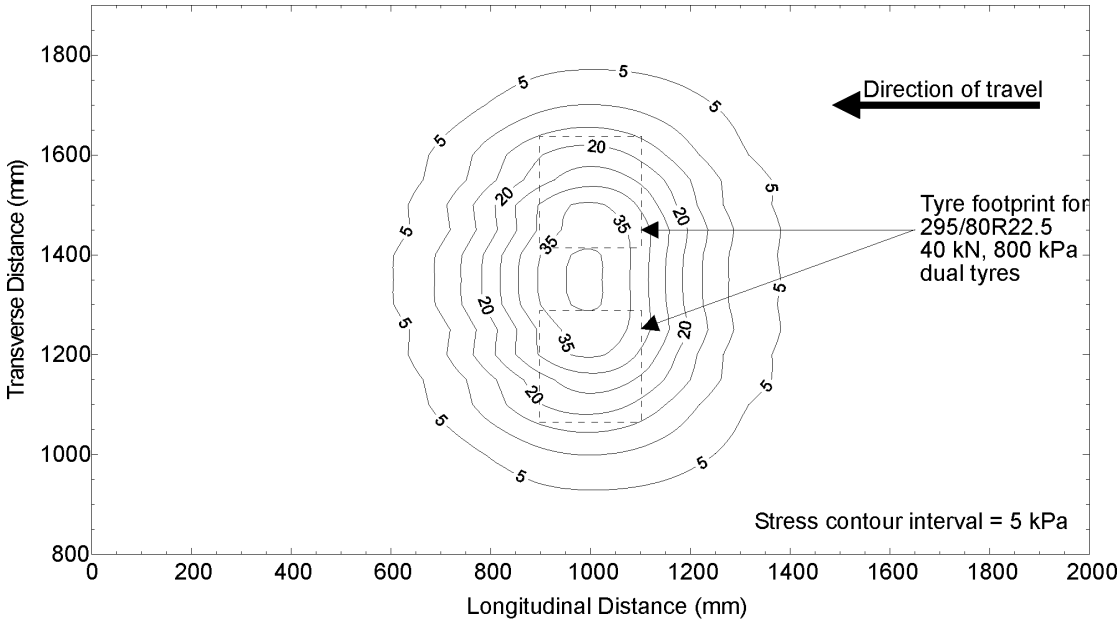

Figure 4.7 Stress contour for station 7, depth = 300 mm.

4.3.4 Vertical Stress Variation With Load

At the start of the PR3-0610 test, a set of measurements was taken with the SLAVE's loaded with different weights. The different test weights were 23, 35, 40, 50 and 60 kN. The measurements were done with the centre of the dual tyre assembly over the pressure cells.

The measured stresses for station 7 are shown in Figure 4.8 and the measured stress at the top of the subgrade for stations 7, 17, 28 and 38 are shown in Figure 4.9. The parameters for a least squares regression are shown in Table 4.3 and show that the measured stress varies linearly with load.

These tests were repeated twice at the end of the experiment with the measurements taken when the centre of the dual tyre assembly was over the pressure cells and for the second set, the centre of the inner tyre was positioned over the pressure cells. The results are shown in Figure 4.10 and Figure 4.11 when the centre of the dual tyre assembly is over the gauge array and when the centre of one tyre is over the gauge array respectively (ram positions of 135 and 153 cm). The vertical stresses measured between the tyres at depth of 75 mm are less than those measured at a depth of 150 mm because the upper pressure cell lies outside of the measured load cone (Section 4.3.2) and is possibly subjected to an amount of upwards pressure by

the interaction between the two tyres near to the surface. The pressure cell at a depth of 150 mm lies within the load cone of both tyres and therefore is subjected to downwards stress only. The parameters for a least squares regression are shown in Table 4.4 and show that the measured stress varies linearly with load, confirming the measurements carried out at the start of the test. The results for the pressure cell at a depth of 375 mm are not included as there was a problem with the instrument during these measurements.

These results show that the measured stresses confirm the theory developed by Boussinesq, namely that the variation of vertical stress at a fixed depth is a linear function of load.

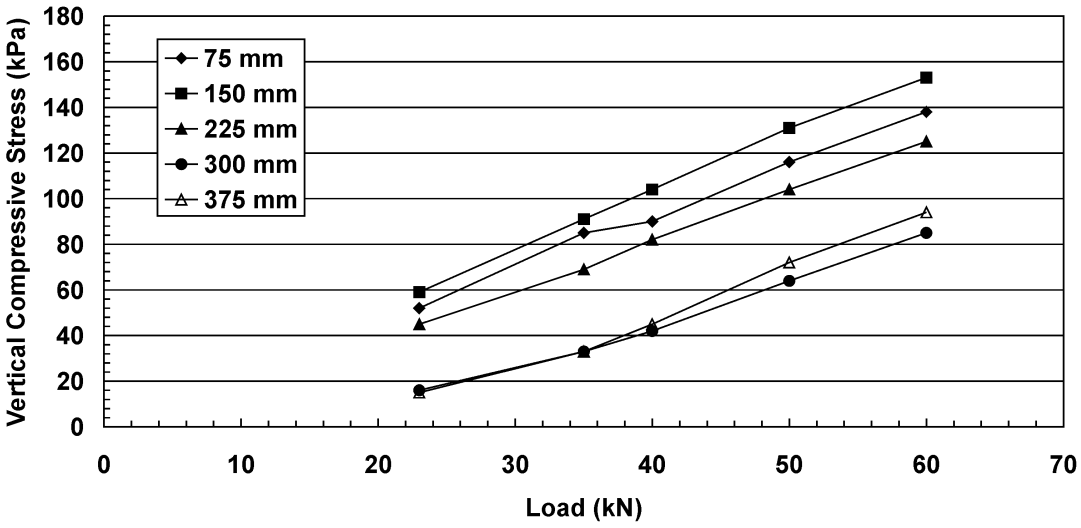

Figure 4.8 Variation of stress with different loads at station 7, PR3-0610 pavement.

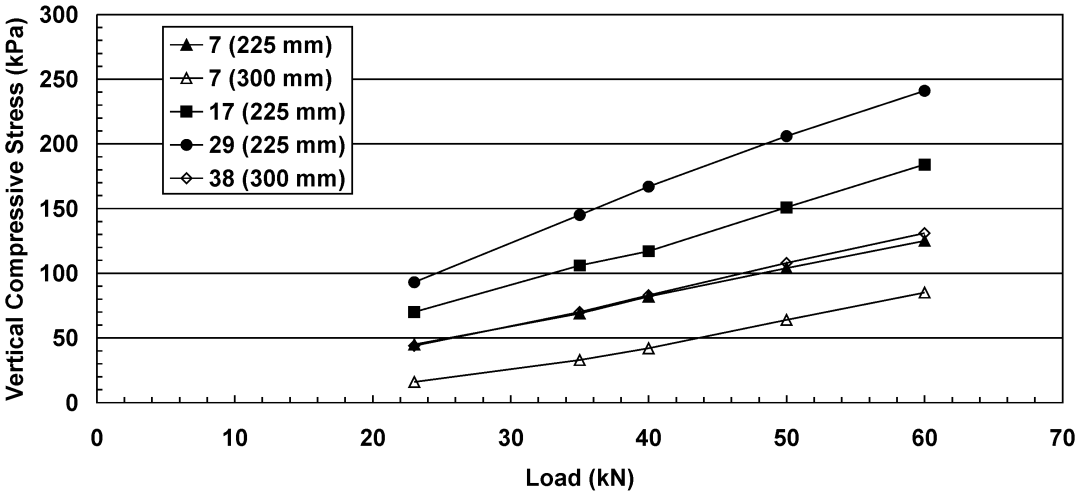

Figure 4.9 Variation of stress with different loads at the top of the subgrade/lower basecourse, PR3-0610 pavement.

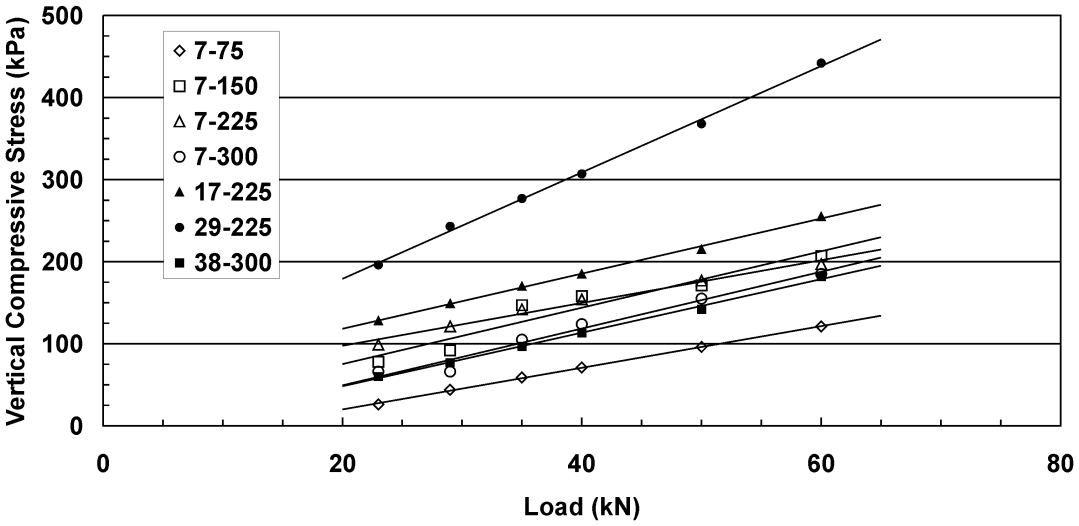

Figure 4.10 Variation of stress with load, 1447k laps, gauges between the tyres, PR3-0610 pavement

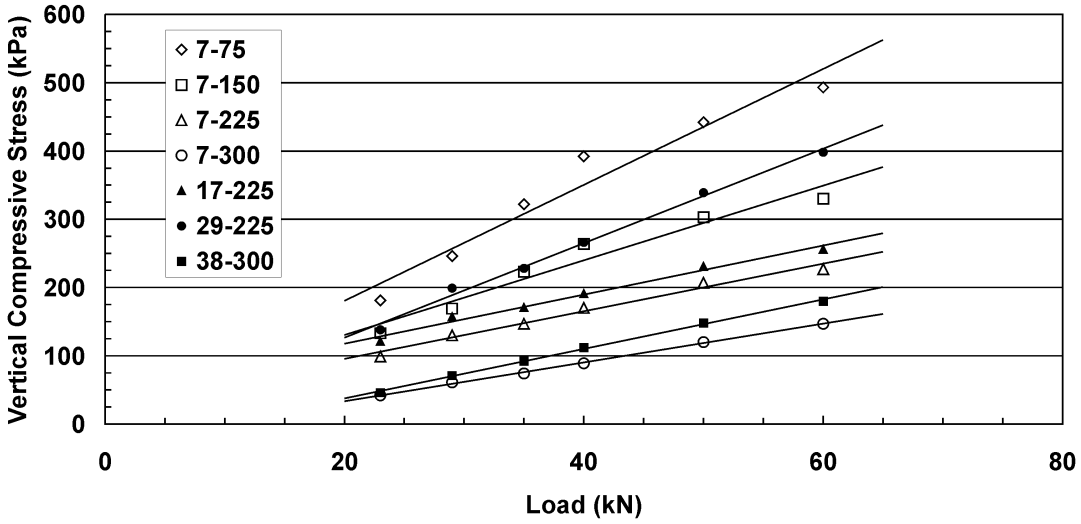

Figure 4.11 Variation of stress with load, 1447k laps, gauges beneath a tyre, PR3-0610 pavement.

Table 4.3 Least squares regression parameters for stress measurements with varying weights at 0k laps, gauges between the tyres, PR3-0610 pavement.

Station	7					17	29	38
Depth (mm)	75	150	225	300	375	225	225	300
Slope (kPa/kN)	2.298	2.560	2.184	1.896	2.204	3.077	4.007	2.377
Intercept (kPa)	0.6	1.1	-5.9	-30.9	-39.9	-2.4	3.7	-11.7
R^2 Value	0.994	0.999	0.999	0.990	0.987	0.997	0.998	0.999

Table 4.4 Least squares regression parameters for vertical stress measurements with varying weights at 1447k laps, gauges between the tyres, PR3-0610 pavement.

Ram = 135 cm							
Station	7				17	29	38
Depth (mm)	75	150	225	300	225	225	300
Slope (kPa/kN)	2.536	3.432	2.604	3.457	3.359	6.477	3.260
Intercept (kPa)	-30.7	6.6	45.5	-19.7	51.0	49.6	-16.9
R^2	0.999	0.921	0.983	0.973	0.998	0.998	0.997
Ram = 153 cm							
Station	7				17	29	38
Depth (mm)	75	150	225	300	225	225	300
Slope (kPa/kN)	8.490	5.470	3.484	2.840	3.593	6.919	3.622
Intercept (kPa)	10.7	20.9	25.7	-23.4	45.9	-12.0	-34.9
R^2	0.951	0.951	0.983	0.998	0.986	0.994	0.998

4.3.5 Relationship Between Vertical and Horizontal Stresses

In both the PR3-0404 and PR3-0610 pavements, pressure cells were installed to measure compressive horizontal longitudinal and/or transverse stresses. This was achieved by installing the pressure cells on their edges so that the pressure membrane was in the vertical plane. For the PR3-0404 pavement, six cells were installed in a horizontal orientation at the top of the subgrade: three cells were in a longitudinal orientation and the other three cells were in a transverse orientation. The cells were installed in groups of two (one transverse and one longitudinal) in three different pavement sections. For the PR3-0610 pavement, only one cell was installed in a horizontal orientation to measure longitudinal stresses. This cell was installed at a depth of 75 mm below the pavement surface.

For the PR3-0404 pavement, a limited set of measurements was taken at different loads (40, 50, 60 kN), tyre inflation pressures (750 and 850 kPa) and vehicle speeds (6, 20 and 45 km/h). These measurements were taken with a single wide based single tyre (385/60R22.5). The horizontal stress is plotted as a function of vertical

stress and is shown in Figure 4.12. All the data from the various loading configurations is plotted in this figure, accounting for some of the scatter in the results. In addition, the data was collected over a small weight range (40-60 kN). The slope and intercept for the line of best fit are 0.187 kPa/kPa and -9.7 kPa respectively. The R-squared value was 0.32. The data from 1447k laps, ram position 153 cm (one tyre of the dual tyre assembly above the cells) for the PR3-0610 pavement is shown in Figure 4.13. The slope and intercept for the line of best fit are 0.153 kPa/kPa and -8.8 kPa respectively. The r-squared value was 0.93.

While the two sets of measurements are taken at two different depths and from two different pavements, there are similarities in the relationship between the vertical and horizontal stresses; both have similar intercepts and slopes. This implies that the relationship between the vertical and horizontal stresses is constant, irrespective of the applied load and the depth below the pavement surface. If the least squares regressions are recalculated with the intercept set to zero, the slope coefficients are 0.119 and 0.130 for the PR3-0404 and PR3-0610 pavements respectively. The R-squared terms drop to 0.27 and 0.90. If the two slope coefficients were averaged, an approximate relationship would be:

$$\sigma_h = 0.125\sigma_v \tag{4.2}$$

This relationship is similar to findings of Freeman and Harr (2004) who reported measured stress ratios of 0.14 for a crushed limestone. If Boussinesq's equations are used to determine the ratio of horizontal and vertical stresses, then an appropriate value of Poisson's ratio can be determined for an analysis on the centerline.

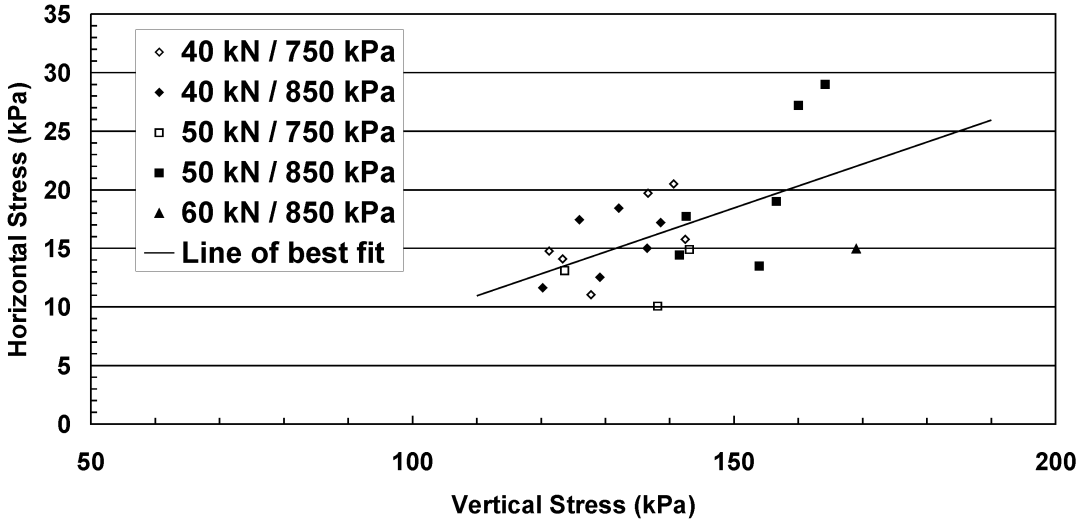

Figure 4.12 Horizontal stress versus vertical stress for the PR3-0404 pavement (all loads/pressures/stations, top of subgrade, z=300 mm).

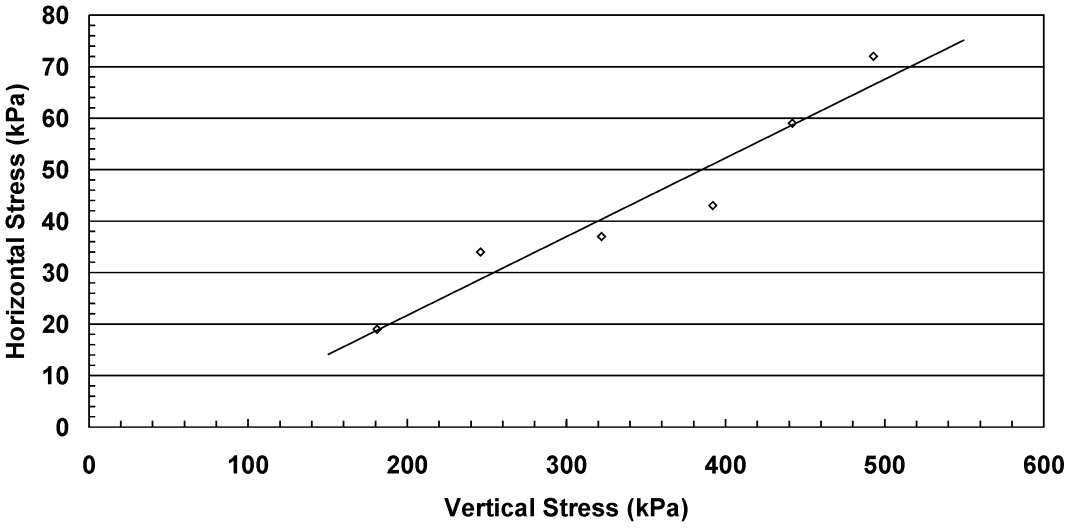

Figure 4.13 Horizontal stress versus vertical stress for the PR3-0610 pavement (Station 7, z=75 mm), gauges between the tyres.

Using Equations (2.6), (2.7) at a depth of 300 mm and for a loaded area with a radius of 187 mm (see Sections 4.2 and 5.4 for the calculation of the radius of the loaded area), the value of the Poisson's ratio can be calculated in order to satisfy Equation (4.2). The result of this calculation gives a value of Poisson's ratio of 0.61. Since this value is greater than 0.5, it implies that the material exhibits some degree of anisotropic behaviour.

4.4 Strain Measurements

A series of vertical and horizontal strain measurements were taken at the end of the PR3-0610 test. The strains were measured under a number of different loads; 23, 29, 35, 40, 50 and 60 kN loads on a 295/80R22.5 dual tyre assembly. The vehicle speed was 6 km/h and the measurements were repeated with a) the centre of one of the tyres of the dual tyre assembly over the centre of the strain coil array (ram position = 1530 mm) and b) with the centre of the dual tyre assembly over the strain coil array (ram position = 1350 mm).

4.4.1 Verification of the εmu Soil Strain System

In order to verify the accuracy of the εmu Soil Strain system, the measured strains were integrated over the depth of the pavement and compared against the surface deflections measured with the CAPTIF Deflectometer and a FWD. In order to reduce the effect that the vehicle speed may have on the results, the strain data for comparing the Deflectometer results was captured when the SLAVE units were moving at a steady speed of 6 km/h over the coils. The strain data for the FWD results was captured as the FWD was dropped over the coils. The pavement response was measured under three different loading configurations for the Deflectometer check and under four different drop heights for the FWD check. These checks were done on the pavement constructed for the PR3-0404 project after the application of 600,000 load cycles.

In order to integrate the measured strains over the full depth of the pavement, several assumptions were made to account for the sections of pavement that were not monitored by the soil strain system. These assumptions were:

- To calculate a linear regression for the basecourse strains, the resulting line of best fit was extrapolated to the top of the basecourse and to the basecourse/subgrade interface. A linear extrapolation was chosen because the strains measured at the three depths showed that the strains varied linearly with depth;

- That there was zero strain in the thin asphalt concrete layer. This layer was 30 mm thick, therefore any compression of the layer would be small compared to the overall deflection/compression of the pavement structure;

- To fit a straight line to the top two strain points in the subgrade and to extrapolate this line up to the basecourse/subgrade interface to determine the strain at the top of the subgrade;

- That the strain decreased at a constant rate from the measured value at lowest coil pair to a value of zero at the bottom of the pavement tank (1500 mm);

The different steps in the computations carried out to integrate the strains are detailed below:

1) The as-constructed thicknesses of the asphalt concrete and basecourse layers were determined from the construction records.

2) The actual εmu coil depths below the surface were calculated from the construction records.

3) A straight line was fitted to the basecourse strains (3 values) by the method of least squares. The fitted line was extrapolated to the asphalt concrete/basecourse and basecourse/subgrade interface depths in order to determine the basecourse strains at the top and bottom of the basecourse layer.

4) The extrapolated basecourse strains were integrated over the thickness of the basecourse layer to calculate the compression in the basecourse layer.

5) A straight line was fitted to the top two strain points in the subgrade and this line was extrapolated up to the basecourse/subgrade interface to determine the strain at the top of the subgrade.

6) The subgrade strains were integrated over the gauge length of the coil pairs and summed to calculate the compression in the subgrade layer.

7) The calculated deflections were compared with the measured deflection from the SLAVE unit or FWD.

A representative plot of the strain versus depth and the lines that are fitted to the strains is shown in Figure 4.14. The area under the dashed line is calculated in order to determine the surface deflection. A summary of the calculations for the strain/deflections measured by the Deflectometer is shown in Table 4.5. The calculated results for stations 9 and 23 are within the range of –2.4 to +9.8% of the measured values; this would be considered a good result considering the various assumptions that were made. The calculated results for station 37 show a greater variation against the measured values, the calculated values range from 20.5 to 29.0% of the measured values. A possible reason for the bigger percentage difference for the station 37 results is that the actual deflection and strain values are lower than the other two stations (approximately 0.73 versus 1.18 mm and 1151 versus 2355 and 3960 microstrain for the average strains at the top of the subgrade), and any inaccuracies in the assumptions will have a bigger effect on the computed deflections.

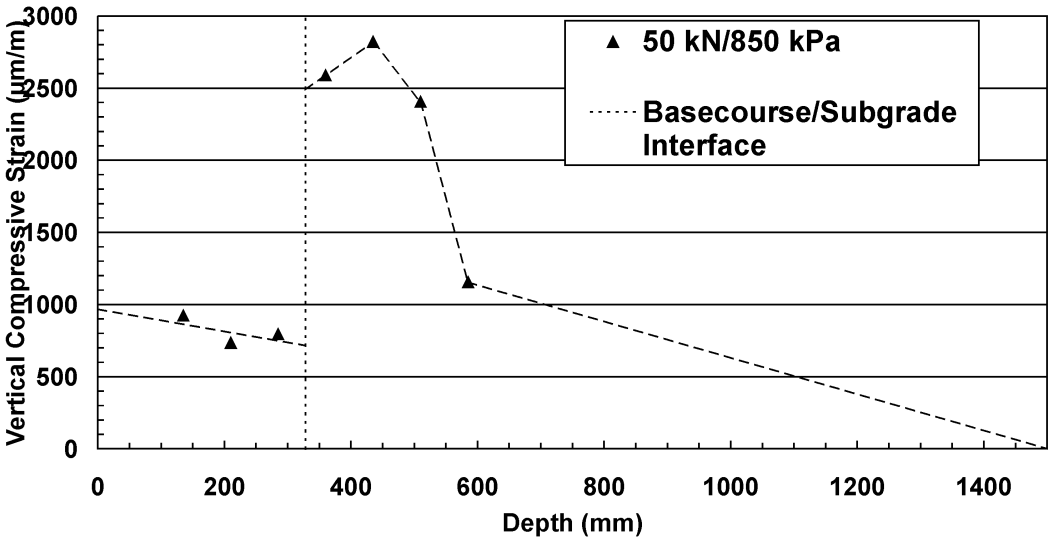

Figure 4.14 Strain profile at station 9 for 50 kN / 850 kPa wheel load at 6 km/h, PR3-0404 pavement.

The same procedure was followed for the FWD measurements, for this test the FWD weights were dropped from four different heights and the response of the εmu coils was recorded for each drop height. The FWD contractor carried out the testing in two visits to the CAPTIF facility. Due to other work requirements, the contractor was required to use two different FWD machines for the two visits, even though the visits were only 3 days apart.

A summary of the calculations for the strain/deflections measured by the FWD is shown in Table 4.6. The deflections obtained by integrating the strains from the FWD loading show a greater difference with the deflections measured by the FWD device. For this comparison, the differences are up to 25%, although most (13/16) of the differences are 15% or less and 14 of the 16 measurements have differences that are less than 0.150 mm.

In conclusion, these measurements show that the strains measured by the εmu soil strain system are realistic, and that they can be verified against an independent measurement method.

Table 4.5 Results from strain integration calculations for a rolling wheel.

Station 9			
Load/Pressure (kN/kPa)	40/650	40/850	50/850
Integrated deflection (mm)	1.155	1.205	1.388
Deflectometer deflection (mm)	1.065	1.098	1.281
% Difference	8.5%	9.8%	8.4%
Absolute difference (mm)	0.090	0.107	0.107
Station 23			
Load/Pressure (kN/kPa)	40/650	40/850	50/850
Integrated deflection (mm)	1.139	1.161	1.349
Deflectometer deflection (mm)	1.167	1.146	1.310
% Difference	-2.4%	1.3%	3.0%
Absolute difference (mm)	-0.028	0.015	0.039
Station 37			
Load/Pressure (kN/kPa)	40/650	40/850	50/850
Integrated deflection (mm)	0.855	0.860	1.039
Deflectometer deflection (mm)	0.710	0.686	0.805
% Difference	20.5%	25.3%	29.0%
Absolute difference (mm)	0.145	0.174	0.234

4.4.2 Vertical Strain Variation With Load

The relationship between load and vertical strain for each measurement point is plotted in Figure 4.15. These measurements were taken at the conclusion of the PR3-0610 test in the inner wheelpath, at station 38 and at a speed of 6 km/h. Here it can be seen that the strain increases with load at each measurement point in the pavement but the increase is not linear. The type of relationship that gave the best fit to the data was logarithmic, $y = a \times \ln(x) + b$, but due to the variation in the coefficients, it was decided not to include any curve fitting for the data. Additional strain measurements for stations 38 and 29 are included in Appendix A. It is interesting to note that the maximum strain is not recorded with the uppermost coil pair in the subgrade as expected, but in the next coil pair (z=412.5 mm).

Table 4.6 Results from strain integration calculations for the FWD.

Station 9 (old FWD)				
Drop Height	1	2	3	4
Integrated deflection (mm)	0.735	0.947	1.369	1.773
FWD deflection (mm)	0.642	0.837	1.200	1.426
% Difference	14.5%	13.1%	14.1%	24.3%
FWD load (kN)	25.3	33.2	51.8	71.7
Absolute difference (mm)	0.093	0.110	0.169	0.347
Station 23 (old FWD)				
Drop Height	1	2	3	4
Integrated deflection (mm)	0.624	0.808	1.219	1.556
FWD deflection (mm)	0.578	0.765	1.184	1.413
% Difference	8.0%	5.7%	3.0%	10.1%
FWD load (kN)	23.8	31.2	48.3	67.6
Absolute difference (mm)	0.046	0.043	0.035	0.143
Station 9 (new FWD)				
Drop Height	1	2	3	4
Integrated deflection (mm)	0.603	1.129	1.424	1.658
FWD deflection (mm)	0.502	1.023	1.324	1.550
% Difference	20.1%	10.3%	7.5%	7.0%
FWD load (kN)	20.3	42.5	57.1	70.8
Absolute difference (mm)	0.101	0.106	0.100	0.108
Station 37 (new FWD)				
Drop Height	1	2	3	4
Integrated deflection (mm)	0.473	0.811	1.034	1.216
FWD deflection (mm)	0.359	0.713	0.899	1.067
% Difference	31.8%	13.7%	15.0%	13.9%
FWD load (kN)	20.4	42.7	57.5	71.3
Absolute difference (mm)	0.114	0.098	0.135	0.149

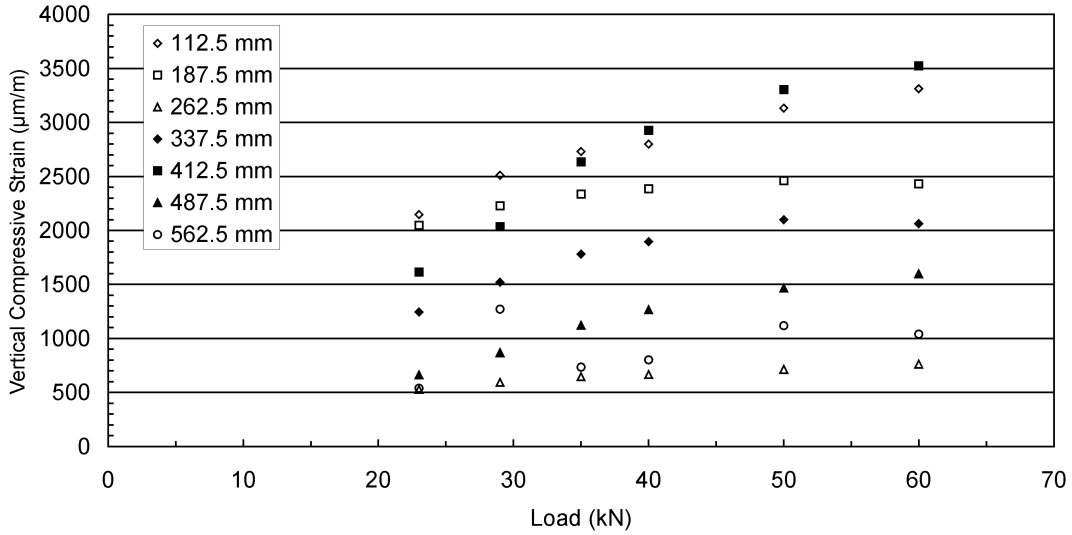

Figure 4.15 Vertical compressive strain versus load for various depths at station 38, inner wheelpath, gauges between the wheels, PR3-0610 pavement.

This could be attributed to two factors; firstly the location of the upper coil in the top pair of subgrade coils is not exactly on the interface due to the pavement construction methods employed at CAPTIF – the bottom coil in the array is placed relative to the target level for the finished surface and the subsequent coils are placed exactly 75 mm above each other, due to construction tolerances, the interface may not be at the exact height, although every endeavour is made to do so. The second factor could be that due to the aggregate particles penetrating into the top of the subgrade, there may be an intermediate transition layer which is a mix of aggregate and subgrade which has a stiffness between the stiffness of the basecourse and subgrade layers.

It is recommended that in a subsequent project, this effect is investigated by placing a coil array so that a coil pair "bridges" the transition zone between the two materials, this coil pair may be able to either determine the existence and/or extent of such a transition zone.

4.4.3 Horizontal Strain Variation With Load

The relationship between load and longitudinal horizontal strain for each measurement point is plotted in Figure 4.16 and the relationship between load and transverse horizontal strain for each measurement point is plotted in Figure 4.17.

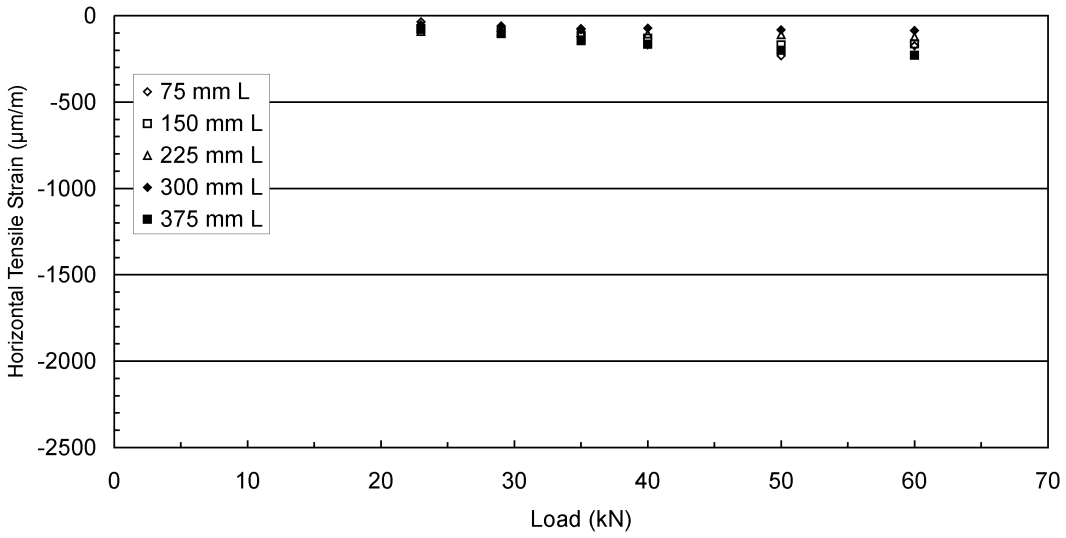

Figure 4.16 Longitudinal horizontal tensile strain versus load for various depths at station 38, gauges between the wheels, PR3-0610 pavement.

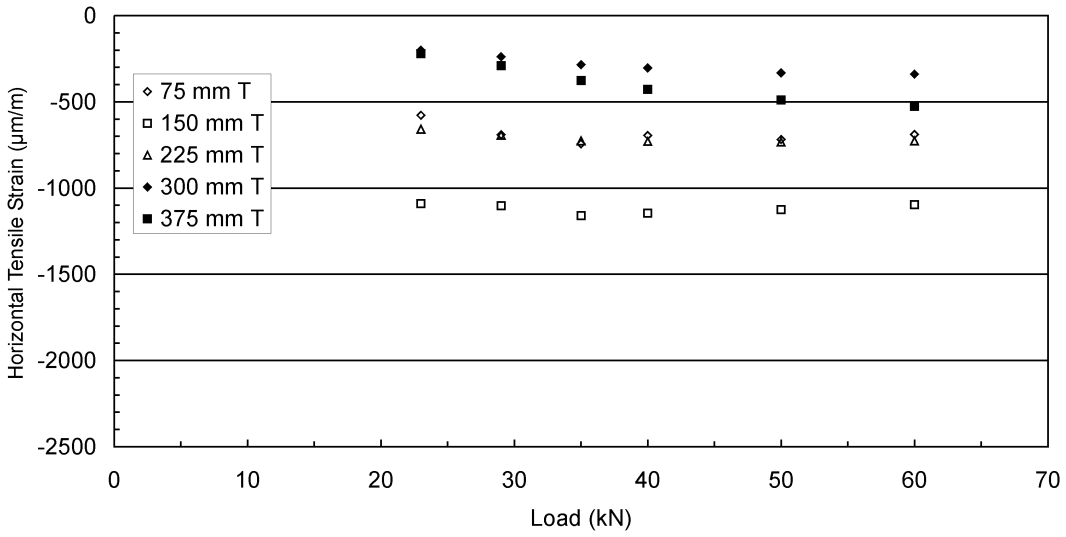

Figure 4.17 Transverse horizontal tensile strain versus load for various depths at station 38, gauges between the wheels, PR3-0610 pavement.

These measurements were taken at the conclusion of the PR3-0610 test in the 1350 mm wheelpath, at station 38 and at a speed of 6 km/h. Here it can be seen that there is a marked difference between the transverse and longitudinal strains. The longitudinal strains are smaller than the transverse strains and both show an approximately linear relationship to load. It should be remembered that the longitudinal strains undergo a reversal as the wheel approaches and departs as shown in Figure 4.18.

From a modelling perspective where the load is applied as a static load, the transverse strains should be used, as the response will be more representative of the static load case, i.e. the coil pair undergoes little or no shear reversal as the wheel moves past.

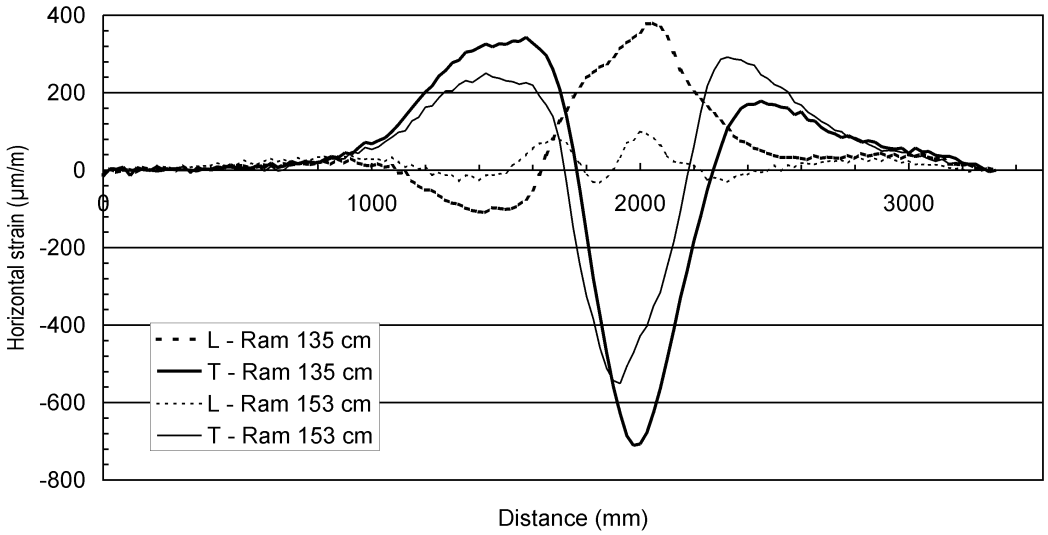

Figure 4.18 Longitudinal (L) and transverse (T) horizontal strain traces for two ram positions near the bottom of the basecourse (z=225 mm), at station 38, load = 40 kN and speed = 6 km/h.

4.4.4 The Effect of the Wheel Position on Measured Strains

A limited set of strain measurements was taken with the centreline of the dual tyre assembly over the soil strain array. The results of these measurements are plotted against the measurements taken in Sections 4.4.2 and 4.4.3 and are shown in Figure 4.19 and Figure 4.20 for the vertical and horizontal strains respectively. It is interesting to note that for all but the upper two measurements for both types of

strains, that the higher strain is measured between the two tyres. From this observation it can be concluded that for measurements in the top 150-200 mm of the granular material, the maximum values are obtained when the centre of one tyre is directly above the instrument array and for measurements at lower depths, the maximum values are obtained when the centre of the dual tyre assembly is over the instrument array.

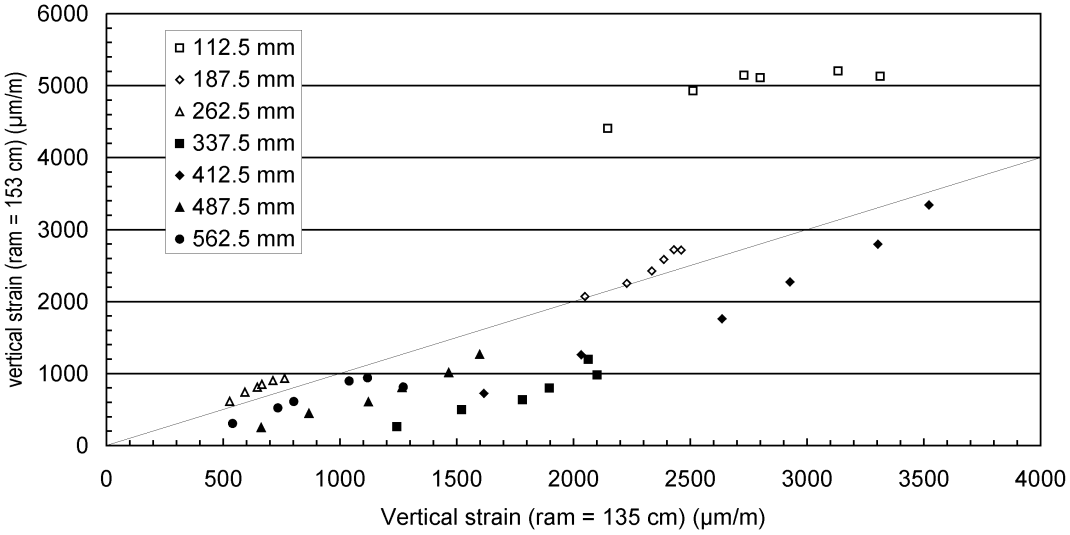

Figure 4.19 Vertical strains for gauges between the tyres and beneath a tyre, at station 38, speed = 6 km/h, measured with various loads.

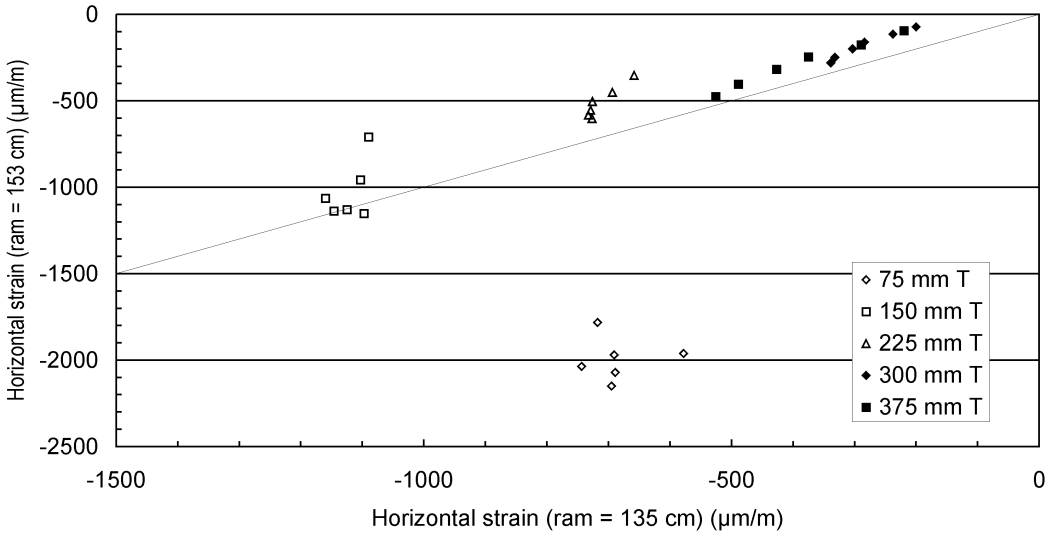

Figure 4.20 Horizontal transverse strains for gauges between the tyres and beneath a tyre, at station 38, speed = 6 km/h, measured with various loads.

By using the earlier calculations for the stress measurements in determining the angle of load spreading (approximately 60°) and the separation distance between the tyres of 125 mm, the depth at which the stress cones intersect for the two tyres is calculated to be 108 mm. Therefore, at depths in the pavement greater than 110 mm, the stresses and strains between the tyres will be influenced by both tyres.

4.5 Pavement Response to Varying FWD Loads

The strain response of the pavement to four different levels of loading by the FWD was measured. The loading plate pressures varied from approximately 300 kPa to 1000 kPa (21 to 70 kN load for the standard plate diameter of 300 mm). The central deflections (D_0) recorded under the various FWD loads are shown in Figure 4.21. The results show that the surface deflection under the centre of the loading plate, D_0, varied linearly with load. The least squares regression parameters for fitting a linear line to each dataset are given in Table 4.7. The measured vertical strains induced by different FWD load levels at the top of the subgrade are shown in Figure 4.22. The measured responses for other depths are shown in Table A.1. The least squares regression parameters for fitting a linear line to each dataset are given in Table 4.8. These results show that the vertical strain varies linearly with load as well. Boussinesq's theory states that at the surface of a body, the deflection

at the centre of the load/loaded area is proportional to the load for a given material stiffness. This would imply that the pavement structure is behaving as a linear elastic solid. When the corresponding strain measurements are analysed, the results show that at a particular point in the pavement, the vertical strain also varies linearly with load. However, the relationship between the strain measurements at different depths in the pavement is not constant, thus showing that while the response of the whole pavement may appear linear, the response within the pavement structure is non-linear with respect to load. Boussinesq's theory states that: for vertical strain, the strain is proportional to the load at a given point in the pavement structure. However, because the modulus of the material in the pavement structure is a function of the imposed stress state, the effective or apparent depth used in the solution of Boussinesq's equations for the point in question must vary to compensate for the change in modulus.

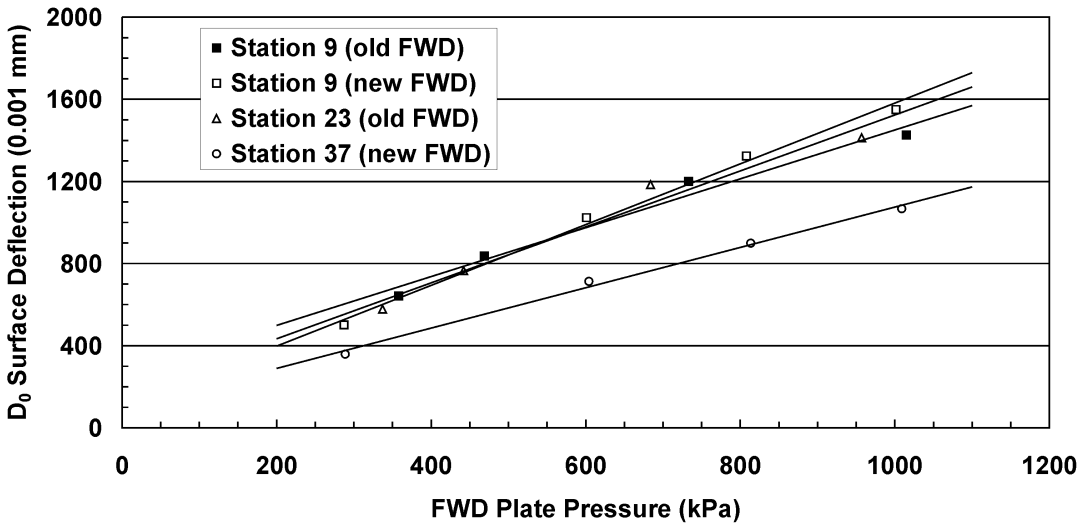

Figure 4.21 Surface deflection versus plate pressure for varying FWD loads.

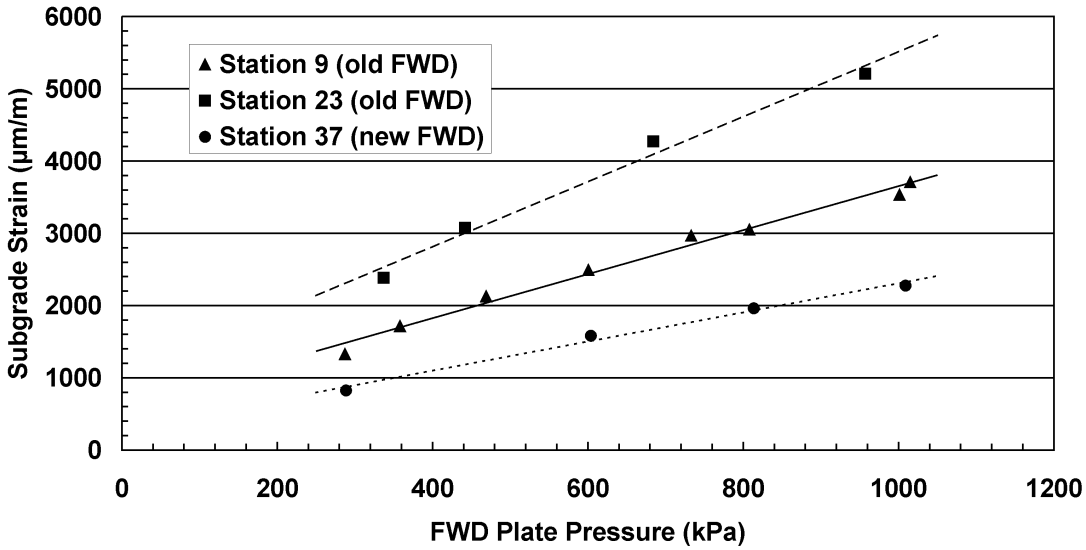

Figure 4.22 Measured strains at a depth of 337.5 mm induced by various FWD load levels (PR3-0404 pavement, 600k load cycles).

Table 4.7 Least squares regression parameters for surface deflection measurements with varying FWD loads, inner wheelpath, PR3-0404 pavement.

	Station 9 (old FWD)	Station 9 (new FWD)	Station 23 (old FWD)	Station 37 (new FWD)
Slope (0.001 mm/kPa)	1.189	1.479	1.362	0.982
Intercept (0.001 mm)	261	102	161	93
RSQ	0.977	0.994	0.971	0.995

The stresses measured at the top of the subgrade due to FWD loading are shown in Figure 4.23. The relationship between the applied surface stress and the stress at a depth of 300 mm is linear for all granular materials and applied stress levels. This data would reinforce the findings in Sections 4.3.2 and 0 that show that the centreline vertical stress distribution is a function of the depth below the surface and not a function of material stiffness.

The vertical strains measured under a rolling wheel and the FWD were compared and are shown in Table 4.9. The regression equations developed earlier were used

to determine the FWD strain in the pavement for an applied load of 40 kN and the rolling wheel strains were those that were measured after the application of 600k load cycles. The 600k load cycle data was used as the FWD measurements were also taken at this time. In the basecourse the rolling wheel strains are on average 1.47 times greater than the FWD strains. This difference can be attributed to two main reasons. Firstly, the rolling wheel was a dual tyre, so the strains near the surface will be influenced by the space between the dual tyres and secondly, the approach and departure of the wheel will cause a shear stress reversal which could influence the vertical strain measurement, while the FWD loads the pavement with a single plate and a vertical impulse. The first reason for the difference is actually counter intuitive, as it would be expected that the FWD induced strain would be greater than the rolling wheel, especially nearer to the surface.

It could also be argued that the relative rigidity of the FWD loading plate compared to the pavement allows a non-uniform stress distribution to develop under the FWD plate, in which the vertical stress at the centre of the plate is much lower than the stress near the edge of the plate. This argument could be tested by measuring the strain response of the pavement when the edge of the FWD loading plate is located above the coil array. Since the total pavement deflections are similar for the two loading mechanisms, the difference in strains in the basecourse must be compensated for by an opposite difference in the strains in the subgrade, which is indeed true because in the subgrade the wheel strains are an average of 0.84 times the FWD strains.

Table 4.8 Least squares regression parameters for vertical strain measurements with varying FWD loads, inner wheelpath, PR3-0404 pavement.

		Station		
Depth (mm)		9	23	37
112.5	Slope (um/m/kPa)	0.426	0.725	0.321
	Intercept (um/m)	252	142	175
	RSQ	0.991	0.999	0.994
187.5	Slope (um/m/kPa)	No data	0.520	0.406
	Intercept (um/m)		212	222
	RSQ		0.995	0.976
262.5	Slope (um/m/kPa)	0.322	0.443	0.366
	Intercept (um/m)	265	276	213
	RSQ	0.970	0.996	0.978
337.5	Slope (um/m/kPa)	3.045	4.509	2.020
	Intercept (um/m)	607	1008	290
	RSQ	0.987	0.985	0.990
412.5	Slope (um/m/kPa)	3.291	2.772	1.547
	Intercept (um/m)	415	-59	164
	RSQ	0.993	0.993	0.998
487.5	Slope (um/m/kPa)	3.129	No data	0.939
	Intercept (um/m)	178		410
	RSQ	0.994		0.964
562.5	Slope (um/m/kPa)	1.510	1.337	1.205
	Intercept (um/m)	84	37	119
	RSQ	0.997	0.993	0.997

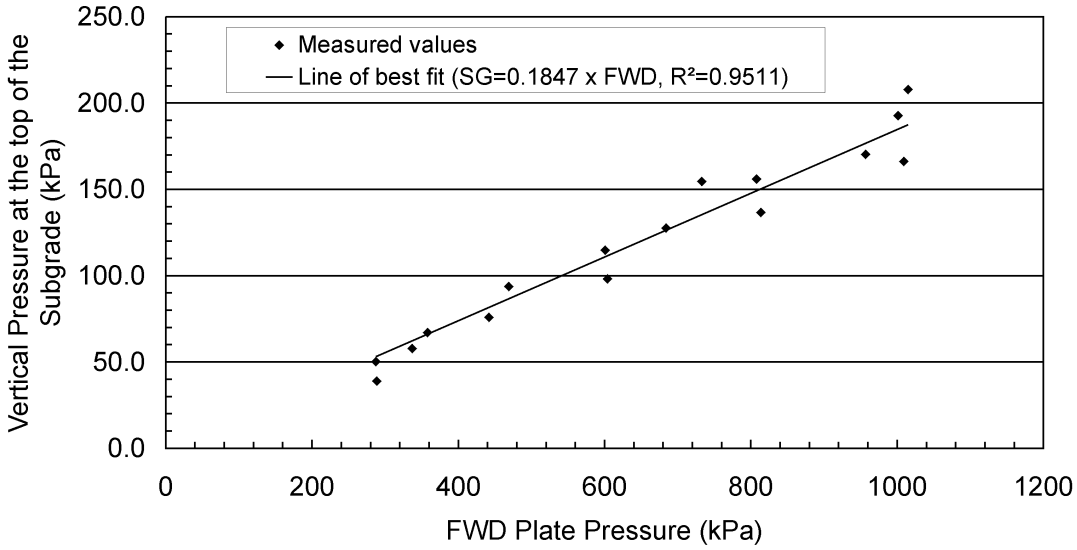

Figure 4.23 Measured stress at the top of the subgrade due to varying FWD loads.

It was found in Section 4.4.4 that the maximum strain in the subgrade was between the tyres so for this case, the rolling wheel and FWD comparison is appropriate as the strain coils are measuring the maximum vertical strains for both loading methods.

Table 4.9 Comparison of rolling wheel and FWD vertical strain measurements, PR3-0404 pavement.

Depth (mm)		40 kN wheel (μm/m)	40 kN FWD (μm/m)	$\frac{\text{wheel}}{\text{FWD}}$
112.5	Base-course	647	493	1.31
187.5		513	NA	
262.5		729	447	1.63
337.5	Sub-grade	2030	2330	0.87
412.5		2038	2278	0.89
487.5		1602	1948	0.82
562.5		706	939	0.75

4.6 In Situ Material Characterisation for Varying Loads

The measured values of horizontal and vertical stress and strain can be used to determine some in-situ properties of the pavement materials, namely the resilient modulus and Poisson's ratio.

4.6.1 Poisson's Ratio Calculations

The strain measurements taken at the end of the PR3-0610 test were used to determine the Poisson's ratio at station 29 and 38. Because the horizontal strains are determined from the co-planar coil pairs, strains from adjacent pairs were averaged to give a horizontal strain measurement at the same depth as the vertical strains. In addition to this, since vertical strains were measured with all the possible coils pair combinations; adjacent vertical strain measurements were averaged as well. This meant that the Poisson's ratio was calculated in the centre of a 75 x 75 square of material. This arrangement is shown in Figure 4.24. The Poisson's ratio was calculated for horizontal strains measured in the transverse direction only. The maximum tensile strains were used for the calculations. The calculated values for stations 29 and 38 are shown in Table 4.10 and Table 4.11 respectively. The calculated values of Poisson's ratio for the subgrade were in the range 0.18 to 0.34 with an average value of 0.25. The subgrade results showed little sensitivity to load and were comparable for the two pavement thicknesses. The Poisson's ratio between the tyres at the bottom of the granular material for the thicker pavement (Station 38) was on average 0.7. If the material was isotropic, it could be inferred that the material was dilating ($\upsilon > 0.5$) or that the material was anisotropic, where the maximum permissible value of υ_{21} is 1.0.

4.6.2 Resilient Modulus Calculations

For the PR3-0610 pavement, actual resilient modulus values can be calculated from the measured values of stress and strain. The observation that the stress varied linearly with depth was used to interpolate the stress values at the mid points between the pressure cells. This gave a vertical stress value at the same depth as the vertical strain measurement point. The calculated modulus values for the various depths are shown in Figure 4.25.

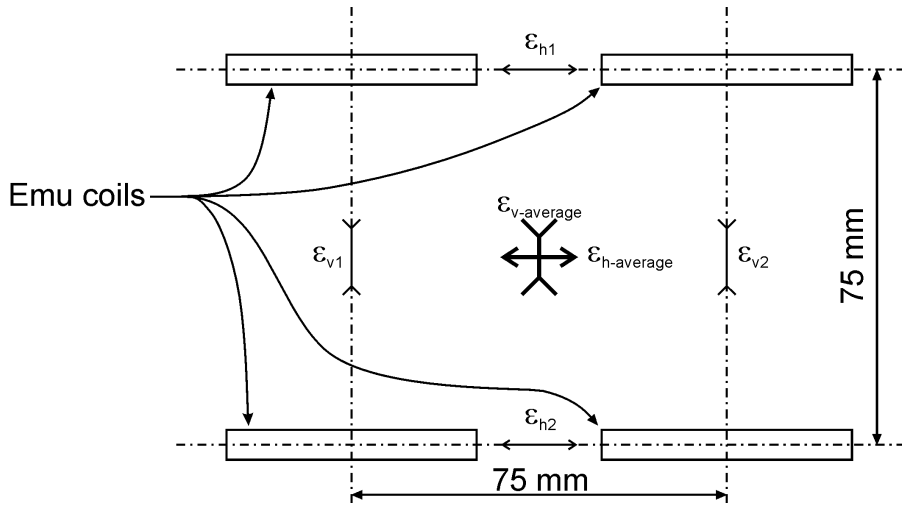

Figure 4.24 εmu coil pairs used to calculate the Poisson's ratio for stations 29 and 38, PR3-0610 pavement.

This figure shows that for the granular material the modulus varies with depth in the pavement structure and applied wheel load. This confirms that the stiffness of the granular material is non-linear. The modulus of the granular material between the tyres at a depth of 112.5 mm is low compared to the values deeper in the pavement; this can be attributed to the fact that at a shallow depth between the tyres, the major stress direction is likely to be non-vertical and thus, the vertical resilient modulus will not be the maximum value at that depth.

4.7 Response Over the Life of a Pavement

4.7.1 Resilient Strain Measurements

During the accelerated pavement loading phases of the PR3-0404 and PR3-0610 tests, vertical resilient strains were measured at various depths in the two pavements. The measurements were taken with the centre of the dual tyre assembly over the centre of the εmu coil array and with a vehicle speed of 45 km/h. The dual tyre load was 40, 50 or 60 kN depending on the stage in the loading. Plots of the strains versus laps for the segments that were constructed with the TNZ M4 granular material are shown in Figure 4.26 to Figure 4.30 and the strain values are listed in Table A.2 to Table A.6.

Table 4.10 Calculated Poisson's ratio for station 38, inner wheelpath, 1447k laps, PR3-0610 pavement.

Poisson's ratio under one tyre (ram = 153 cm)							
	Depth	Dual tyre load (kN)					
	(mm)	23	29	35	40	50	60
Base	112.5	0.33	0.34	0.33	0.36	0.32	0.35
Base	187.5	0.28	0.34	0.35	0.35	0.34	0.35
Base	262.5	0.31	0.36	0.38	0.41	0.43	0.43
Subgrade	337.5	0.29	0.28	0.31	0.32	0.34	0.33
Poisson's ratio between two tyres (ram = 135 cm)							
	Depth	Dual tyre load (kN)					
	(mm)	23	29	35	40	50	60
Base	112.5	0.49	0.46	0.45	0.41	0.37	0.35
Base	187.5	0.48	0.46	0.46	0.44	0.43	0.42
Base	262.5	0.74	0.72	0.72	0.71	0.69	0.64
Subgrade	337.5	0.18	0.19	0.2	0.21	0.21	0.23

Table 4.11 Calculated Poisson's ratio for station 29, inner wheelpath, 1447k laps, PR3-0610 pavement.

Poisson's ratio under one tyre (ram = 153 cm)							
	Depth	Dual tyre load (kN)					
	(mm)	23	29	35	40	50	60
Base	112.5	0.46	0.5	0.51	0.52	0.52	0.52
Base	187.5	0.23	0.25	0.26	0.28	0.32	0.35
Subgrade	262.5	0.22	0.24	0.26	0.27	0.32	0.33
Subgrade	337.5	0.18	0.21	0.22	0.24	0.24	0.24
Poisson's ratio between two tyres (ram = 135 cm)							
	Depth	Dual tyre load (kN)					
	(mm)	23	29	35	40	50	60
Base	112.5	0.45	0.49	0.49	0.49	0.48	0.5
Base	187.5	0.24	0.26	0.28	0.28	0.3	0.3
Subgrade	262.5	0.28	0.3	0.29	0.3	0.29	0.29
Subgrade	337.5	0.21	0.23	0.23	0.23	0.23	0.24

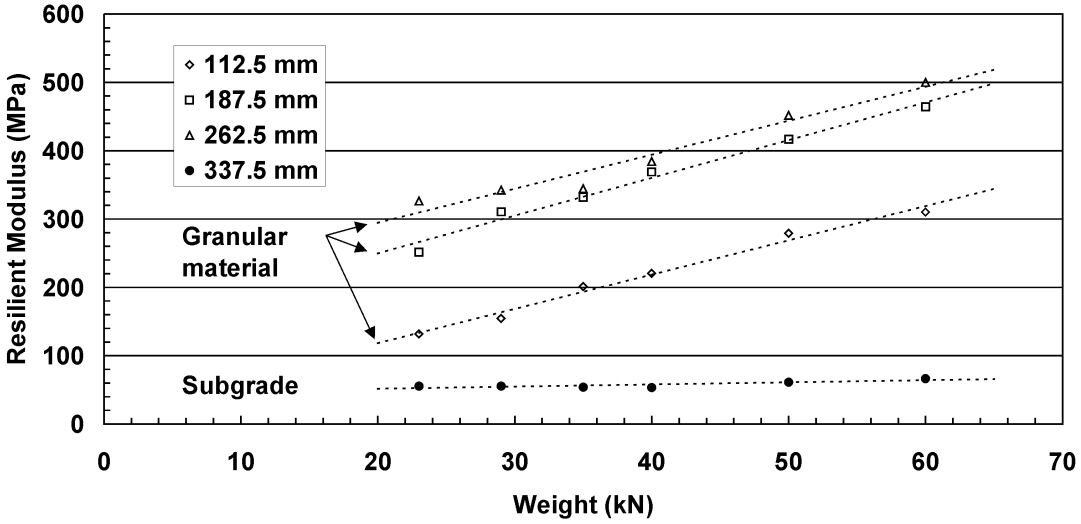

Figure 4.25 Calculated resilient modulus values for station 7 at various depths in the PR3-0610 pavement.

For the PR3-0404 pavement, the strains were reasonably constant during the 40 kN loading phase, then they increased when the load was increased to 50 kN and remained at the higher value for the remainder of the test.

The vertical strains in the PR3-0610 test showed an interesting relationship to the VSD measurements. The strains in the granular material, in the inner wheelpath, which was trafficked exclusively by the 60 kN load, were relatively constant for the majority of the test until near the end when they started to increase.

This increase in the strain was also matched by an increase in the corresponding VSD data for both stations 29 and 38, indicating that the pavement was starting to undergo Range C Shakedown behaviour, i.e. rapid failure. In the outer wheelpath, which was trafficked initially with a 40 kN load and then increased to 60 kN after 1 million load cycles, the strains again were relatively constant under the 40 kN loading and showed an increase after the wheel load was increased. Near to the end of the test, large changes in the strain values were matched by increasing rates of VSD for both stations. In Figure 4.28, it is observed that the strain near the pavement surface increased rapidly near the end of the test and this was matched with a decrease in the strains measured at the top of the subgrade. A possible explanation for this is that as the magnitude of the resilient response of the granular material increases, the stress distribution in the granular material with regards to

depth is altered, which has resulted in a decrease in the strains measured in the subgrade.

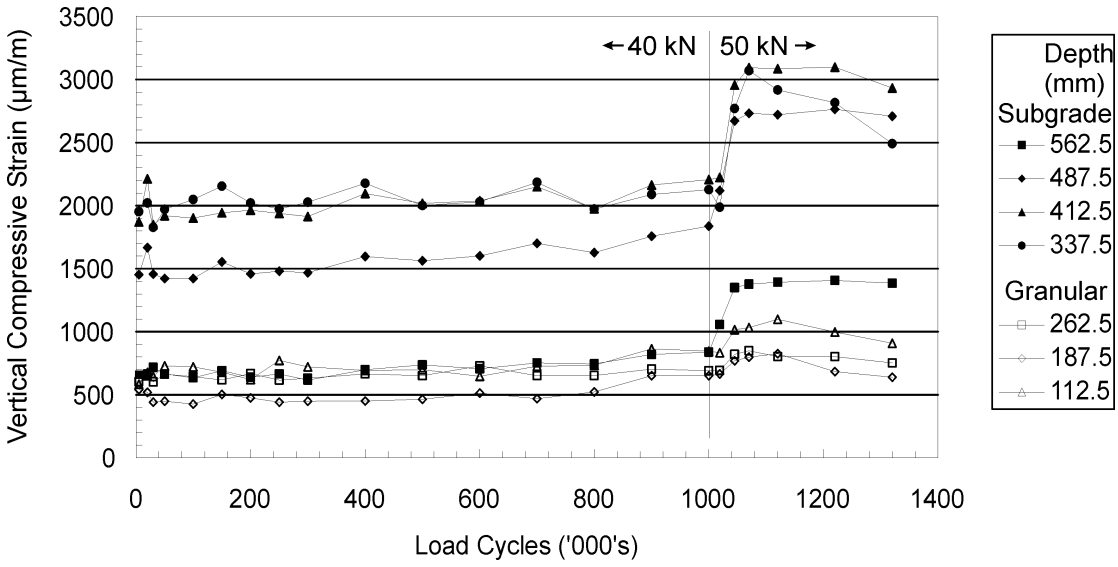

Figure 4.26 Vertical strains versus laps for Station 9, inner wheelpath, PR3-0404 pavement.

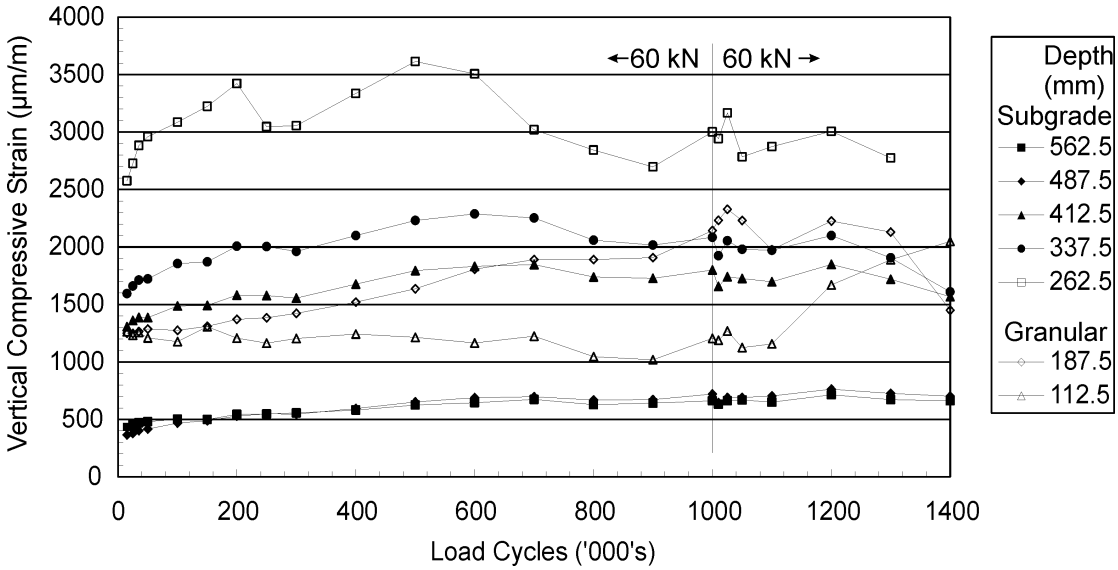

Figure 4.27 Vertical strains versus laps for Station 29, inner wheelpath, PR3-0610 pavement.

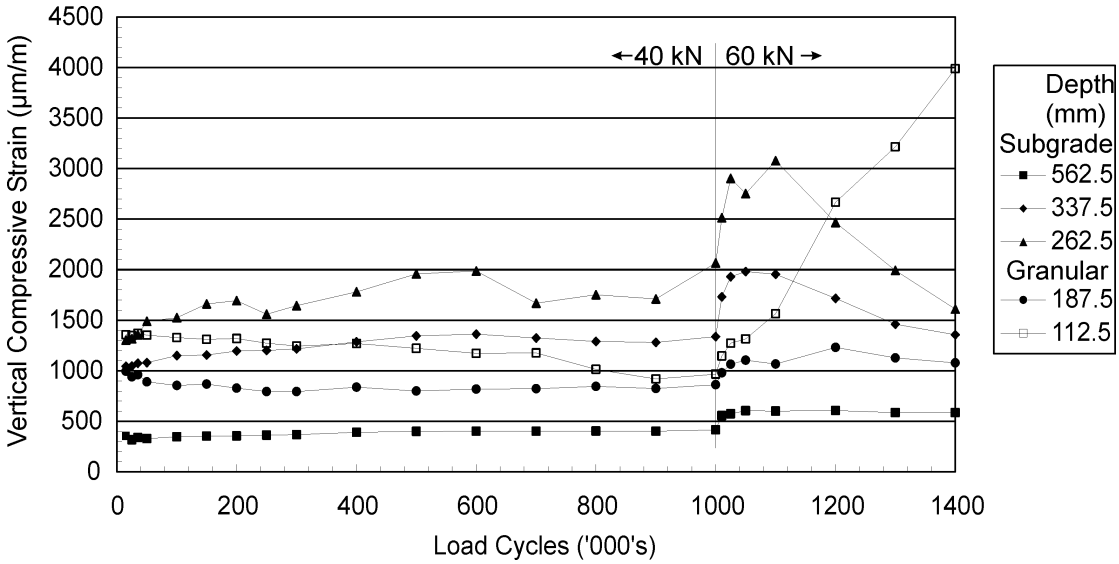

Figure 4.28 Vertical strains versus laps for Station 29, outer wheelpath, PR3-0610 pavement.

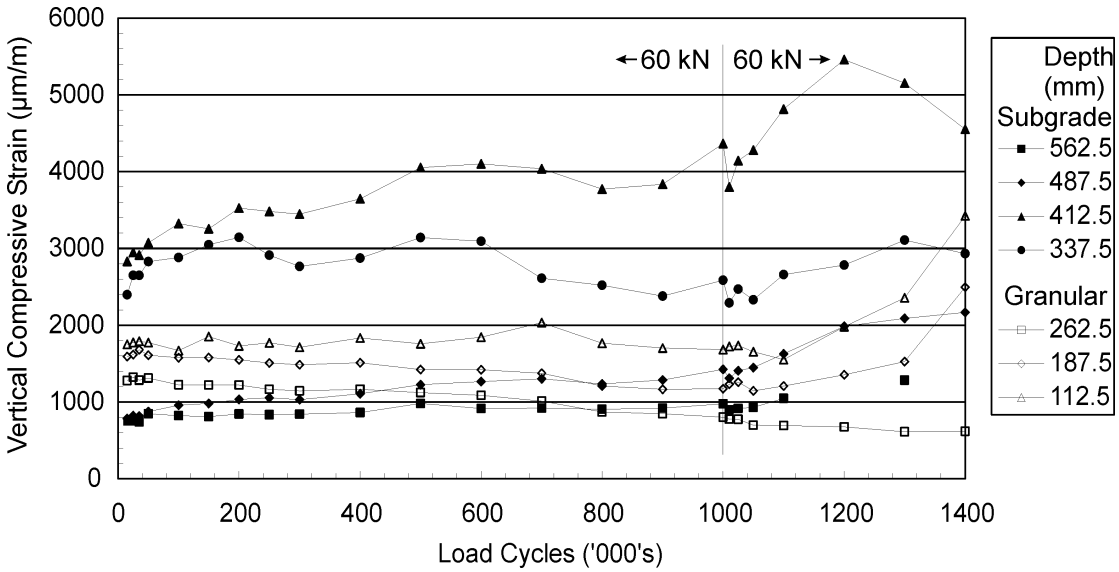

Figure 4.29 Vertical strains versus laps for Station 38, inner wheelpath, PR3-0610 pavement.

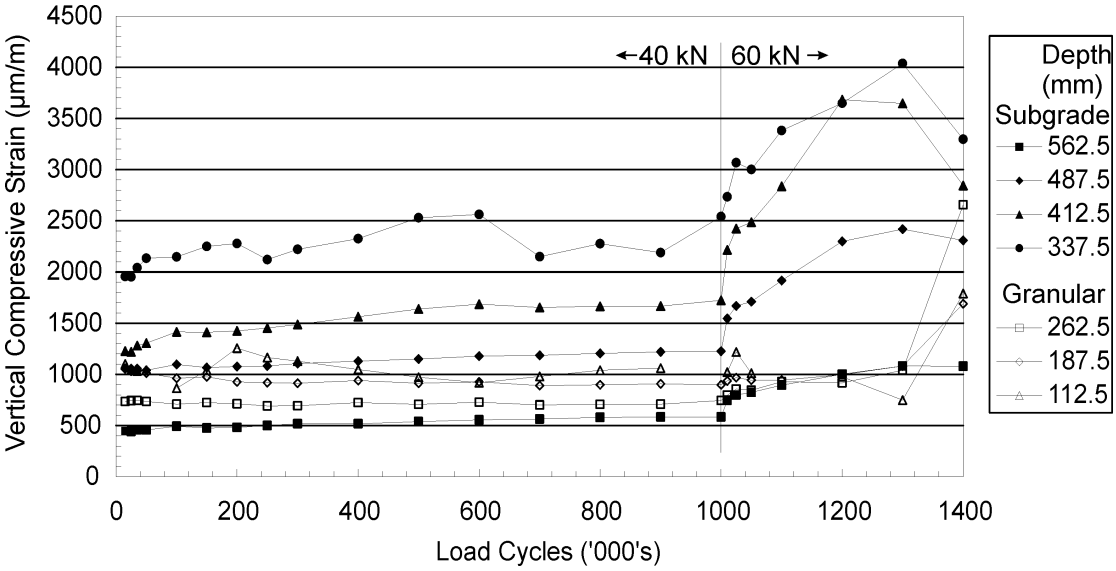

Figure 4.30 Vertical strains versus laps for Station 38, outer wheelpath, PR3-0610 pavement.

4.7.2 Resilient Stress Measurements

The resilient stress measurements taken during the PR3-0404 and PR3-0610 pavements are shown in Figure 4.31 and Figure 4.32 and the values are listed in Table A.8 and Table A.9 respectively. In both cases, the measurements are from the stress cells that were located at the top of the subgrade in the TNZ M4 segments. For the results from the PR3-0404 pavement, the stress values are reasonably constant for the two loading levels (40, then 50 kN). The results are more variable in the latter stages of the PR3-0610 pavement, although this is when the pavement is starting to show signs of accelerated failure. The average values over the accelerated testing phase for the 300 mm thick granular sections are plotted with the data from Section 0 and shown in Figure 4.33. In this figure, it can be seen that the stress measurements are in agreement with each other with respect to the effect of load.

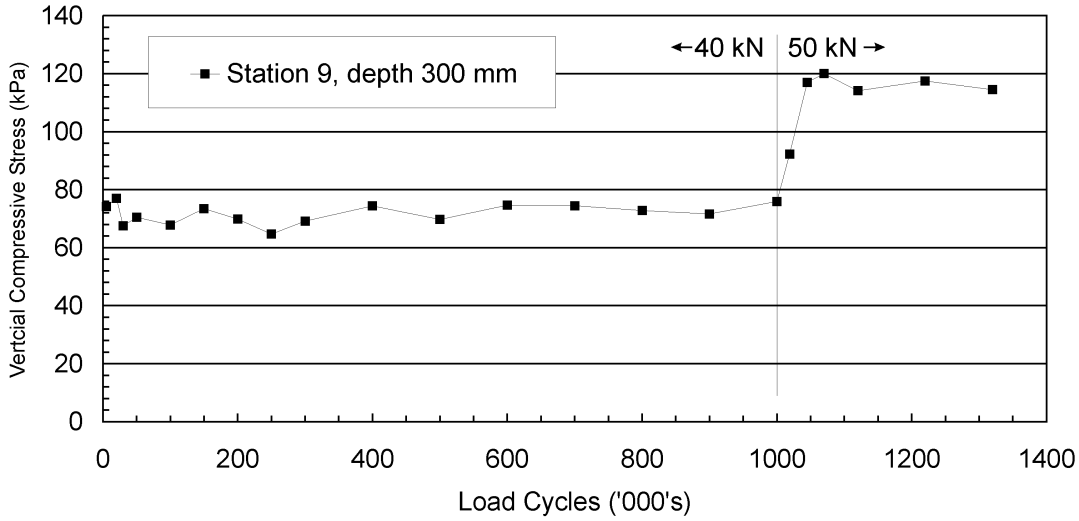

Figure 4.31 Vertical stress at the top of the subgrade versus load cycles, Station 9, PR3-0404 pavement.

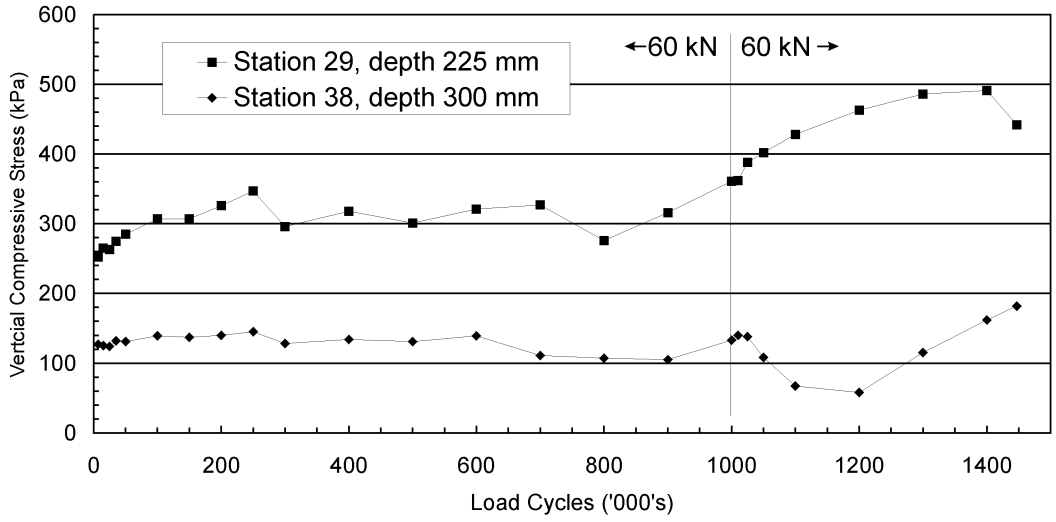

Figure 4.32 Vertical stress at the top of the subgrade versus load cycles, Stations 29 and 38, PR3-0610 pavement.

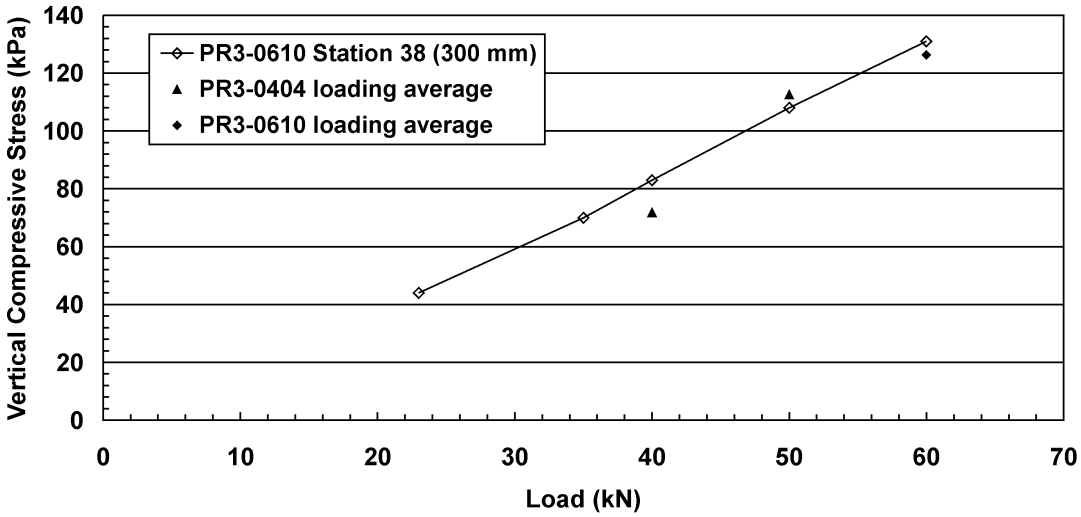

Figure 4.33 Vertical stress measurements on the top of the subgrade versus load for the 300 mm thick granular sections.

4.7.3 Resilient Modulus Calculations

Using the stress and strain measurements presented in Sections 4.7.1 and 4.7.2, the in situ resilient modulus was calculated, assuming that the measured stress was equal to the deviatoric stress in the RLT test. The calculated values for the PR3-0404 and PR3-0610 pavements are shown in Figure 4.34 and Figure 4.35 and the values are listed in Table A.8 and Table A.9 respectively. For the two pavement segments with the thickness of granular material (300 mm), the calculated resilient modulus values at the top of the subgrade are similar (approximately 35 versus 45 MPa for the PR3-0404 and PR3-0610 pavements respectively). The resilient modulus values for the thin segment (150 mm granular material) in the PR3-0610 pavement are higher, with an average of 100 MPa. One explanation for this is that the measurements were taken while the instruments were located between the wheels, so with the thin granular cover, the strain values may be lower as the maximum strain value may still be located closer to the centre of one tyre rather than directly between the tyres.

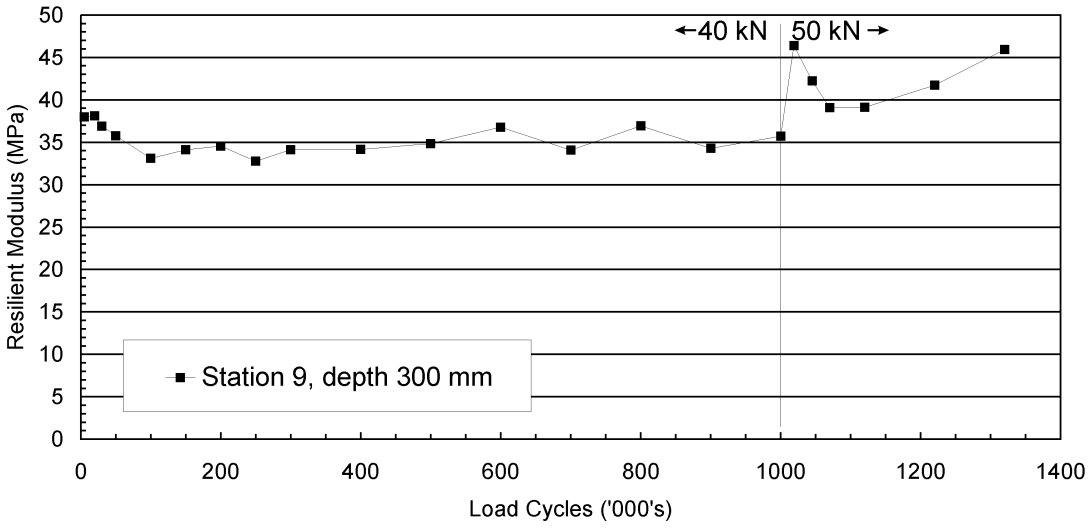

Figure 4.34 Resilient modulus at the top of the subgrade versus load cycles, Station 9, PR3-0404 pavement.

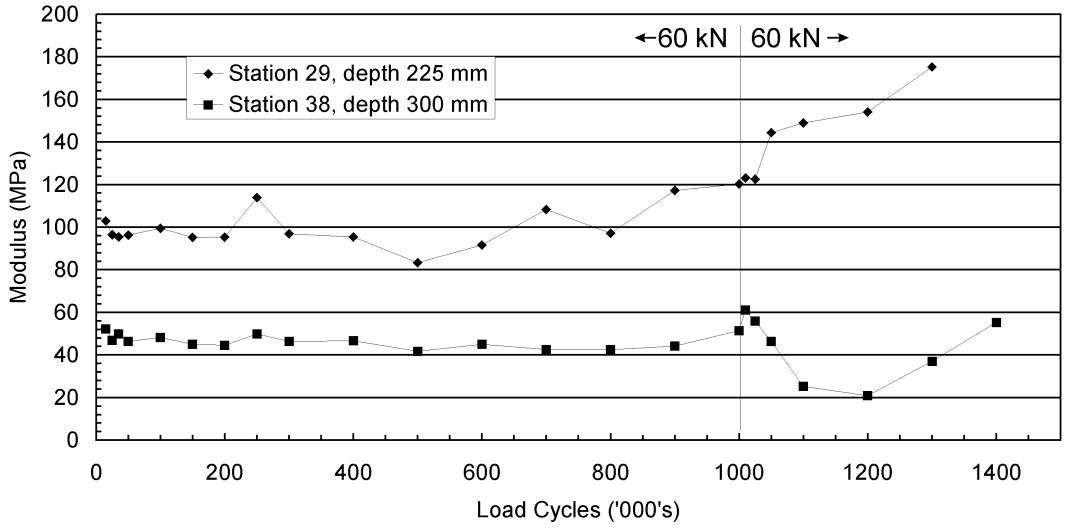

Figure 4.35 Resilient modulus at the top of the subgrade versus load cycles, Stations 29 and 38, PR3-0610 pavement.

4.7.4 Pavement Rutting

The progression of VSD for the segments that were constructed with the TNZ M4 granular material are shown in Figure 4.36 and Figure 4.37 and the VSD values are listed Table A.7 and Table A.10. In the PR3-0404 test, the VSD increases rapidly at the start of the test; this initial phase could be seen as a post-construction phase where the final compaction of the pavement is completed with the SLAVE units.

After 100,000 load cycles the rate of accumulation of VSD reduces and then increases at a linear rate until 1 million load cycles. This behaviour is apparent for both the inner (40 kN) and outer (50 kN) wheelpaths. After the application of 1 million load cycles, the load on the inner wheelpath is increased to 50 kN, whilst the load on the outer wheelpath is reduced from 50 to 30 kN in order to reduce the loading and extend the life of other sections of the pavement. In the inner wheelpath, the level of VSD increases sharply after the increase in load and then after 50,000 load cycles the rate of increase is linear until the end of the test. The VSD in the outer wheelpath continued to increase, albeit at a much lower rate after the reduction in load level.

For the PR3-0610 test the initial VSD accumulates rapidly in the first 50,000 load cycles and then the rate of accumulation reduces and is either constant or reducing until 1 million load cycles when the load in the outer wheelpath is increased from 40 to 60 kN. After 1 million load cycles the thin section in the inner wheelpath (Station 29, 200 mm, 60/60 kN) shows no change in the rate of VSD accumulation. This would be expected, as the pavement has not undergone any change in the loading. After 1 million load cycles the VSD in the thick sections of pavement (Station 38) increases at a similar rate for both the inner (40 then 60 kN) and outer (all 60 kN) loads. The implication of this is that the loading history of a "well-behaved" pavement is not relevant when determining the potential effect of an increased loading. The outer thin section (station 29, 200 mm, 40 kN) had a small amount of VSD after 1 million load cycles but when the load was increased to 60 kN the pavement started to undergo accelerated rutting.

In order to determine the relative contribution of the granular and subgrade layers to the surface rutting, trenches were excavated in the pavement at the end of the PR3-0404 and PR3-0610 tests. The trenches were approximately 500 mm wide and excavated by making two parallel saw cuts in the surfacing layer, removing the surfacing layer and the majority of the granular material by mechanical means and finally carefully removing the remaining granular material by hand to expose the top of the subgrade.

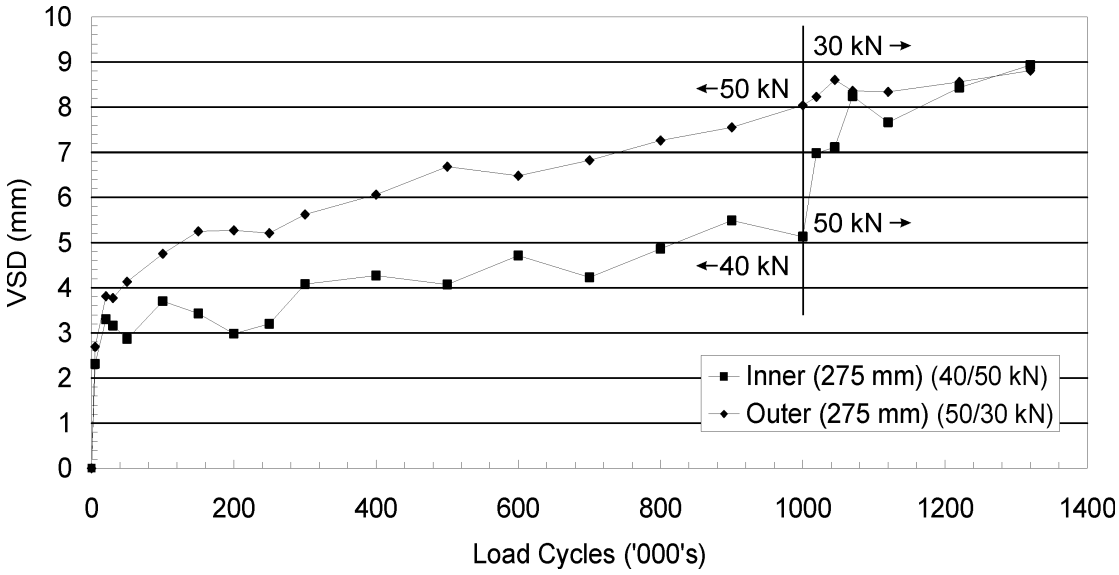

Figure 4.36 VSD versus laps for Station 9, inner wheelpath, PR3-0404 pavement.

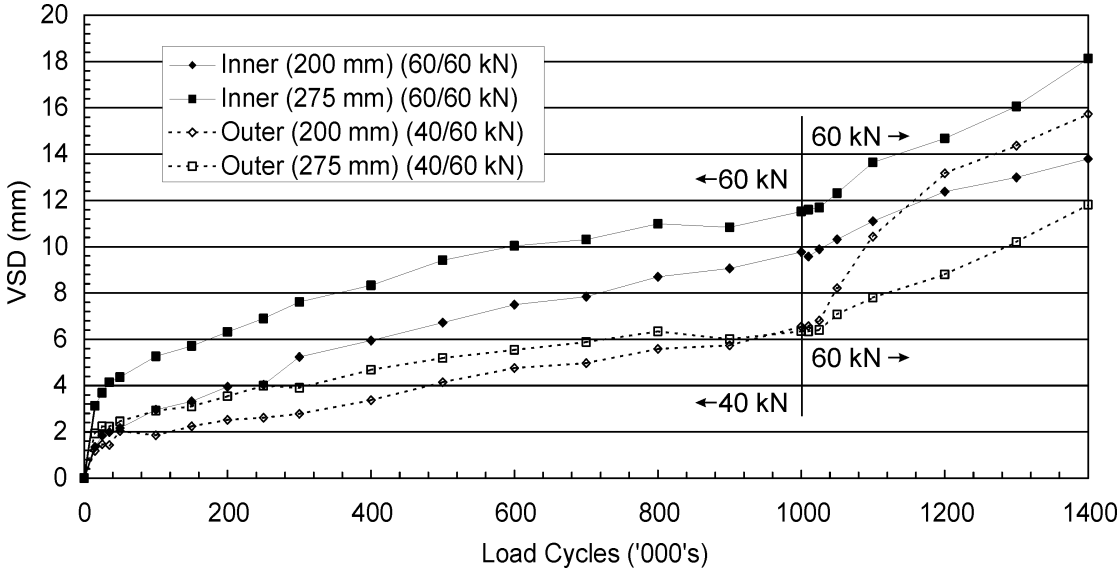

Figure 4.37 VSD versus laps for Stations 29 and 38, both wheelpaths, PR3-0610 pavement.

Transverse profile measurements were made on the surface of the pavement prior to the disturbance of the surfacing layer and again on the top of the subgrade. These profiles were then compared with the corresponding profiles taken during the pavement construction in order to determine the amount of permanent deformation or rutting in each layer.

Because of the high degree of bond that exists between the granular material and the asphalt concrete surfacing layer, it is difficult to get a sound surface on top of the granular material after the removal of the surfacing layer. The lack of a sound surface makes it difficult to determine the permanent deformation of the asphalt concrete layer, so this profile is omitted and the combined deformation of the asphalt concrete and granular layers is attributed to the granular layer.

Three trenches were excavated in segment A in the PR3-0404 pavement and two trenches in each of the thick and thin segments (D and C respectively) in the PR3-0610 pavement. The manual profile measurements were averaged over ±250 mm from the centreline of the appropriate wheelpath and are shown in Table 4.12. The granular layer in the pavement contributed on average 70% of the total amount of rutting. There were only three trenches where the contribution of the subgrade to the surface rutting was greater than 50%, and at these locations, the pavement was showing signs of accelerated failure. This implies that the granular material had lost the ability to effectively distribute the stresses imposed by the wheel, thus increasing the stress on the subgrade.

4.8 Laboratory Measurements

The results of the Permanent Deformation (PD) tests on the TNZ M4 aggregate and the subgrade materials are shown in Figure 4.38 and Figure 4.39 respectively. The stress states for the PD tests were chosen to be representative of the stress states in the pavement under the standard loading (40 kN half axle load) (Section 3.4), with the higher stress state chosen to recreate the stress state in the upper part of the relevant material and the lower stress state selected to represent the stress state deeper in the pavement structure. For the granular material it is observed that the resilient response was constant for the duration of the high stress state test and reduced as the test proceeded during the low stress state test. This effect is reversed for the subgrade material; the high stress state test has a decreasing resilient response and the low stress state test has a constant resilient response.

Table 4.12 Contribution of each pavement layer to surface rutting.

Station	Wheelpath	Thickness of granular layer (mm)	Subgrade Value (mm)	Subgrade % of Total	Basecourse Value (mm)	Basecourse % of Total	Total Value (mm)
PR3-0404 pavement							
5	inner	275	2.0	27	5.3	73	7.3
7	inner	275	4.2	63	2.5	38	6.7
8	inner	275	2.8	53	2.5	47	5.3
PR3-0610 pavement							
26	Inner	200	4.0	28	10.2	72	14.2
26	Outer	200	8.0	70	3.5	30	11.5
31	Inner	200	2.8	24	9.2	76	12.0
31	Outer	200	2.0	18	9.2	82	11.2
36	Inner	275	1.0	14	6.0	86	7.0
36	Outer	275	1.3	20	5.5	80	6.8
40	Inner	275	0.8	8	9.7	92	10.5
40	Outer	275	0.5	5	9.7	95	10.2
	Average			30%		70%	

In both materials the change in resilient modulus over the tests was less than 20%, apart from the initial part of the test when the test specimens were "bedding in". The results for the multi-stage resilient modulus tests for the subgrade and TNZ M/4 materials are listed in Table A.11 and Table A.12 respectively.

4.9 Conclusions

In this chapter, the results of a large number of pavement response tests were presented. The pavement responses that were measured were vertical and horizontal stress and strains and pavement surface deflections and deformation. A linear relationship was found to exist between the stress and strain values and the applied load, although the proportionality between the applied load and pavement response varied at different depths in the pavement. The measurements were used to calculate the in situ modulus and Poisson's ratio. The modulus showed a linear dependency on the load level and the Poisson's ratio varied according to the location in the pavement. At the bottom of the granular layer, directly beneath the wheels, the magnitude of the Poisson's ratio was greater than 0.5 indicating either dilation if the material is isotropic in nature or that the granular material is cross-

anisotropic. Both the results from the accelerated pavement testing and the PD laboratory tests showed that the resilient response remained constant if the rate of accumulation of PD was constant. Excavations at the end of the pavement testing showed that on average 70% of the surface deformation could be attributed to the granular layer in the pavement.

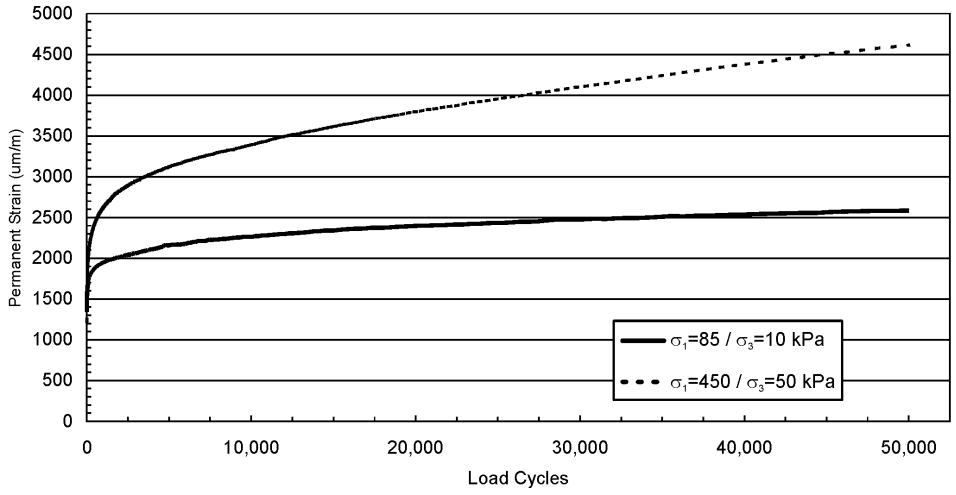

(a)

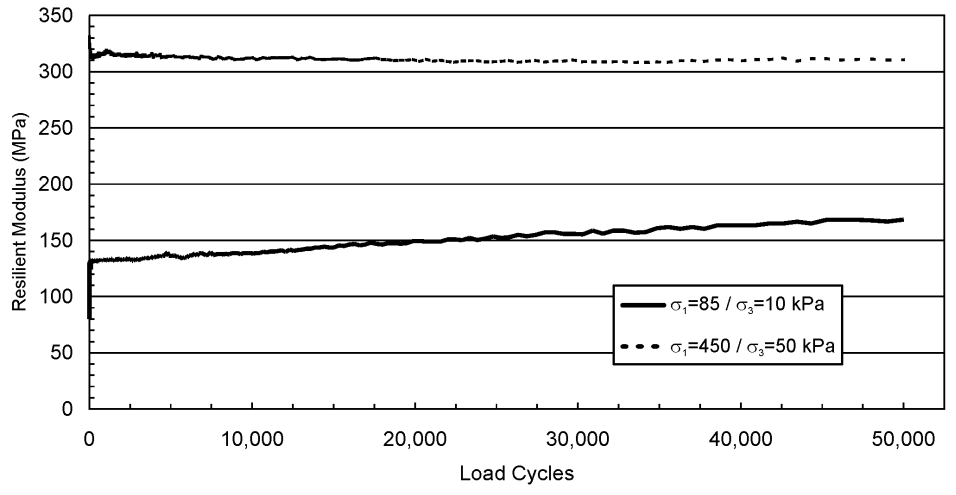

(b)

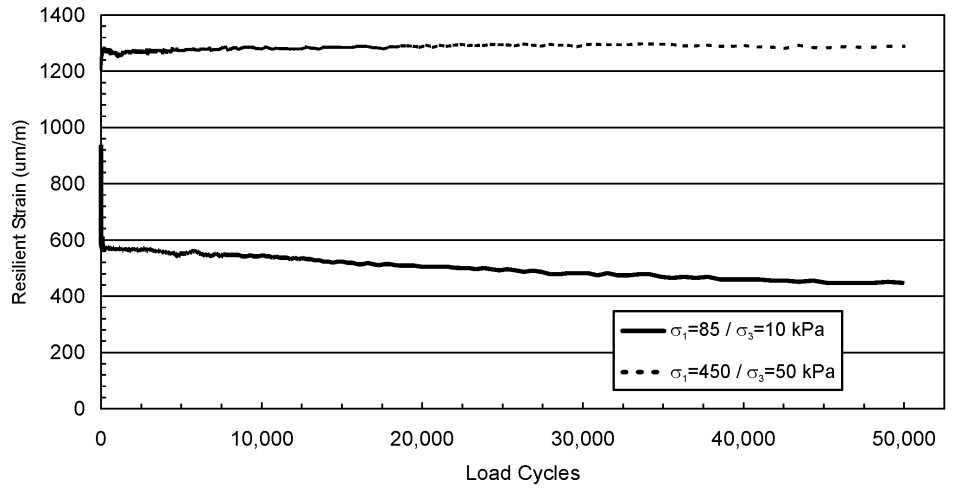

(c)

Figure 4.38 Permanent deformation RLT results for TNZ M4 granular material: (a) Permanent strain, (b) Resilient modulus, (c) Resilient strain.

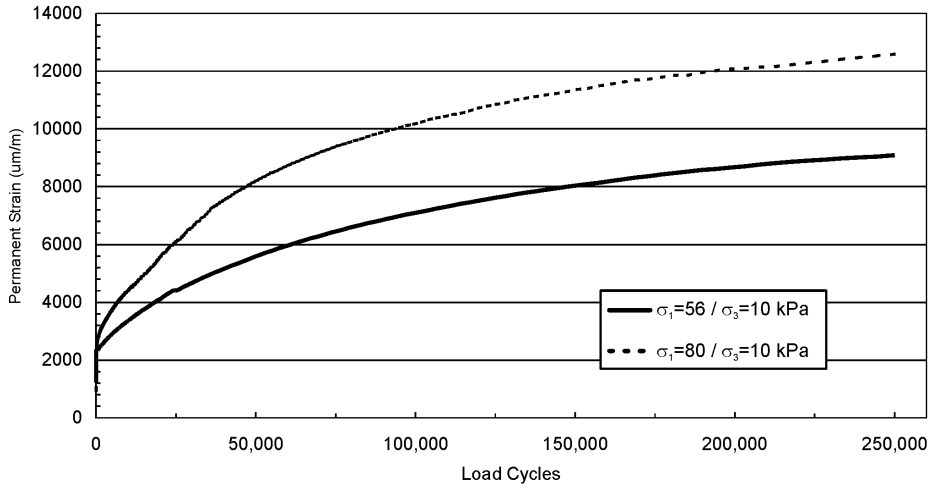

(a)

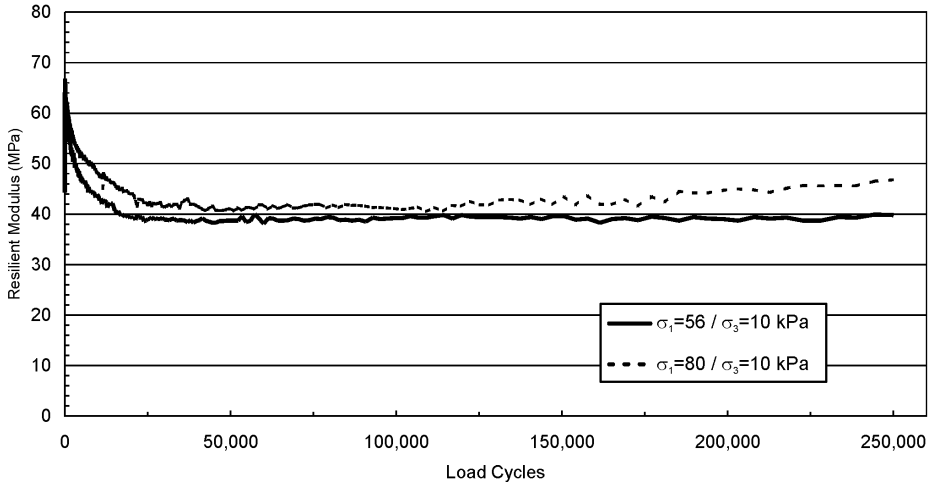

(b)

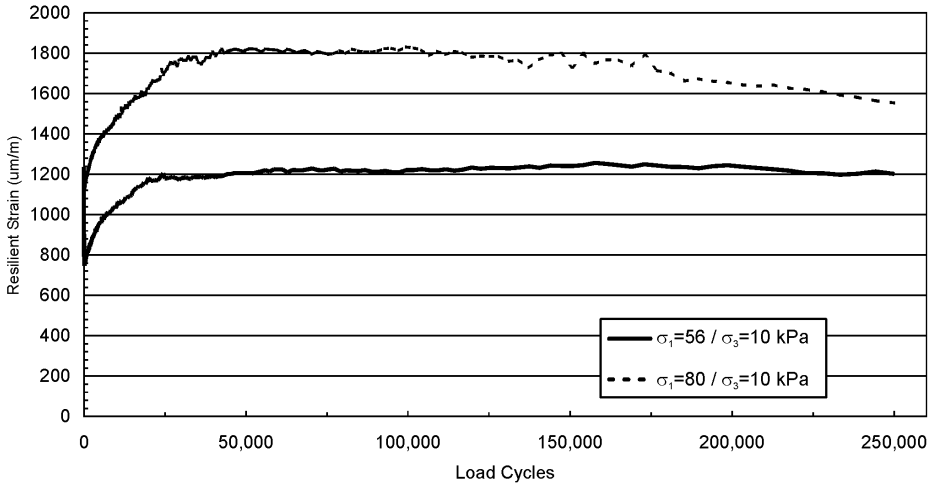

(c)

Figure 4.39 Permanent deformation RLT results for subgrade material: (a) Permanent strain, (b) Resilient modulus, (c) Resilient strain.

This page is intentionally left blank.

Chapter 5 Pavement Response Modelling

5.1 Introduction

This chapter covers the development, calibration and verification of the pavement response model. This model was used to predict the resilient response of the pavement to the monotonic static application of a single/dual tyre. The stages in developing two different pavement models, a Multi Layer Linear Elastic Theory (MLLET) and a Finite Element Method (FEM) model, are described. The stiffness of the granular and subgrade materials that are used in the models are calculated as a function of the applied and in situ stress state and then the model is solved as a first-order linear elastic continuum. The two models are checked initially against theoretical solutions to verify their initial development and then compared to the pavement response measurements collected at CAPTIF.

5.2 Model Verification

The MLLET and FEM models developed in this thesis were tested against accepted analytical solutions at appropriate stages of their development. The first verification level was to compare a single layer model with Boussinesq's solution for an infinite elastic half space. The second verification level was to compare a layered model where all the layers are assigned the same material properties with Boussinesq's solution for an infinite elastic half space. This verification stage will check the stress transfer across layer boundaries. The third verification stage is to compare the MLLET and FEM models with each other when they have identical layer, material and loading characteristics.

5.3 Material Model

The modified Shackel/Uzan model, Equation (2.20) was used to determine the stress dependant stiffness that the granular and subgrade materials used in the MLLET and FEM models. One advantage of this form of model is that if either or both of the exponent coefficients are set to zero, the model decomposes to the k-Theta (k_3=0), deviator (k_2=0) or linear elastic ($k_2 = k_3$=0) models. The material

parameters were determined by decomposing the equation into a linear form by using a log-log transformation,

$$M_r = k_1 p_a \left(\frac{\theta}{p_a}\right)^{k_2} \left(\frac{\tau_{oct}}{p_a} + 1\right)^{k_3}$$

$$\log\left(\frac{M_r}{p_a}\right) = \log(k_1) + k_2 \log\left(\frac{\theta}{p_a}\right) + k_3 \log\left(\frac{\sigma_{oct}}{p_a} + 1\right) \tag{5.1}$$

which has the form

$$Y' = a + b_1 X_1 + b_2 X_2 \tag{5.2}$$

A three variable least squares regression (Edwards 1976) was used to determine the three *k* coefficients. This particular model was chosen because of the reasons given in section 2.6.1 and since the Repeated Load Triaxial (RLT) equipment in the laboratory did not have the capability to measure radial strains, a model that required volumetric strains for the determination of the material parameters was not suitable. The applied stress states and resilient modulus values from the RLT tests are shown in Table A.11 for the subgrade and Table A.12 for the basecourse. The coefficients for the resilient modulus equations are listed in Table 5.1. The goodness of fit for the two models is shown in Figure 5.1 for the basecourse material and in Figure 5.2 for the subgrade material. The goodness of fit for the basecourse is very good with a R-squared value of 0.995, but the fit is not as good for the subgrade material, which has a R-squared value of 0.855. The absolute variations between the measured and calculated resilient modulus values for the subgrade are less than 10 MPa, which is approximately 10% of the magnitude of the measured values. Although the goodness of fit is reasonable, the absolute variations are close to the accuracy/repeatability limits of the RLT system, considering that the RLT system used in this research used an external axial displacement measurement system.

If an asphalt concrete layer was used in a pavement model, it was represented as a linear elastic material with an assumed modulus of 2000 MPa.

Table 5.1 Parameters for Modified Uzan Resilient Modulus model for the basecourse and subgrade materials.

	Basecourse	Subgrade
k_1	1.3131	1.1438
k_2	0.7600	0.4644
k_3	-0.3068	-2.2663
p_a	100 kPa	100 kPa
R^2	0.994	0.855

5.3.1 Limits on Modulus Values

The RLT resilient modulus test determines the modulus for a range of stress conditions, however care must be taken when modelling as the calculated stress conditions used to calculate the modulus might be outside the range of stress conditions used in the RLT test. This is more likely to be an issue in the granular material at points that are outside the cone of influence of the loaded area where the stress state may be lower than the RLT conditions.

For the granular material, the minimum modulus value determined from the RLT test was 107 MPa when the confining stress was 5 kPa and the deviatoric stress was 65 kPa. As the overall stress state tends to a limit of zero, the modulus calculated for a minimum stress value of 1 kPa for each of the confining and axial stresses is 9 MPa. A contour plot of resilient modulus values for different combinations of axial and confining stress states is shown in Figure 5.3. This shows that the maximum probable value for the resilient modulus is likely to be about 900 MPa. If the limit argument that was put forward by Kramer (1996) is used, then monotonic shear test results from Arnold (2004), shown in Figure 5.4, for the TNZ M/4 aggregate give minimum elastic moduli of 23, 40 and 36 MPa for confining pressures of 25, 50 and 75 kPa respectively. These values were averaged to give a lower modulus limit of 33 MPa. Thus, when the calculated resilient modulus was less than 33 MPa, the value was set to equal 33 MPa.

The lower limit of the resilient modulus from the RLT tests for the subgrade was 68 MPa, at a confining pressure of 16 kPa and a deviatoric stress of 55 kPa. The lower limit of the calculated values of the resilient modulus is 22 MPa when the mean stress is 1 kPa in an isotropic stress state.

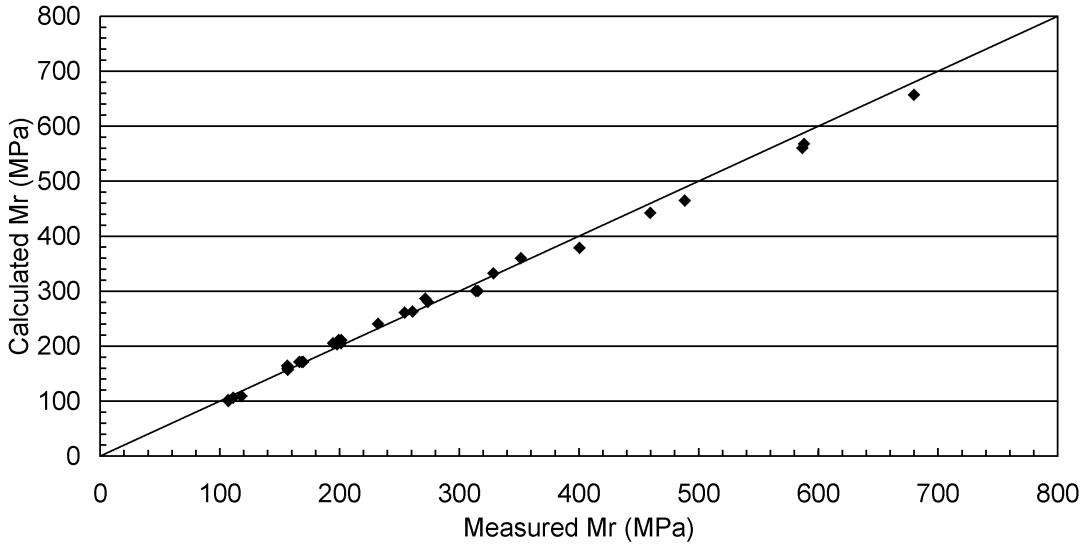

Figure 5.1 Calculated versus measured resilient modulus for the basecourse material.

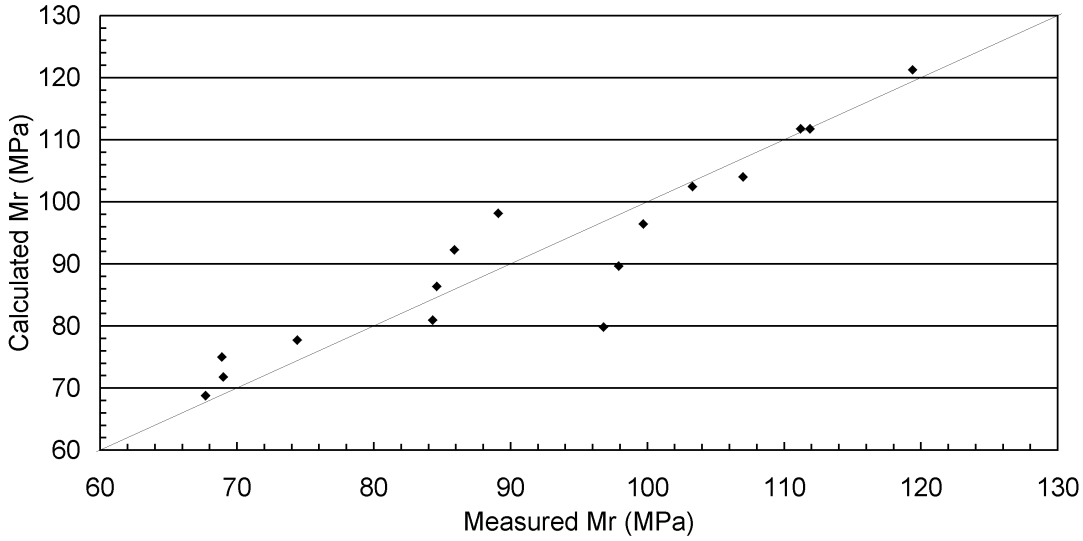

Figure 5.2 Calculated versus measured resilient modulus for the subgrade material.

Monotonic shear results for the subgrade material were not available, so the lower limit was set at 20 MPa. A contour plot of subgrade resilient modulus values for different combinations of axial and confining stress states is shown in Figure 5.5.

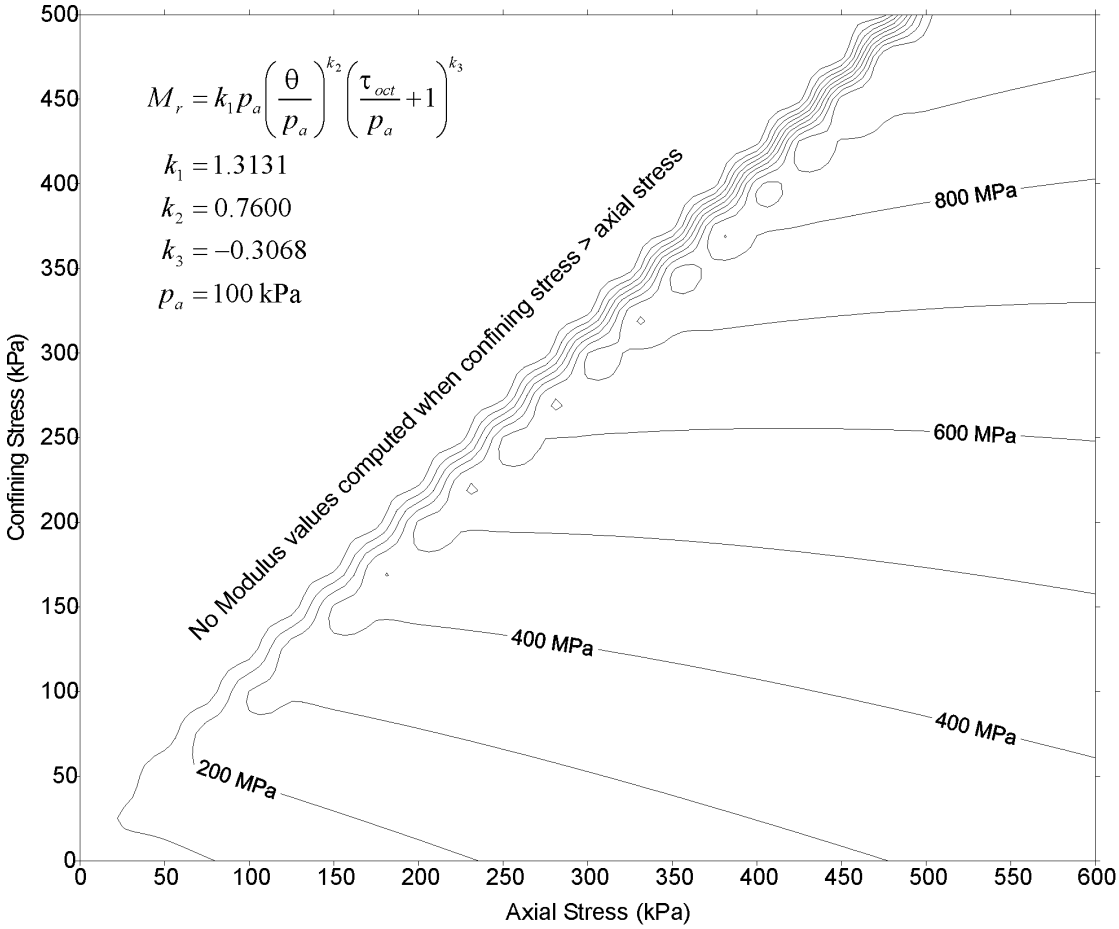

Figure 5.3 Basecourse resilient modulus contours for the Uzan model.

This figure shows that the subgrade material is a stress softening material: the material becomes softer as the stress level increases.

5.3.2 Initial Stresses

The at rest or initial stresses in the pavement should be considered when determining the resilient modulus, as the conditions under which the RLT test is conducted and the model parameters are subsequently determined include the at rest or cell confining pressure. Due to the existence of residual horizontal stresses (Section 2.9) and the assumed value of 3 for K_0, it was decided that a single value of 2.0 t/m³ for the unit mass of the overburden would be adopted. Typical values for the density of asphalt concrete, aggregate and silty-clay are 2.4, 2.2 and 1.8 t/m³ respectively and since the granular layer is relatively thin, small deviations from the actual values would not unduly effect the resulting value.

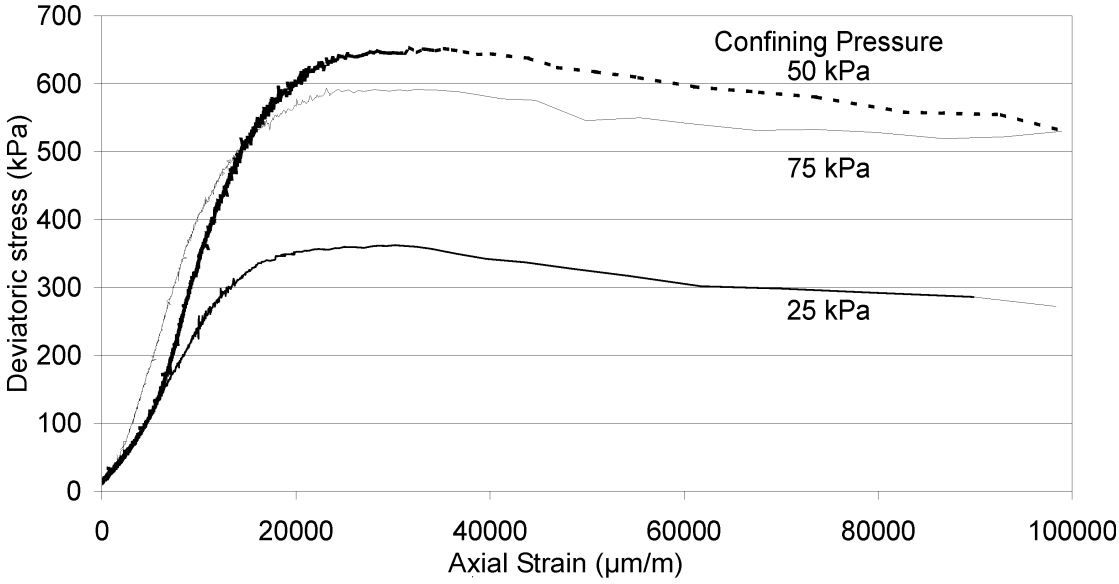

Figure 5.4 Monotonic shear test plots for basecourse material (Arnold 2004).

The adoption of a single value would also simplify the computation of the initial stresses. At a depth of 300 mm in the pavement, the estimated initial stresses will be:

$$\begin{aligned}\sigma_{v_o} &= \gamma \times g \times h \\ &= 2.0 \times 9.81 \times 0.3 \\ &= 5.9 \text{ kPa} \\ \sigma_{h_o} &= K_0 \sigma_{v_o} \\ &= 3 \times 5.9 \\ &= 17.7 \text{ kPa}\end{aligned}$$

The prediction of tensile stresses at the bottom of the granular layer is a recognized problem in modelling granular pavements, however the consideration of residual horizontal stresses will partially compensate for this. Additional compensation for the predicted tensile stresses can be obtained by accounting for the matric suction of the partially saturated granular materials. Practical evidence of this has been observed during the excavation of pavements at CAPTIF: blocks of aggregate with dimensions of approximately 300 x 200 x 200 mm could be picked up without the blocks disintegrating. The blocks would only break apart after the application of a moment or shear force. This would indicate the presence of matric suction in the material, although the magnitude is unknown.

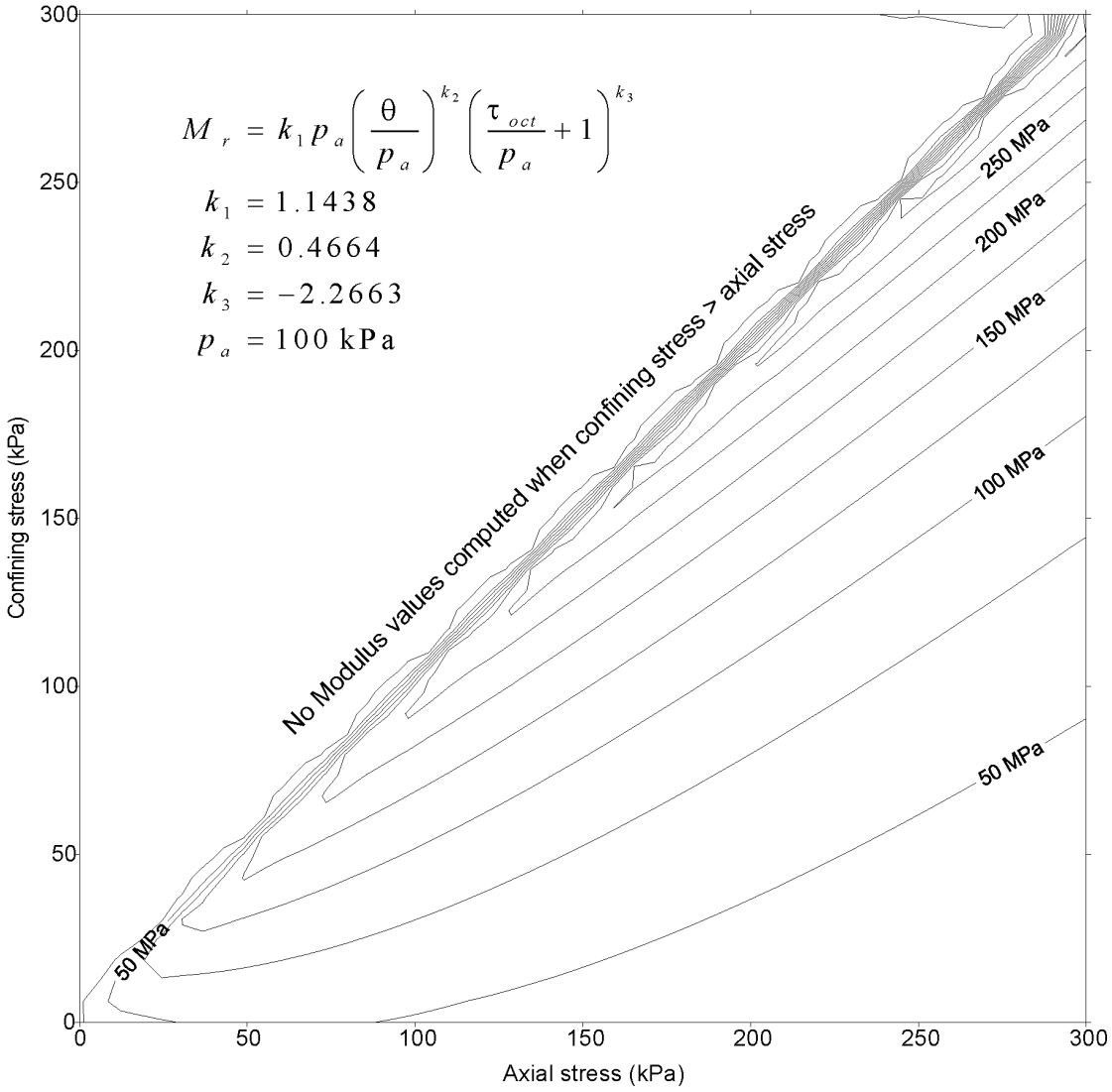

Figure 5.5 Subgrade resilient modulus contours for the Uzan model.

From the sum of the values of suction presented in Section 2.5.3 and the residual compaction/consolidation stresses, it could be conceivable to have a confining stress state in excess of 100 kPa at the bottom of the granular layer. If the sum of the residual stress, matric suction and the horizontal stress due to loading is greater than zero (i.e. compressive), then the material will not have gone into a tensile failure state. The effect of the matric suction is not included in the model formulation, with the expectation that tensile horizontal stresses will be predicted, but offset by the matric suction in reality.

5.3.3 Limits on Stress Values

In order to limit the calculation and subsequent effect of unrealistic stiffness values, checks were implemented to detect two different stress states. The two stress states are: the existence of high values of octahedral shear stress when the vertical stress caused by the applied load is low and when the net vertical stress caused by the initial stresses is greater than the vertical stress caused by the applied load.

When the vertical stress caused by the applied load was less than 5 kPa at any point within the pavement, the octahedral shear stress term in Equation (2.20) was set to a value of zero. The effect of setting the octahedral shear stress term to zero eliminated any shear effects created by the static confining stresses when the influence of the applied load was low. This condition would only be activated at points outside the load cone. When the net vertical stress caused by the stresses due to the overburden was greater than the vertical pressure applied by the load, the octahedral shear stress term was also set to a value of zero. This condition would be true when the value of K_0 is greater than one and at lower depths in the pavement where the overburden stresses increase and the load induced stresses decrease with increasing depth. The effect of setting the octahedral shear stress term to zero is to reduce the *Modified Uzan* stiffness model to the *K-Theta* stiffness model.

5.4 Loaded Area

When the model is formulated as either a non-linear axisymmetric FEM or a MLLET model, the modeller is restricted to using one loaded area. For the FEM approach, superposition is not valid to combine multiple load areas, as the influence of the load in each part is not recognised by the other parts, thus not allowing the combined stress state to be used to determine the stiffness of the material. In the instance of the MLLET model, only one stiffness value can be assigned to each layer, therefore removing the ability to accurately model the stiffness variation beneath and between multiple load areas. Therefore it was decided to use a single loaded area for the MLLET and axisymmetric FEM models, the contact pressure was the same that was calculated in Section 4.3.2 and the radius was calculated as a function of the load and contact pressure. For a 40 kN dual tyre load with a contact pressure of 366 kPa, this resulted in a radius of:

$$p = \frac{F}{A}$$

$$A = \frac{F}{p}$$

$$= \frac{40{,}000}{0.366}$$

$$= 109{,}290 \text{ mm}^2$$

$$A = \pi r^2$$

$$r = \sqrt{\frac{109{,}290}{\pi}}$$

$$r = 187 \text{ mm}$$

where

p = contact pressure (MPa)
F = half axle load (N)
A = area (mm^2)
r = radius loaded area (mm)

5.5 Multi Layer Linear Elastic Model

The historical method of using linear elastic models is to define the model with three layers. The three layers represent the structural asphalt concrete layer, the granular base layer and the subgrade. A single set of material characteristics is defined for each layer (modulus and Poisson's ratio). The material characteristics could be based on; assumed values, the experience or knowledge of the user, previously published values, values determined from laboratory tests or field tests. When a thin surfaced unbound flexible pavement is analysed in this manner, inaccuracies can exist in the solution when a single constant value is used to represent the non-linear properties of the granular and subgrade materials. One method that allows for the non-linearity of the materials is to divide the layer in question into a number of sub layers, each with a different modulus value. This approach can account for the variation in modulus with depth, but not in the horizontal direction.

The computer program Circly was selected for the MLLET model in this research. It has evolved from software developed at CSIRO (Harrison et al. 1972; Wardle

1977). In the current version of Circly (v5.0), a Graphical User Interface (GUI) steps the user through the creation of a pavement model. When the model is solved, an ASCII text file is created and passed to a command line program for solving. Another ASCII text file is created by the command line program that contains the user specified responses and this file is read by the GUI and displayed to the user.

The reasons for choosing the Circly computer program for the MLLET model were: (a) it is the pavement analysis program recommended for use in the Austroads Pavement Design Guide (AUSTROADS 2004a), and (b) it is widely used in New Zealand and Australia. The European Commission project on Advanced Models for Analytical Design of European Pavement Structures (AMADEUS) (FEHRL 2000) compared a number of MLLET programs and concluded that these programs generally gave similar answers to each other and that both MLLET and FEM programs under-estimated the vertical stresses and strains in the pavement.

5.5.1 Stage One Circly Verification

For the Stage One verification, a pavement model was created in Circly v5.0 with the parameters listed in Table 5.2. The following responses were checked on the model centreline: surface deflection and vertical stress and strain at a depth of 300 mm. The results from the Circly analysis and the analytical solution are shown in Table 5.3. There is no difference between the Circly and analytical solutions. An additional check was done to determine the effect of the concrete pavement tank. The Circly model was altered to include a rigid boundary at a depth of 1500 mm; this change was made to simulate the concrete tank. The analytical solution was determined by subtracting the calculated vertical displacement in an infinite half space at a depth of 1500 mm from the surface displacement. The results are also shown in Table 5.3. The inclusion of the concrete tank has a noticeable effect on the surface displacement (-9%) and a negligible effect on the vertical strain (1%) and vertical stress (3%) at a depth of 300 mm.

Table 5.2 Parameters for verifying Circly with elastic theory.

Parameter	Value
p (MPa)	0.366
r (mm)	187
E (MPa)	100
ν	0.35
Anisotropy factor, *n*	1
Depth (mm)	∞

Table 5.3 Results for initial Circly verification.

Response	Infinite halfspace		Rigid boundary	
	Circly	Theory	Circly	Theory
Surface Deflection (mm)	1.201	1.201	1.094	1.069
Vertical Stress (MPa) (z=300 mm)	0.1423	0.1423	0.1427	
Vertical Strain (μm/m) (z=300 mm)	1398	1398	1413	

5.5.2 Stage Two Circly Verification

A three layer Circly model with a rigid bottom at a depth of 1500 mm was created and compared with the single layer model with a rigid base for the Stage Two verification. The layer thicknesses were 25, 275 and 1200 mm. The interface conditions were defined as full contact with no slip. The load and material properties were the same as the Stage One verification model. The results are shown in Table 5.4 and show an interesting problem: while the surface deflection is the same for the one and three layer models, the stress and strains for the three layer model are approximately 15 % less than the corresponding values for the single layer model. The difference is greater closer to the surface and reduces with increasing depth.

A number of additional Circly analyses were performed with varying numbers of layers and layer thicknesses. The results of these analyses show that for an arbitrarily fixed analysis point in the pavement, the computed stress or strain take one of two values. If the analysis point is in the uppermost layer, then the results

are equal to the values obtained from the single layer model. If the analysis point is in the second or subsequent layer, then the results are a constant percentage less than the values obtained from the single layer model. In all cases, the surface deflection remained constant.

The only rational explanation for this anomaly is in the formulation and numerical solution of the Bessel functions used to transfer the load between the different layers. Further analysis of this problem with the computer programs BISAR and ELSYM5 showed that this problem is unique to Circly. However, both BISAR and ELSYM5 have limitations that make them unsuitable for use in this research, namely a maximum of five layers and limited to isotropic materials. Circly permits an unlimited number of layers and allows the user to specify the degree of cross-anisotropy, therefore it was decided to continue using Circly in this research, but to flag any significant differences between the FEM and Circly analyses.

Table 5.4 Results for single and three layer Circly comparison.

Response	Single Layer Model	Three Layer Model
Surface Deflection (mm)	1.094	1.094
Vertical Stress (MPa) (z=300 mm)	0.1427	0.1236
Vertical Strain (μm/m) (z=300 mm)	1411	1194

5.6 Multi Layer Non-linear Elastic Model

A Multi Layer Non-linear Elastic (MLNLE) model of a CAPTIF pavement was constructed using Circly. The model was constructed by creating 30 layers, with the stiffness of each layer specified as a function of the stresses at the mid depth of each layer. The coefficients for the non-linear resilient modulus or stiffness models are those listed in Table 5.1. A value of 0.5 was used for the anisotropic factor *n*. The non-linear solution was found using an automatic iterative approach. A Microsoft Visual Basic for Applications (Excel) program was written to loop through the iterative process of creating the input file, running the command line program, reading the output file, recalculating the material stiffness and determining the change in the material stiffness from the input and calculated

moduli (error function). Once the error function is within the specified tolerance the loop is exited. After each iteration the input moduli, calculated vertical and horizontal stress, vertical strain and calculated moduli are written to a summary file. A summary of the key parameters is also written to the excel spreadsheet. The process is illustrated in Figure 5.6. The program can automatically work through a number of different pavement models.

For a nominal pavement design of: 25 mm of asphalt concrete, 275 mm of granular material and 1200 mm of subgrade, a number of different analyses were done to examine the effect of the stiffness of the asphalt concrete. Two different values of stiffness were used, 2000 and 4000 MPa. In addition, the asphalt concrete was removed and the thickness of the granular layer was increased to 300 mm to compensate for the removal of the asphalt concrete. The load conditions correspond to the measurements taken when the FWD was dropped on top of the εmu instrumentation in the PR3-0404 test. The results of the FWD analysis are given in Table 5.5 and show that the surface deflection remains almost unchanged (less than 2% reduction), but the vertical stress at the top of the subgrade is reduced by 13% if a stiff surface layer is used. At equivalent depths in the granular layer, the vertical stress values for the two asphalt concrete models are on average 10 (2000 MPa) and 14% (4000 MPa) less than the values for the full depth granular model. The vertical strain at the top of the subgrade decreased by 10% for the asphalt models compared to the granular model.

These results suggest that the inclusion of a thin stiff surfacing layer will not reduce the surface deflection, but the vertical stress 300 mm below the surface is reduced by 13%. One possible explanation of this is that the materials are all modelled as linear elastic materials with no failure criteria, therefore from a modelling perspective, the thin surfacing layer can act like a membrane supported on a foundation with a relatively low stiffness (the granular layer). In the model the surfacing layer is then able to transfer a larger proportion of the applied vertical load out horizontally through the thin layer of asphalt concrete whilst being subjected to significant curvature and deflection, which is caused by the low level of support provided by the underlying layers.

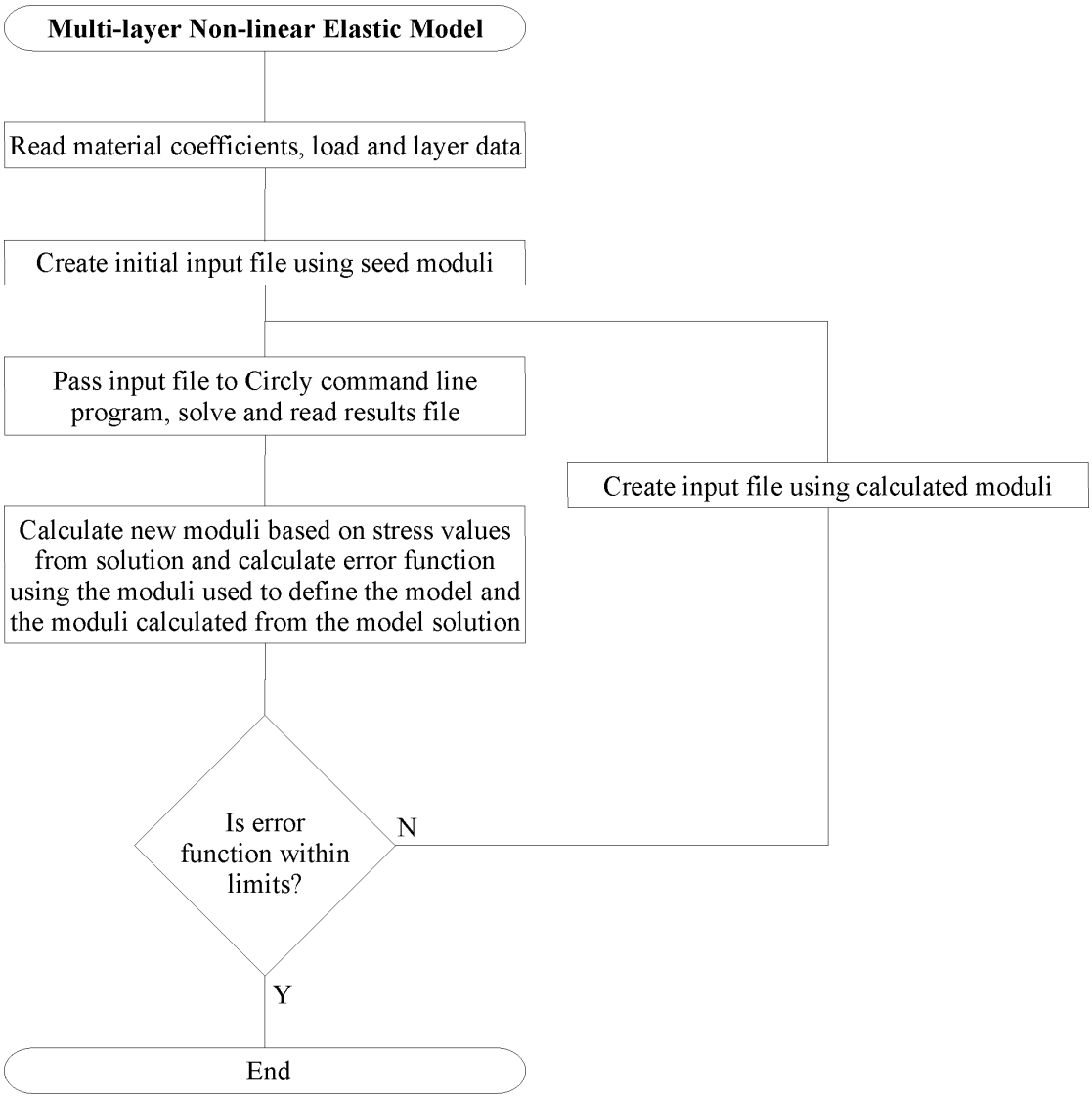

Figure 5.6 Modular Flowchart for MLNLE model.

It is the experience of the writer, that a section of thin asphalt concrete material can be pulled apart relatively easily by hand, especially when a small moment is applied to the material. This would indicate that the material has little tensile capacity when acting as a membrane, therefore it would seem that there is little potential to transfer the vertical force outwards in the horizontal direction.

Thus, it is proposed that when an unbound granular pavement is surfaced with a thin asphalt concrete layer, it is modelled with the thickness of the asphalt concrete layer added to the thickness of the unbound granular layer and there is no distinct asphalt concrete layer. When a pavement is surfaced with a chipseal, no allowance should be made for the thickness of the chipseal.

Table 5.5 Results for non-linear calculations considering the influence of the surfacing layer, *n*=0.5.

	No AC	2000 MPa AC	4000 MPa AC	Non-linear FEM – no σ_3	Non-linear FEM
Asphalt Concrete thickness (mm)	0	25	25	0	0
AC Modulus (MPa)	-	2000	4000	-	-
Basecourse thickness (mm)	300	275	275	300	300
Load radius (mm)	150	→			
Contact Pressure (MPa)	0.358	→			
Surface Deflection (mm)	0.803	0.788	0.782	0.947	0.606
Vertical Strain at top of SG (z=325 mm) (μm/m)	1287	1168	1140	1640	1285
Vertical Stress at top of SG (z=325 mm) (MPa)	0.059	0.052	0.050	0.085	0.085
Measured FWD surface deflection (mm)	0.642	→			
Ratio Calc/Meas Deflection	1.250	1.228	1.218		
Backcalculated Deflection (mm)	0.643	0.642	0.642		
Vertical Strain at top of SG (z=325 mm)[1] (μm/m)	1029	951	936		
Ratio initial/final SG strain	1.250	1.228	1.218		
Vertical Stress at top of SG (z=325 mm) (MPa)	0.059	0.052	0.050		

[1] Depth corresponds to the mid-height of the top subgrade layer which was 50 mm thick

5.6.1 MLNLE Model Backcalculation

Even though an iterative process using a stress dependent stiffness model was used to create a stress dependent pavement model, the model is still a multi-layered linear elastic model. Using the principles put forward by Odemark, that the stress or strain at a point in the pavement is related to the ratio of interlayer stiffnesses of the structure above the point in the pavement, then if the stiffness of the overall model is scaled proportionally, the response will be scaled by the same amount. Thus, by scaling the stiffness of each layer by the same proportion, the system response will change by the same proportion. Ullidtz's suggestion of a non-linear backcalculation procedure that adjusted the k_1 or scalar term of a non-linear material model, such as Equation (2.17) can be utilised in the framework outlined above.

The ratio of a particular response from a solution obtained by using the procedure outlined in Figure 5.6 to a response obtained from a field measurement can be calculated and the scalar coefficients of the constitutive models for the granular and subgrade materials can be multiplied by this ratio.

$$k_1' = \frac{y_{model}}{y_{measured}} \cdot k_1 \qquad (5\ 3)$$

where

y_{model} = a response calculated by the model
$y_{measured}$ = the same response measured in the field
k_1 = scalar coefficient of constitutive model
k_1' = adjusted scalar coefficient

If a fixed modulus asphalt concrete layer is incorporated in the model, then the modulus of this layer should also be adjusted by the field/calculated ratio as well in order to maintain the proportionality of the results. If the model is solved again using the adjusted scalar coefficients, then the model and measured responses should be equal. The modular flowchart for this process is shown in Figure 5.7.

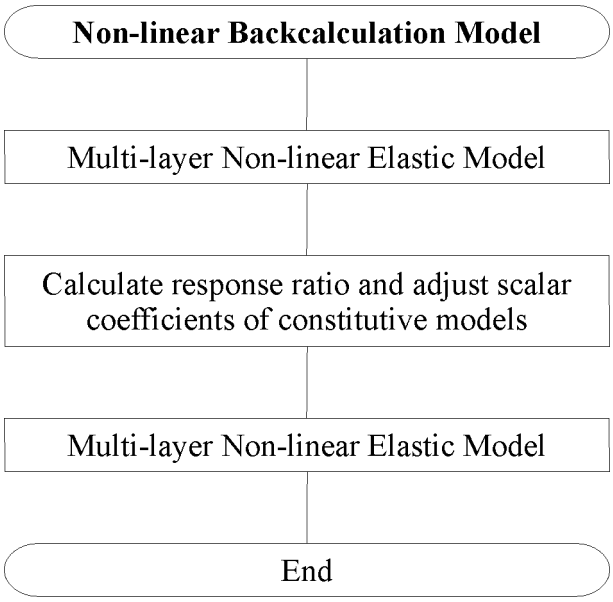

Figure 5.7 Modular Flowchart for MLNLE backcalculation model.

The response that is compared can be a surface deflection or strain value(s) as the underlying stress equation (Equation (2.6)) determines the stress distribution as a function of position. Normally the only response that is readily available is a surface deflection, usually obtained from a FWD test.

The stress and strain instrumentation installed in CAPTIF pavements allows these alternative responses to be used in the backcalculation of the properties of the pavement structure. The results of an analysis conducted using this procedure are given in Table 5.5. The results show that after the scalar coefficients have been adjusted, the central deflection of the model matches the measured deflection and the ratio of the initial and final strains is the same as the ratio of initial and final deflections. The vertical stress values remain unchanged. The results of the analysis of the pavements that incorporated an asphalt concrete layer were included as a comparison, even though the use of an asphalt concrete layer had previously been discounted.

This approach would have some benefits for the backcalculation of FWD results as the pavement response is still controlled by the laboratory derived non-linear material characteristics. The process outlined above determines the shift factor between the laboratory and field conditions and does not rely on seed values or limits imposed by the user. However due to the problems found earlier with the

stress transfer across the layer interfaces, the accuracy of the results may be questionable. This inaccuracy may be mitigated if Circly is used for any forward calculations using the "shifted" material properties. In addition, reasonably accurate layer thickness values would be required as well as some indication of the non-linear properties of the materials in order to fully realise the potential of this approach.

5.7 Finite Element Method Model

The general-purpose Finite Element Method (FEM) program ABAQUS/Standard was chosen for the FEM modelling. While ABAQUS/Standard has extensive libraries of element and material definitions, the option exists for the user to create user defined material models and elements. The ability to create user material definitions and the availability of the program were the two reasons for choosing the software.

General purpose FEM software, such as ABAQUS is written in the traditional manner of solid mechanics, that is tensile forces/displacements are positive and compressive forces/displacements are negative. The FEM work reported in this thesis is based on the geotechnical approach which uses the opposite sign conventions, i.e. tensile forces/displacements are negative and compressive forces/displacements are positive. The results from the FEM work have been translated to the geotechnical convention where required.

The creation of FEM models in ABAQUS/Standard can either be done with an ASCII text file created by the user or from within ABAQUS/CAE, a graphical user interface covering model creation, solution and visualisation of the results. This research was started prior to the release of ABAQUS/CAE so the models created for this research were created as ASCII text files. ABAQUS/CAE was used to view the results. Both 2D axisymmetric (2D) and three-dimensional (3D) models were created during the course of the research. The 2D and 3D models were used to model the pavement response due to loading by the FWD and dual tyre assembly respectively. The 2D formulation was chosen for the FWD loading because of the reduced computational requirement that is associated with an axisymmetric formulation and the ability of the model geometry to accurately represent the

loaded area. The 3D formulation was chosen for the dual tyre assembly, as the model geometry would allow the two tyres to be modelled by two separate load areas. By using two planes of symmetry, the computational requirements could be reduced to a quarter of those required for a full 3D model. Details of the loaded area and the planes of symmetry are shown in Figure 5.8.

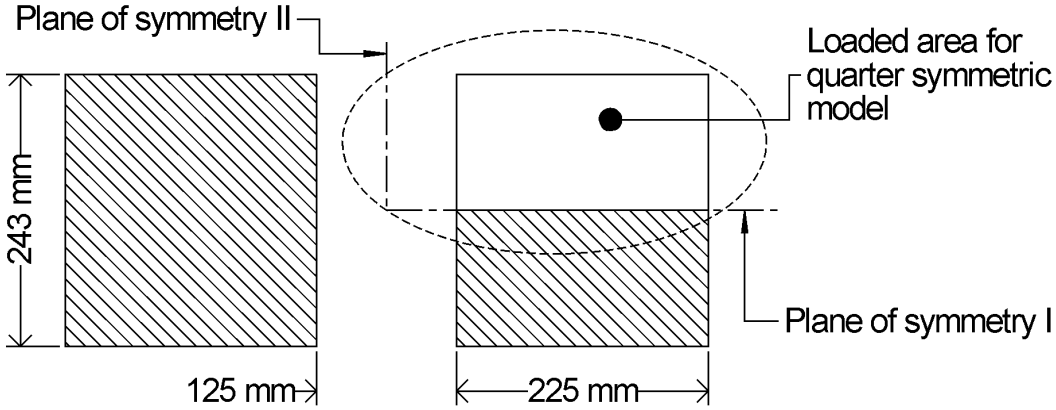

Figure 5.8 Details of 40kN loaded area for 3D FEM model using quarter symmetry.

5.7.1 Model Size

The pavement structure in the pavement tank is effectively a long trapezoidal prism, albeit slightly curved, so modelling the pavement as an axisymmetric solid could create a potential discrepancy with regard to either the transverse or the longitudinal boundary conditions.

If the transverse boundary dictates the radial dimension of the model, then the longitudinal boundary would be closer than it actually was and if the longitudinal boundary dictates the radial dimension, then the transverse boundary would be further away than it actually was. The axisymmetric model was primarily developed to simulate the FWD testing, so sufficient "model space" was required to obtain a realistic response for all of the FWD geophones without undue influence of the model boundaries. The outermost measurement point for the FWD was 1.5 m from the centre of the load plate in the tangential direction of the tank. Due to the limited distance, 1.6 and 1.3 m for the inner and outer wheelpaths respectively, from the instrument arrays to the edge of the pavement tanks as shown in Figure 5.9, it was decided to let the longitudinal dimension control the radial dimension of

the axisymmetric model. Duncan et al. (1968) concluded that if the radial boundary was at least 12 time the radius of the loaded area, then the radial boundary would have no practical effect on the results. Based on this assumption, the radial boundary should be at least 1800 mm when modelling the FWD load plate.

For the 2D axisymmetric model, the radial boundary was set at 2000 mm and the model was 1500 mm high, which equates to the depth of the CAPTIF pavement tank. Because the direction of interest for the analysis was along the track centreline, the radial boundary was defined as a vertical boundary rather than a sloped boundary similar to the sidewall of the tank.

The size of the 3D model was defined using the pavement tank geometry and the location of the instrument arrays within the tank. Using the dimensions shown in Figure 5.9, the width of the model was set at 1300 mm and the length of the model was the same as the axisymmetric model, 2000 mm.

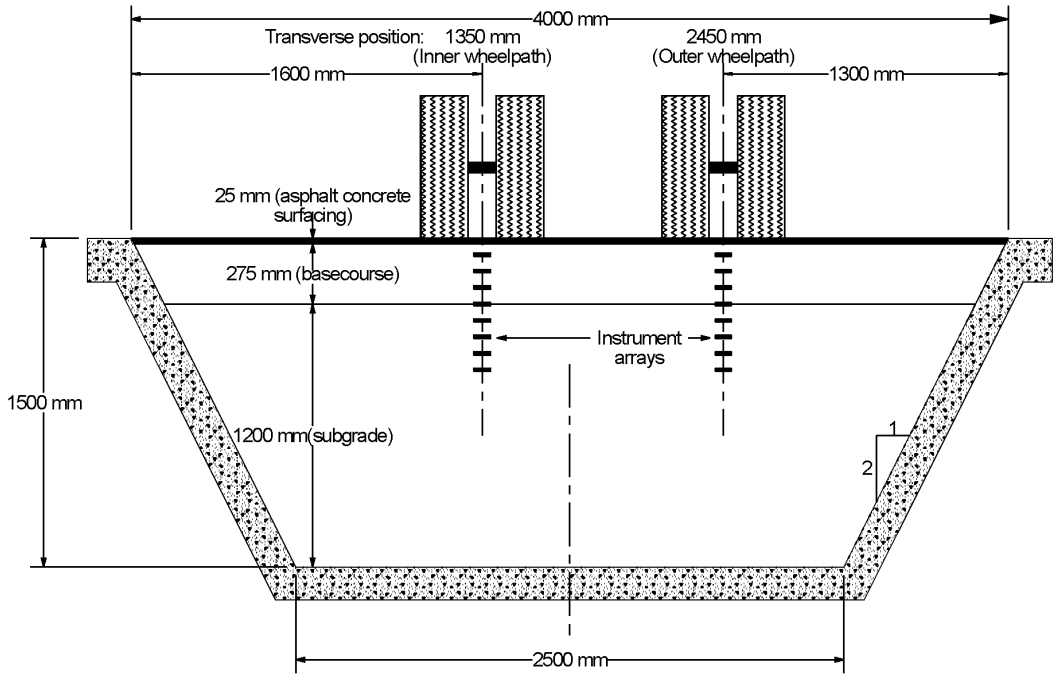

Figure 5.9 Location of instrument arrays with respect to pavement tank boundaries.

5.7.2 Element Size

The element size is always a tradeoff between the desire to increase the accuracy of the results and optimizing or reducing the computational effort. If the measured stress values are used as inputs to the laboratory derived material model for the granular material, the computed values of the resilient modulus range from 1500 to 100 MPa over the depth of the granular layer (300 mm). The range of predicted values mean that a relatively small element would be required to accurately represent the full range of resilient modulus values in the granular layer without having large modular ratios between adjacent elements.

The granular material has a maximum particle size of 40 mm therefore 40 mm should be the lower limit for the element dimension. The thickness of the granular layer was either 225 or 300 mm, allowing for the inclusion of the 25 mm thick asphalt concrete surfacing layer. Therefore it was decided to model the 225 mm thick granular layer as 4 elements 56.25 mm high and the 300 mm thick layer as 6 elements 50 mm high. The horizontal dimensions were set to be of the same order as the vertical dimension and to be compatible with the dimensions of the loaded area. In order to reduce the required computation effort, the element dimensions should increase as the distance from the loaded area increases, however this normally requires the use of transition elements in order to satisfy the requirements of element connectivity.

One of the features of ABAQUS/Standard is the ability to tie discrete blocks of elements together. This is achieved by defining two surfaces, one each on the outer faces of two adjacent blocks of elements. One surface is defined as the slave surface and the other as the master as shown in Figure 5.10. The two surfaces are then tied together by mapping the nodes on the slave surface to phantom nodes on the master surface. The phantom nodes are created by interpolating the degrees of freedom and reaction forces from adjacent nodes to the phantom node. This feature was used in the 3D model outside of the locations of the instruments where the element sizes were increased from approximately 50 mm cubes to 150 mm cubes. The 2D axisymmetric model formulation is quite efficient so the smaller element size was used throughout the model. The meshes used in the two models are shown in Figure 5.11 and Figure 5.12 for the 2D and 3D meshes respectively.

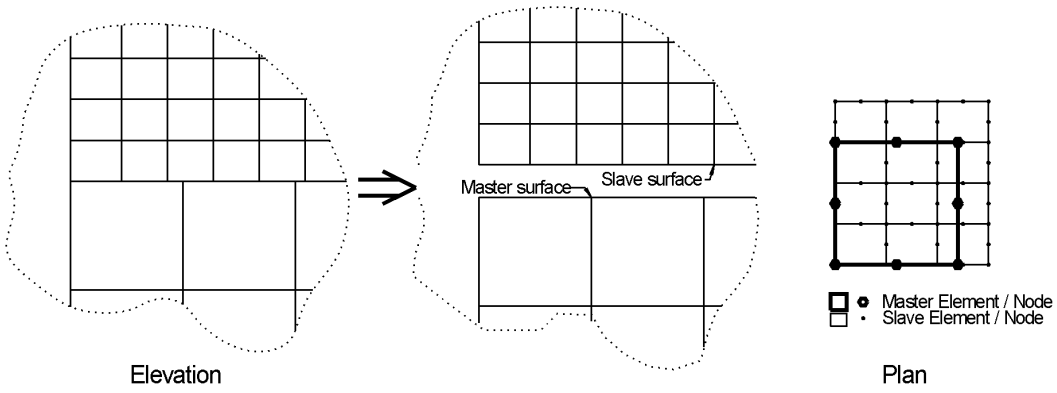

Figure 5.10 Details for change in FEM mesh density.

5.7.3 Element Selection

The models were created with isoparametric solid continuum elements that have been formulated for the analysis of general displacement/stress problems. Quadratic or second order elements were selected for both models as these types of elements provide a more accurate solution for straight-forward problems that do involve complex contact conditions, impact, or severe element distortions.

These elements are defined by nodes at each corner and at the mid point of each edge, 8 nodes are required for the 2D axisymmetric elements (Figure 5.13) and 20 nodes for the 3D elements (Figure 5.14). The second order elements are solved numerically using Gauss integration over 27 points inside the element. ABAQUS/Standard also includes reduced integration elements where the integration scheme is formulated at the next lower order. For the 3D second-order elements, the number of integration points reduces to eight, with the required computational effort reducing by a factor of 3.5. The second-order reduced integration elements are recommended over the full integration elements when the solution is expected to be "smooth" (ABAQUS Inc. 2004) (Section 14.1.1). The ABAQUS/Standard designation for the elements is CAX8R and C3D20R for the 2D axisymmetric and 3D elements respectively.

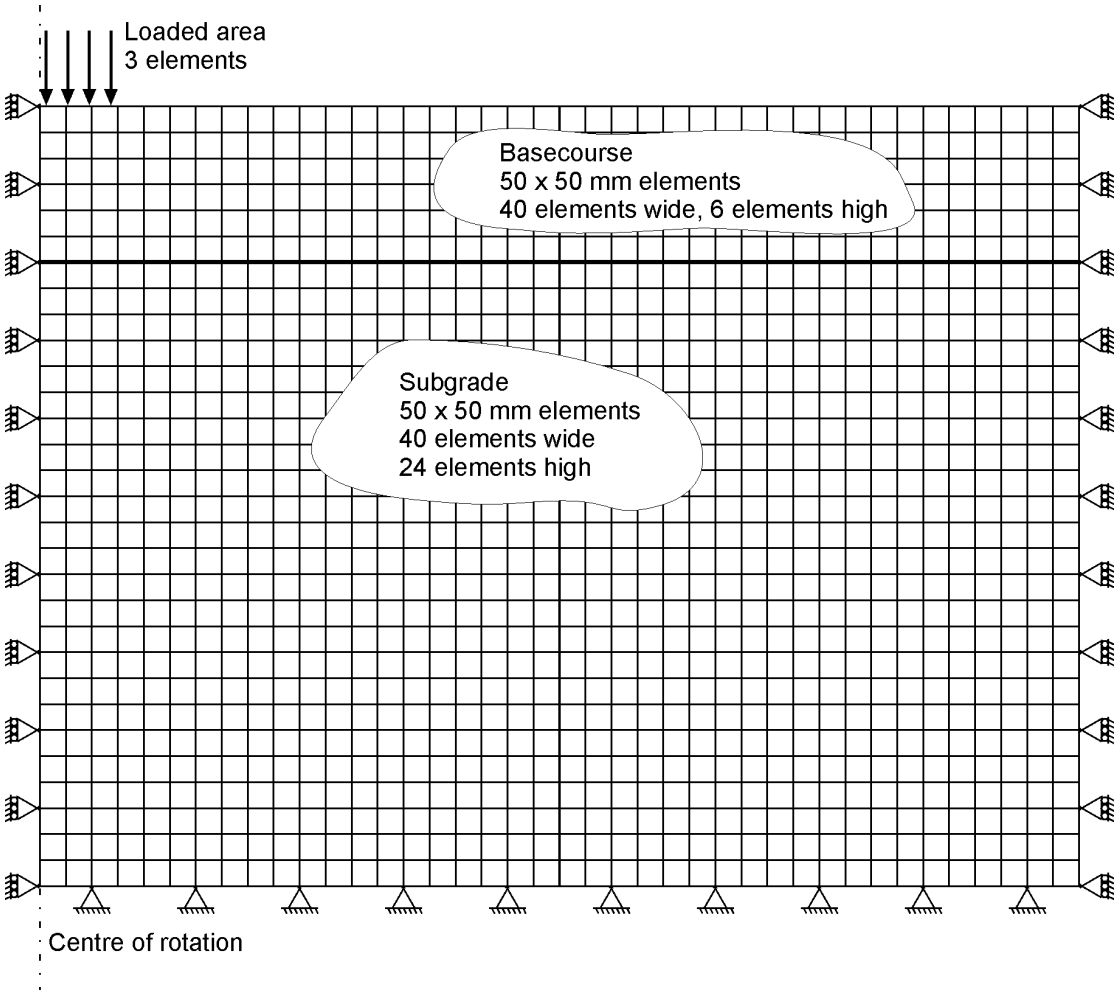

Figure 5.11 Mesh details for the 2D axisymmetric mesh.

5.7.4 Boundary Conditions

For the 2D model, the nodes on the centre of rotation and the radial boundary were allowed to move in the vertical direction and were fixed in the radial direction. The nodes on the bottom surface of the model were fixed in the vertical and radial directions. For the 3D model, the nodes on the planes of symmetry were allowed to move on the plane of symmetry but not out of the plane. The nodes on the sloping side and the bottom of the model were fixed in all three directions and the nodes on the back face of the model were allowed to move in the vertical direction.

These degrees of freedom were chosen to match the boundary conditions of the pavement tank (semi-rough concrete), no movement, or for the continuation of the material beyond the model, i.e. along the tank centreline, vertical movement only.

5.7.5 Orientation of Stresses for Modulus Determination

Material models that are developed from the repeat load triaxial test use stress orientations that correspond to the principal stress orientations, thus no shear stresses are induced in the test specimens. Therefore, in order to use such a material model in any type of analysis, the co-ordinate system should ideally be one in which the shear stresses are zero.

This approach works well for the FEM when the material stiffness is calculated directly beneath the centre of the loaded area/s, however if the calculation points are not located on the model centreline, there is a difference in the orientation of the system (σ_{11}, σ_{22}, σ_{33}) and principal (σ_1, σ_2, σ_3) stresses. At shallow depths away from the loaded area, the horizontal stresses can be greater than the vertical stresses and it makes sense to use the principal stress values.

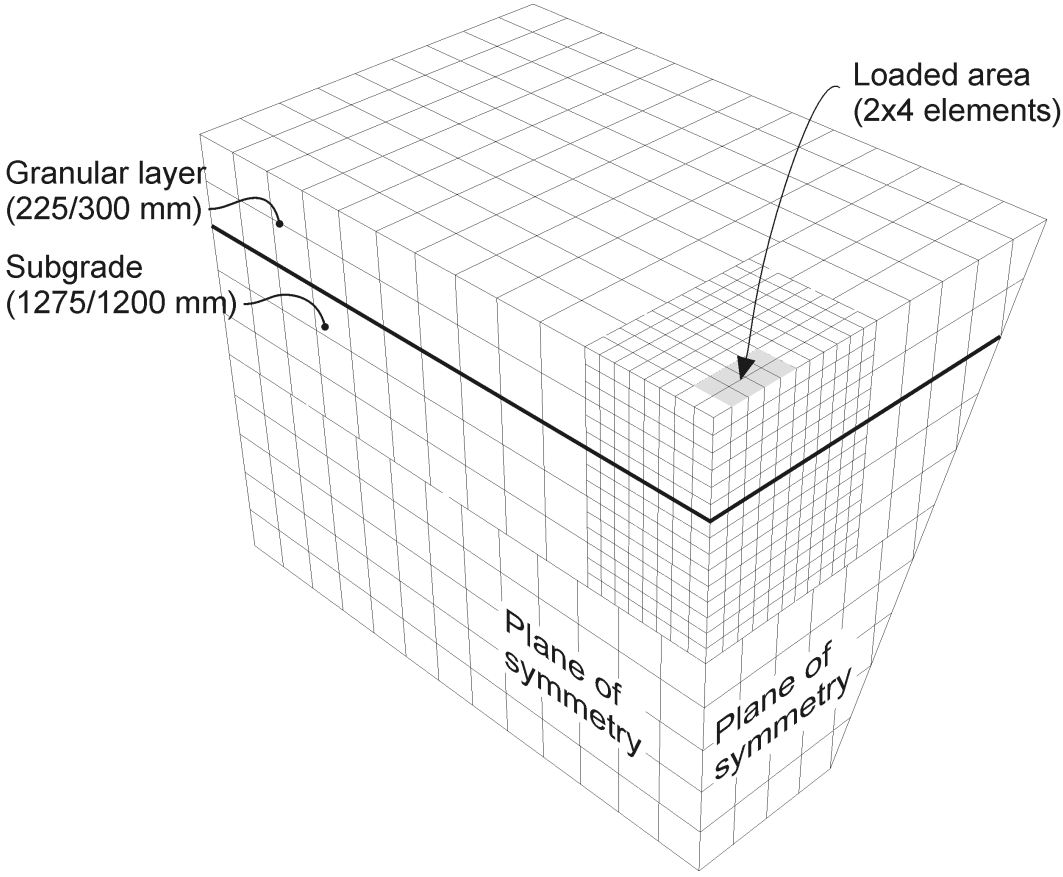

Figure 5.12 Mesh details for the 3D mesh.

For an isotropic material the material stiffness can be calculated after the principal stress have been determined as the orientation of the principal stresses relative to the model orientation is irrelevant. For a cross-isotropic material, the angle of the major principal stress relative to the cross-isotropic plane needs to be accounted for in determining the vertical modulus. First the principal stresses and their orientation to the system co-ordinates need to be determined.

The material stiffness can then be determined from the principal stresses and the resulting material stiffness can then be modified according to Equation (2.35), based on the angle between the normal of the plane of isotropy and the orientation of the major principal stress.

For the 2D axisymmetric model, the principal stress values can be calculated from the stresses aligned with the system axes by the use of Mohr's Circle as shown in Figure 5.15.

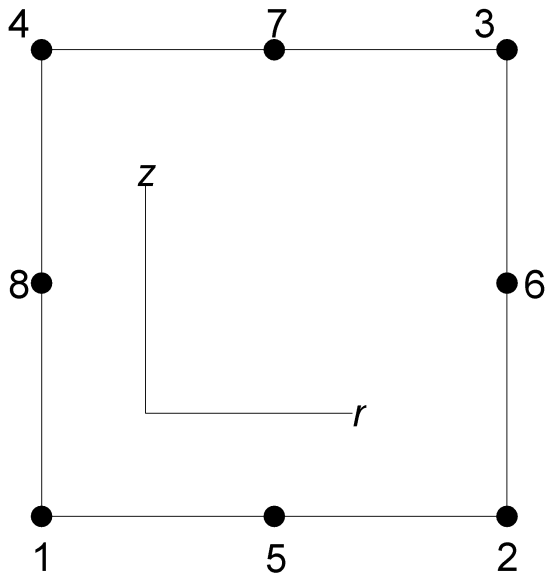

Figure 5.13 Second-order 2D axisymmetric solid continuum element.

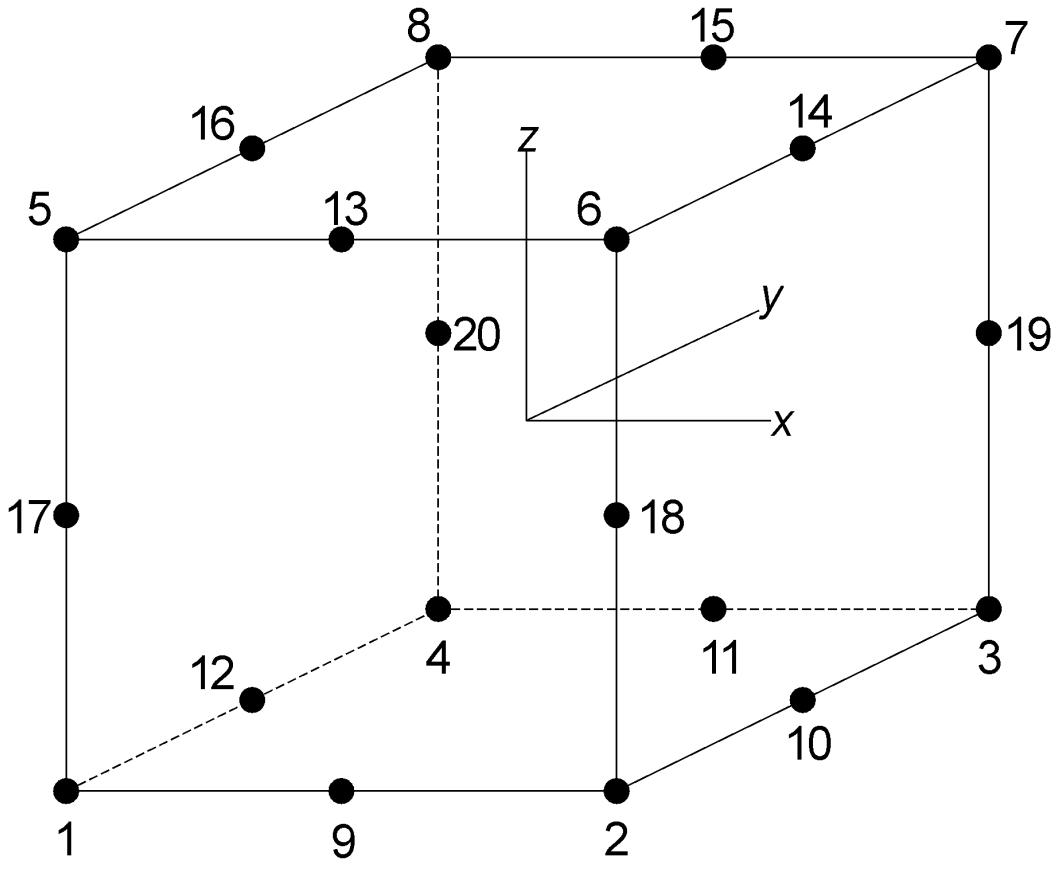

Figure 5.14 Second-order 3D solid continuum element.

$$\sigma_1 = \frac{\sigma_{11}+\sigma_{33}}{2} + \sqrt{\left[\frac{\sigma_{11}-\sigma_{33}}{2}\right]^2 + {\sigma_{13}}^2}$$
$$\sigma_3 = \frac{\sigma_{11}+\sigma_{33}}{2} - \sqrt{\left[\frac{\sigma_{11}-\sigma_{33}}{2}\right]^2 + {\sigma_{13}}^2} \qquad (5.4)$$

where

σ_{11} = radial stress
σ_{33} = axial stress
σ_{13} = shear stress on radial plane due to axial stress

The inclination of the major principal stress to the axial stress can be found by substituting the principal stresses into the solution of the transformation matrix

required to move between the original coordinate and principal stress systems as follows

$$\begin{aligned} (\sigma_{11} - \sigma_1) l_1 + \sigma_{13} l_3 &= 0 \\ \tan\theta &= \frac{l_1}{l_3} \\ &= \frac{-\sigma_{13}}{(\sigma_{11} - \sigma_1)} \end{aligned} \tag{5.5}$$

where

l_i = components of the unit normal for the major principal stress
θ = inclination between axial stress and major principal stress

For the 3D case, ABAQUS/Standard provides utility routines for use within the UMAT to determine the principal stress values and the direction cosines for each principal stress.

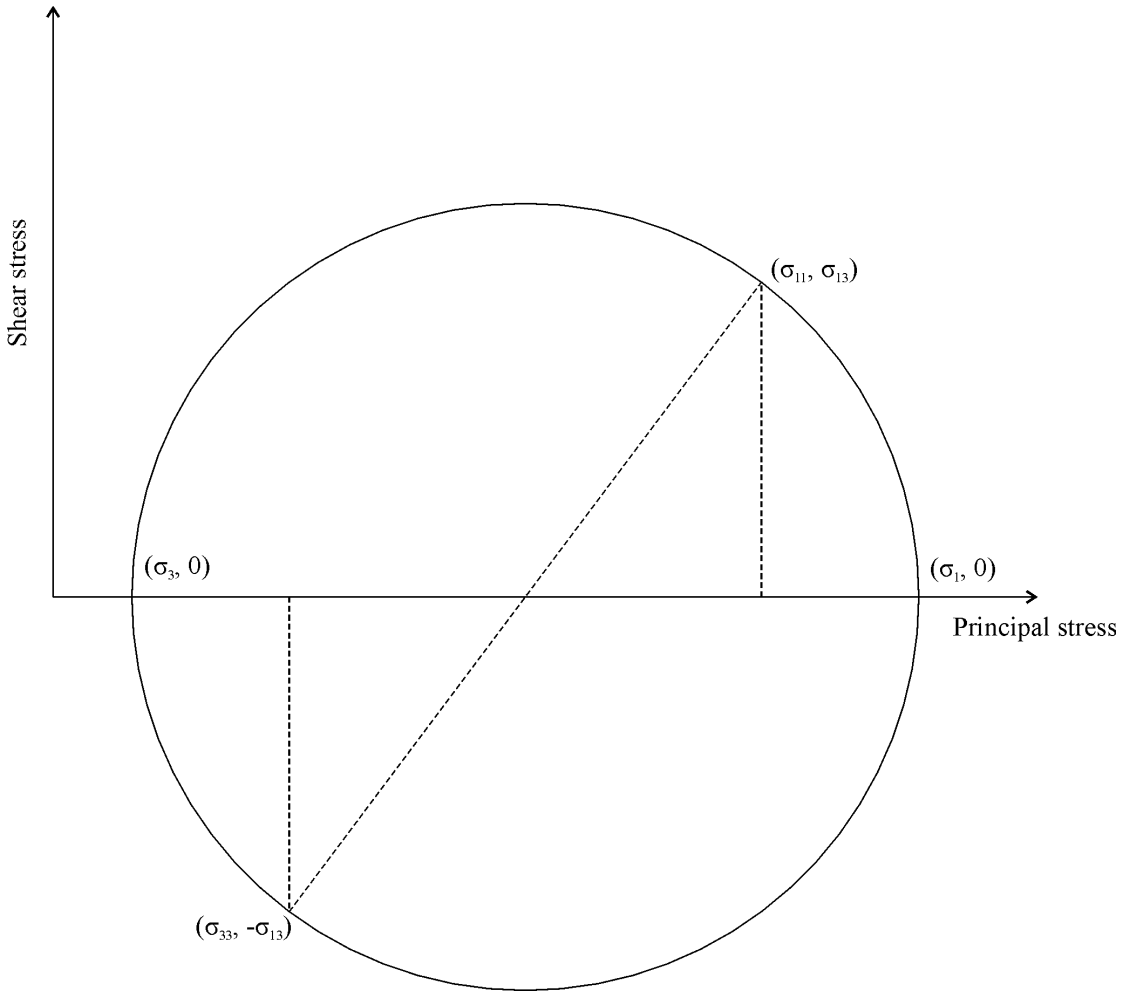

Figure 5.15 Mohr's Circle for determining the principal stress values for the 2D axisymmetric case.

5.7.6 Non-linear Modelling

In a general approach to non-linear modelling, the load is applied in small increments and the displacement for each load increment (c_a) is determined using the current stiffness matrix (K_0) of the model. This approach is shown in Figure 5.16. The difference between the applied load increment and the load increment determined from the specified load-displacement relationship is determined (R_a) and if the difference is within the specified tolerance the increment is deemed to have converged and the next load increment is applied. If the difference is not within the tolerance, then the stiffness matrix is recalculated (K_1) and an additional displacement amount (c_b) is determined as shown in Figure 5.17. This iterative process continues until the difference between the applied and calculated load is

within the tolerance value. This approach to solving the non-linear problem is known as the *Newton Method* (ABAQUS Inc. 2004).

This method of solution accumulates the system response (stress/strain) for each increment and it relies on the determination of the stiffness matrix at loads ranging from 0 to 100% of the applied load. This is also called a path dependent solution. However, because of the methods and equations used to determine the material stiffness, the stiffness is defined as the secant stiffness if the confining or initial stresses are ignored or the chord stiffness if the initial stresses are taken into account and is path independent. For this approach, the final stress state needs to be known in order to determine the material stiffness, rather than the intermediate stress states.

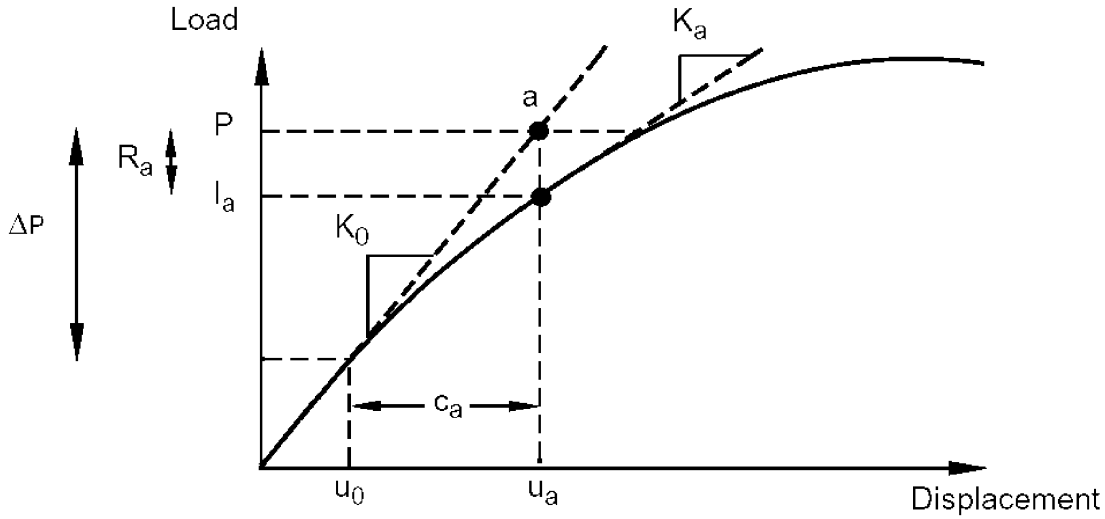

Figure 5.16 First iteration for non-linear modelling (ABAQUS Inc. 2004).

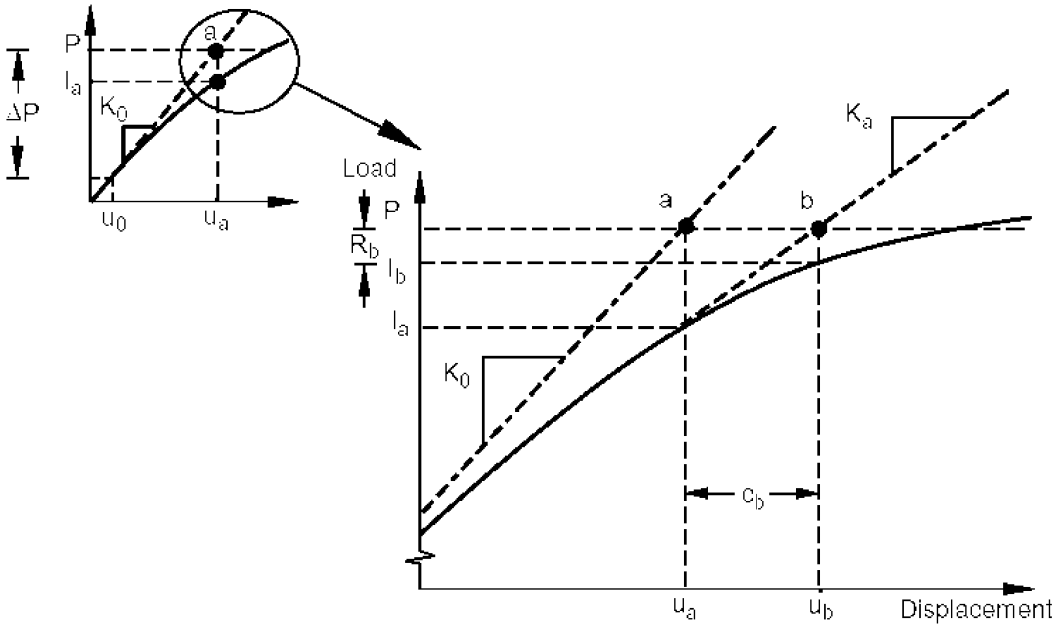

Figure 5.17 Second iteration for non-linear modelling (ABAQUS Inc. 2004).

The use of intermediate stress states will results in material stiffness values that are too low, resulting in the overestimation of the strain values. When ABAQUS/Standard is used to solve a non-linear problem, the user specifies the size or the initial load increment as a percentage of the total load. Because the initial stiffness matrix must be defined before the first load increment is applied, the stiffness matrix is generated using an arbitrary value for the modulus, 1000 MPa. This high value, along with a small increment size (1% of total) was chosen to minimize the contribution of the first increment to the final solution. The program uses the inverse of the current stiffness matrix and the stress tensor to determine the strain tensor that is used to initiate the solution process. The stress tensor is based on the percentage of the total load that is going to be applied in the current increment.

5.7.7 User-defined Material Model (UMAT)

In ABAQUS/Standard the user can define the constitutive material behaviour using the *USER MATERIAL option and a UMAT subroutine in place of the *ELASTIC material option. The UMAT subroutine is developed by the user using the FORTRAN programming language. A standard header for the subroutine is

provided by ABAQUS/Standard that passes a range of variables and values into the subroutine from the main program. Within the UMAT, the user is required to calculate the Jacobian Matrix (incremental stiffness matrix) and update the total stress tensor using the incremental strain tensor that is supplied for the current load increment. The response modelling work undertaken in this thesis is based on the first order Cauchy formulation, so the definition of the stiffness matrix is straightforward once the elastic parameters are defined. The UMAT contains a number of different steps, which are shown in Figure 5.18.

To call the UMAT from an input file, the required declaration block for an elastic material:

```
*SOLID SECTION,ELSET=ALLELEMENTS,MATERIAL=BASECOURSE
*MATERIAL,NAME=BASECOURSE
*ELASTIC
200,0.35
```

where the `200,0.35` which correspond to the modulus and Poisson's ratio respectively, is replaced with

```
*SOLID SECTION,ELSET=ALLELEMENTS,MATERIAL=BASECOURSE
*MATERIAL,NAME=BASECOURSE
*USER MATERIAL, TYPE=MECHANICAL, CONSTANTS=11
1,0.35,1.3131,0.76,-0.3068,0.5,1,3
2,33,1000
*DEPVAR
9
```

The `CONSTANTS=11` term refers to PROPS(1) to PROPS(11) in the UMAT and the values are given in the following lines (with a maximum of eight values per line). The current definitions for the values 1-11 are given in Table 5.6. The `*DEPVAR` term initialises the solution dependent variable array (SDV) which is populated from within the UMAT and can be called as output variables either as SDV for all values or SDV(i) to only request a particular variable. The variables that are stored in the SDV array are given in Table 5.7. It is important to remember that indexes for arrays in the Fortran programming language start at 1.

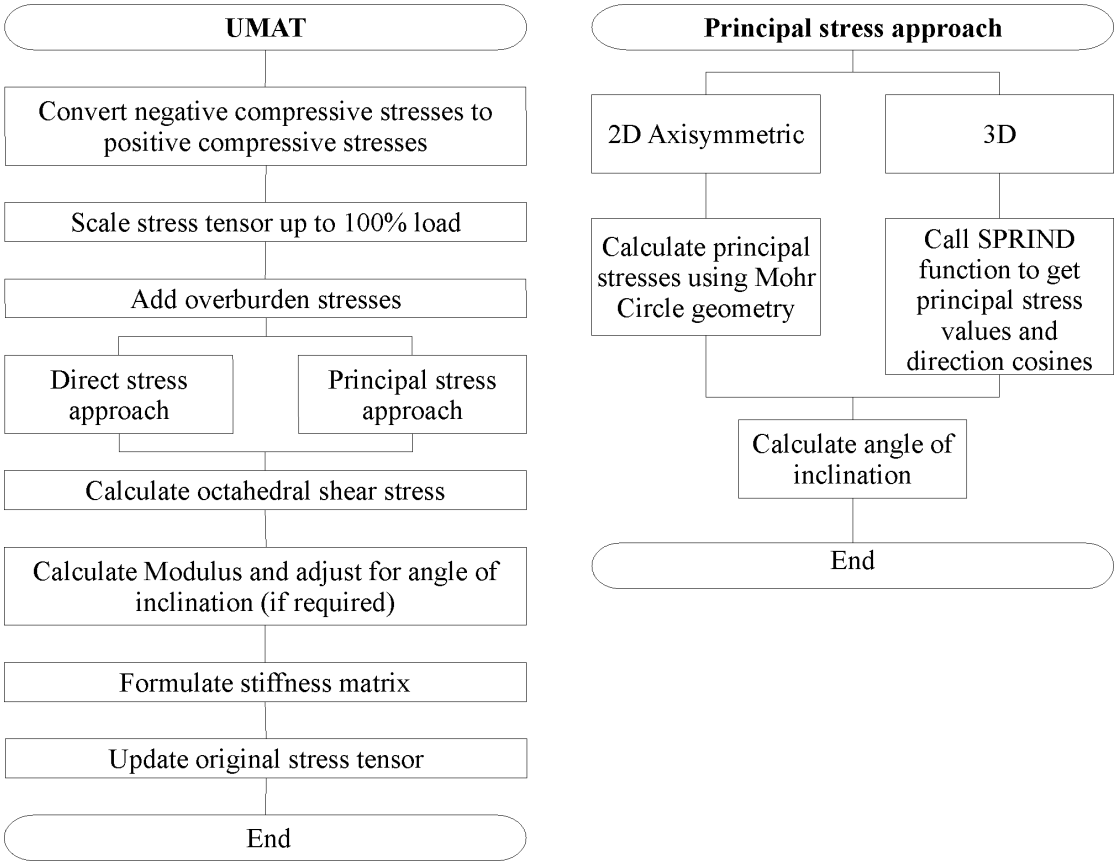

Figure 5.18 Flow diagram for UMAT program.

Table 5.6 Definitions for PROPS(i) values.

i	Description	Units
1	Model no, currently only 1 available (1)	-
2	Poisson's ratio	-
3	Model coefficient k_1	-
4	Model coefficient k_2	-
5	Model coefficient k_3	-
6	n factor for anisotropy E_h/E_v	-
7	Stress orientation for the determination of the modulus 0=direct coordinate system (1-2-3) 1=principal stress directions	-
8	K_0 coefficient for determination of lateral at rest stress	-
9	Density of material for calculation of overburden and lateral stresses (assuming a constant/composite value for entire pavement)	t/m^3
10	Minimum value of resilient modulus	MPa
11	Value of resilient modulus for the first increment	MPa

Table 5.7 Definitions for SDV(i) values.

i	Description	Units
1	σ_1 Major principal stress or stress in dir^n 1	MPa
2	σ_2 Intermediate principal stress or stress in dir^n 2	MPa
3	σ_3 Minor principal stress or stress in dir^n 3	MPa
4	τ_{oct} Octahedral shear stress	MPa
5	Horizontal stress due to overburden	MPa
6	Vertical stress due to overburden	MPa
7	Angle between the major principal stress and the vertical axis	Radians
8	Resilient modulus as calculated	MPa
9	Resilient modulus after adjusted for angle of inclination	MPa

The model was developed using the assumption that the z axis was the vertical axis and that z=0 corresponded to the surface of the pavement structure. The direction of the z axis is not critical.

For a non-linear analysis in ABAQUS/Standard, the program will automatically increase the size (percentage) of the next increment by 50% if the previous two increments converged in less than five iterations. For an initial increment size of 1%, the solution would require 11 iterations if the problem behaves normally and the default automatic increment control is used. In the UMAT developed for this research, the current stress state in each increment is scaled up to 100% of the full load to determine the resilient modulus; therefore, there is little change in the value of the modulus for each increment. The value of the parameter that increases the size of the next increment was changed from its default value of 150% to 1000%. This reduced the number of required increments to four with a subsequent reduction in time required to solve the problem. The variation of the value of the resilient modulus at one point in the model for the default and modified increment sizing factors is shown in Figure 5.19 and it can be seen that the values could be regarded as constant (1% variation) after the second increment.

Once the program was working correctly it was packaged into a library file using the `ABAQUS make` command, this enabled the UMAT to be used on other computers without having to install the FORTRAN compiler on each computer where the UMAT was used.

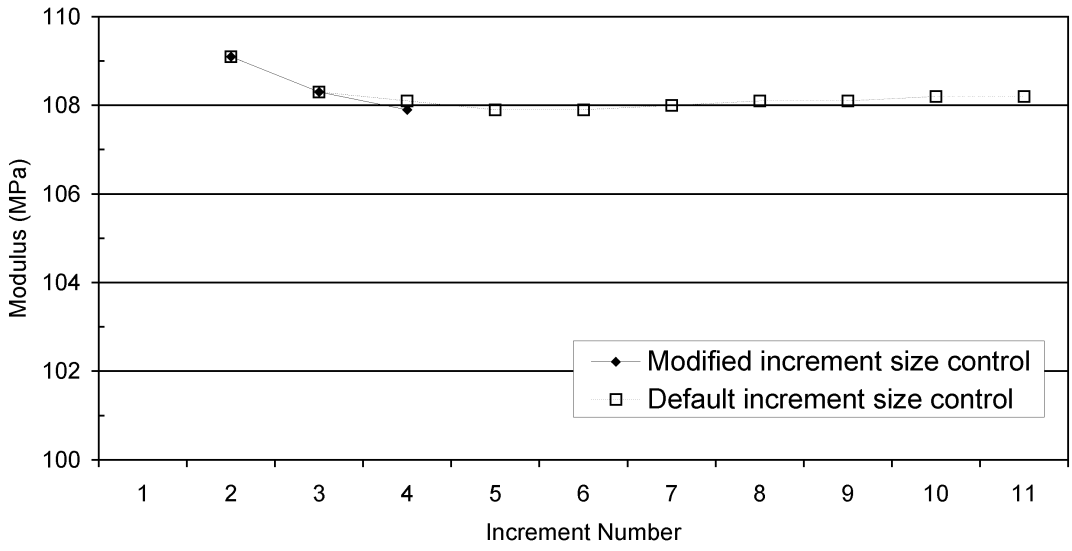

Figure 5.19 Variation of Resilient Modulus with increment number.

5.7.8 Stage One/Two FEM Verification

By nature of the FEM process, the stage one and two verification procedures are identical because each element effectively has its own material definition. The 2D model was setup to match the MLLET Circly model using the material properties that are listed in Table 5.2. In order to verify the 3D model, a mesh was created with a square shaped loaded area that was centred on the central axis of the model as shown in Figure 5.20. The element sizes were selected so that the loaded area was equal to the loaded area of the 2D model.

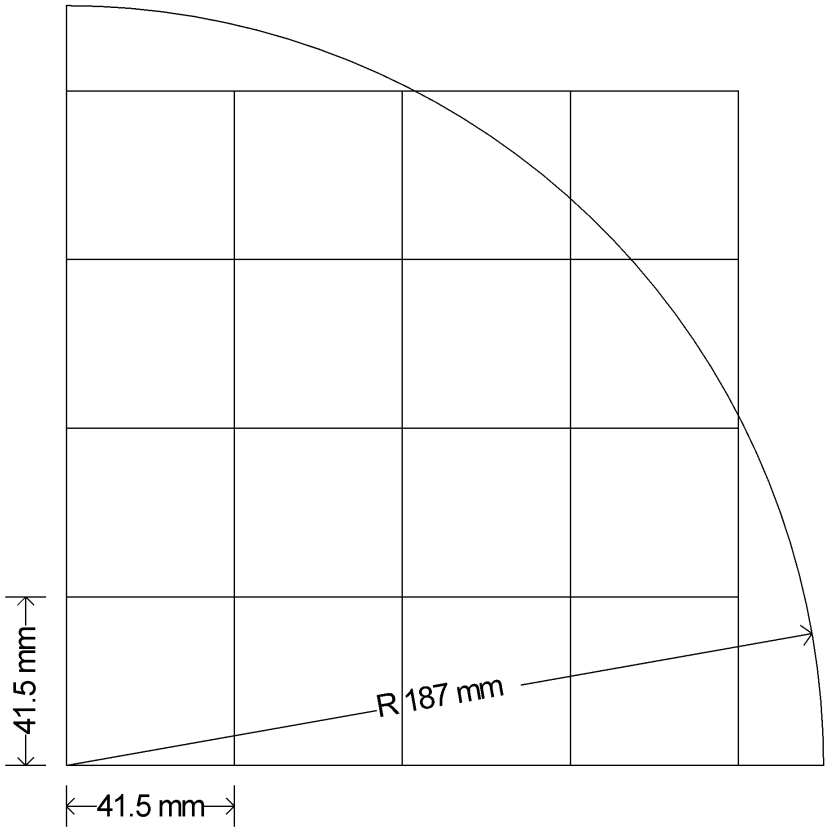

Figure 5.20 Comparison of loaded areas for 2D and 3D FEM meshes.

2D axisymmetric case

$$F = Ap$$
$$= 187^2 \pi \times 0.366$$
$$= 40{,}208 \text{ N}$$

3D quarter symmetric case

$$A = \frac{F}{p}$$
$$= \frac{40{,}208}{4 \times 0.366}$$
$$= 27{,}464 \text{ mm}^2$$

$$\text{length of side of a square} = \sqrt{27{,}464}$$
$$= 166 \text{ mm}$$

The 2D and 3D models were solved as isotropic linear elastic models and the key results are shown in Table 5.8. There is an excellent agreement between the results of the Circly and 2D FEM models and a reasonable agreement between the 2D and

3D models. The difference is –2.8% for the central surface deflection and this could be attributed to the irregular surface area and the difference for the stress and strain values at a depth of 300 mm is less than -2%. In addition, differences in the element geometry and the fact that the values at the nodes are averaged from the adjacent elements, of which the value for each element has been extrapolated from the internal integration points, also contribute to the difference in the results. The stress results on the model centreline and a distance of 300 mm from the centreline are plotted against depth for both the 2D and 3D models in Figure 5.21. These results show that the 2D and 3D formulations within ABAQUS/Standard give similar results. For the 3D case, elements that were on the x-direction axis were chosen because the x and y directions in the 3D space correspond to the radial and tangential directions in the axisymmetric space respectively.

The anisotropic formulation of the stiffness matrix in the UMAT was checked by comparing the output from the Circly single layer model with the 2D and 3D FEM models when the anisotropic factor *n*, was set to a value of 0.5. The single layer model was used because of the difficulties found with the multi layer Circly model (Section 5.5.2). The k_1 coefficient of the material model was set to equal 1 and the k_2 and k_3 coefficients were set to equal 0, this made the stiffness a constant value of 100 MPa.

Table 5.8 Results for initial FEM verification.

Response	Rigid boundary		
	Circly	2D FEM	3D FEM
Surface Deflection (mm)	1.094	1.090	1.063
Vertical Stress (MPa) (z=300 mm)	0.1423	0.1425	0.1398
Vertical Strain (μm/m) (z=300 mm)	1398	1412	1384

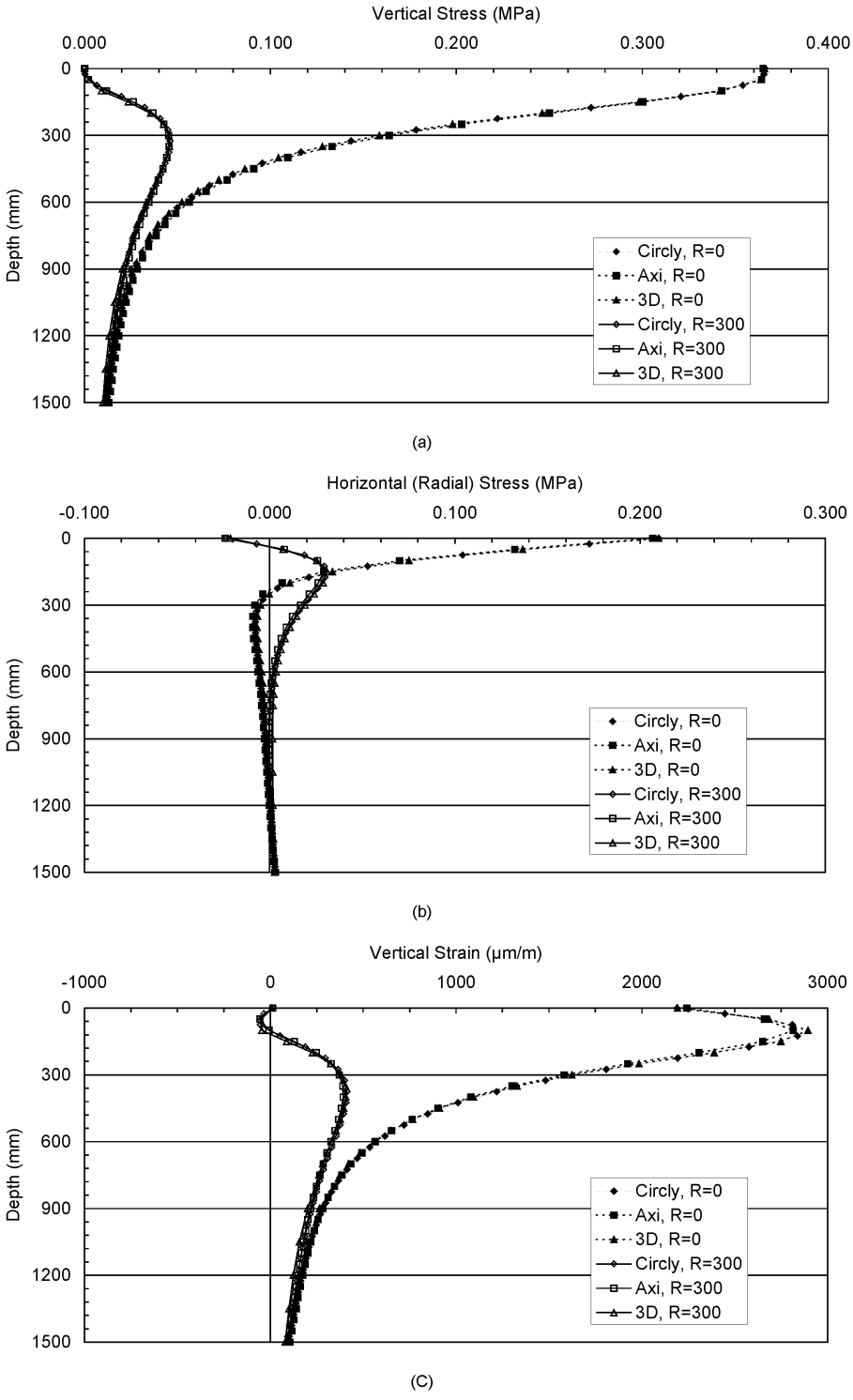

Figure 5.21 Comparison of computed stresses and strains on centreline and a distance of 300 mm from the centreline for the Circly, 2D and 3D FEM models (single layer, anisotropic (n=0.5)): (a) vertical stress, (b) horizontal stress, and (c) vertical strain.

The key response parameters are listed in Table 5.9 and the vertical stress, strain and horizontal stress versus depth at a radial distance of 0 and 300 mm are shown in Figure 5.21. The results show that the FEM and Circly solutions agree, with the variation of values being less than 4%. In addition, the FEM and Circly models were compared when the anisotropy factor, *n* was set to 0.25 and the variation of vertical and horizontal stresses were compared at a depth of 300 mm below the surface. The results of this analysis is shown in Figure 5.22 and show that the results from the two models agree, although there is a small (2 kPa) offset between the two models in the horizontal stress values.

From these verification results it can be assumed that the FEM models and the UMAT code have been correctly formulated when compared to an accepted analytical solution.

5.7.9 The Effect of Anisotropy

In order to study the effect of the degree of anisotropy a series of constant stiffness axisymmetric FEM models were analysed and a series of outputs (surface deflection, vertical and horizontal stress on the centreline and on a radial line 300 mm below the surface) were compared with each other. The model was the same as that was used in the previous section, except that the anisotropy factor *n*, was varied from 1 to 0.1. The surface deflections are shown in Figure 5.23, the maximum deflection increased by 54% as the value of *n* changed from 1 (isotropic) to 0.1. The vertical and horizontal stresses on the centre of rotation versus depth are shown in Figure 5.24 and the variation in stresses at varying distances from the centre of rotation at a depth of 300 mm below the surface are shown in Figure 5.25. The increase in vertical stress on the centreline at depth of 300 mm is 54% as the anisotropy factor changes from 1.0 to 0.1, at the same point in the model, the horizontal stress decreases by 52% as the value of *n* changes from 1.0 to 0.1.

The results presented in this section shows that the inclusion of any allowance of anisotropy will influence the results, even though the work in this section was limited to a linear elastic model. Additional analysis using the non-linear material model will be presented later in the chapter.

Table 5.9 Verification of anisotropic solution for axisymmetric and 3D FEM models.

Response	Isotropic	Anisotropic, n=0.5		
	Circly	Circly	Axisymmetric FEM	3D FEM
Surface Deflection (mm)	1.094	1.254	1.227	1.228
Vertical Stress (MPa) (z=300 mm)	0.143	0.161	0.164	0.159
Vertical Strain (μm/m) (z=300 mm)	1413	1645	1583	1624

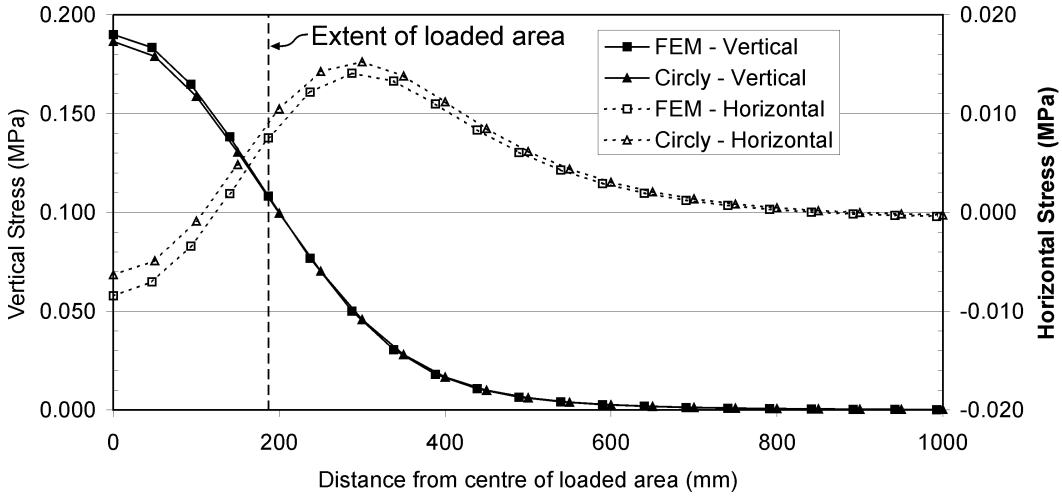

Figure 5.22 Vertical and horizontal stresses at a depth of 300 mm for the axisymmetric linear FEM and Circly models, n=0.25.

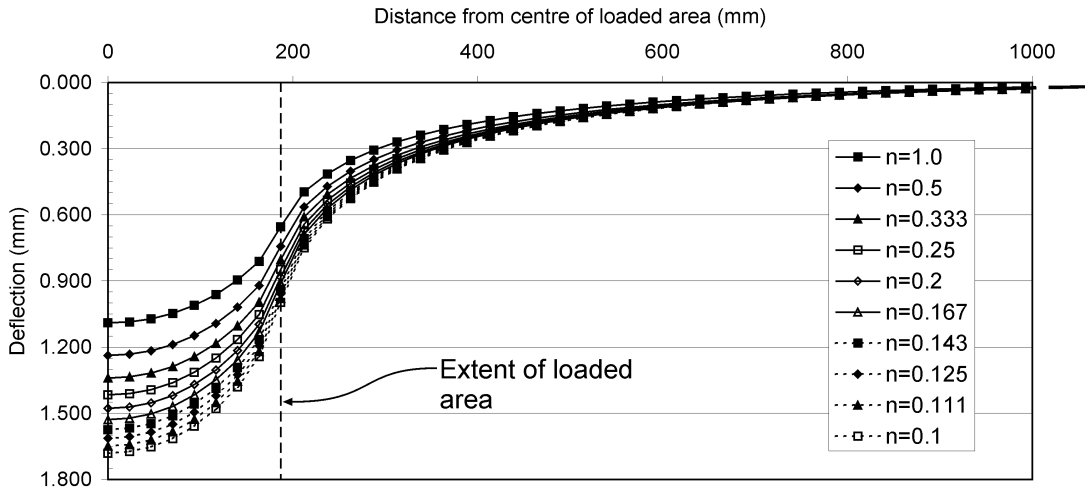

Figure 5.23 Surface deflections for different values of anisotropy factor, *n*, for axisymmetric linear FEM model.

5.7.10 Stage Three FEM Verification

In this verification exercise, the axisymmetric and 3D models used in Section 5.7.8 were used with three changes. The changes were:

1) The loaded area was changed to a radius of 150 mm (axisymmetric model) or a square with a side dimension of 133 mm (3D model) and a surface pressure of 366 kPa to allow a comparison with the "No AC" results presented in Table 5.5;

2) The model was divided into 2 layers, 300 mm of basecourse and 1200 mm of subgrade;

3) The non-linear stiffness model was implemented, using the parameters listed in Table 5.1. The anisotropy factor, *n*, was set to equal 0.5.

An initial axisymmetric FEM model was created and solved where each row of elements (30 rows each being 50 mm high) was assigned the same modulus value that was used in the corresponding layer in the final Circly run. This created a FEM model that was the same as the Circly model, i.e. a multilayer linear elastic model and allowed the comparison of a numerical and closed form solution (using Circly) to the same problem. The next step was to extend the FEM model to incorporate

the full stress dependant material stiffness model that was coded in the UMAT. Initially the unit weight of the material was set to zero, removing the influence of the stresses caused by the overburden on the calculation of the material stiffness. This was done to determine the effect of allowing the stiffness to vary in the radial direction as well as the vertical direction and was the only difference between the multilayer and full nonlinear FEM models.

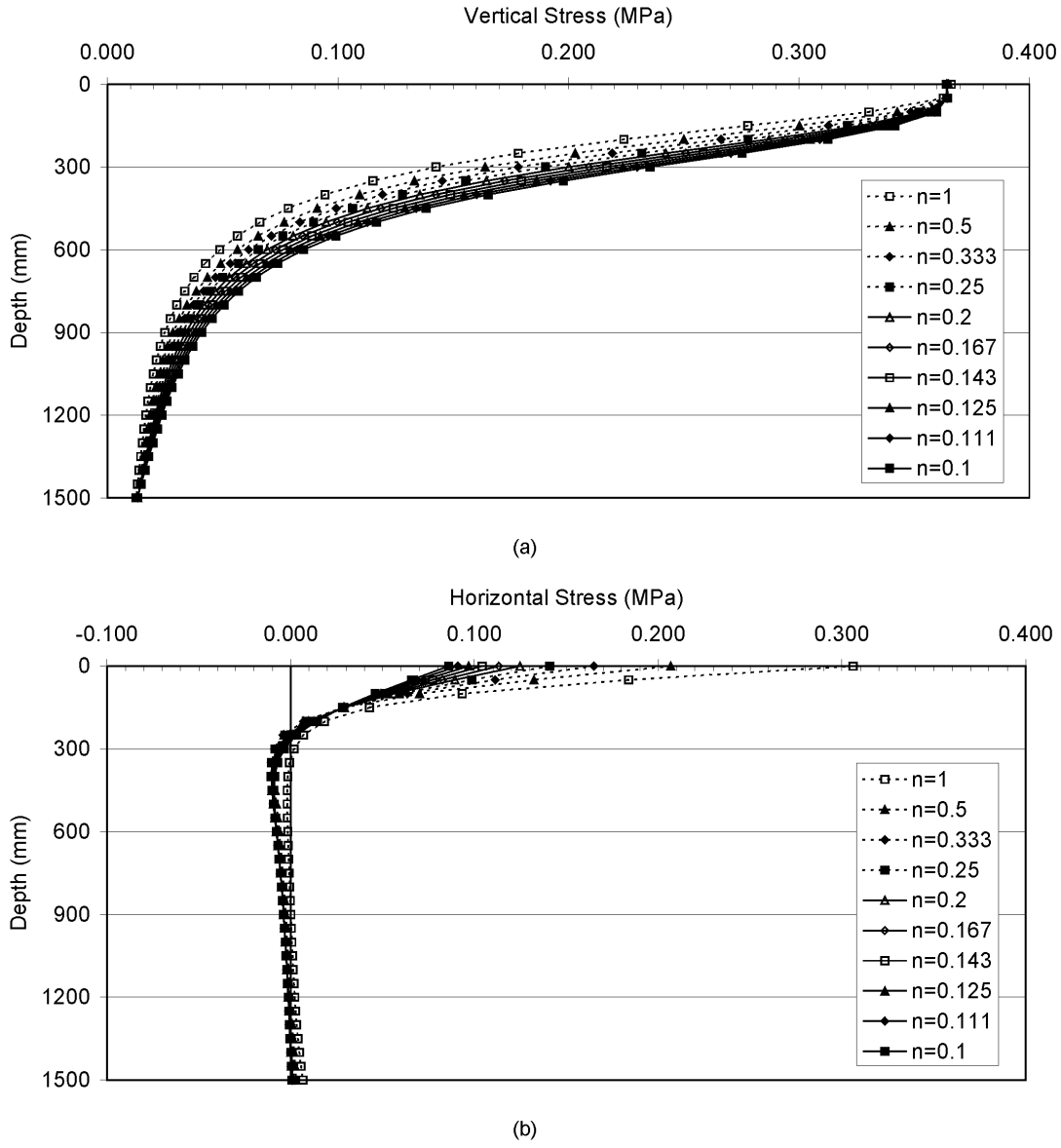

Figure 5.24 Vertical and horizontal stresses on the centre of rotation for an axisymmetric linear FEM for different values of the anisotropy factor, *n*.

The solutions to the two multilayer models were similar to each other, as shown by the co-incident traces in Figure 5.26 for the vertical stress and strain on the model centreline. Figure 5.27 shows the vertical and horizontal stress at a depth of 275 mm (bottom of the granular layer) and Figure 5.28 shows the surface deflections, with the difference between stress, strain and surface deflection responses differing by less than 5%. This type of analysis appeared to reduce the effect of the problems with the Circly model that were identified earlier.

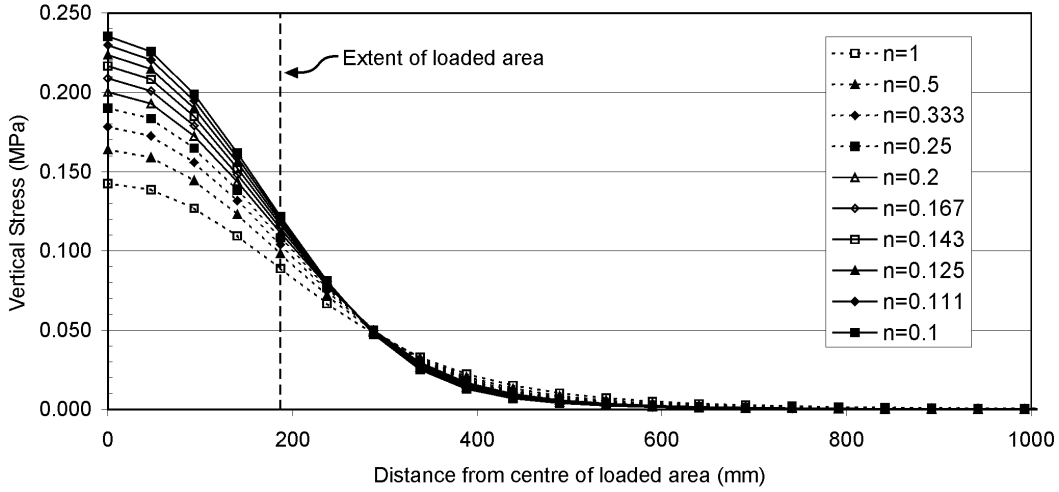

(a)

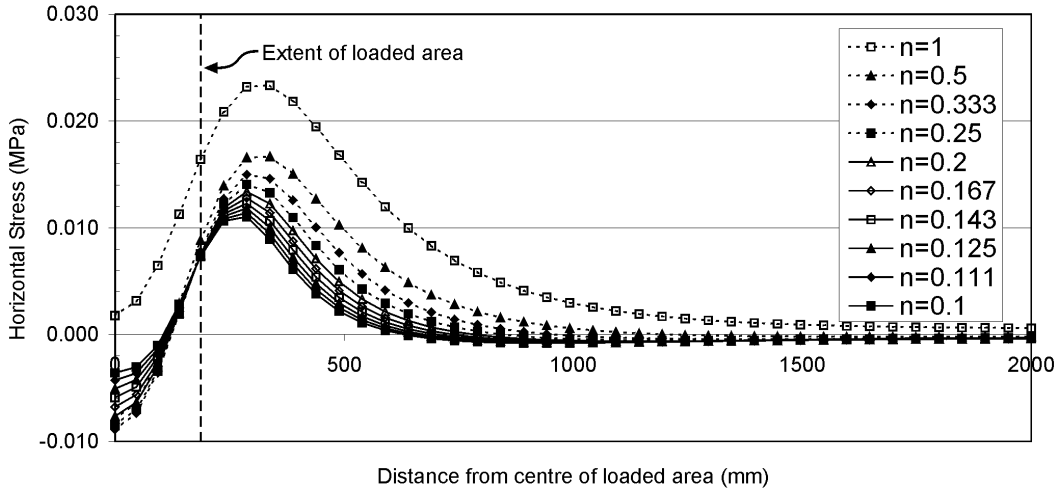

(b)

Figure 5.25 Vertical and horizontal stresses at a depth of 300 mm for an axisymmetric linear FEM for different values of the anisotropy factor, *n*.

The results of the full non-linear analysis show a significant difference to the results obtained from the multilayer approached described above. When comparing the multilayer Circly and "no confining" nonlinear FEM models, the FEM responses were all greater than the Circly responses. The maximum surface deflection increased by 18%, the vertical strain at the top of the subgrade increased by 27% and the vertical stress at the top of the subgrade increased by 44%.

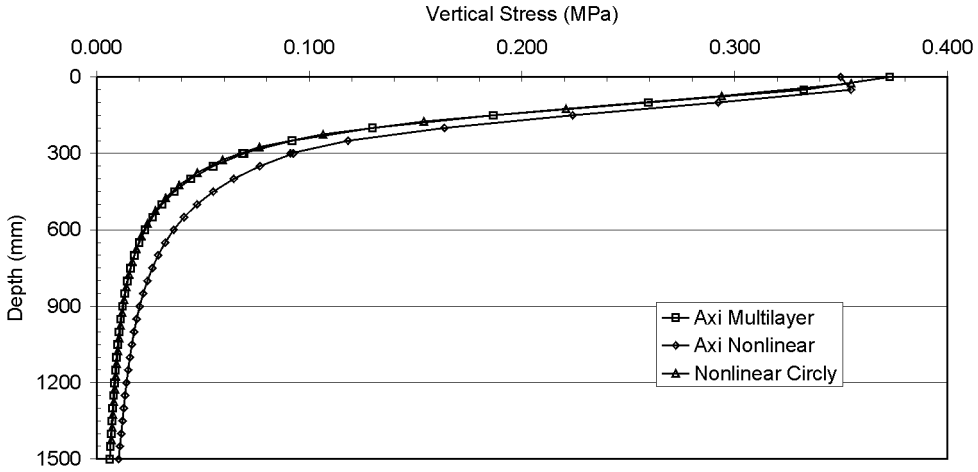

(a)

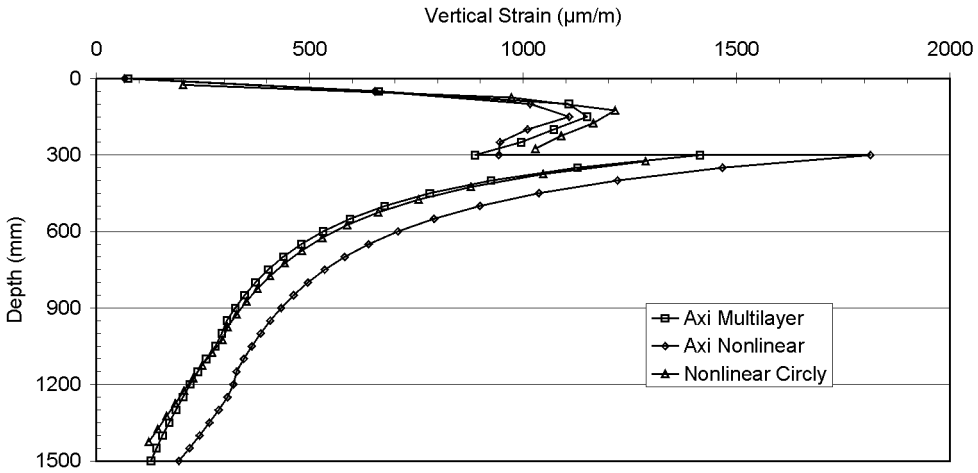

(b)

Figure 5.26 Comparison of nonlinear Circly, multilayer FEM and nonlinear FEM models: (a) vertical stress and (b) vertical strain on model centreline.

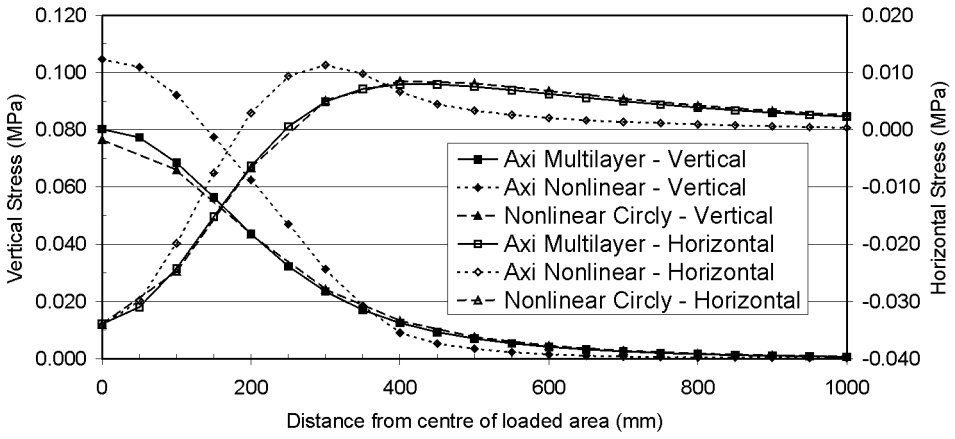

Figure 5.27 Comparison of vertical and horizontal stresses at a depth of 275 mm for nonlinear Circly, multilayer FEM and nonlinear FEM models.

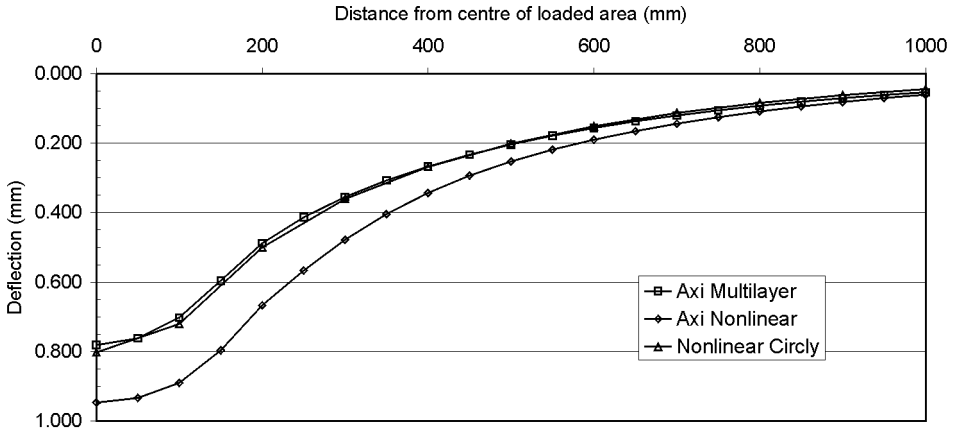

Figure 5.28 Comparison of surface deflection bowls for nonlinear Circly, multilayer FEM and nonlinear FEM models.

The increase in magnitude of the selected responses of the nonlinear FEM can be explained as follows: the multilayer approach has a constant stiffness for a particular layer and the stiffness is usually determined from the stress state on the model centreline at the mid depth of the layer, where the stress state usually has the greatest magnitude. As the radial distance increases, the magnitude of the stress state reduces, but the stiffness does not, as it has been determined at the model

centreline, thus the overall stiffness of the layer and therefore the model, is greater than would be for a fully nonlinear system. This leads to higher stresses/strains and deflections for the nonlinear FEM model when compared to the multilayer model.

When the multilayer Circly model and nonlinear FEM model which accounts for the confining effect of the overburden stresses are compared, the FEM model produces smaller responses than the Circly model. The reason for the difference in the responses can be seen in Figure 5.29, in which the calculated stiffness versus depth for the stiffness values on the model centreline are plotted. The stiffness values for the Circly and no confining FEM models are similar, as expected, but the there is a significant variation in the stiffness values for the subgrade material in the FEM model which incorporates the effect of the confining stress. By examining the different parts of the equation that is used to calculate the stiffness, along with the relative magnitudes of the stresses caused by the load and the overlying material, the relative contributions of the bulk and shear terms to the stiffness can be determined.

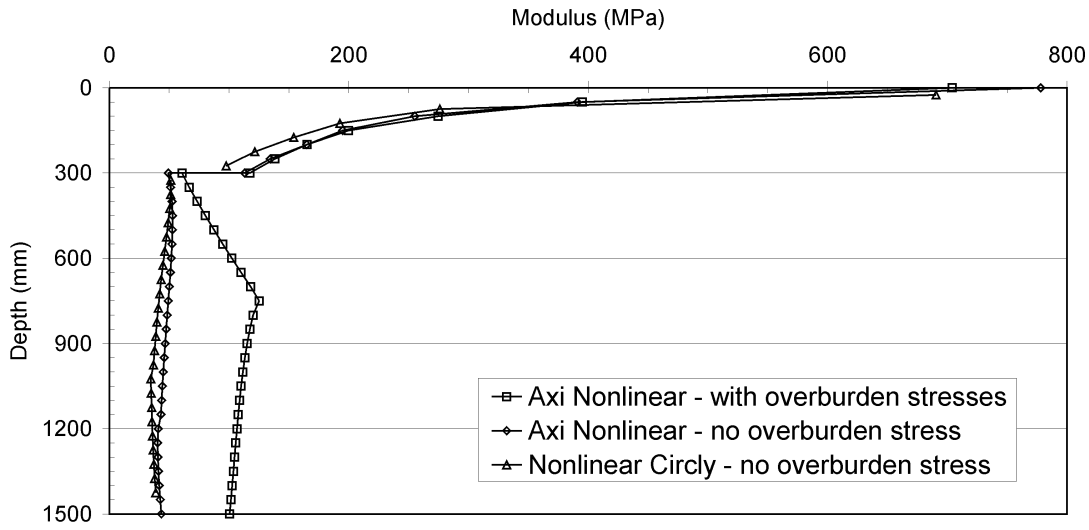

Figure 5.29 Variation of computed modulus values versus depth for the multilayer and full nonlinear models.

At increasing depths in the model, the stresses caused by the load decrease and the in situ stresses caused by the overlying material increase, therefore at shallow depths in the model the load induced stresses dictate the calculated stiffness and at greater depths, the in situ stresses control the stiffness. The relative effect of the bulk and shear terms can be determined by looking at the values of the exponents in the equation. The exponent for the bulk stress term for the subgrade model is positive and less than unity (0.4644); therefore, as the bulk stress increases, the value of the term also increases, albeit at a lower rate. The exponent for the octahedral shear term is negative (-2.2663); therefore, the value of the term will increase to an upper limit of 1.0 as the octahedral shear stress decreases to a lower limit of zero. Therefore, high levels of shear stress will have the effect of reducing the stiffness. The addition of 1.0 to the term prior to the application of the power function ensures that the base number is greater than or equal to 1.0 and prevents any numerical singularities in the calculation. The bulk and octahedral shear stresses are plotted in Figure 5.30, along with the components of the bulk stress that are caused by the load and overburden material. The octahedral shear stress is at a minimum when the total stress state is isotropic, i.e. when the total horizontal and vertical stresses are equal. In addition, at this depth in the pavement the bulk stress is comprised largely of the overburden stresses. It is coincidental that the bulk and shear terms combine to produce a nearly constant value of stiffness in the lower half of the subgrade material.

5.7.11 The Effect of the FWD Loading Plate on the Pavement Response

A series of nodes and elements were added to the 2D axisymmetric FEM model in order to model the FWD loading plate. The plate dimensions and material characterisation were the same as those given in section 2.14.1, namely a composite plate made up of three layers: aluminum, PVC and rubber. A relatively fine element size (5x5 mm) was used to avoid numerical problems with high stress concentrations at the outer edge of the plate. The mesh for the FWD loading plate was incorporated into the main mesh using the *SURFACE and *TIE options in ABAQUS/Standard.

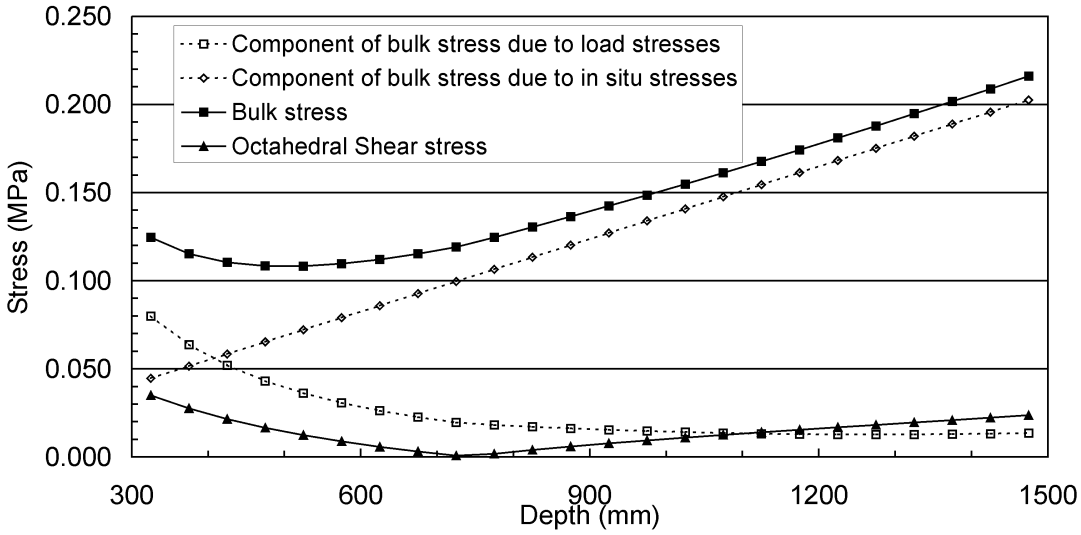

Figure 5.30 Contribution of stress components to the subgrade stiffness.

The loading plate system was bonded to the pavement surface because in practice, the rubber pad would mould to the micro texture of the pavement surface and no slippage would occur between the rubber pad and pavement surface.

The model was configured with two layers: granular material (300 mm) and subgrade (1200 mm). The granular material and subgrade were modelled as non-linear materials using the coefficients given in Table 5.1.

The results were compared with a model where the load was applied as a uniform pressure and it was found that the relative rigidity of the plate compared to the granular material resulted in high vertical stress values at the edge of the plate and low values at the centre of the plate. This resulted in unrealistic stress and thus, modulus distributions in the granular material. It was decided to eliminate the FWD loading plate from the FEM model as it appeared to introduce anomalies into the analysis that were unable to be verified by the available measurements. The FWD load was applied in subsequent analyses using a uniformly distributed pressure.

5.8 The FEM Modelling of a Pavement to Loading by a FWD

In this section, the axisymmetric FEM model is calibrated using one of the four load cases presented in Section 4.5 and then the response of the FEM model is determined for the remaining three load cases. The load case chosen for the model calibration was the 2nd FWD load case where the measured FWD plate pressure was 0.469 MPa and the loading plate diameter was 150 mm. This equated to a pavement loading of 33.2 kN and it was the load case that was closest to the standard half axle load of 40 kN. The FEM model comprised of a 300 mm thick layer of granular material on top of a 1200 mm thick layer of subgrade material. The subgrade material was modelled as two layers, the upper layer was 50 mm thick (one row of elements) and the lower layer was 1150 mm thick. The upper layer was created to provide a quasi transition layer between the granular and cohesive materials. The only difference in material properties between the two layers was in the value of the scalar (k_1) coefficient of the material model. The value of k_1 for the lower layer was set to 50% of the value of the upper layer, the value of k_1 that was used for the initial modelling of the upper layer was the value given in Table 5.1.

Some initial attempts were made at calibrating the model and two problems were encountered. The first problem was the existence of negative eigenvalues in the solution at the top of the subgrade. This was traced to the use of different n values for the granular and subgrade materials (0.5 and 2.0 respectively). This can be explained by considering the stress state in each material adjacent to the material boundary and the requirement of stress compatibility across the boundary. If one material is stiffer in the vertical direction than in the horizontal direction and the adjacent material has the opposite characteristics, then incompatibilities will arise in the stress continuity across the boundary.

This problem was resolved by making the subgrade material isotropic (n=1). The second problem was that the stress attenuation with depth was too great and this resulted in unreasonably low stiffness values of less than 20 MPa at the top of the subgrade. Even with the use of low stiffness values, the resulting vertical strain value was only 80% of the measured value.

The measured values of stress and strain at the top of the subgrade were used to give an idea of the required stiffness. The in situ modulus calculated for the 2nd FWD load case (FWD plate pressure 0.469 MPa) was:

$$\begin{aligned} M_r &= \frac{\sigma_d}{\varepsilon_r} \\ &= \frac{0.0937}{2125 \times 10^{-6}} \\ &= 44.1\,\text{MPa} \end{aligned} \tag{5.6}$$

This value of field stiffness was twice the value calculated by the material model, thus in order to achieve an acceptable solution, the vertical stress would have to be double the value that was being determined by the FEM model. In Section 5.6.1 it was observed that the vertical stress distribution remained unchanged when the scalar coefficient was changed, this means that once the relative stiffness of the different layers is determined, changing the scalar coefficients will not have a significant effect on the stress distribution. It was shown in Figure 5.24 that decreasing the value of *n* from 1.0 to 0.1 caused the vertical stress at a depth of 300 mm in the pavement to increase by 60%. This observation was used to reduce the stress attenuation by setting the value of *n* equal to 0.15.

It is recognised that the published values of *n* do not generally support such low values, however the methodologies used to measure the values in the laboratory may not give a true indication of the degree of anisotropy. It could be considered that the use of such a low value of *n* is an empirical or arbitrary condition placed upon the model, but without going to a higher order or elasto-plastic continuum formulation it would be difficult to arrive at a numerical solution that approximated the three different measured values (surface deflection, subsurface stress and strain). Another benefit of using a lower value of *n* is the reduction in the calculated horizontal tensile stresses at the bottom of the granular layer.

Other possible reasons may exist for the difference between the measured responses and the initial numerical results. One reason could be the effect of the dynamic nature of the loading on the pavement response and the time lag between the peak surface load and the peak pavement response at different depths and radial distances. The effect of wave travel time through geo-materials is well recognised

in the field of seismic engineering and was also noted by Al-Khoury (2002). The use of full dynamic simulation of the loading method, either FWD or rolling wheel, may improve the accuracy of the results but at a greater computational cost and difficulty in obtaining the required material parameters.

Once the values of n had been finalised (0.15 and 1.0 for the basecourse and subgrade respectively), the FEM model was solved using the laboratory derived material coefficients and the measured and computed pavement responses were compared. The computed surface deflection at the centre of the loaded area was 31% greater than the measured value, so the values of the k_1 coefficients were increased by 31% and the model was solved again. The measured and computed central deflections were equal, but the vertical strains at the bottom of the basecourse and the top of the subgrade differed by +81 and –9% respectively.

The values of the k_1 coefficients for the different layers were altered in turn until the computed vertical strains at the bottom of the basecourse and the top of the subgrade matched the measured values to within a tolerance of 5%. The k_1 value of the lower subgrade layer was always set to equal 50% of the value used for the upper layer. It took two iterations to get a satisfactory match for the basecourse strains and a further four iterations to get a satisfactory match for the subgrade strains. It was interesting to note that once the coefficient for the basecourse was finalised, the vertical strains in the basecourse changed very little despite changes to the scalar coefficient of the subgrade model in subsequent model solutions.

Once the difference between the measured and computed values for the vertical strains was acceptable, the computed values for the vertical stress at the top of the subgrade and the surface deflection at the centre of the loaded area were compared with the measured values and found to differ by –6 and 1% respectively. The strains, stresses and deflections obtained at the different stages of the calibration process are listed in Table 5.10. The final values of the model coefficients are listed in Table 5.11. It can be seen that the value for the basecourse material was increased by a factor of 2.43 while the value for the subgrade decreased by a factor of 0.78. This highlights the need to determine a shift factor or function when translating test results from the laboratory to the field.

The computed surface deflection bowls for the three stages (laboratory coefficient, surface deflection matched and strain matched) are plotted with the measured deflection bowl in Figure 5.31. The shape of the deflection bowl obtained after the calibration is flatter than the deflection bowl obtained after the laboratory coefficients were scaled to get a match for the central deflection. This result agrees with the changes in the model coefficients: the basecourse was made stiffer because of the calibration process, resulting in a flatter deflected shape. The measured and computed vertical strains are shown in Figure 5.32. It can be seen that the match between the strains at six of the seven points in the pavement is excellent; the maximum variation of the six "good" points was 7%. The second lowest point in the subgrade varies by 32%, but the overall shape of the strain curve is smooth.

The variation between the measured and modelled response at a depth of 487.5 mm may indicate that the subgrade is behaving as a series of distinct layers. The subgrade was constructed in 150 mm thick layers and the coil pair that is centred at a depth of 487.5 mm bridges across one such layer. The choice of material stiffness models and/or assumptions made in the modelling process also may not fully represent the behaviour of the subgrade material.

Table 5.10 Results of FEM calibration using 33.2 kN FWD loading.

		Measured	FEM						
			Lab Coefficient	% diff	Deflection ratio	% diff	Strain matched	% diff
Vertical Strains (μm/m)								
Depth (mm)	Base-course	112.5	449	1079	141%	823	83%	438	-2%
		262.5	438	1041	137%	794	81%	426	-3%
	Subgrade	337.5	2125	2544	20%	1935	-9%	2191	3%
		412.5	2016	1814	-10%	1383	-31%	1966	-2%
		487.5	1636	1269	-22%	970	-41%	1113	-32%
		562.5	796	964	21%	738	-7%	852	7%
Vertical Stress @ z=300 mm (MPa)									
		0.094		0.130	39%	0.130	39%	0.088	-6%
Central Deflection (mm)									
		0.837		1.098	31%	0.838	0%	0.848	1%

The model was solved for the three other load cases using the coefficients given in Table 5.11 and the results are shown in Table 5.12. Here it can be seen that the match between the measured and computed values could be considered very good overall, with the variation in results less 10% for three of the four load cases, the accuracy of the model for the highest load case is less than that for the other load cases (up to 17% variation). The measured and computed vertical strains for the other three load cases are shown in Figure C.1, Figure C.2 and Figure C.3.

Table 5.11 Coefficients for the FWD calibrated Uzan model.

	Basecourse	% change from laboratory value	Upper Subgrade	% change from laboratory value	Lower Subgrade
k_1	3.1885	143%	0.8868	-22%	0.4434
k_2	0.7600		0.4644		0.4644
k_3	-0.3068		-2.2663		-2.2663
p_a	100 kPa		100 kPa		100 kPa

The stress results are not in complete agreement, the model under-estimates the stress as the load increases. This highlights the potential issue that the stress distribution in the pavement may not be Hookean, as assumed in the model. It should be noted that the load varies by a factor of 2.8 from smallest to largest.

These results show that the pavement response can be successfully modelled using a numerical model that accounts for the stress dependant stiffness of the materials and that the model works over a reasonable range of loads. It should be noted that due to the assumptions and simplifications made in setting up the model, the range over which it would be accurate should be limited to a specified interval centred around the calibration load.

5.9 The FEM Modelling of a Pavement to Loading by a Rolling Wheel

In this section a series of 3D quarter symmetric FEM models were used to model the response of the PR3-0404 and PR3-0610 pavements to loading by a rolling dual tyre assembly. The models were calibrated using the same steps outlined in the previous section. Two different types of analysis were undertaken, the first analysis was to calibrate a single model at one load level, and then determine the model response to a range of load levels. The results of this analysis were then compared with the measured vertical strain data presented in Section 4.4.2. The second type of analysis was to model five different pavement sections from the two test pavements.

Table 5.12 Measured and computed pavement responses for all FWD load cases.

Applied Load (kN)			25.3			33.2			51.8			71.7		
			Measured	FEM	% diff	Measured	FEM	% diff	Measured	FEM	% diff	Measured	FEM	% diff
Vertical Strains (μm/m)														
Depth (mm)	Base-course	112.5	383	384	0%	449	438	-2%	573	549	-4%	676	640	-5%
		262.5	378	378	0%	438	426	-3%	509	528	4%	573	616	8%
	Subgrade	337.5	1714	1706	0%	2125	2191	3%	2966	3241	9%	3707	4331	17%
		412.5	1558	1542	-1%	2016	1966	-2%	2928	2947	1%	3740	3983	6%
		487.5	1233	880	-29%	1636	1113	-32%	2497	1653	-34%	3317	2258	-32%
		562.5	593	675	14%	796	852	7%	1198	1256	5%	1611	1716	7%
Vertical Stress @ z=300 mm (MPa)			0.067	0.073	8%	0.094	0.088	-6%	0.155	0.118	-23%	0.208	0.146	-30%
Central Deflection (mm)			0.642	0.684	7%	0.837	0.848	1%	1.200	1.212	1%	1.426	1.602	12%

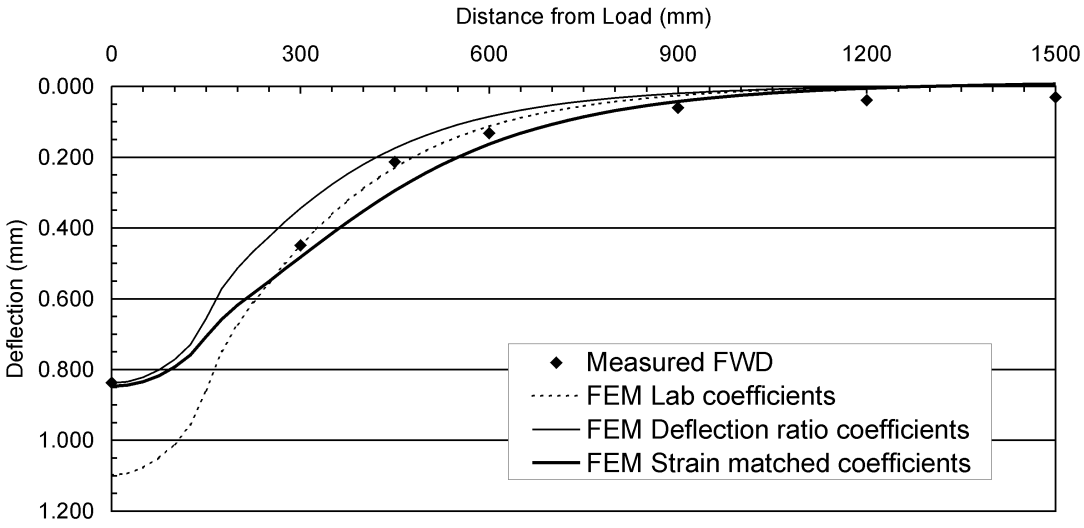

Figure 5.31 Surface deflection bowls for the different calibration stages.

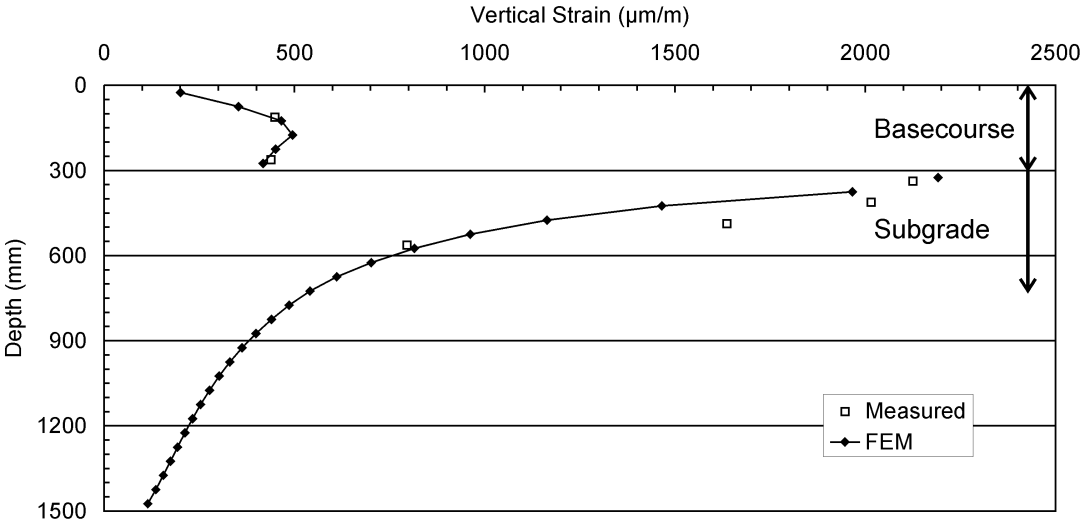

Figure 5.32 Measured and computed strains for a FWD load of 33.2 kN.

Each pavement section was calibrated with the strains measured at the mid point in the history of the pavement loading. The results of this analysis were used in Chapter 6 as an input to the performance model.

5.9.1 The Response of a Pavement Model to Varying Loads.

In this section, the data collected at the end of the PR3-0610 test was used to calibrate, and then verify the response model. The vertical strain data from Section D, outer wheelpath (Station 38) was used in this section. The model was calibrated with the data from the 40 kN dual tyre load and then the model response was determined for the remaining five load cases (23, 29, 35, 50 and 60 kN). Examination of the measured strain data for this coil array (Table A.6) showed that the maximum strain in the subgrade was measured with the uppermost coil pair rather than the second coil pair as had been the case for the data measured in the PR3-0404 pavement. Therefore, it was decided to model the subgrade as a single layer, rather than incorporating a thin transition layer between the basecourse and subgrade materials. The model UMAT parameters for anisotropy and overburden were the same as used for the FWD modelling in the previous section. The length and contact pressure of the load area for the different load levels was adjusted to match the actual measured values using the data presented in Section 4.2.

The calibration process followed the same steps as before, the k_1 coefficient of the basecourse was modified on an iterative basis until the computed vertical strain at the bottom of the basecourse was within 10% of the measured value. Then the k_1 coefficient of the subgrade was modified on an iterative basis until the computed vertical strain at the top of the subgrade was within 10% of the measured value. The measured strain values from between the wheels were used in the calibration process. The measured and computed vertical strains for the 40 kN calibration case are shown in Figure 5.33. It can be seen the match between measured and computed strains is good for both the strains between the tyres and directly beneath the centre of one tyre. The percentage difference between the measured and computed values is less than 7% for the top two coil pairs in the subgrade and less than 14% for the bottom coil pair in the basecourse. The large difference between the computed and measured vertical strains at the top of the basecourse, between the tyres, can be attributed to the lack of a surfacing layer in the model.

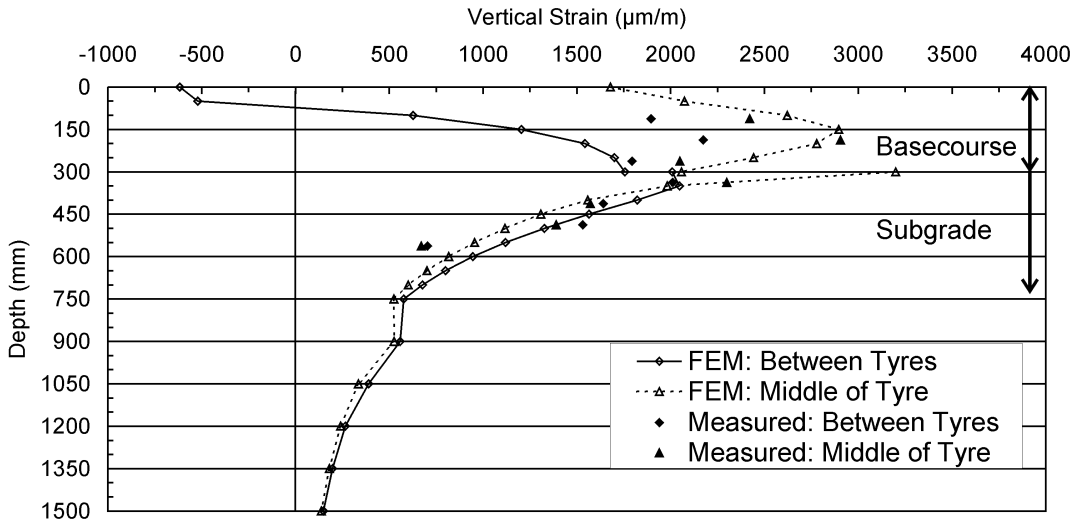

Figure 5.33 Measured and computed vertical strains for a 40 kN dual wheel load, Station 38, outer wheelpath, PR3-0610 pavement, 1447k laps.

In CAPTIF pavements, the asphalt concrete surfacing would provide resistance against any vertical heaving or upward movement between the wheels, however the surfacing layer was eliminated because of a membrane effect that reduced the effect of vertical loads deeper in the pavement. The lack of restraint against heaving in the model allowed the calculation of much smaller vertical strains compared to the measured strains. The final model coefficients are listed in Table 5.13 and it can be seen that the values of k_1 for the basecourse and subgrade are less than the initial laboratory values. These coefficients were then used to model the pavement to a series of loads ranging from 23 to 60 kN and the resulting strains are shown in Table 5.14, Table 5.15, Figure 5.33 and Figure C.4 through Figure C.8. A plot of the modulus distribution for the 40 kN load case is shown in Figure 5.34, here it can be seen that the maximum vertical modulus is 446 MPa beneath the tyre and drops to one third of this value at the bottom of the basecourse layer.

The computed modulus distribution is compared with the distribution that would be obtained if the Austroads granular material modulus sub-layering procedure was used (AUSTROADS 2004a, Equation 8.4, page 8.5, Section 8.2.3). In the Austroads approach, a modular ratio is determined so that there is a smooth

progression in the sub-layer stiffness from the top of the subgrade to the top of the granular layer. The modular ratio is defined by

$$R = \left[\frac{E_{\text{top of granular layer}}}{E_{\text{top of subgrade}}} \right]^{\frac{1}{nlayer}} \tag{5.7}$$

where

$$\begin{aligned} R &= \text{Modular ratio between adjacent sub - layers} \\ E_{\text{top of granular layer}} &= \text{Modulus at the top of the granular layer} \\ E_{\text{top of subgrade}} &= \text{Modulus at the top of the subgrade} \\ nlayer &= \text{Number of sub - layers in the granular layer} \end{aligned}$$

For this case, the modulus of the subgrade and top of the granular layer were 35 and 450 MPa respectively. The values were chosen from the values computed by the FEM model. The modulus for the top of the granular layer is comparable to normal design values for high quality basecourse material, but the subgrade modulus may be considered too low given the material classification. The modulus distribution for the six sub-layers in the granular material is shown on the left-hand side in Figure 5.34. It can be seen that the Austroads approach for determining the modulus values for the sub-layers results in moduli values that are much lower than those which are calculated in the lower part of the granular material (54 versus 114 MPa). The modular ratio for the calculated modulus values in the granular material is approximately 1.25, compared to a value of 1.53 as determined by Equation (5.7).

A plot of the percentage difference between the measured and modelled strains is shown in Figure 5.35. It can be seen that the differences between the measured and computed values at the bottom of the basecourse and top of the subgrade are on the whole around ±10-15%, with a slightly greater difference in the subgrade values at the minimum and maximum loads. Two possible reasons for this greater difference at the ends of the load range is that the chosen material model is not the best model to use for the subgrade material and that the stress distribution in the model does not reflect the actual field conditions.

Table 5.13 Coefficients for the rolling wheel load calibrated Uzan model.

	Basecourse	% change from laboratory value	Subgrade	% change from laboratory value
k_1	0.5325	-59%	0.6853	-40%
k_2	0.7600		0.4644	
k_3	-0.3068		-2.2663	
p_a	100 kPa		100 kPa	

Even though the model was calibrated using strain values measured between the wheels, the model predicts the strains directly under the wheel with a reasonable degree of accuracy across all of the load levels.

The computed vertical stress values at the top of the subgrade, between the wheels are shown in Figure 5.36 and Table 5.16. It can be seen that the computed values vary linearly with load. This is expected as the model is based on first order elastic theory and the fact that the relative stiffness of the different materials used in the model remains constant. The measured and computed stress values compare favourably, although there is a difference in the rates of change of the two sets of values. The measured data were presented in Table 4.4.

The surface deflections are shown in Figure 5.37. As with the other responses (stress and strain), the values vary linearly with load. This result is similar to that shown with the FWD measurements, i.e. the overall system response is linear with load.

5.9.2 Model Calibration Using FWD Measurements

The only cost effective method of assessing the stiffness of pavements is with the FWD device. It would be beneficial to be able to use these measurements to calibrate the FEM models. By using the calibration results from the previous two sections a framework was developed to use the FWD measurements to calibrate the 3D model for use with dual tyre loading. It was previously observed that when the model was calibrated to predict strains that were comparable to the measured values, the deflection of the surface was close to the measured value.

Table 5.14 Measured and computed vertical strain measurements for varying loads (23, 29 & 35 kN).

		Between the wheels			Middle of Tyre		
		Measured	FEM		Measured	FEM	
Dual tyre load (kN)	Depth (mm)	Vertical Strain (μm/m)		% diff	Vertical Strain (μm/m)		% diff
23	112.5	1445	700	-52%	2592	2470	-5%
	187.5	1789	1252	-30%	2681	2421	-10%
	262.5	1393	1371	-2%	1673	1863	11%
	337.5	1317	1134	-14%	1663	1284	-23%
	412.5	860	978	14%	821	840	2%
	487.5	867	654	-25%	841	655	-22%
	562.5	403	508	26%	411	520	27%
29	112.5	1482	724	-51%	2567	2577	0%
	187.5	1934	1348	-30%	2714	2597	-4%
	262.5	1558	1515	-3%	1764	2063	17%
	337.5	1581	1449	-8%	1832	1637	-11%
	412.5	1163	1250	8%	1001	1070	7%
	487.5	1142	836	-27%	989	834	-16%
	562.5	520	648	25%	491	660	34%
35	112.5	1893	735	-61%	3096	2643	-15%
	187.5	2082	1418	-32%	2902	2721	-6%
	262.5	1690	1632	-3%	1938	2225	15%
	337.5	1873	1767	-6%	2157	1988	-8%
	412.5	1463	1524	4%	1353	1300	-4%
	487.5	1389	1017	-27%	1257	1012	-19%
	562.5	639	789	23%	611	800	31%

Table 5.15 Measured and computed vertical strain measurements for varying loads (40, 50 & 60 kN).

		Between the wheels			Middle of Tyre		
		Measured	FEM		Measured	FEM	
Dual tyre load (kN)	Depth (mm)	Vertical Strain (μm/m)		% diff	Vertical Strain (μm/m)		% diff
40	112.5	1896	771	-59%	2421	2690	11%
	187.5	2174	1458	-33%	2906	2808	-3%
	262.5	1794	1714	-4%	2049	2346	14%
	337.5	2011	2037	1%	2299	2286	-1%
	412.5	1641	1757	7%	1571	1496	-5%
	487.5	1531	1171	-23%	1390	1164	-16%
	562.5	703	908	29%	670	921	37%
50	112.5	2104	671	-68%	3052	2721	-11%
	187.5	2220	1480	-33%	2915	2868	-2%
	262.5	1916	1820	-5%	2160	2502	16%
	337.5	2205	2524	14%	2415	2817	17%
	412.5	1858	2197	18%	1745	1866	7%
	487.5	1695	1470	-13%	1536	1456	-5%
	562.5	794	1140	44%	758	1154	52%
60	112.5	1991	653	-67%	2901	2771	-4%
	187.5	2193	1528	-30%	3067	2953	-4%
	262.5	2153	1933	-10%	2384	2661	12%
	337.5	2383	3058	28%	2728	3382	24%
	412.5	2171	2667	23%	2139	2259	6%
	487.5	1910	1782	-7%	1809	1764	-3%
	562.5	896	1382	54%	880	1398	59%

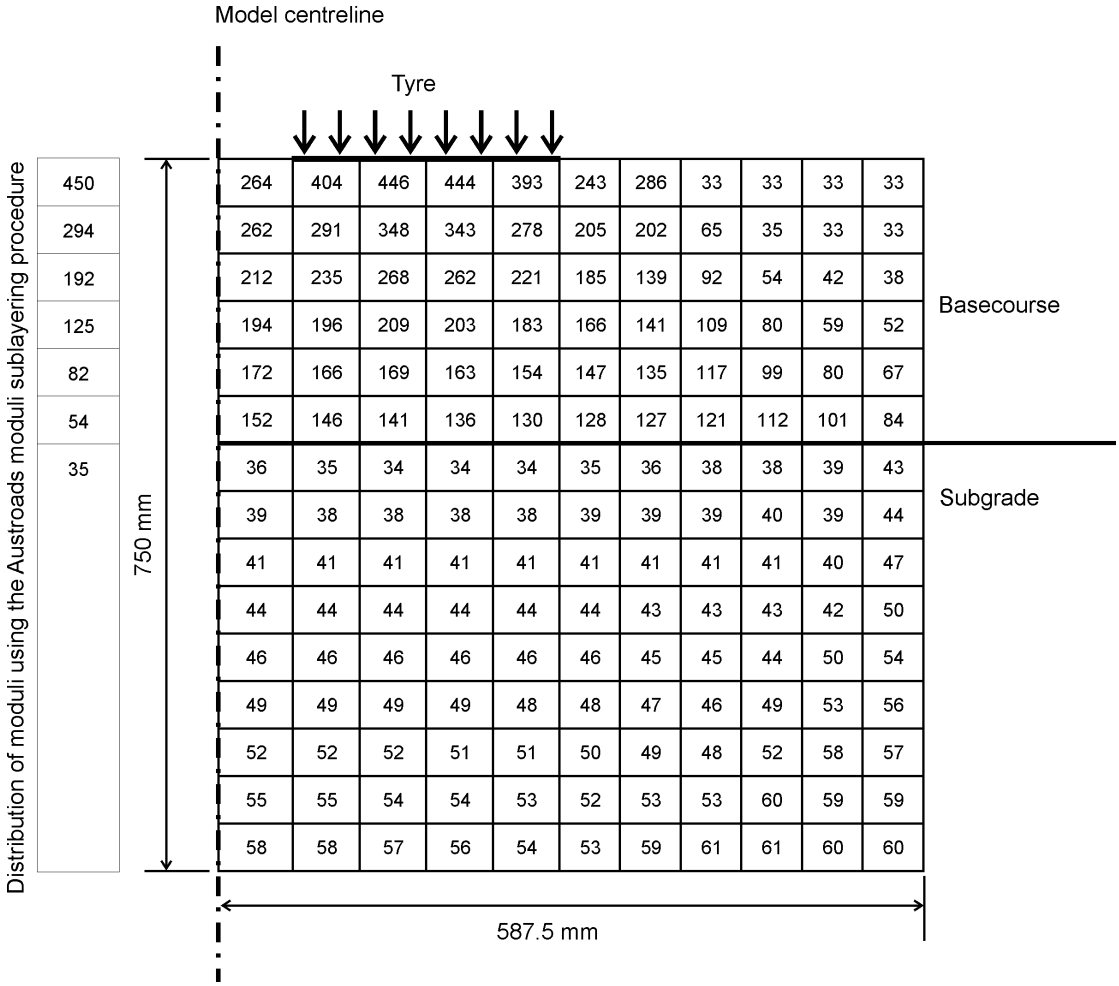

Figure 5.34 Distribution of vertical moduli values for the fine mesh area for the 40 kN load case, Station 38, outer wheelpath, PR3-0610 pavement.

It was also calculated that the surface deflection measured under a rolling wheel was on average 16% greater than the deflection measured under the FWD for the same load. Therefore if the FWD deflection was increased by 16% and the FEM model was then calibrated with the adjusted deflection, this should give a reasonable prediction of the strain values.

The validity of this methodology was tested with the data from station 38, outer wheelpath, PR3-0610 pavement after 500,000 load applications. The FWD load level was 43.6 kN and this was converted to a dual tyre load with the same load using the tyre footprint dimensions listed in Table 4.1 for the 40 kN dual tyre load. This resulted in a contact pressure of 0.400 MPa.

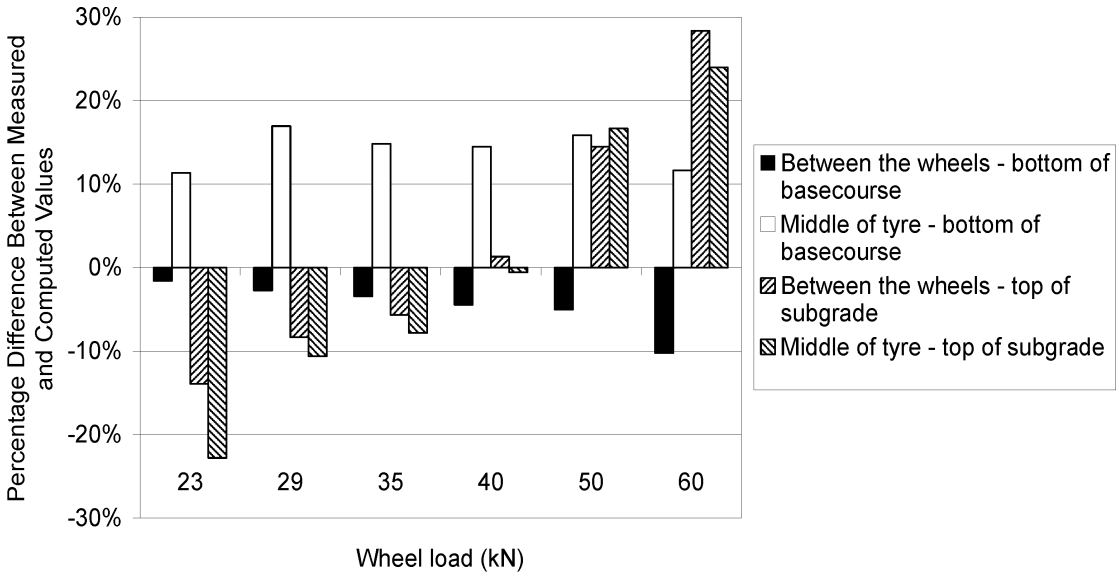

Figure 5.35 Percentage differences for measured versus computed strains, Station 38, outer wheelpath, PR3-0610 pavement, 1447k laps.

The measured deflection was increased by 16% to a value of 0.995 mm. The initial FEM solution was found using the laboratory derived material coefficients. The maximum surface deflection beneath a tyre and the deflection between the tyres was averaged and this value was 0.680 mm. The original k_1 coefficients (1.3131 & 1.1438) were multiplied by the ratio of the measured (adjusted) to computed values to give new values of 0.8895 and 0.7778 and the model was solved again. The average FEM deflection was 0.997 mm and the deflection bowls are plotted along the longitudinal axis of the model in Figure 5.38. Here it can be seen that there are some differences between the computed and measured values although these differences are explained by the technique used by the FWD to capture the maximum value rather than deflections at the same time as the peak load. The vertical strains are plotted in Figure 5.39 and while the FEM basecourse strains are 600 μm/m greater than the measured values, the subgrade strains match reasonably well. This example shows that the FWD measurements can be adjusted in a transparent manner and be used to calibrate a FEM model to predict the pavement response to loading by a rolling wheel.

Table 5.16 Computed stress values at the top of the subgrade, Station 38, Outer wheelpath, 1447k laps, PR3-0610 pavement.

Load (kN)	FEM Computed (MPa)
23	0.083
29	0.101
35	0.117
40	0.129
50	0.153
60	0.174
Least squares regression	
Slope (MPa/kN)	0.002453
Intercept (MPa)	0.029
R^2	0.996

5.9.3 The Response of Different Pavement Designs

In this section, five different load/pavement configurations were modelled. The objective of this section was to calibrate the models at a fixed point in time during the accelerated testing phase of the CAPTIF tests. The computed surface deflection from the calibrated models would be compared with FWD measurements taken at the same time and then the calculated strain distribution within the pavement would be used as an input into the pavement performance model that will be developed in Chapter 6.

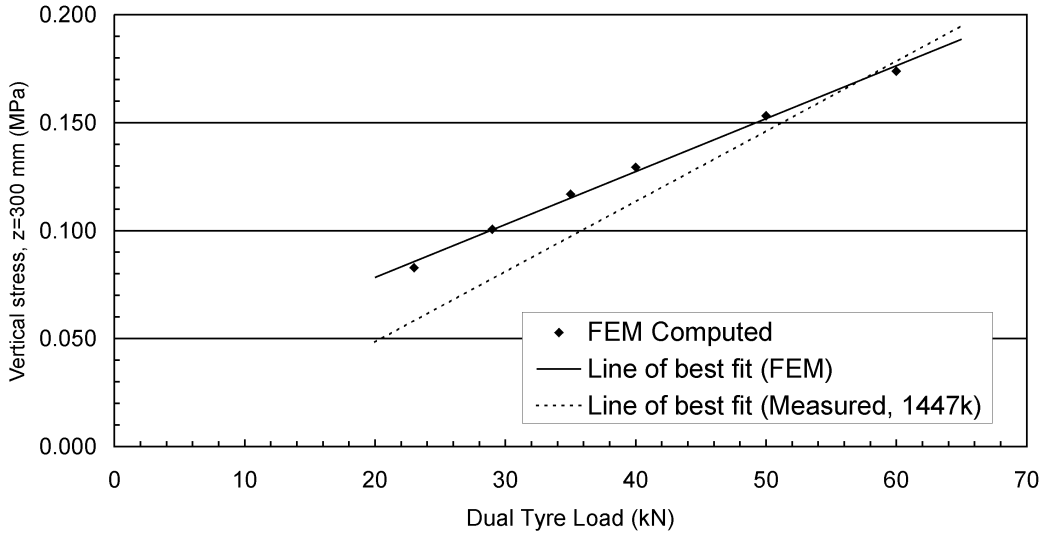

Figure 5.36 Computed vertical stresses at the top of the subgrade, Station 38, outer wheelpath, PR3-0610 pavement, 1447k laps.

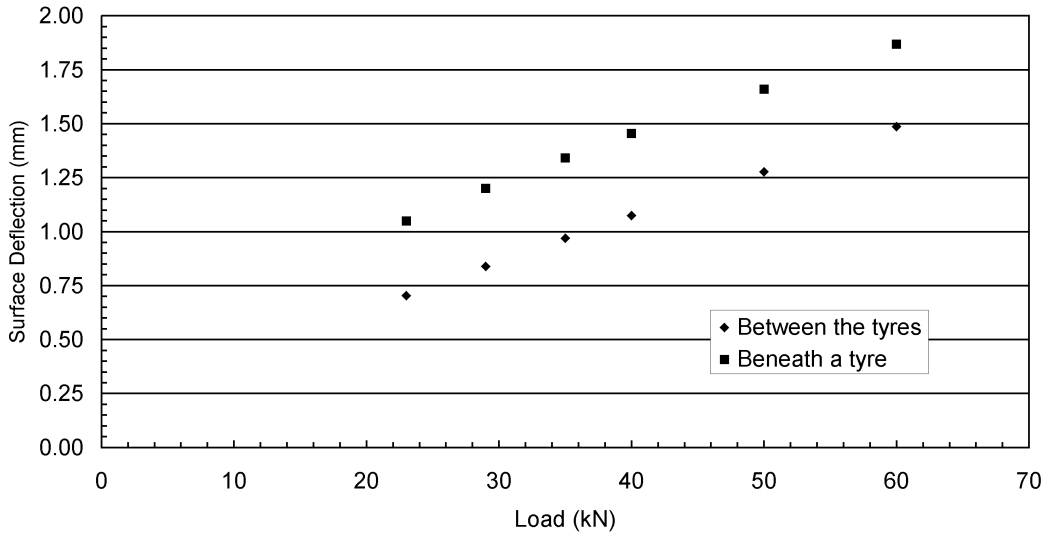

Figure 5.37 Computed surface deflections for varying load levels, Station 38, outer wheelpath, PR3-0610 pavement, 1447k laps.

The different pavement sections and loads are given in Table 5.17. It was recognised that each of the five models would require separate calibration processes since there was sufficient variation in the moisture content and compaction of the materials to make the overall response of each section unique. The calibration for Model I was done with data measured at 600,000 load applications and at 500,000

load applications for Models II to V. After examining the shape of the distribution of measured strains with depth for each model, it was decided that Models I and IV would be modelled with a transition layer at the top of the subgrade and Models II, III and V would be modelled without the transition layer.

If a FEM model was being calibrated solely with surface deflection measurements, it would be difficult to judge whether or not a transition layer would be required. A conservative or historical approach would be to not include a transition layer. The calibration was done following the procedure outlined previously. A summary of the k_1 coefficients and model responses is given in Table 5.18. In this table, it can be seen that there is a reasonable spread in the values of the k_1 coefficients for both the basecourse (0.5560 to 1.3892) and subgrade (0.5365 to 1.3018) materials.

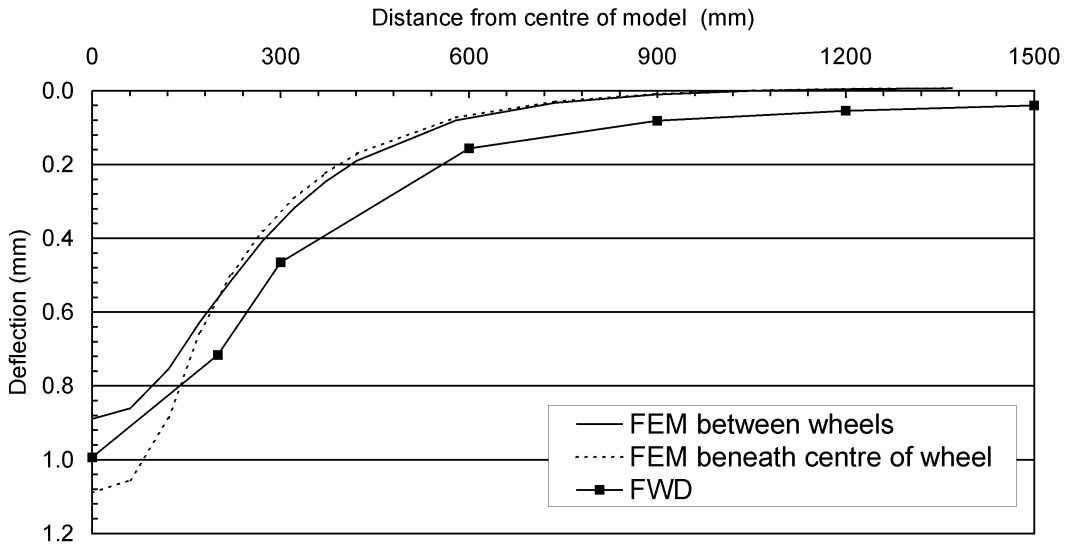

Figure 5.38 Computed and measured surface deflections for the rolling wheel model calibrated with FWD measurements.

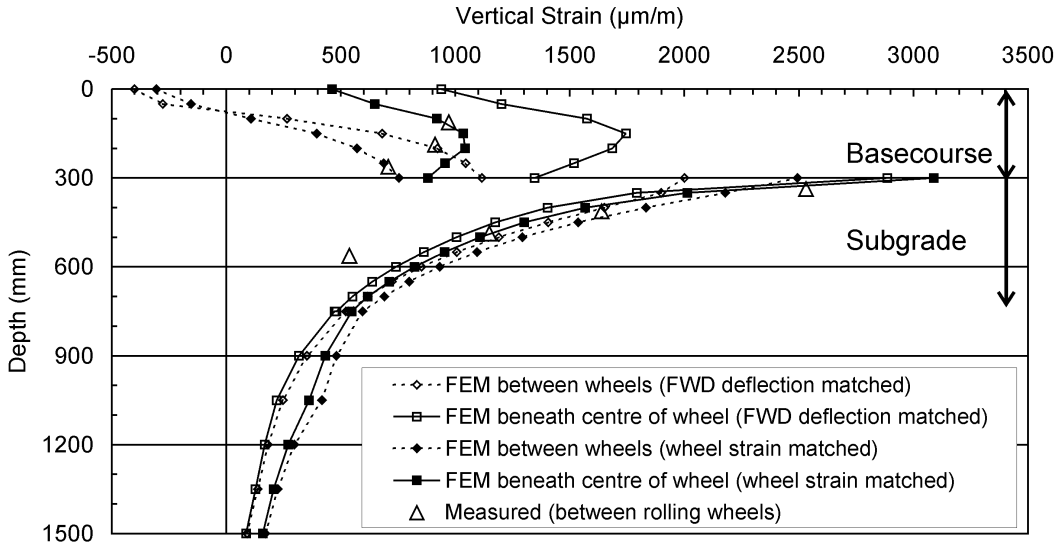

Figure 5.39 Computed and measured strain values for the rolling wheel model calibrated with FWD measurements.

Table 5.17 Model configuration for FEM response loading.

ID	Project	Segment	Wheelpath	Thickness of granular base (mm)	Load Level (kN)
I	PR3-0404	A	Inner	300	40
II	PR3-0610	C	Inner	225	60
III	"	C	Outer	225	40
IV	"	D	Inner	300	60
V	"	D	Outer	300	40

The model that was used in the previous section was based on data collected at the end of the PR3-0610 test at the same location as Model V and it can be seen that the k_1 coefficients (listed in Table 5.13) changed from 1.3892 to 0.5325 for the basecourse and from 0.5365 to 0.6853 for the subgrade. This change was not unexpected as an additional 847,000 load applications had been applied, of which 447,000 were at a much higher level (60 versus 40 kN) and the pavement at that point was showing signs of accelerated failure (see Figure 4.30 and Figure 4.37). The large reduction in the value of the basecourse coefficient can be interpreted as a loss of load carrying ability of the granular material.

The maximum computed surface deflection was compared with measured deflections from the FWD and it is seen in Table 5.13 that the computed deflections are on average 27% higher than the FWD deflections for the same level of loading. The FWD deflections were scaled to the level of the appropriate wheel load by using the average load/deflection relationships for Stations 9 and 23 that were presented in Table 4.7. The deflections that were measured by the FWD and CAPTIF Deflectometer (Table 4.5 and Table 4.6) were compared and it was found that the rolling wheel deflection was 16% greater than the FWD deflection for the same level of applied load. This is another observation that the FWD does not induce the same response as a rolling wheel. After the FWD/Rolling wheel difference (16%) was subtracted, the overall difference between the measured and computed deflections was 12%. This difference is considered acceptable given the differences between the measurement and modelling spaces.

Table 5.18 Summary of model coefficients and computed and measured responses for different pavement models.

Model ID	k_1 value		Transition layer	FWD Deflection at APT load (mm)	Max FEM Deflection (mm)	% Difference between FWD and FEM deflection	% Difference between measured and computed strains		
	Basecourse	Subgrade					Bottom of basecourse	Top of subgrade	2nd pair in subgrade
I	1.3892	0.8094	Yes	0.935	1.146	+23	-7	0	3
II	0.5560	1.3018	No	1.222	1.551	+27	-5	-44	3
III	1.0667	0.8781	No	0.854	0.954	+12	-8	-15	18
IV	1.0479	0.8218	Yes	1.150	1.726	+50	-10	-6	-23
V	1.3892	0.5365	No	0.785	1.025	+31	0	-11	7

The differences between the measured and computed strains for the five models could be considered to be good, the basecourse variations are less than 10 percent with a higher level of scatter in the subgrade. The scatter in the subgrade could be attributed to small variations in the vertical position of the coil pairs, imhomogniety in the in situ material properties or the different loading/permanent deformation history at each coil array.

5.10 Conclusions

In this chapter the development of a multi layer non-linear elastic, 2D axisymmetric and 3D quarter symmetric FEM models is described. The formulation of the models was checked against accepted theoretical solutions and the models were found to have been formulated correctly. A potential error in the Circly program was found, but the effect of the error was reduced when a high number of layers, each with a different value of stiffness were used. The effect of anisotropy on the model response was investigated and it was found that as the degree of anisotropy increased, the stress attenuation reduced. This finding was used to decrease the model anisotropy factor, n, from 0.5 to 0.15.

A process of determining a transfer function to translate laboratory measured model coefficients to field coefficients was developed. This process was used to calibrate models by either using measured surface deflections or subsurface strain values.

The pavement response to loading by the FWD was modelled using the 2D axisymmetric FEM model. One of the data sets was used to calibrate the model at one load level and then the model was used to predict the pavement response at the other three load levels. The match between the measured and computed responses (vertical stress and strain and surface deflection) was considered very good considering the range of applied loading (25 to 71 kN).

A 3D quarter symmetric model was calibrated at one load level of a rolling wheel and then the model was used to predict the pavement response (vertical stress and strain) for load levels ranging from 23 to 60 kN. The match between the measured and computed responses was found to be good, given the wide range of loads that were modelled.

An additional five 3D quarter symmetric pavement models were calibrated to provide input data for the pavement performance model developed in Chapter 6. It was found that there was considerable variation in the final model coefficients for the different models, even though good matches were found between the measured and computed pavement responses (vertical strain and surface deflection) for each model. It was also found that the surface deflection measured beneath a rolling wheel was 16% greater than the deflection measured under a FWD at the same load level. The difference between the computed surface deflection and the estimated (from FWD measurements) surface deflection was found to be 12%. The implication of this is that while the FWD and associated analysis techniques are widely accepted by engineers and the outputs from the backcalculation process may seem to be realistic, the measurements presented in this thesis show that the subsurface response of the pavement is very much dependant on the loading mechanism (vertical impact pulse versus smooth rolling approach and departure). This makes it problematic to compare the FWD derived outputs with outputs measured/derived from other loading systems, however specific FWD responses (applied load and deflection of the centre of the loading plate) can be modified and used to calibrate rolling wheel models with some degree of success.

This page is intentionally left blank.

Chapter 6 Pavement Performance Modelling

6.1 Introduction

This chapter develops a framework to predict the permanent deformation of the basecourse layer in the pavement structure. The framework is based on similarities observed between RLT and field data and uses the resilient axial strain to predict the rate of development of the plastic strain or Permanent Deformation (PD). The relationships developed using the laboratory data are applied to the vertical strains predicted in the previous chapter and integrated over the depth of the granular layer and a number of laps to determine the permanent deformation occurring in the granular layer. The match between the predicted and measured permanent deformation was not strong, however the magnitude of the accumulated PD measured in the test pavements was small (<5 mm) after 1,000,000 load applications.

6.2 Laboratory RLT Measurements

Arnold (2004) conducted three multi-stage CCP PD RLT tests at the University of Nottingham on the TNZ M/4 basecourse material that was used in the test pavements. For each RLT test, the specimen was subjected to repeated loading at a number of different stress states. In each test the specimen was subjected to 50,000 load cycles at a loading frequency of 5 Hz of each stress state and each subsequent stress state was more severe than the previous stress state. In the three tests, the mean stress was held at a constant value of either 75, 150 or 250 kPa and as each test progressed, the confining stress decreased as the deviatoric stress increased in successive stages until the specimen failed. The specimens were compacted to achieve a dry density of 95% of MDD and 70% of OMC (target values of 2120 kg/m³ and 3.6%), strain measurements were done with two on-specimen LVDT's mounted over the middle half of the specimen and the specimen height and diameter were 300 and 150 mm respectively. Arnold analysed the PD data in his thesis as a function of stress state and the number of load applications.

The author has postulated two hypotheses based on observations of RLT tests conducted over a period of time. The first observation is that there appears to be a physical limit to the magnitude of the resilient axial strain that a specimen can sustain before it fails. This limiting strain appears to be independent of the stress state and could possibly be a function of the interface between the specimen and the confining medium in the RLT cell. Near the perimeter of the specimen, the particles are constrained by a constant stress applied by the confining medium (air, oil or water) acting through the impermeable membrane. In the middle of the specimen, the interparticle forces are much higher due to the point to point contact of the particles and this may help contain the resilient straining that occurs when the load is cycled. Therefore, due to the physical limitations of the test device, the specimen may not be able to be subjected to the range of resilient strains that may be generated in a pavement.

The second observation is that when a specimen exhibits shakedown behaviour of either type A or B (Section 2.10.5), the resilient axial strain is a constant value over the duration of the test (ignoring the initial "bedding in" cycles). This type of response mirrors the behaviour that is seen in CAPTIF tests. Because the PD RLT tests are generally conducted over either 10,000 or 50,000 load cycles, it can be difficult to accurately determine whether the form of the long term PD response is either linear ($PD = a + bN$) or logarithmic ($PD = aN^b$). The selection of the PD-N equation can have a significant effect, especially when the PD model is extrapolated to a higher number of load applications (>500,000). The cost and time required to conduct RLT testing to 1 million or more load cycles would be prohibitive, although a better understanding of the long-term behaviour would be obtained.

In light of these two hypotheses, the raw RLT data was obtained from Arnold and reanalysed in terms of resilient axial strain and the rate of PD development. A representative plot of the resilient and PD versus the number of load cycles is shown in Figure 6.1. Because the initial part of the PD curve is often influenced by the technique employed to setup the specimen in the RLT cell it was decided to focus on the steady state response of the specimen.

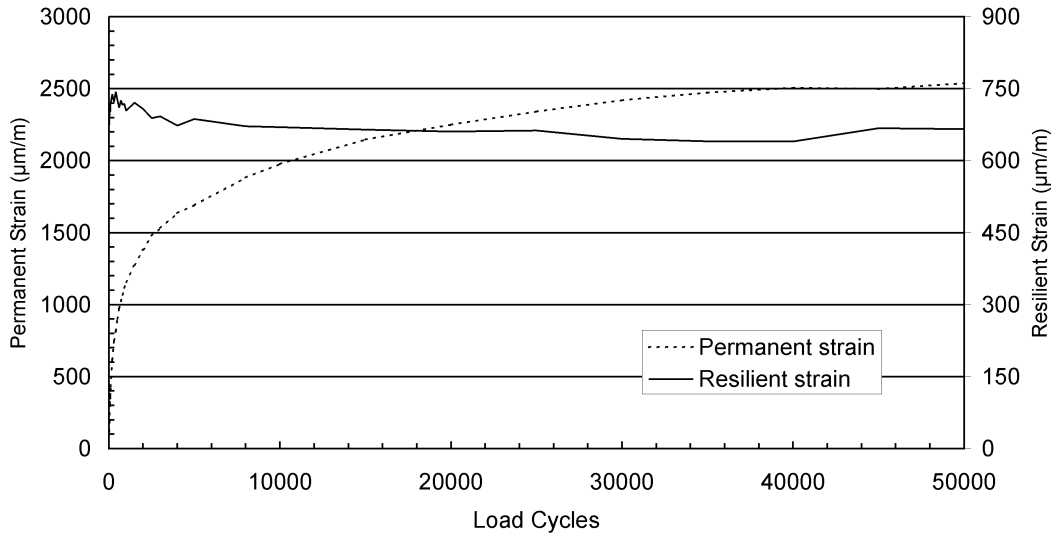

Figure 6.1 Permanent and resilient strains versus load cycles (confining stress = 11 kPa, deviatoric stress = 183 kPa).

The PD strain rate ($\dot{\varepsilon}_p$) was determined by undertaking a least squares linear regression analysis using the data from 20,000 to 50,000 cycles, likewise the resilient strain (ε_r) was averaged over the same interval to give an average value of ε_r. The test conditions and results are summarised in Table 6.1. The results show that stable behaviour (Shakedown Range A or B) was evident when the axial resilient strain was below 1,000 µm/m. The values of $\dot{\varepsilon}_p$ are plotted against ε_r and are shown in Figure 6.2. The function which gave the best fit was of an exponential form and is:

$$\dot{\varepsilon}_p = 0.4908 \times 10^{-3} \cdot e^{3.9479 \times 10^{-3} \cdot \varepsilon_r} \tag{6.1}$$

The coefficients were determined by decomposing the equation into a linear form by taking the logarithm of each side and then using the technique of least squares to determine the coefficients for the transformed equation, the R-Squared value was 0.92. It was observed that a small change in the power coefficient would result in a significant difference in the value of $\dot{\varepsilon}_p$ for a given value of ε_r when the resilient strain is close to the observed upper limit of 1000 µm/m.

Table 6.1 Summary of Arnold (2004) PD RLT data

Specimen	Mean Stress (kPa)	Deviatoric stress (kPa)	Confining stress (kPa)	Resilient axial strain[1] (μm/m)	Permanent axial strain rate[2] (μm/m/cycle)
1	73	43	58	158	0.001233
(p=75 kPa)	73	91	43	347	0.001465
	73	139	27	530	0.003749
	72	183	11	655	0.009021
	68	203	0	[3]	
2	145	135	100	296	0.001319
(p=150 kPa)	150	183	88	399	0.002291
	146	229	70	493	0.003129
	145	274	54	588	0.004982
	146	319	40	[4]	
3	242	324	134	691	0.002963
(p=250 kPa)	243	376	118	836	0.013456
	245	419	105	930	0.015353
	238	465	83	1056	0.032766
	244	515	72	[5]	

[1] average of data from 20,000 to 50,000 cycles
[2] linear approximation over data from 20,000 to 50,000 cycles
[3] 775 μm/m but Type C behaviour, lasted 50k cycles
[4] peaked @ 1130 μm/m then dropped after 10k cycles, Type C behaviour, lasted 50k cycles
[5] 1150 μm/m until failure @ 8k cycles

6.3 Performance Modelling of Test Pavements

Because of the difficulty in determining the initial post-construction compaction of a pavement, it was decided to calculate the amount of PD that occurred over the steady state phase of the testing. The steady state phase was deemed to have started when the change in PD accumulation became linear with respect to the number of load applications and it usually starts within the first 100,000 load applications in CAPTIF tests. Therefore, the amount of PD that occurred from 100,000 load applications to the end of the tests was calculated in the following manner:

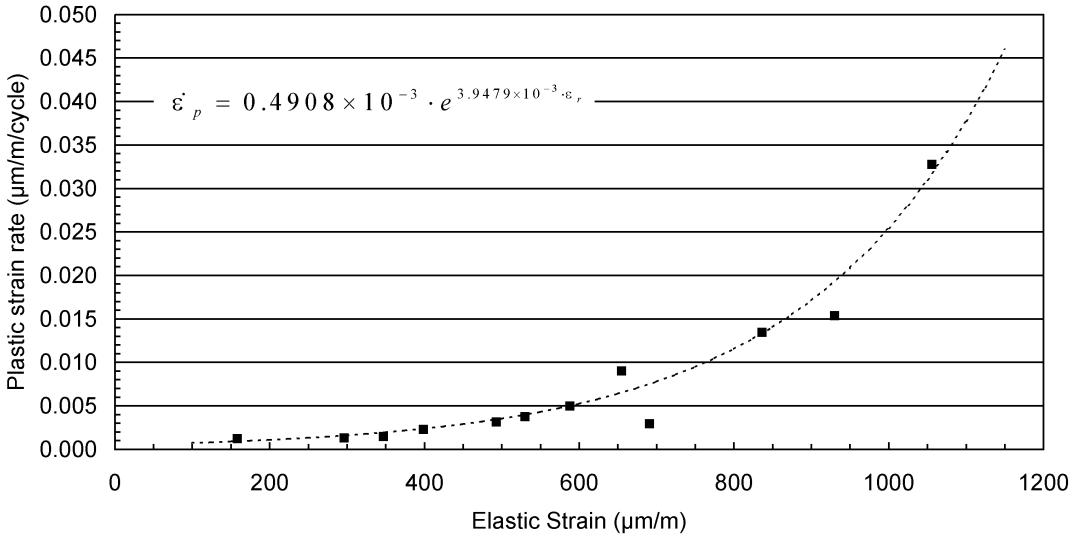

Figure 6.2 Resilient strain versus Plastic strain rate for RLT data.

1) The vertical strain profile of the pavement when it was subjected to the standard loading was determined at a point near to the mid point in the history of the pavement loading.

2) The basecourse layer was divided into a number of sublayers and the vertical resilient strain at the midpoint of each layer was used to determine the value of $\dot{\varepsilon}_p$ for each layer.

3) The contribution of each sublayer in the basecourse was determined by calculating the product of the thickness of the sublayer (50 mm for 300 mm thick basecourse layer and 56.25 mm thick for the 225 mm thick basecourse layer), the number of load applications (1,000,000 – 100,000 = 900,0000) and $\dot{\varepsilon}_p$.

4) The total amount of PD in the basecourse layer was calculated by summing the contributions of the sublayers.

The strain profile was determined between the two tyres and beneath the centre of one tyre. The two profiles were chosen because the limited transverse wander used in the CAPTIF tests (for operational reasons) resulted in the development of a small ridge between the two tyres of the dual tyre assembly. This type of response is not

typical of in-service pavements where the vehicle wander is greater, resulting in a smooth rut shape in each wheelpath.

The actual values of PD were calculated by subtracting the transverse profile measured after 1,000,000 load applications from the profile measured after 100,000 load applications and then averaging the resulting VSD values from the nominal transverse position and ± 1 reading either side. For the value beneath the centre of the tyre, the values from beneath the middle of both tyres were averaged to eliminate any imbalance in PD between the two tyre paths (average of six values). The values obtained were reduced to 70% of the calculated value to remove the PD that occurred in the subgrade (Table 4.12). The PD values for the different test sections are given in Table 6.2. It can be seen that the actual values are small (<4 mm), so any inaccuracies in the calculations or models used in the process could have a significant effect on the results.

The strain profiles that were calculated in Section 5.9.3 were used in the calculations carried out in this section. The possibility that a shift factor may be required to translate from the laboratory to the field was recognised, since the laboratory analysis showed that a vertical strain of 1000 μm/m or greater resulted in unstable or rapid failure, but vertical strains in excess of this boundary value were measured and subsequently predicted from the test pavements and these particular pavements were not showing any signs of accelerated distress.

Model II was not included in the analysis as the strain measurements at the bottom of the basecourse and top of the subgrade showed continual change throughout the project, indicating that the internal response of the pavement was not stable. Given the thin basecourse layer (200 mm) and the high level of loading (60 kN) it is not surprising that this section did not exhibit stable behaviour. The calculation process for Station 38, outer wheelpath, PR3-0610 pavement (Model V) is detailed in Table 6.3. In the calculations shown in this table, there is no modification of the parameters. The computed values were 0.6 mm less and 2.9 mm greater than the measured values for the locations between the tyres and beneath a tyre respectively. A shift factor was included to reduce the model strains to fit within the limits of the laboratory model. Reducing the computed elastic strains to 70% of the original values prior to calculating the plastic strain rate produced the closest fit to the

measured values across the five models. The differences for Model V reduced to 1.1 and 0.5 mm less than the measured values for the positions between and beneath the tyres respectively.

Table 6.2 PD of basecourse layer from measured values (100-1000k load applications).

Model ID		Between tyres PD (mm)	Beneath tyre PD (mm)
I	VSD 0-1000k	2.8	4.8
	VSD 0-100k	1.5	2.6
	VSD 100-1000k	1.3	2.2
	Basecourse PD (70% of 100-1000k value)	**0.9**	**1.5**
II	VSD 0-1000k	6.5	8.1
	VSD 0-100k	1.9	2.5
	VSD 100-1000k	4.6	5.6
	Basecourse PD (70% of 100-1000k value)	**3.2**	**3.9**
III	VSD 0-1000k	4.2	5.5
	VSD 0-100k	1.5	1.8
	VSD 100-1000k	2.7	3.7
	Basecourse PD (70% of 100-1000k value)	**1.9**	**2.6**
IV	VSD 0-1000k	7.8	9.6
	VSD 0-100k	3.5	4.2
	VSD 100-1000k	4.3	5.4
	Basecourse PD (70% of 100-1000k value)	**3.0**	**3.8**
V	VSD 0-1000k	4.6	5.6
	VSD 0-100k	2.4	2.6
	VSD 100-1000k	2.2	3.0
	Basecourse PD (70% of 100-1000k value)	**1.5**	**2.1**

Table 6.3 PD calculations for Station 38, outer wheelpath, PR3-0610 pavement (300 mm / 40 kN).

Model V, Station 38, outer wheelpath (300 mm / 40 kN), PR3-0610 pavement
h=50 mm
N=900,000
$\dot{\varepsilon}_p = 0.4908 \times 10^{-3} \cdot e^{3.9479 \times 10^{-3} \cdot \varepsilon_r}$, $\Delta\varepsilon_p = \dot{\varepsilon}_p \times h \times N$

Depth to midheight of sublayer (mm)	Between tyres			Beneath tyre		
	ε_r (μm/m)	$\dot{\varepsilon}_p$ (μm/m/cycle)	$\Delta\varepsilon_p$ (mm)	ε_r (μm/m)	$\dot{\varepsilon}_p$ (μm/m/cycle)	$\Delta\varepsilon_p$ (mm)
25	-229	0.0[1]	0.0	555	0.004391	0.2
75	-23	0.0[1]	0.0	784	0.010857	0.5
125	251	0.001325	0.1	978	0.023296	1.0
175	483	0.003305	0.1	1039	0.029656	1.3
225	629	0.005888	0.3	999	0.025348	1.1
275	721	0.008458	0.4	918	0.018413	0.8
PD in basecourse layer	(mm)		0.9			5.0

[1]Value set to zero because of tensile vertical strain

The calculations for the remaining models are given in Table D.1, Table D.2 and Table D.3. A summary of the original and reduced PD values is given in Table 6.4.

Table 6.4 Summary of computed PD values for original and reduced strain values.

	Between tyres			Beneath tyre		
Model ID	Measured PD (mm)	Calculated PD (mm)	Difference PD (mm)	Measured PD (mm)	Calculated PD (mm)	Difference PD (mm)
I	0.9	0.8	-0.1	1.5	4.5	3.0
III	1.9	0.7	-1.2	2.6	12.9	10.3
IV	3.0	2.4	-0.6	3.8	22.5	18.7
V	1.5	0.9	-0.6	2.1	5.0	2.9

Computed strains reduced to 70% of original values

	Between tyres			Beneath tyre		
Model ID	Measured PD (mm)	Calculated PD (mm)	Difference PD (mm)	Measured PD (mm)	Calculated PD (mm)	Difference PD (mm)
I	0.9	0.4	-0.5	1.5	1.5	0.0
III	1.9	0.3	-1.6	2.6	2.8	0.2
IV	3.0	0.8	-2.2	3.8	4.6	0.8
V	1.5	0.4	-1.1	2.1	1.6	-0.5

6.4 Conclusions

The framework presented in this chapter is a development of observed behaviour in both the laboratory and field. The strain based approach was chosen over the more widely accepted stress based approaches used to model the PD of granular pavements as the results from both the field measurement and pavement modelling chapters showed that the stress responses tended to be somewhat insensitive to both the materials used and the thickness of the various layers in the pavement structure. The measurement of stresses within the pavement structure is also problematic. The modelling work was able to accurately predict the strain response of the pavement using stress dependant material stiffness models. Because, in modelling terms, the modelling framework employed by most researchers, i.e. a first order Cauchy stress distribution and static monotonic loading, the model predictions are never going to accurately reflect the actual stress history that a particle is subjected to as a driven, rolling wheel passes over the point of interest. Therefore, numerical predictions are always going to be a simplification of reality and maybe the focus of the modelling work should to be on the relative magnitude and trend of the results when comparing them to measured field values.

The PD results that are presented in this chapter are generally in agreement with the measured values. Although the percentage difference is high, the absolute differences are low.

This page is intentionally left blank.

Chapter 7 Conclusions

7.1 Pavement Response Measurements

The research described in this thesis showed that the (resilient) response of the pavement could be reliably measured by using εmu soil strain coils and that the measurements taken by this system could independently be verified by other measurements. The measurements that were collected gave a comprehensive set of data over a range of pavement designs and vehicle loads.

Relationships between the load and response were developed which showed that while the response at a point in the pavement was linear with respect to load, the relationship varied according to the depth in the pavement. This showed that the different pavement materials exhibit load or stress dependent stiffness. The implication of this is that pavements should be modelled with some sort of non-linear model: either a Multi Layer Non-Linear Elastic (MLNLE) model for simple cases or where great accuracy is not required, or where there is a limited amount of information available on the non-linear properties of the materials; or a 3D-FEM for situations where a greater degree of certainty is needed.

The subsurface response of the pavement that was subjected to loading by the FWD and a rolling wheel was compared. In the basecourse, the vertical strains induced by the rolling wheel were on average 1.5 times the strains induced by the FWD for the same equivalent static load. In the subgrade, the rolling wheel strains were 84 % of the FWD strains. The effect of the loading mechanism, vertical impulse versus rotating stress field, clearly has a significant effect on the response of the granular material. In addition it was found that while the surface deflection and subsurface stresses and strains were linear with respect to the applied load, the rate of change was not constant for the different measurements, indicating that while the surface deflections show that the pavement responded as a linear system, the subsurface responses suggest otherwise.

The tyre footprints were measured and the nominal average contact pressure was found to be approximately 50% of the inflation pressure. An attempt was made to verify the accuracy of the stress gauges, however the computed result showed a large variation from the nominal static load. Several explanations for these differences were proposed, and the main effect was thought to be the effect of shear stresses on the surface of the gauges when the tyre was not directly over the gauge. Vertical and horizontal stress measurements taken at the same depth in the pavement and at the same time showed that the ratio of horizontal to vertical stress was a constant value (0.125) for the two depths at which gauges of both orientation were installed; being the top of the granular material and the top of the subgrade.

Strain measurements were taken with the εmu soil strain system and the system was verified by integrating the strains over the height of the coil array and comparing with the integrated value with the surface deflections that was measured at the same time as the strain measurements were taken. The verification was done with both a FWD device and a rolling wheel. Allowing for the assumptions that were made during the verification process, the results were within 10% for the rolling wheel measurements and within 15% for the majority of the FWD measurements.

The measured stresses and strains were used to calculate in situ resilient modulus and Poisson's ratio values. The resilient modulus values in the mid to lower levels of the granular material were proportional to the applied load, with the modulus values approximately doubling when the load increased from 23 to 60 kN. The subgrade exhibited a small degree of non-linearity with the modulus increasing by 20% when the load increased from 23 to 60 kN. The values of the calculated Poisson's ratios at different positions in the pavements showed a small relationship to load and a greater dependency on position relative to the wheels. This implies that the value of Poisson's ratio is sensitive to the applied stress state in the pavement.

During the accelerated testing of the pavements both the vertical strains and permanent deformation increased quickly at the beginning of the tests and then after 50,000 – 100,000 load applications, the vertical strains remained reasonably constant, while the permanent deformation accumulated at a constant rate. This type of behaviour was mirrored in the results from the laboratory RLT tests.

7.2 Pavement Response Modelling

A model framework based on the monotonic static loading of a first-order (linear) Cauchy elastic model was selected to build a mathematical model of the pavement. The material stiffness was derived as a function of the applied and in-situ stress states using the modified Uzan model. This material model that was selected because it was judged to be a good compromise between complexity and completeness and the ability to determine the parameters from standard laboratory tests. The parameters for the material models were determined from RLT laboratory tests and it was accepted that a "shift" factor would be required to enable the models to be used with field data as there are sufficient differences between the laboratory and field conditions.

The user material (UMAT) facility in the General Purpose Finite Element Program ABAQUS was used to implement the chosen material model. This allowed the non-linear stiffness of the aggregate and subgrade materials to be modelled. The cross-anisotropic properties of the materials were also taken into account as well as the effect of rotation of the principal stress state. A non-linear 3D FEM model was constructed to represent the CAPTIF pavements and the resilient response of the model to various pavement configurations and applied loads was determined.

The non-linear material models were calibrated at one load level and then they were able to predict with reasonable accuracy the strain distribution with depth in the pavement and the pavement response to varying loads. The accuracy of the predicted responses reduced near the minimum and maximum load levels, however the load level range was ±50 % (23 to 60 kN) of the standard load (40 kN) for the rolling wheel measurements.

The 3D FEM model was also able to predict the variation of vertical strain in a horizontal plane in the pavement due to loading by a dual tyre assembly.

The MLLET programs are of limited accuracy when they are used to model dual tyre assemblies due to the constant modulus in the horizontal direction. The non-linear FEM results show a significant variation of the modulus in the horizontal direction. This variation in the modulus is critical to the accurate prediction of the pavement response.

The variations between the measured and predicted responses could be improved by using a more complex relationship to determine the stress distribution in the pavement and/or a different model to determine the material stiffness. In addition, the use of a model that incorporates the dynamic nature of the loading should improve the results. The use of more complex models will increase the computational effort and laboratory testing required to solve the model.

7.3 Pavement Performance Modelling

After observing the performance of the pavement over time, similarities were observed between the laboratory tests and CAPTIF results. After the initial "bedding-in" stage, the development of the plastic strain was linear with an increasing number of load cycles and the resilient response of the pavement was constant. It was also found that there was also a limit to the resilient strain within which the laboratory specimens exhibited stable behaviour and this strain value was independent of the stress state.

An exponential relationship between the resilient strain and the plastic strain rate was developed from the laboratory tests. This relationship was used with the strain fields predicted by the elastic FEM models to predict the accumulation of rutting in the pavement during the steady state response of the pavement tests. It was observed that the limiting strain in the laboratory tests was lower than both the measured and predicted strain values for some of the pavement sections, yet those pavements were exhibiting stable behaviour.

7.4 Recommendations for Further Research

Further investigation is required into determining the stress distribution within the pavement. Current response models usually rely on a first order linear stress distribution, but there was enough evidence to suggest that this classical approach was not entirely appropriate.

Additional measurements need to be undertaken to determine the thickness and or characterisation of the interface zone between the layers of different materials in the pavement.

More research is required to consider the effects of including a thin asphalt concrete surface layer on the responses of the pavement response model. In addition, more work should be done on investigating the influence of the size of the loaded area and the pressure distribution on the model responses.

The permanent deformation model needs to be validated with data from pavements that have higher levels of permanent deformation.

Methods to determine the amount of initial post construction rutting need to be developed.

The effects of either varying density and/or moisture content need to be incorporated into the response and performance models.

This page is intentionally left blank.

Chapter 8 References

ABAQUS Inc. (2004). *ABAQUS Analysis User's Manual (v6.5)*, Providence, Rhode Island, USA.

Adu-Osei, A. (2000). "Characterization Of Unbound Granular Layers In Flexible Pavements." *Report No. ICAR/502-3*, Texas Transportation Institute, The Texas A&M University System, College Station, Texas 77843-3135.

Adu-Osei, A., Lytton, R. L., and Little, D. N. (2000) "System identification method for determining the anisotropic resilient properties of unbound aggregates." *Unbound Aggregates in Road Construction, UNBAR5*, University of Nottingham, UK, 249-256.

Akou, Y., Heck, J. V., Kazai, A., Hornych, P., Odeon, H., and Piau, J.-M. (1999) "Modelling of Flexible Pavements Using the Finite Element Method and a Simplified Approach." *Unbound Granular Materials: Laboratory testing, In-Situ Testing and Modelling*, Lisbon, Portugal, 207-220.

Akram, T., Scullion, T., and Smith, R. E. (1994) "Comparing Laboratory And Backcalculated Layer Moduli On Instrumented Pavement Sections." *Nondestructive Testing of Pavements and Backcalculation of Moduli (Second Volume) ASTM STP 1198*, 170-202.

Al-Khoury, R. (2002). "Parameter Identification Technique for Layered Systems," PhD thesis, University of Technology of Delft, Delft.

Allen, J. J., and Thompson, M. R. (1974a). "Resilient Response of Granular Materials Subjected to Time-Dependent Lateral Stresses." *Transportation Research Record*(510), 1-13.

Allen, J. J., and Thompson, M. R. (1974b). "Significance of Variably Confined Triaxial Testing." *Journal of Transportation Engineering*, 100(4), 827-843.

American Association of State Highway and Transportation Officials (AASHTO). (1999). "Determining the Resilient Modulus of Soils and Aggregate Materials." AASHTO Standard Test Designation T–307–99, Washington, D.C.

Andrei, D., Witczak, M. W., Schwartz, C. W., and Uzan, J. (2004). "Harmonized resilient modulus test method for unbound pavement materials." *Transportation Research Record*(1874), 29-37.

Arnold, G. (2004). "Rutting of Granular Pavements," PhD Thesis, The University of Nottingham, Nottingham.

Arnold, G., Steven, B. D., Alabaster, D. J., and Fussell, A. W. (2005a). "Effect on pavement wear of increased mass limits for heavy vehicles - Concluding Report." Land Transport New Zealand Research Report 281, Wellington, New Zealand.

Arnold, G., Steven, B. D., Alabaster, D. J., and Fussell, A. W. (2005b). "Effect on pavement wear of increased mass limits for heavy vehicles - Stage 3." Land Transport New Zealand Research Report 279, Wellington, New Zealand.

Arnold, G., Steven, B. D., Alabaster, D. J., and Fussell, A. W. (2005c). "Effect on pavement wear of increased mass limits for heavy vehicles - Stage 4." Land Transport New Zealand Research Report 280, Wellington, New Zealand.

Askegaard, V., Brink, A., and Ullidtz, P. (1998) "Pressure Cell Applicability." *Fifth International Conference on Bearing Capacity of Roads and Airfields*, Trondheim, Norway, 1481-1490.

AUSTROADS. (1992). *Pavement design : a guide to the structural design of road pavements*, Austroads, Sydney.

AUSTROADS. (2004a). *Pavement Design : A Guide to the Structural Design of Road Pavements*, Austroads, Sydney.

AUSTROADS. (2004b). "Technical Basis of Austroads Pavement Design Guide." *AP-T33/04*, Austroads Incorporated, Sydney.

Balay, J., Correia, A. G., Jouve, P., Hornych, P., and Paute, J. L. (1997) "Mechanical Behaviour of Soils and Unbound Granular Materials, Modelling." *Eighth International Conference on Asphalt Pavements*, Seattle, Washington, 823-842.

Barksdale, R. D. (1972) "Laboratory Evaluation Of Rutting In Base Course Materials." *Third International Conference on the Structural Design of Asphalt Pavements*, London, England, 161-174.

Barksdale, R. D., Alba, J., Khosla, N. P., Kim, R., and Lambe, P. C. (1997). "Laboratory Determination of Resilient Modulus for Flexible Pavement Design." *NCHRP Web Document 14*, 486.

Barnes, G. E. (1995). "Soil Mechanics - Principles and Practice." MacMillan Press, 365.

Bellotti, R., Jamiolkowski, M., Lo Presti, D. C. F., and O'Neill, D. A. (1996). "Anisotropy of small strain stiffness in Ticino sand." *Geotechnique*, 46(1), 115-131.

Biarez, J. (1961). "Contribution à l'étude des propriétés mécaniques des sols et des matériaux pulvérulents.," D.Sc, Grenoble.

Boddapati, K. M., and Nazarian, S. (1994) "Effects of pavement-falling weight deflectometer interaction on measured pavement response." *Proceedings of the Symposium on Nondestructive Testing of Pavements and Backcalculation of Moduli, Jun 23-24 1993*, Atlanta, GA, USA, 326-340.

Bonaquist, R. F., and Witczak, M. W. (1997) "A Comprehensive Constitutive Model for Granular Materials in Flexible." *Eighth International Conference on Asphalt Pavements*, Seattle, Washington, 783-802.

Boussinesq, J. (1878). "Équilibre d'élasticité d'un solide isotrope sans pesanteur, supportant différents poids." *C. Rendus Acad. Sci. Paris*, 86, 1260-1263.

Boyce, H. R. (1980) "A non-linear model for the elastic behaviour of granular materials under repeated loading." *International Symposium on Soils under Cyclic and Transient Loading*, Swansea, 285-294.

Brown, S. F. (1977). "State-of-the-Art Report on Field Instrumentation for Pavement Experiments." *Transportation Research Record*(640), 13-28.

Brown, S. F., and Hyde, A. F. L. (1975). "Significance of Cyclic Confining Stress in Repeated-Load Triaxial." *Transportation Research Record*(537), 49-58.

Brown, S. F., and Pappin, J. W. (1981). "Analysis of Pavements with Granular Bases." *Transportation Research Record*(810), 17-23.

Brown, S. F., and Selig, E. T. (1991). "The Design of Pavement and Rail Track Foundations." Cyclic loading of soils : from theory to design, M. P. O'Reilly and S. F. Brown, eds., Blackie, Glasgow, 249-305.

Budiman, J., Sture, S., and Ko, H.-Y. (1992). "Constitutive Behavior Of Stress-Induced Anisotropic Cohesive Soil." *Journal of Geotechnical Engineering*, 118(9), pp 1348-59.

Burmister, D. M. (1943). "The Theory Of Stress And Displacements In Layered Systems And Applications To The Design Of Airport Runways." *Highway Research Board Proceedings*, 23, 126-148.

Collins, I. F., and Boulbibane, M. (2000). "Geomechanical Analysis Of Unbound Pavements Based On Shakedown Theory." *Journal of Geotechnical and Geoenvironmental Engineering*, 126(1), 50-59.

Correia, A. G. (1985). "Contribution a L'Etude Mecanique des sols Soumis a des Chargements Cycliques," Dr Eng Thesis, Ecole Nationale des Ponts et Chausseess, Paris.

Crovetti, J. A., Shahin, M. Y., and Touma, B. E. (1989) "Comparison of Two Falling Weight Deflectometer Devices, Dynatest 8000 and KUAB 2M-FWD." *Nondestructive Testing of Pavements and Backcalculation of Moduli ASTM STP 1026*, 59-69.

Davis, R. O., and Selvadurai, A. P. S. (1996). *Elasticity and geomechanics*, Cambridge University Press, Cambridge ; New York, NY, USA.

Dawson, A. R. (1994). "The e-mu System, Users Manual." *2nd Edition*, University of Nottingham, Nottingham, UK.

Dawson, A. R., and Gomes Correia, A. (1996). "The effects of subgrade clay condition on the structural behaviour of road pavements." Flexible Pavements, A. Gomes Corriea, ed., A. A. Balkema, Rotterdam, 113-120.

Dawson, A. R., and Little, P. H. (1997). "Measurement of Stress and Strain in an Unsurfaced Haul Road at a Soft Clay Site in Scotland." *Transportation Research Record*(1596), 15-22.

Dawson, A. R., Paute, J.-L., and Thom, N. H. (1996). "Mechanical characteristics of unbound granular materials as a function of condition." Flexible Pavements, A. Gomes Corriea, ed., A. A. Balkema, Rotterdam, 35-44.

de Almeida, J. R., Brown, S. F., and Thom, N. H. (1994) "A Pavement Evaluation Procedure Incorporating Material Non-Linearity." *Nondestructive Testing of Pavements and Backcalculation of Moduli (Second Volume) ASTM STP 1198*, 218-232.

de Beer, M., Fisher, C., and Jooste, F. (1997) "Determination of Pneumatic Tyre/Pavement Interface Contact Stresses Under Moving Loads and Some Effects on Pavements with Thin Asphalt Surfacing Layers." *Eighth International Conference on Asphalt Pavements*, Seattle, Washington, 179-227.

de Beer, M., Horak, E., and Visser, A. T. (1989) "The Multidepth Deflectometer (MDD) System for Determining the Effective Elastic Moduli of Pavement Layers." *Nondestructive Testing of Pavements and Backcalculation of Moduli ASTM STP 1026*, 70-89.

de Pont, J., Alabaster, D. J., Steven, B. D., and Fussell, A. W. (2003). "Effect on pavement wear of an increase in mass limits for heavy vehicles. Stage 2." *Transfund New Zealand Research Report No. 231*, Transfund New Zealand, Wellington.

de Pont, J., Steven, B. D., Alabaster, D. J., and Fussell, A. W. (2001). "Effect on Pavement Wear of an Increase in Mass Limits for Heavy Vehicles." *Transfund New Zealand Research Report No. 207*, Transfund New Zealand, Wellington.

de Pont, J., Steven, B. D., and Pidwerbesky, B. D. (1999). "The relationship Between Dynamic Wheel Loads and Road Wear." *Transfund New Zealand Research Report No. 144*, Transfund New Zealand, Wellington.

de Pont, J., Thakur, K., Pidwerbesky, B. D., and Steven, B. D. (1998) "Validating A Whole Life Pavement Performance Model." *Proceedings of the Fifth International Symposium on Heavy Vehicle Weights and Dimensions*, Queensland, Australia, 91-111.

Desai, C. S., and Christian, J. T. (1977). *Numerical methods in geotechnical engineering*, McGraw-Hill, New York.

Desai, C. S., and Siriwardane, H. J. (1984). *Constitutive laws for engineering materials, with emphasis on geologic materials*, Prentice-Hall, Englewood Cliffs, New Jersey.

Desai, C. S., Somasundaram, S., and Frantziskonis, G. (1986). "Hierarchical Approach for Constitutive Modelling of Geologic Materials." *International*

Journal for Numerical and Analytical Methods in Geomechanics, 10(3), 225-257.

Dormon, G. M. (1962) "The Extension to Practice of a Fundamental Procedure for the Design of Flexible Pavements." *International Conference on the Structural Design of Asphalt Pavements*, Ann Arbor, Michigan, 785-793.

Dormon, G. M., Edwards, J. M., and Shell International Petroleum Co. Ltd. (1964). *Shell 1963 design charts for flexible pavements : an outline of their development*, Shell International Petroleum Company, London.

Drucker, D. C., and Prager, W. (1952). "Soil mechanics and plastic analysis or limit design." *Quarterly of Applied Mathematics*, 10(2), 157-165.

Duncan, J. M., and Chang, C.-Y. (1970). "Nonlinear analysis of stress and strain in soils." *ASCE Journal of Soil Mechanics and Foundations Division*, 96(SM5), 1629-1653.

Duncan, J. M., and Dunlop, P. (1969) "Behavior of Soils in Simple Shear Tests." *Proc. 7th Int. Conf. on Soil Mechanics and Foundation Engineering*, Mexico, 101-109.

Duncan, J. M., Monismith, C. L., and Wilson, E. L. (1968). "Finite Element Analyses of Pavements." *Highway Research Record, Hwy Res Board*, 228, 18-33.

Duncan, J. M., and Seed, R. B. (1986a). "Compaction-Induced Earth Pressures under K_0-Conditions." *Journal of Geotechnical Engineering*, 112(1), 1-22.

Duncan, J. M., and Seed, R. B. (1986b). "FE Analyses: Compaction-Induced Stresses and Deformations." *Journal of Geotechnical Engineering*, 112(1), 23-43.

Edwards, A. L. (1976). *An introduction to linear regression and correlation*, W. H. Freeman, San Francisco.

Elhannani, M. (1991). "Modelisation et Simulation Numerique des Chaussees Souples," Ph.D thesis, University of Nantes, France.

Emeriault, F., and Chang, C. S. (1997). "Anisotropic Elastic Moduli Of Granular Assemblies From Micromechanical Approach." *Journal of Engineering Mechanics*, 123(12), 1289-1293.

European Committee for Standardization CEN. (2004). *EN 13286-7 : 2004 - Unbound and hydraulically bound mixtures - Part 7 : Cyclic load triaxial test for unbound mixtures*, Brussels.

FEHRL. (2000). "AMADEUS Advanced Models for Analytical Design of European Pavement Structures." *RO-97-SC.2137*.

Felippa, C. A. (2001). "A historical outline of matrix structural analysis: a play in three acts." *Computers & Structures*, 79(14), 1313-1324.

FHWA. (1987). "ELSYM5 Interactive Microcomputer Version." *Report FHWA-TS-87-217*, Federal Highway Administration, Washington, D.C.

Fredlund, D. G., Gan, J.-M., Guan, Y., and Richardson, N. (1997). "Suction Measurements on a Saskatchewan Soil Using a Direct-Measurement, High-Range Suction Sensor." *Transportation Research Record*(1596), 84-92.

Freeman, R. B., and Harr, M. E. (2004). "Stress Predictions for Flexible Pavement Systems." *Journal of Transportation Engineering*, 130(4), 495-502.

Galjaard, P. J., Paute, J.-L., and Dawson, A. R. (1996). "Comparison and performance of repeated load triaxial test equipment for unbound granular materials." Flexible Pavements, A. Gomes Corriea, ed., A. A. Balkema, Rotterdam, 7-22.

Gazetas, G. (1982). "Stresses And Displacements In Cross-Anisotropic Soils." *ASCE Journal of the Geotechnical Engineering Div*, 108(GT4), pp 532-553.

Gomes Correia, A., and de Almeida, J. R. (1998) "Mechanical Behaviour Of Unbound Granular Materials For Modelling Of Flexible Pavements." *Fifth International Conference on Bearing Capacity of Roads and Airfields*, Trondheim, Norway, 1211-1220.

Graham, J., and Houlsby, G. T. (1983). "Anisotropic elasticity of a natural clay." *Geotechnique*, 33(2), 165-180.

Guezouli, S., Elhannani, M., and Jouve, P. (1996). "NOEL: A non linear finite element code for road pavement analysis." Flexible Pavements, A. Gomes Corriea, ed., A. A. Balkema, Rotterdam, 193-200.

Harichandran, R. S., and Yeh, M.-S. (1988). "Flexible Boundary in Finite-Element Analysis of Pavements." *Transportation Research Record*, 1207, 50-60.

Harr, M. E. (1977). *Mechanics of particulate media : a probabilistic approach*, McGraw-Hill, New York.

Harrison, W., Wardle, L. J., and Gerrard, C. M. (1972). "Computer programmes for circle and strip loads on layered anisotropic media." CSIRO Australia Division of Applied Geomechancis Computing Programme No. 1.

Heath, A. C., Pestana, J. M., Harvey, J. T., and Bejerano, M. O. (2004). "Normalizing behavior of unsaturated granular pavement materials." *Journal of Geotechnical and Geoenvironmental Engineering*, 130(9), 896-904.

Helwany, S., Dyer, J., and Leidy, J. (1998). "Finite-Element Analyses Of Flexible Pavements." *Journal of Transportation Engineering*, 124(5), 491-499.

Hildebrand, G. (2002). "Verification of Flexible Pavement Response From a Field Test." *Report 121*, Danish Road Institute, Roskilde, Denmark.

Hjelmstad, K. D., and Taciroglu, E. (2000). "Analysis And Implementation of Resilient Modulus Models For Granular Solids." *ASCE Journal of Engineering Mechanics*, 126(8), 821-30.

Hornych, P., Kazai, A., and Piau, J.-M. (1998) "Study Of The Resilient Behaviour Of Unbound Granular Materials." *Fifth International Conference on Bearing Capacity of Roads and Airfields*, Trondheim, Norway, 1277-1287.

Hugo, F., and Epps-Martin, A. L. (2004). "NCHRP Synthesis of Highway Practice 325: Significant Findings from Full-Scale Accelerated Pavement Testing - A Synthesis of Highway Practice." Transportation Research Board, National Research Council, Washington D.C.

Hveem, F. N. (1955). "Pavement Deflections and Fatigue Failures." *Highway Research Board Bulletin*, 114, 43-87.

Ishihara, K. (1983) "Soil Response in Cyclic Loading Induced by Earthquakes, Traffic and Waves." *Proceedings 7th Asian Regional Conference on Soil Mechanics and Foundation Engineering*, Haifa, Isreal, 42-66.

Jameson, G. W. (1996). "Origins of AUSTROADS design procedures for granular pavements." *Research Report No. 292*, ARRB Transport Research, Vermont South, Vic.

Janoo, V., Irwin, L., Knuth, K., Dawson, A. R., and Eaton, R. (1999) "Use of Inductive Coils to Measure Dynamic and Permanent Pavement Strains." *Proc 1999 International Conference Accelerated Pavement Testing*, Reno, Nevada, USA, Paper CS3-2.

Jiang, G. L., Tatsuoka, F., Flora, A., and Koseki, J. (1997). "Inherent and Stress State-Induced Anisotropy in Very Small Strain Stiffness of a Sandy Gravel." *Geotechnique*, 47(3), 509-521.

Karasahin, M., and Dawson, A. R. (2000) "Anisotropic characteristics of granular material." *Unbound Aggregates in Road Construction, UNBAR5*, Nottingham University, UK, 139-143.

Karasahin, M., Dawson, A. R., and Holden, J. T. (1993). "Applicability of Resilient Constitutive Models of Granular Material For Unbound Base Layers." *Transportation Research Record*(1406), 98-107.

Kenis, W. J. (1977) "Predictive Design Procedures--a Design Method for Flexible Pavements." *4th International Conference on Structural Design of Asphalt Pavements*, Ann Arbor, Michigan., 101-130.

Kohata, Y., Tatsuoka, F., Wang, L., Jiang, G. L., Hoque, E., and Kodaka, T. (1997). "Modelling the non-linear deformation properties of stiff geomaterials." *Geotechnique*, 47(3), 563-580.

Kondner, R. L. (1963). "Hyperbolic Stress-Strain Response: Cohesive soils." *ASCE Journal of Soil Mechanics and Foundations Division*, 89(SM1), 115-143.

Korkiala-Tanttu, L., Laaksonen, R., and Törnqvist, J. (2003). "Effect of the spring and overload to the rutting of a low-volume road." *22/2003*, Finnish Road Administration., Helsinki.

Kramer, S. L. (1996). *Geotechnical earthquake engineering*, Prentice Hall, Upper Saddle River, N.J.

Lade, P. V., and Duncan, J. M. (1973). "Cubical Triaxial Tests On Cohesionless Soil." 99(SM10), 793-81.

Lekarp, F., and Dawson, A. (1998). "Modelling permanent deformation behaviour of unbound granular materials." *Construction and Building Materials*, 12(1), 9-18.

Lekarp, F., and Isacsson, U. (2001). "The Effects of Grading Scale on Repeated Load Triaxial Test Results." *International Journal of Pavement Engineering*, 2(2), 85-101.

Lekarp, F., Isacsson, U., and Dawson, A. (2000a). "State of the art. I: resilient response of unbound aggregates." *Journal of Transportation Engineering*, 126(1), 66-75.

Lekarp, F., Isacsson, U., and Dawson, A. (2000b). "State of the art. II: permanent strain response of unbound aggregates." *Journal of Transportation Engineering*, 126(1), 76-83.

Lim, P. N., and Yandell, W. O. (1988). "Reevaluation of Shell Life by Mechano-Lattice Analysis." *Journal of Transportation Engineering*, 114(4), 435-449.

Lo, S.-C., and Lee, I. (1990). "Response Of Granular Soil Along Constant Stress Increment Ratio Path." *Journal of Geotechnical Engineering*, 116(3), pp 355-376.

Loach, S. C. (1987). "Repeated Loading of Fine Grained Soils for Pavement Design," PhD Thesis, University of Nottingham, Nottingham.

Loi, J., Fredlund, D. G., Gan, J. K., and Widger, R. A. (1992). "Monitoring Soil Suction in an Indoor Test Track Facility." *Transportation Research Record*(1362), 101-110.

Lytton, R. L. (1989) "Backcalculation of Pavement Layer Properties." *First International Symposium on Nondestructive Testing of Pavements and Backcalculation of Moduli - ASTM STP 1026*, Baltimore, Maryland, 7-38.

Maher, M. H., Papp, W. J., Jr., and Gucunski, N. (1996). "Measurement of Soil Resilient Properties Using Noncontacting Proximity Sensors." *Transportation Research Record*(1548), 16-23.

Masad, E., Little, D., and Lytton, R. (2004). "Modeling nonlinear anisotropic elastic properties of unbound granular bases using microstructure distribution tensors." *International Journal of Geomechanics*, 4(4), 254-263.

Mayhew, H. C. (1983). "Resilient Properties of Unbound Roadbase Under Repeated Triaxial Loading." TRRL Laboratory Report 1088, Transport and Road Research Laboratory, Crowthorne, UK.

McInnes, D. B. (1984). "Total Suction Measurements of Crushed Rock Basecourse Material." *Australian Road Research*, 14(3), 153-156.

Metcalf, J. B. (1996). "NCHRP Synthesis of Highway Practice 235: Application of Full-Scale Accelerated Pavement Testing." Transportation Research Board, National Research Council, Washington D.C.

Monismith, C. L., Seed, H., B., Mitry, F., G., and Chan, C., K. (1967) "Prediction of Pavement Deflections From Laboratory Tests." *Second International Conference on the Structural Design of Asphalt Concrete Pavements*, Ann Arbor, Michigan, USA, 109-140.

Odemark, N. (1949). "Investigations As To The Elastic Properties Of Soils And Design Of Pavements According To The Theory Of Elasticity." *Statens Vaginstitut*, Meddelande 77.

Oloo, S. Y., and Fredlund, D. G. (1998) "The Application of Unsaturated Soil Mechanics Theory to the Design of Pavements." *Fifth International Conference on Bearing Capacity of Roads and Airfields*, Trondheim, Norway, 1419-1428.

Paterson, W. D. O. (1972). "Measurement of Pavement Deformation using Induction Coils." *13*, National Roads Board, Wellington.

Paute, J.-L., Hornych, P., and Benaben, J. P. (1996). "Repeated load triaxial testing of granular materials in the French network of Laboratoires des Ponts et Chaussees." Flexible Pavements, A. Gomes Corriea, ed., A. A. Balkema, Rotterdam, 53-64.

Pearson-Kirk, D. (1976). "Lateral earth pressures exerted by compacted granular materials." *Australian Road Research Board Conference Proc*, 8(4).

Peattie, K. R. (1962) "A Fundamental Approach to the Design of Flexible Pavements." *International Conference on the Structural Design of Asphalt Pavements*, Ann Arbor, Michigan, 403-411.

Peutz, M. G., Van Kempen, H. P., and Jones, A. (1968). "Layered Systems Under Normal Surface Loads." *Highway Research Record, Hwy Res Board*, 228, 34-45.

Pickering, D. J. (1970). "Anisotropic Elastic Parameters for Soil." *Geotechnique*, 20(3), 271-276.

Pidwerbesky, B. D. (1989) "Commisioning the Canterbury Accelerated Pavement Testing Facility." *Proceedings IPENZ annual conference, 1989 : engineering our natural resources*, Dunedin, 317-328.

Pidwerbesky, B. D. (1995). "Accelerated Dynamic Loading Of Flexible Pavements At The Canterbury Accelerated Pavement Testing Indoor Facility." *Transportation Research Record*, 1482, 79-86.

Pidwerbesky, B. D. (1996). "Fundamental behaviour of unbound granular pavements subjected to various loading conditions and accelerated trafficking," PhD thesis, University of Canterbury, Christchurch.

Ping, W. V., and Ge, L. (1997). "Field Verification of Laboratory Resilient Modulus Measurements on Subgrade Soils." *Transportation Research Record*(1577), 53-61.

Porter, O. J. (1942). "Foundations For Flexible Pavements." *Highway Research Board Proceedings*, 22, 100-36.

Potter, D. W., and Donald, G. S. (1985). "Revision Of Naasra Interim Guide To Pavement Thickness Design." *Australian Road Research Journal*, 15(2), 106-112.

Raad, L., and Figueroa, J. L. (1980). "Load Response of Transportation Support Systems." *Transportation Engineering Journal*, 106(1), 111-128.

Raad, L., Minassian, G. H., and Gartin, S. (1992). "Characterization of Saturated Granular Bases under Repeated Loads." *Transportation Research Record*(1369), 73-82.

Rada, G., and Witczak, M. W. (1981). "Comprehensive Evaluation of Laboratory Resilient Moduli Results For Granular Material." *Transportation Research Record*, 810, 23-33.

Richardson, I., Chapman, D., and Brown, S. (1996). "Relating Failure Tests Performed In Hollow Cylinder Apparatus To Inherent Anisotropy." *Transportation Research Record*, 1526, pp 149-156.

Sauer, E. K., and Monismith, C. L. (1968). "Influence of soil suction on behavior of glacial till subjected to repeated loading." *National Research Council -- Highway Research Board -- Highway Research Record*(215), 8-23.

Scarpas, A., Al-Khoury, R., and Van Gurp, C. (1998) "Finite Elements Investigation Of Pavement -FWD Interaction." *Fifth International Conference on Bearing Capacity of Roads and Airfields*, Trondheim, Norway, 253-262.

Schofield, A. N., and Wroth, P. (1968). *Critical State Soil Mechanics*, McGraw-Hill.

Scullion, T., Briggs, R. C., and Lytton, R. L. (1989) "Using the Multidepth Deflectometer to Verify Modulus Backcalculation Procedures." *Nondestructive Testing of Pavements and Backcalculation of Moduli ASTM STP 1026*, 90-101.

Seed, H., B., Mitry, F., G., Monismith, C. L., and Chan, C., K. (1967a). "Factors Influencing the Resilient Deformations of Untreated Aggregate Base in Two-

Layer Pavements Subjected to Repeated Loading." *Highway Research Record, Hwy Res Board*, 190, 19-55.

Seed, H., B., Mitry, F., G., Monismith, C. L., and Chan, C., K. (1967b). "Prediction of Flexible Pavement Deflections From Laboratory Repeated-Load Tests." *NCHRP Repprt No 35*.

Seed, H. B., Chan, C. K., and Lee, C. E. (1962) "Resilience Characteristics of Subgrade Soils and Their Relation To Fatigue Failures In Asphalt Pavements." *International Conference on the Structural Design of Asphalt Pavements*, Ann Arbor, Michigan, 77-113.

Selig, E. T. (1987). "Tensile zone effects on performance of layered systems." *Geotechnique*, 37(3), 247-254.

Selig, E. T., Zhang, J., and Ebersohn, W. (1997). "Evaluation of Dynamic Earth Pressure Cells for Subgrade." *Transportation Research Record*(1596), 1-6.

Semmelink, C., and de Beer, M. (1995). "Rapid Determination of Elastic and Shear Properties of Road-Building Materials With the K-Mould." Unbound Aggregates in Roads, A. R. Dawson and R. H. Jones, eds., Department of Civil Engineering, University of Nottingham, UK, Nottingham, 151-1641.

Semmelink, C., Jooste, F., and de Beer, M. (1997) "Use of the K-Mould in Determination and Analysis of the Elastic and Shear Properties of Road Materials for Flexible Pavements." *Proc. Eighth International Conference on Asphalt Pavements*, Seattle, Washington, USA, 1643-1658.

Seyhan, U., and Tutumluer, E. (2002). "Anisotropic modular ratios as unbound aggregate performance indicators." *Journal of Materials in Civil Engineering*, 14(5), 409-416.

Shackel, B. (1973). "Repeated Loading of Soils - A Review." *Australian Road Research*, 5(3), 22-49.

Sharp, R. W., and Booker, J. R. (1984). "Shakedown of Pavements under Moving Surface Loads." *Journal of Transportation Engineering*, 110(1), 1-14.

Shell International Petroleum Company Ltd. (1978). *Shell pavement design manual - : asphalt pavements and overlays for road traffic*, London.

Standards Australia International Limited. (1995). *AS 1289.6.8.1-1995 : Methods of testing soils for engineering purposes - Soil strength and consolidation tests - Determination of the resilient modulus and permanent deformation of granular unbound pavement materials*, Standards Australia International, Strathfield, NSW.

Standards New Zealand. (1986a). *NZS 4402.4.1.1:1986 : Determination of the dry density/water content relationship - Test 4.1.1 New Zealand standard compaction test*, Standards New Zealand, Wellington, NZ.

Standards New Zealand. (1986b). *NZS 4402.4.1.3:1986 : Determination of the dry density/water content relationship - Test 4.1.3 New Zealand vibrating hammer compaction test*, Standards New Zealand, Wellington, NZ.

Steven, B., de Pont, J., Pidwerbesky, B. D., and Arnold, G. (1999) "Accelerated Dynamic Loading of Flexible Pavements at CAPTIF." *Proc 1999 International Conference Accelerated Pavement Testing*, Reno, Nevada, USA, Paper GS2-3.

Steven, B. D. (1993). "The Response of an Unbound Granular Flexible Pavement to Loading by Super-Heavy Vehicles.," ME, University of Canterbury.

Steven, B. D., Pidwerbesky, B. D., and de Pont, J. (1998) "Evaluation of Pavement Response Models Using Measured Pavement Response Data." *Proc. Roading Geotechnics '98*, Auckland, New Zealand, 53-8.

Steven, B. D., Sharp, K., and Arnold, G. (2001). "Comparison of Accelerated Pavement Test Facilities in New Zealand and Australia." *Transfund New Zealand Research Report No. 198*, Transfund New Zealand, Wellington.

Stewart, H. E., Selig, E. T., and Norman-Gregory, G. M. (1985). "Failure Criteria and Lateral Stresses in Track Foundations." *Transportation Research Record*(1022), 59-64.

Strack, O. D. L., and Cundall, P. A. (1978). "The Distinct Element Method As A Tool For Research In Granular Media." *Rep. Concerning NSF Grant ENG76-20711, Part I*, National Science Foundation, Arlington, Va.

Sture, S., and Desai, C. S. (1979). "Fluid Cushion Truly Triaxial or Multiaxial Testing Device." 2(1), 20-33.

Sweere, G. T. H. (1990). "Unbound Granular Bases for Roads," Delft University of Technology, Delft.

Tam, W. S., and Brown, S. F. (1989) "Back-Analyzed Elastic Stiffnesses: Comparison Between Different Procedures." *Nondestructive Testing of Pavements and Backcalculation of Moduli ASTM STP 1026*, 189-200.

Theyse, H. L. (1997) "Mechanistic-Empirical Modelling of the Permanent Deformation of Unbound Pavement Layers." *Eighth International Conference on Asphalt Pavements*, Seattle, Washington, 1579-94.

Thom, N. H., and Brown, S. F. (1987). "Effect of Moisture on the Structural Performance of a Crushed-Limestone Road Base." *Transportation Research Record*(1121), 50-56.

Thom, N. H., and Brown, S. F. (1988) "The effect of Grading and Density on the Mechanical Properties of a Crushed Dolomatic Limestone." *Proceedings 14th ARRB Conference*, Canberra, Australia, 94-100.

Thom, N. H., and Dawson, A. R. (1996). "The permanent deformation of a granular material modelled using hollow cylinder testing." Flexible Pavements, A. Gomes Corriea, ed., A. A. Balkema, Rotterdam, 65-78.

Timoshenko, S. P., and Goodier, J. N. (1970). *Theory of Elasticity*, McGraw-Hill Book Company, New York.

Transit New Zealand. (1975). *M/10: 1975. Specification for Asphaltic Concrete.*, Transit New Zealand, Wellington, NZ.

Transit New Zealand. (2000). "NEW ZEALAND SUPPLEMENT TO THE DOCUMENT, Pavement Design – A Guide to the Structural Design of Road Pavements (AUSTROADS, 1992)." Transit New Zealand, Wellington.

Turnbull, W. J., Maxwell, A. A., and Ahlvin, R. G. (1961) "Stresses and Deflections in Homogeneous Soil Masses." *Proceedings Fifth International Conference on Soil Mechanics and Foundation Engineering*, Paris.

Turner, M. J., Clough, R. W., Martin, H. C., and Topp, L. J. (1956). "Stiffness and Deflection Analysis of Complex Structures." *Journal of Aeronautical Sciences*, 23(9), 805-823.

Tutumluer, E., and Barksdale, R. D. (1995) "Behaviour of Pavements with Granular Bases - Prediction and Performance." *UNBAR4*, Nottingham, 173-183.

Tutumluer, E., and Seyhan, U. (1999). "Laboratory Determination Of Anisotropic Aggregate Resilient Moduli Using An Innovative Test Device." *Transportation Research Record*, 1687, pp 13-21.

Tutumluer, E., and Seyhan, U. (2000) "Effects of fines content on the anisotropic response and characterisation of unbound aggregate bases." *Unbound Aggregates in Road Construction, UNBAR5*, University of Nottingham, UK, 153-160.

Tutumluer, E., and Thompson, M. R. (1997). "Anisotropic Modeling of Granular Bases in Flexible Pavements." *Transportation Research Record*(1577), 18-26.

Tutumluer, E., and Thompson, M. R. (1998). "Anisotropic Modeling of Granular Bases, FAA Center of Excellence for Airport Pavement Research Report No. 2,." Department of Civil Engineering, University of Illinois at Urbana-Champaign, Urbana, Illinois.

Ullidtz, P. (1997) "Modelling of Granular Materials Using the Discrete Element Method." *Eighth International Conference on Asphalt Pavements*, Seattle, Washington, 757-769.

Ullidtz, P. (1998). *Modelling Flexible Pavement Response and Performance*, Polyteknisk Forlag, Lyngby, Denmark.

Ullidtz, P., and Busch, C. (1979). "Laboratory Testing of a Full-Scale Pavement: The Danish Road-Testing Machine." *Transportation Research Record*(715), 52-62.

Uzan, J. (1985). "Characterization of Granular Material." *Transportation Research Record*, 1022, 52-59.

Uzan, J. (1992). "Resilient Characterization Of Pavement Materials." *International Journal For Numerical And Analytical Methods In Geomechanics*, 16, 453-459.

Uzan, J. (1994) "Advanced Backcalculation Techniques." *Nondestructive Testing of Pavements and Backcalculation of Moduli (Second Volume) ASTM STP 1198*, 3-37.

Uzan, J. (1999). "Permanent Deformation of a Granular Base Material." *Transportation Research Record*, 1673, 89-94.

Van Cauwelaert, F. J., Alexander, D. R., White, T. D., and Barker, W. R. (1989) "Multilayer Elastic Program For Backcalculating Layer Moduli In Pavement Evaluation." *First International Symposium on Nondestructive Testing of Pavements and Backcalculation of Moduli - ASTM STP 1026*, Baltimore, Maryland, 171-188.

Vermeer, P. (1982) "A Five-Constant Model Unifying Well-Established Concepts." *International Workshop on Constitutive Behaviour of Soils*, Grenoble, France, 175-197.

Vuong, B. T. (1986). *Non-linear finite element analysis of road pavements*, Australian Road Research Board, Vermont South, Vic.

Vuong, B. T. (1992). "Influence of Density and Moisture Content on Dynamic Stress-Strain Behaviour of a Low Plasticity Crushed Rock." *Road & Transport Research*, 1(2), 88-100.

Vuong, B. T. (1999) "Precision Studies of Resilient Modulus and Permanent Strain Testing." *Unbound Granular Materials: Laboratory testing, In-Situ Testing and Modelling*, Lisbon, Portugal, 63-83.

Walker, P. J. (1997). "Measurement of Total Suction and Matric Suction in Pavement Materials at Dandenong ALF Site." *Road & Transport Research*, 6(4), 48-58.

Wallace, K. (1998). "Tensile response of an unbound granular pavement." *Road and Transport Research*, 7(3), 36-47.

Wardle, L. J. (1977). "Program CIRCLY, User's Manual, Geomechanics Computer program Number 2." Division of Applied Geomechanics, Commonwealth Scientific and Industrial Research Organisation, Melbourne, Australia.

Waterhouse, A. (1967) "Stresses in Layers Systems Under Static and Dynamic Loading." *Second International Conference on the Structural Design of Asphalt Pavements*, Ann Arbor, Michigan, USA, 291-308.

Wellner, F., and Gleitz, T. (1999) "Stress-Strain Behaviour of Granular Materials." *Unbound Granular Materials: Laboratory testing, In-Situ Testing and Modelling*, Lisbon, Portugal, 177-186.

Werkmeister, S. (2004). "Permanent Deformation Behaviour of Unbound Granular Materials in Pavement Constructions," PhD thesis, Technische Universitat, Dresden.

White, T., Zaghloul, S., Anderton, G. L., and Smith, D. M. (1997). "Pavement Analysis for Moving Aircraft Load." *ASCE Journal of Transportation Engineering*, 123(6), 436-446.

Williman, A., and Paterson, W. D. O. (1971). "Track for the accelerated testing of highway pavements." *New Zealand Engineering*, 26(3), 73-7.

Wolff, F. (1982) "Design of Pavements in Tropical Regions with the Finite-Element Method." *Fifth International Conference on the Structural Design of Asphalt Pavements*, Delft, Netherlands, 192-205.

Wolff, H., and Visser, A. T. (1994). "Incorporating elasto-plasticity in granular layer pavement design." *Proceedings of the Institution of Civil Engineers, Transport*, 105(4), 259-272.

Yandell, W. O. (1971). "Prediction of the Behavior of Elastoplastic Roads During Repeated Rolling Using the Mechano-Lattice Analogy." *Highway Research Record, Hwy Res Board*, 374, pp 29-41.

Yandell, W. O. (1982a). "Measurement and Prediction of Forward Movement and Rutting in Pavements." *Transportation Research Record*(888), 77-84.

Yandell, W. O. (1982b). "Residual Stresses and Strains and Fatigue Cracking." *ASCE Journal of Transportation Engineering*, 108(TE1), 103-116.

Yandell, W. O. (1983). "Possible Effect of Relative Plastic Behavior of Pavement Layers On Pavement Life (Abridgment)." *Transportation Research Record*(930), 86-90.

Yandell, W. O., and Behzadi, G. (1997) "Performance Prediction of Accelerated Loading Facility (ALF) Trials." *Eighth International Conference on Asphalt Pavements*, Seattle, Washington, 1041-51.

Yu, S., and Dakoulas, P. (1993). "General Stress-Dependent Elastic Moduli For Cross-Anisotropic Soils." *Journal of Geotechnical Engineering*, 119(10), pp 1568-86.

Zaghloul, S., and White, T. (1993). "Use of a Three-Dimensional, Dynamic Finite Element Program for Analysis of Flexible Pavement." *Transportation Research Record*, 1388, 60-69.

Zamhari, K. A. (1998) "Anisotropy Of Unbound Pavement Materials." *Fifth International Conference on Bearing Capacity of Roads and Airfields*, Trondheim, Norway, 1289-1299.

Zeghal, M. (2004). "Discrete-Element Method Investigation of the Resilient Behavior Of Granular Materials." *Journal of Transportation Engineering*, 130(4), 503-509.

Zienkiewicz, O. C., and Taylor, R. L. (2000). *The finite element method*, Butterworth-Heinemann, Oxford.

Appendix A Field Measurement Data

Table A.1 FWD, Strain and Stress data from Station 9, inner wheelpath, PR3-0404 pavement, 600k load cycles.

FWD Data					
Plate Pressure (kPa)		358	469	733	1015
Plate Load (kN)		25.3	33.2	51.8	71.7
		Deflection (mm)			
Distance from centre of loading plate (mm)	0	0.642	0.837	1.200	1.426
	300	0.340	0.449	0.677	0.923
	450	0.154	0.213	0.346	0.504
	600	0.093	0.132	0.222	0.333
	900	0.044	0.060	0.098	0.148
	1200	0.030	0.039	0.062	0.091
	1500	0.023	0.030	0.047	0.068
Vertical Strains (μm/m)					
Depth (mm)	112.5	383	449	573	676
	262.5	378	438	509	573
	337.5	1714	2125	2966	3707
	412.5	1558	2016	2928	3740
	487.5	1233	1636	2497	3317
	562.5	593	796	1198	1611
Vertical Pressures (kPa) (Top of Subgrade)					
Depth (mm)	300	67.1	93.7	154.5	207.8

Table A.2 Vertical compressive strain versus load cycles for Station 9, Inner Wheelpath, PR3-0404 pavement.

Station 9 Inner Wheelpath									
			Vertical Compressive Strain (μm/m) Depth below surface (mm)						
		Static wheelload (kN)	Subgrade				Basecourse		
			562.5	487.5	412.5	337.5	262.5	187.5	112.5
Load Cycles ('000's)	5	40	659	1452	1871	1952	603	541	584
	20	40	664	1667	2213	2021	650	520	678
	30	40	716	1457	1849	1829	602	442	646
	50	40	665	1422	1920	1970	664	450	729
	100	40	634	1422	1902	2048	644	426	721
	150	40	692	1554	1943	2155	618	503	679
	200	40	639	1459	1964	2022	669	474	621
	250	40	664	1480	1939	1973	616	441	773
	300	40	616	1468	1914	2027	631	449	721
	400	40	699	1597	2096	2178	666	451	693
	500	40	737	1563	2018	2001	651	465	698
	600	40	706	1602	2038	2030	729	513	647
	700	40	752	1700	2151	2185	651	470	726
	800	40	745	1627	1975	1972	652	522	733
	900	40	820	1758	2164	2089	703	651	865
	1000	40	838	1837	2206	2126	692	651	846
	1019	50	1057	2119	2224	1988	693	665	834
	1045	50	1350	2673	2956	2771	822	770	1016
	1070	50	1377	2732	3093	3071	850	799	1033
	1120	50	1393	2722	3086	2918	803	826	1098
	1220	50	1407	2765	3099	2816	804	684	997
	1320	50	1386	2709	2933	2492	753	639	908

Table A.3 Vertical compressive strain versus load cycles for Station 29, Inner Wheelpath, PR3-0610 pavement.

Station 29 Inner Wheelpath									
			Vertical Compressive Strain (μm/m) Depth below surface (mm)						
		Static wheelload (kN)	Subgrade					Basecourse	
			562.5	487.5	412.5	337.5	262.5	187.5	112.5
Load Cycles ('000's)	15	60	434	366	1306	1595	2575	1250	1262
	25	60	451	378	1360	1660	2728	1248	1232
	35	60	469	403	1388	1712	2883	1265	1257
	50	60	479	416	1386	1722	2959	1287	1208
	100	60	502	468	1486	1856	3086	1274	1177
	150	60	499	488	1491	1871	3224	1310	1306
	200	60	544	529	1580	2006	3422	1370	1207
	250	60	547	549	1577	2004	3047	1383	1164
	300	60	555	546	1556	1962	3055	1423	1204
	400	60	580	595	1676	2100	3336	1521	1243
	500	60	624	652	1795	2230	3614	1636	1213
	600	60	645	689	1832	2288	3506	1806	1165
	700	60	673	697	1846	2252	3021	1891	1224
	800	60	628	669	1739	2059	2843	1891	1045
	900	60	641	672	1727	2016	2697	1907	1019
	1000	60	661	720	1799	2084	3002	2143	1205
	1010	60	631	645	1656	1924	2942	2233	1189
	1025	60	661	690	1741	2054	3167	2328	1269
	1050	60	669	691	1725	1979	2785	2231	1124
	1100	60	650	704	1697	1972	2874	1977	1156
	1200	60	713	763	1848	2099	3006	2225	1670
	1300	60	672	725	1719	1906	2774	2129	1889
	1400	60	662	702	1567	1610		1450	2048

Table A.4 Vertical compressive strain versus load cycles for Station 29, Outer Wheelpath, PR3-0610 pavement.

Station 29 Outer Wheelpath									
			Vertical Compressive Strain (μm/m) Depth below surface (mm)						
		Static wheelload (kN)	Subgrade					Basecourse	
			562.5	487.5	412.5	337.5	262.5	187.5	112.5
Load Cycles ('000's)	15	40	354			1044	1303	995	1356
	25	40	317			1045	1316	939	1346
	35	40	339			1073	1355	961	1370
	50	40	327			1079	1488	891	1352
	100	40	347			1149	1525	854	1327
	150	40	352			1156	1661	867	1311
	200	40	354			1195	1693	828	1318
	250	40	362			1200	1559	794	1272
	300	40	368			1216	1644	793	1244
	400	40	391			1286	1780	837	1268
	500	40	399			1345	1958	799	1221
	600	40	401			1362	1986	819	1172
	700	40	402			1323	1669	822	1177
	800	40	404			1289	1752	844	1013
	900	40	402			1281	1710	823	918
	1000	40	415			1337	2066	862	966
	1010	60	554			1731	2514	979	1146
	1025	60	574			1929	2904	1065	1272
	1050	60	605			1982	2751	1104	1315
	1100	60	601			1954	3078	1066	1564
	1200	60	606			1716	2465	1232	2667
	1300	60	586			1461	1993	1127	3216
	1400	60	586			1357	1610	1077	3988

Table A.5 Vertical compressive strain versus load cycles for Station 38, Inner Wheelpath, PR3-0610 pavement.

Station 38 Inner Wheelpath									
			Vertical Compressive Strain (μm/m) Depth below surface (mm)						
		Static wheelload (kN)	Subgrade				Basecourse		
			562.5	487.5	412.5	337.5	262.5	187.5	112.5
Load Cycles ('000's)	15	60	745	783	2830	2397	1278	1591	1749
	25	60	754	821	2947	2650	1320	1617	1774
	35	60	740	816	2915	2648	1282	1680	1790
	50	60	847	874	3074	2829	1311	1609	1773
	100	60	820	958	3322	2881	1223	1577	1669
	150	60	807	980	3255	3048	1220	1579	1851
	200	60	844	1034	3524	3144	1219	1547	1731
	250	60	833	1052	3483	2911	1163	1507	1769
	300	60	840	1030	3448	2766	1145	1486	1713
	400	60	862	1106	3646	2873	1163	1511	1834
	500	60	980	1226	4052	3142	1120	1422	1757
	600	60	914	1265	4101	3093	1085	1420	1844
	700	60	920	1301	4037	2610	1009	1373	2034
	800	60	904	1236	3772	2519	868	1207	1765
	900	60	920	1286	3836	2380	845	1165	1702
	1000	60	975	1423	4366	2587	801	1171	1682
	1010	60	895	1309	3801	2291	774	1231	1722
	1025	60	913	1406	4145	2470	772	1258	1735
	1050	60	929	1446	4280	2331	697	1144	1653
	1100	60	1046	1626	4815	2659	692	1208	1551
	1200	60		1985	5460	2783	674	1353	1981
	1300	60	1284	2088	5154	3108	612	1526	2356
	1400	60		2166	4554	2931	617	2495	3424

Table A.6 Vertical compressive strain versus load cycles for Station 38, Outer Wheelpath, PR3-0610 pavement.

Station 38 Outer Wheelpath								
		Vertical Compressive Strain (μm/m) Depth below surface (mm)						
	Static wheelload (kN)	Subgrade				Basecourse		
		562.5	487.5	412.5	337.5	262.5	187.5	112.5
15	40	445	1058	1228	1956	735	1053	1100
25	40	442	1030	1220	1952	743	1054	1045
35	40	456	1054	1281	2041	745	1034	1033
50	40	456	1039	1304	2134	734	1012	
100	40	492	1096	1414	2148	708	963	866
150	40	476	1067	1411	2250	724	975	1039
200	40	481	1075	1425	2279	712	927	1255
250	40	500	1081	1453	2121	692	919	1164
300	40	517	1107	1486	2221	694	912	1128
400	40	517	1129	1563	2325	723	940	1048
500	40	538	1149	1639	2531	707	912	972
600	40	555	1178	1686	2563	727	926	918
700	40	563	1185	1654	2149	701	890	980
800	40	580	1205	1665	2277	707	898	1039
900	40	583	1219	1667	2190	708	908	1060
1000	40	583	1225	1723	2541	745	898	
1010	60	746	1546	2216	2735	796	935	1021
1025	60	797	1668	2425	3068	857	968	1217
1050	60	823	1710	2487	3001	845	943	1012
1100	60	893	1917	2838	3382	928	943	
1200	60	1001	2300	3684	3649	917	996	976
1300	60	1082	2419	3648	4038	1039	1082	749
1400	60	1080	2308	2844	3297	2657	1690	1790

Load Cycles ('000's)

Table A.7 VSD versus load cycles for Station 9, Inner Wheelpath, PR3-0404 pavement.

Station 9 **Inner Wheelpath**			
		Static wheelload (kN)	VSD (mm)
Load Cycles ('000's)	5	40	0.0
	20	40	2.3
	30	40	3.3
	50	40	3.2
	100	40	2.9
	150	40	3.7
	200	40	3.4
	250	40	3.0
	300	40	3.2
	400	40	4.1
	500	40	4.3
	600	40	4.1
	700	40	4.7
	800	40	4.2
	900	40	4.9
	1000	40	5.5
	1019	50	5.1
	1045	50	7.0
	1070	50	7.1
	1120	50	8.2
	1220	50	7.7
	1320	50	8.4

Table A.8 Vertical stress and modulus values for Station 9, inner wheelpath, PR3-0404 pavement.

Load Cycles ('000's)	Wheelload (kN)	Vertical stress (kPa)	Modulus (MPa)
5	40	74	38
20	40	77	38
30	40	68	37
50	40	70	36
100	40	68	33
150	40	74	34
200	40	70	35
250	40	65	33
300	40	69	34
400	40	74	34
500	40	70	35
600	40	75	37
700	40	74	34
800	40	73	37
900	40	72	34
1000	40	76	36
1019	50	92	46
1045	50	117	42
1070	50	120	39
1120	50	114	39
1220	50	117	42
1320	50	114	46

Table A.9 Vertical stress and modulus values for Stations 29 and 38, inner wheelpath, PR3-0610 pavement.

	Station 29, depth 225 mm			Station 38, depth 300 mm	
Load Cycles ('000's)	Wheelload (kN)	Vertical stress (kPa)	Modulus (MPa)	Vertical stress (kPa)	Modulus (MPa)
15	60	265	103	125	52
25	60	263	96	124	47
35	60	275	95	132	50
50	60	285	96	131	46
100	60	307	99	139	48
150	60	307	95	137	45
200	60	326	95	140	45
250	60	347	114	145	50
300	60	296	97	128	46
400	60	318	95	134	47
500	60	301	83	131	42
600	60	321	92	139	45
700	60	327	108	111	43
800	60	276	97	107	42
900	60	316	117	105	44
1000	60	361	120	133	51
1010	60	362	123	140	61
1025	60	388	123	138	56
1050	60	402	144	108	46
1100	60	428	149	67	25
1200	60	463	154	58	21
1300	60	486	175	115	37
1400	60	491	-	162	55

Table A.10 VSD versus load cycles for PR3-0610 pavement.

Wheelpath		Inner			Outer	
Station		29	38		29	38
Pavement thickness (mm)		200	275		200	275
	Static wheelload (kN)	VSD (mm)		Static wheelload (kN)	VSD (mm)	
Load cycles ('000's) 0	60	0.0	0.0	40	0.0	0.0
15	60	1.3	3.1	40	1.2	1.9
25	60	1.8	3.7	40	1.5	2.2
35	60	2.0	4.1	40	1.4	2.2
50	60	2.2	4.4	40	2.0	2.4
100	60	3.0	5.3	40	1.9	2.9
150	60	3.3	5.7	40	2.2	3.1
200	60	3.9	6.3	40	2.5	3.5
250	60	4.0	6.9	40	2.6	4.0
300	60	5.2	7.6	40	2.8	3.9
400	60	5.9	8.3	40	3.4	4.7
500	60	6.7	9.4	40	4.1	5.2
600	60	7.5	10.0	40	4.8	5.5
700	60	7.8	10.3	40	5.0	5.9
800	60	8.7	11.0	40	5.6	6.3
900	60	9.1	10.8	40	5.7	6.0
1000	60	9.8	11.5	40	6.5	6.4
1010	60	9.6	11.6	60	6.6	6.3
1025	60	9.9	11.7	60	6.8	6.4
1050	60	10.3	12.3	60	8.2	7.1
1100	60	11.1	13.6	60	10.4	7.8
1200	60	12.4	14.7	60	13.2	8.8
1300	60	13.0	16.1	60	14.4	10.2
1400	60	13.8	18.1	60	15.7	11.8

Table A.11 Resilient Modulus test results for Subgrade material.

Confing stress (kPa)	Deviatoric stress (kPa)	Resilient Modulus (MPa)
16	11	97
16	21	74
16	32	69
16	44	69
16	55	68
30	11	103
31	21	89
31	32	86
31	44	85
31	56	84
44	10	119
44	22	111
44	33	107
44	45	100
44	57	98

Table A.12 Resilient Modulus test results for basecourse (TNZ AP40 M4) material.

Confing stress (kPa)	Deviatoric stress (kPa)	Resilient Modulus (MPa)
4	66	107
5	65	107
7	63	111
7	133	157
8	63	118
8	133	157
10	130	157
11	130	156
11	199	198
12	199	195
12	199	201
14	266	232
15	126	170
15	126	167
15	126	169
16	195	199
16	195	201
27	325	272
29	252	254
30	252	261
33	283	274
45	378	329
51	440	352
52	251	316
52	251	314
78	373	400
103	495	460
147	328	489
205	460	587
225	323	588
291	419	680
486	231	854

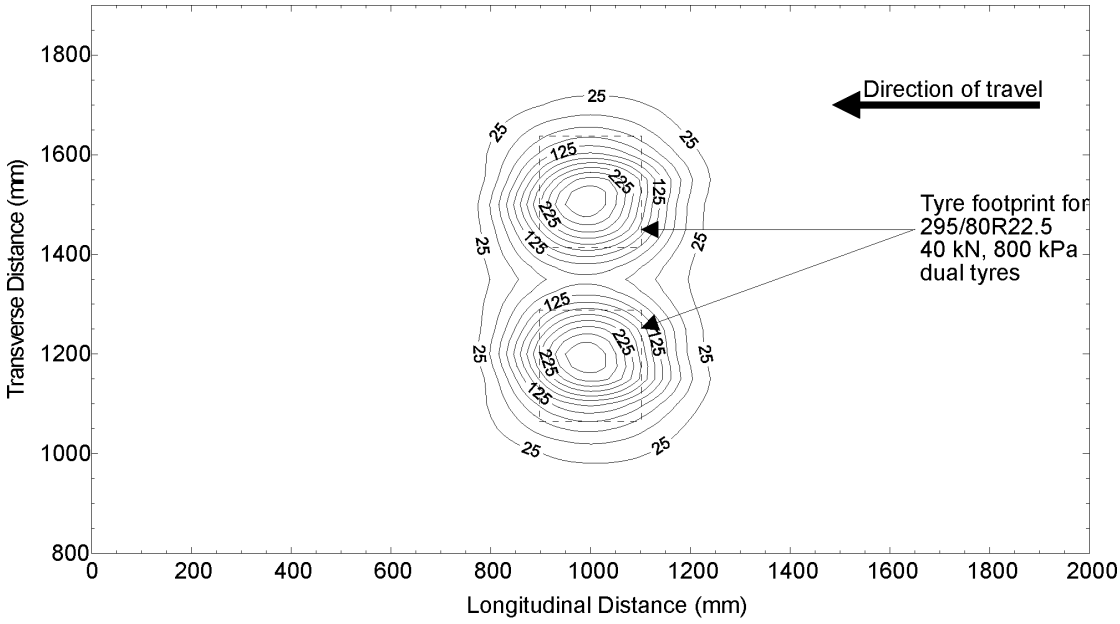

Figure A.1 Stress contour for station 7, depth = 75 mm.

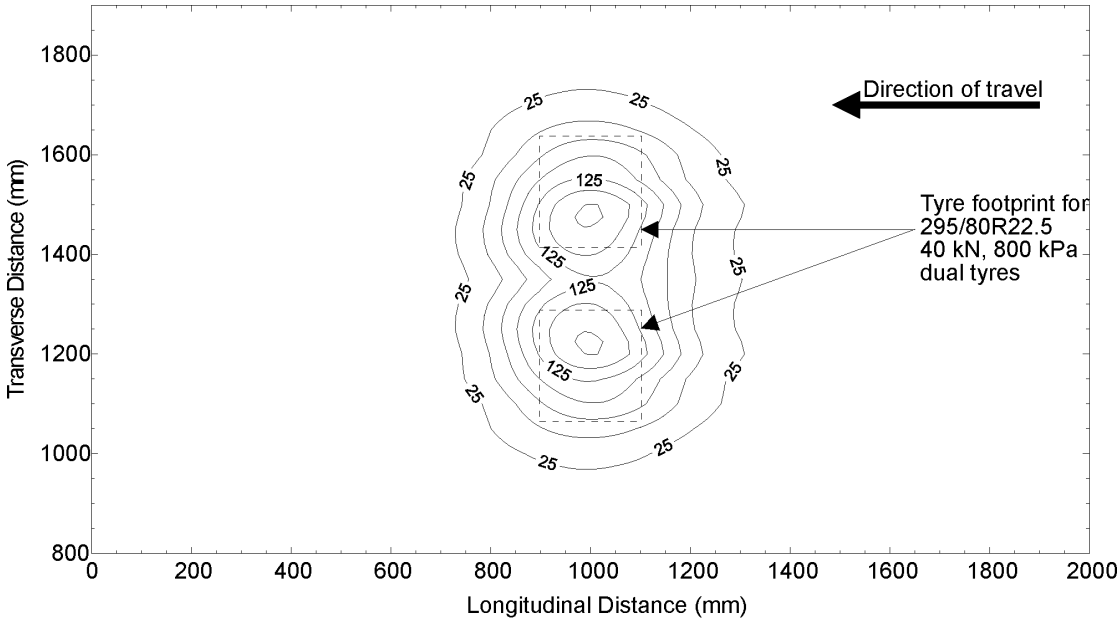

Figure A.2 Stress contour for station 7, depth = 150 mm.

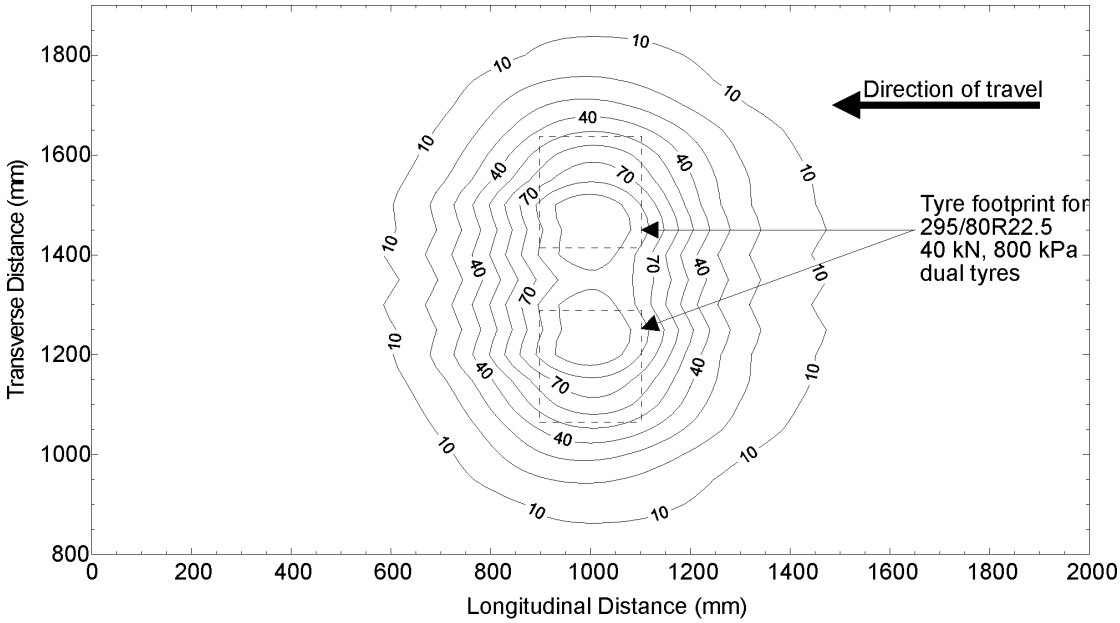

Figure A.3 Stress contour for station 7, depth = 225 mm.

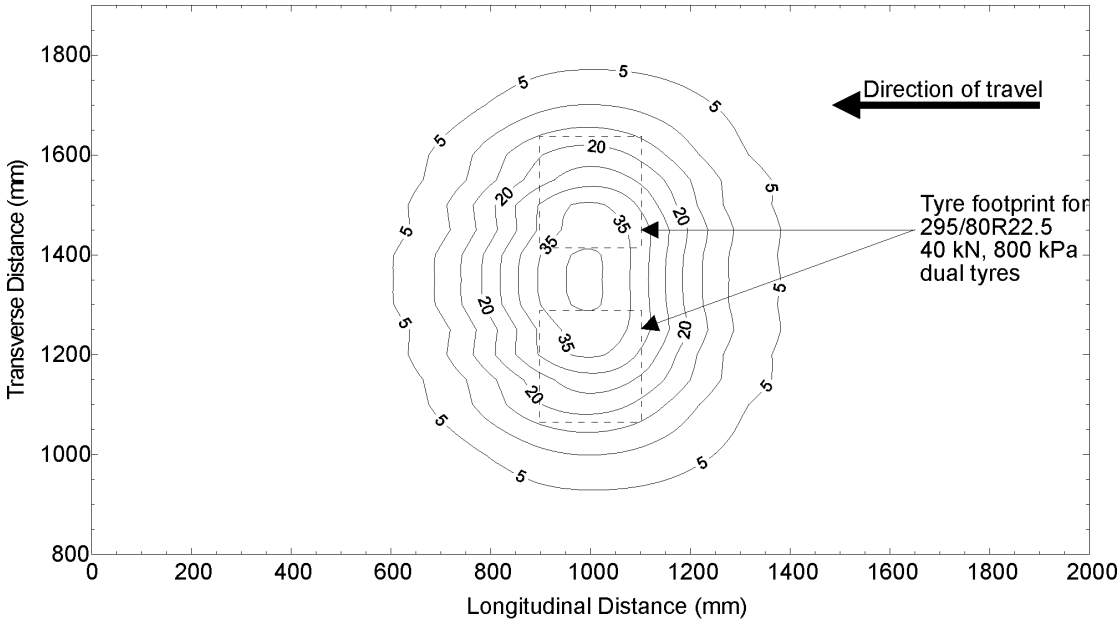

Figure A.4 Stress contour for station 7, depth = 300 mm.

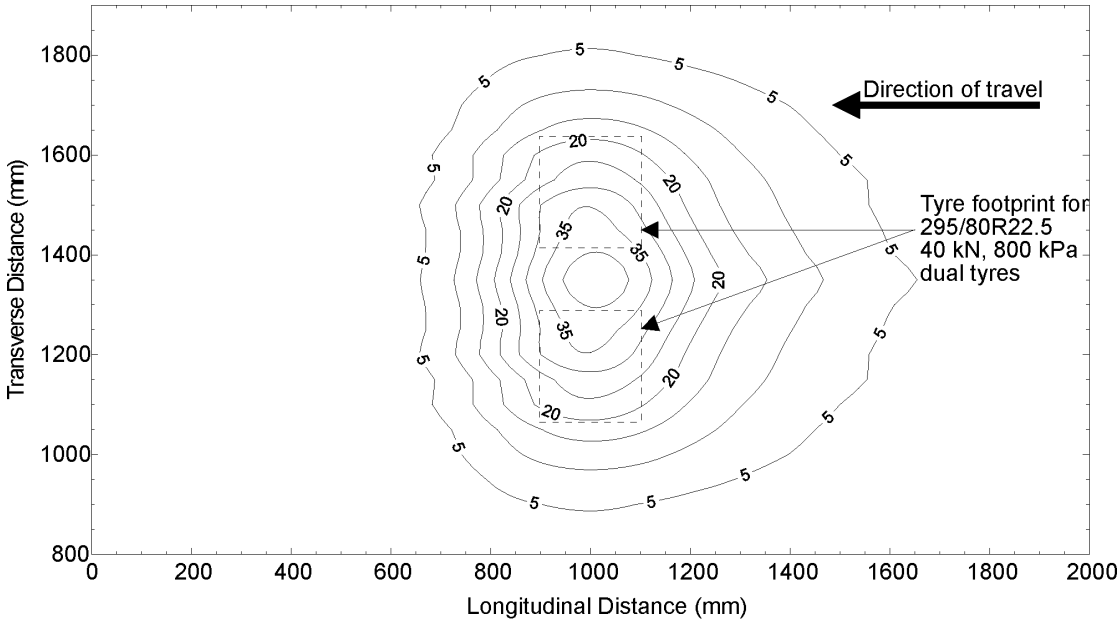

Figure A.5 Stress contour for station 7, depth = 375 mm.

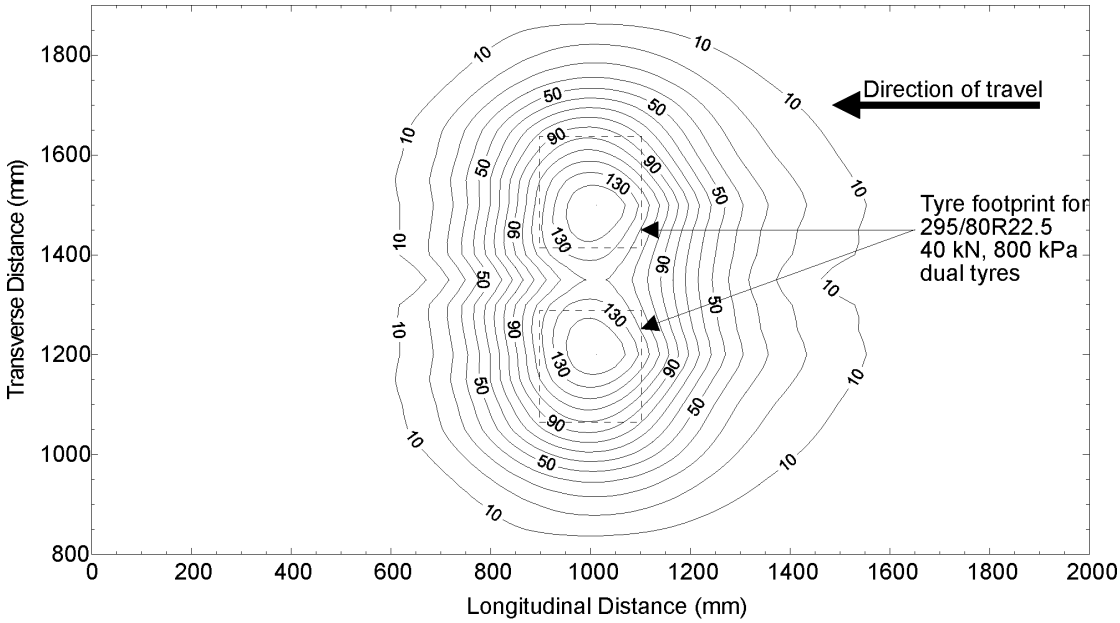

Figure A.6 Stress contour for station 17, depth = 225 mm.

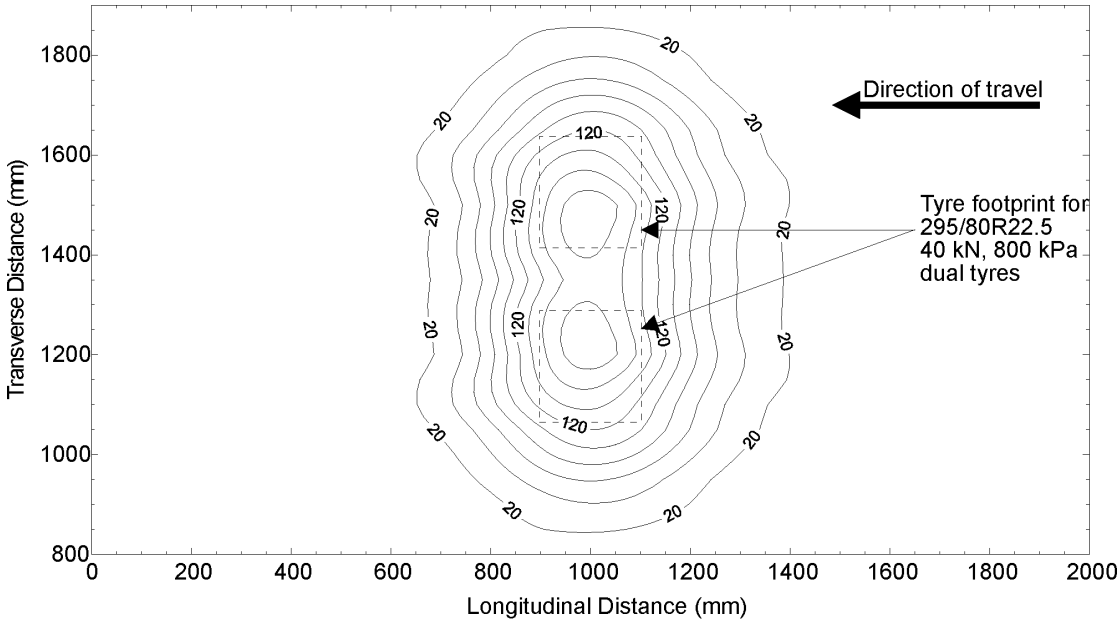

Figure A.7 Stress contour for station 29, depth = 225 mm.

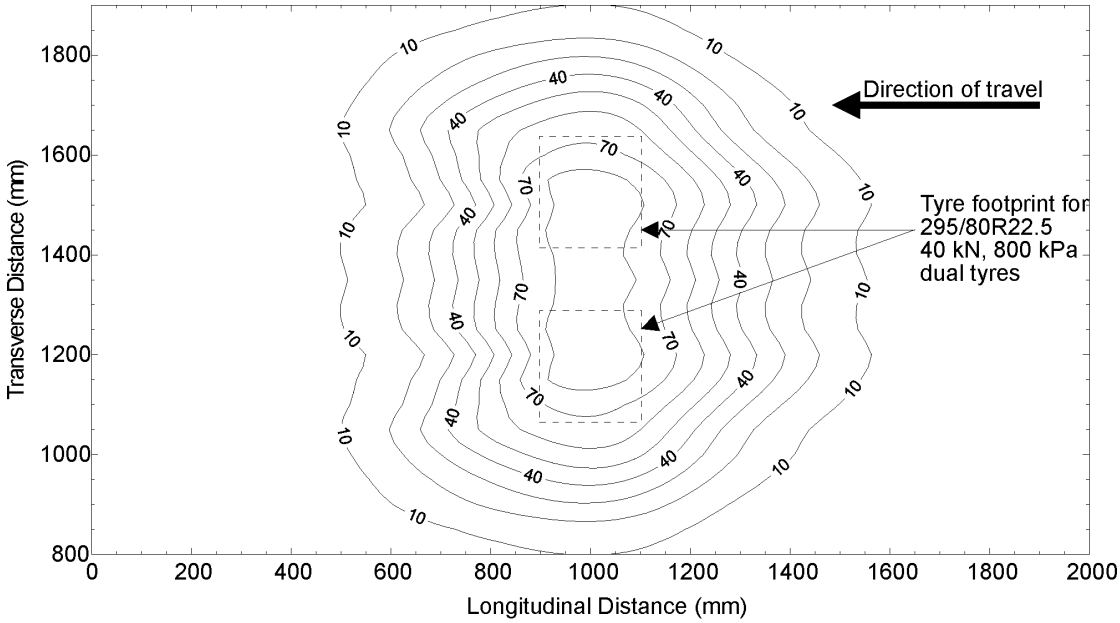

Figure A.8 Stress contour for station 38, depth = 300 mm.

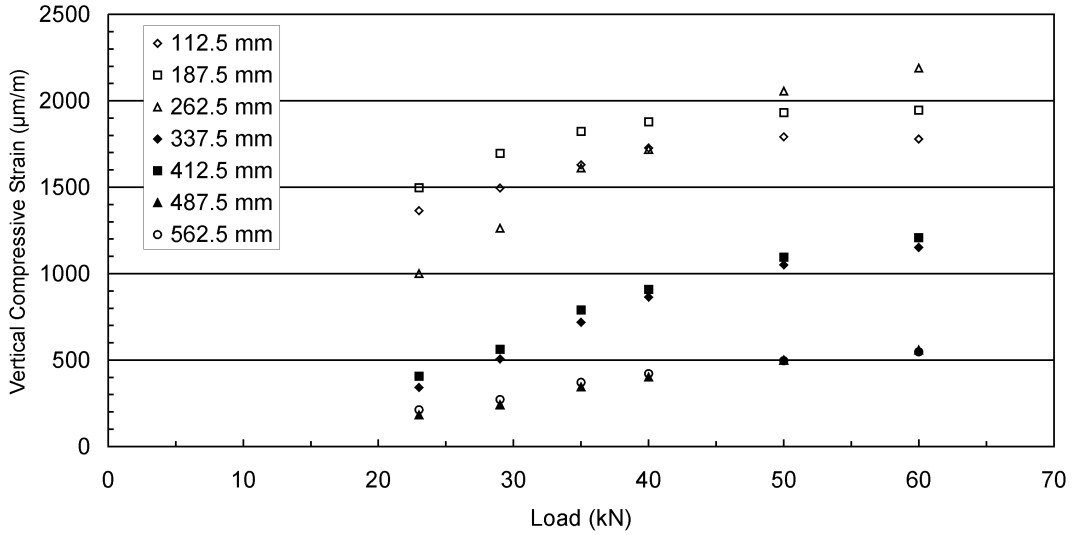

Figure A.9 Vertical compressive strain versus load for various depths at station 29, inner wheelpath, ram 135 cm, PR3-0610 pavement.

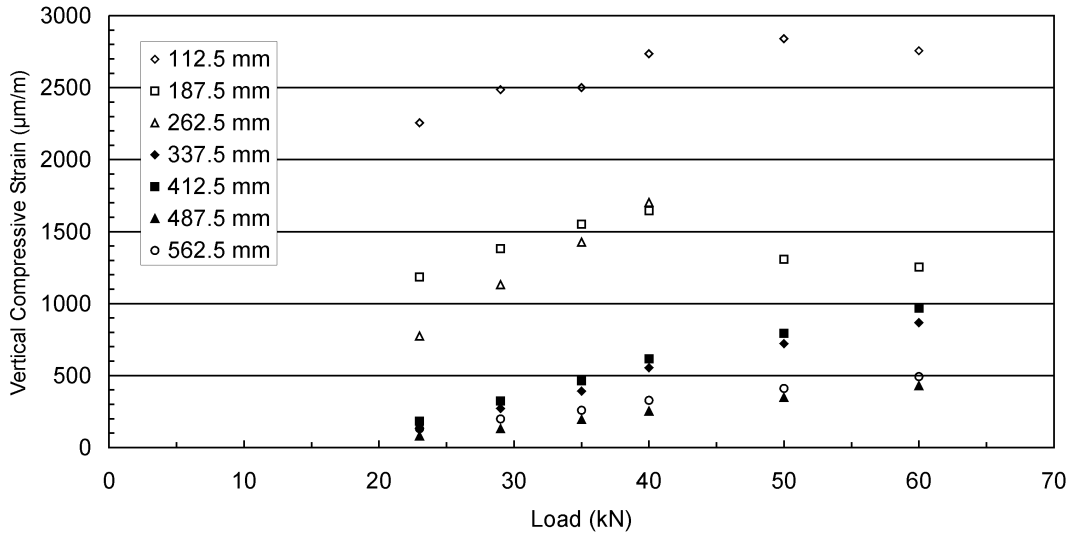

Figure A.10 Vertical compressive strain versus load for various depths at station 29, inner wheelpath, ram 153 cm, PR3-0610 pavement.

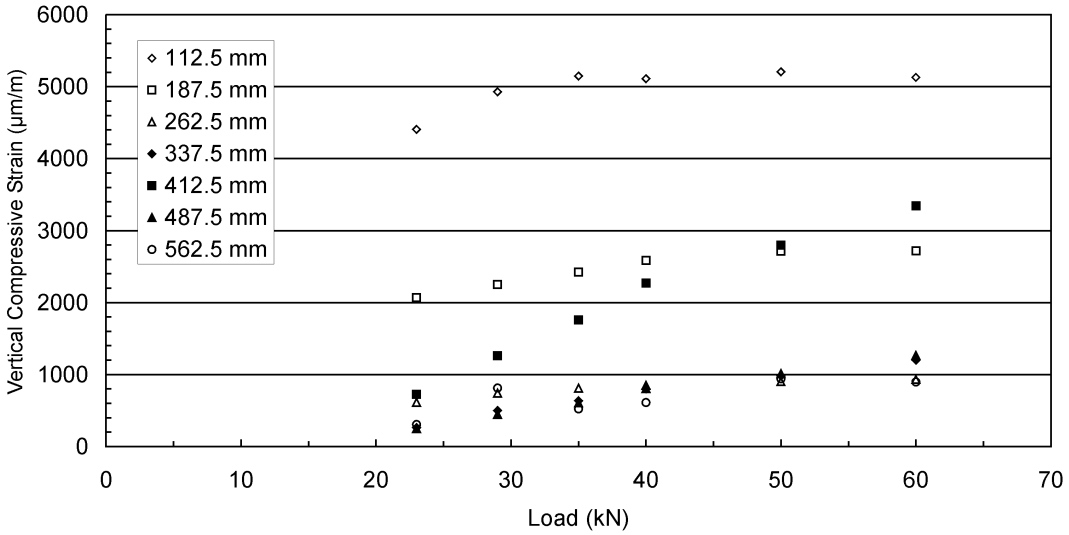

Figure A.11 Vertical compressive strain versus load for various depths at station 38, inner wheelpath, ram 153 cm, PR3-0610 pavement.

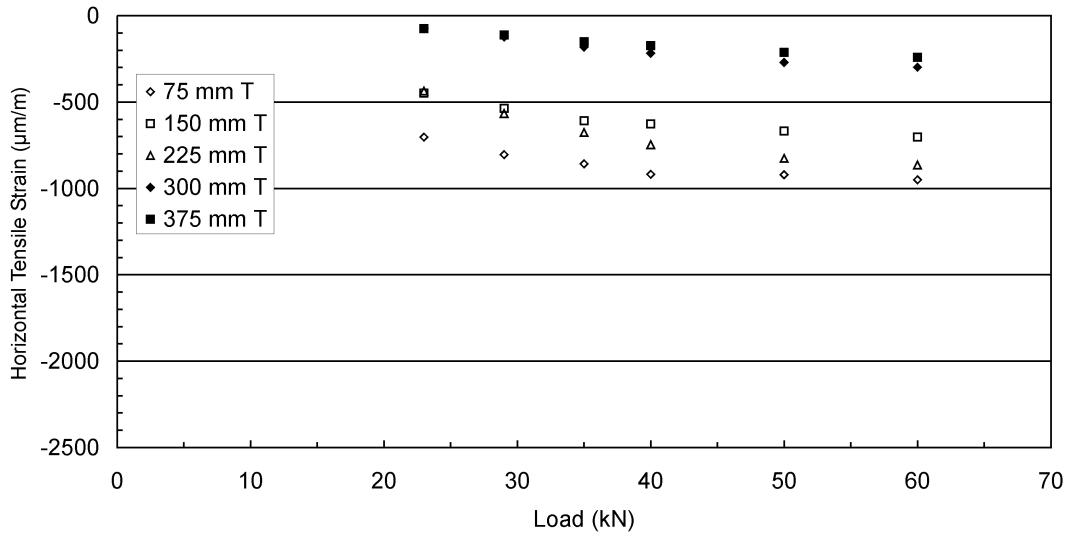

Figure A.12 Horizontal transverse tensile strain versus load for various depths at station 29, ram 135 cm, PR3-0610 pavement.

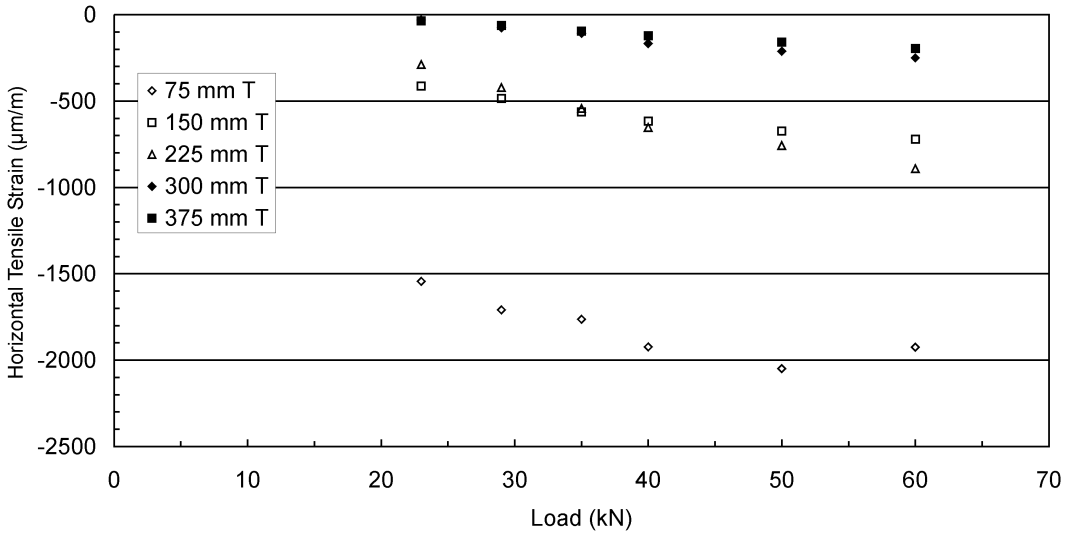

Figure A.13 Horizontal transverse tensile strain versus load for various depths at station 29, ram 153 cm, PR3-0610 pavement.

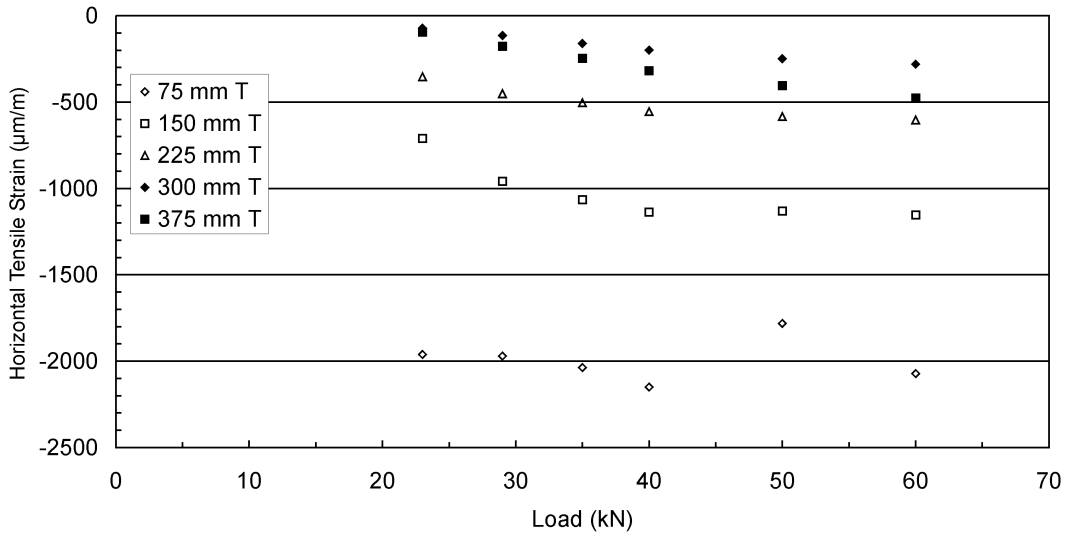

Figure A.14 Horizontal transverse strain versus load for various depths at station 38, ram 153 cm, PR3-0610 pavement.

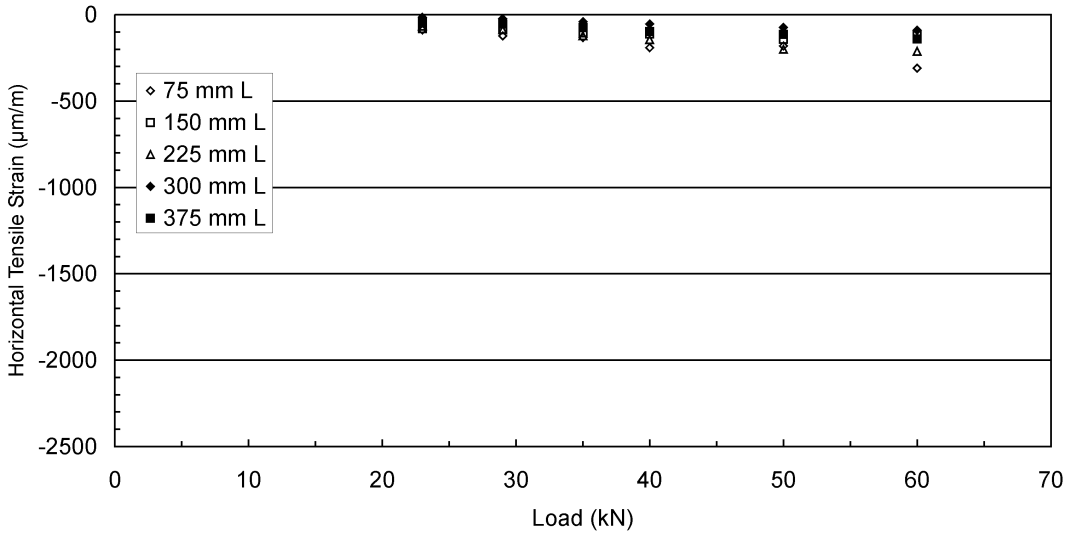

Figure A.15 Horizontal longitudinal strain versus load for various depths at station 29, ram 135 cm, PR3-0610 pavement.

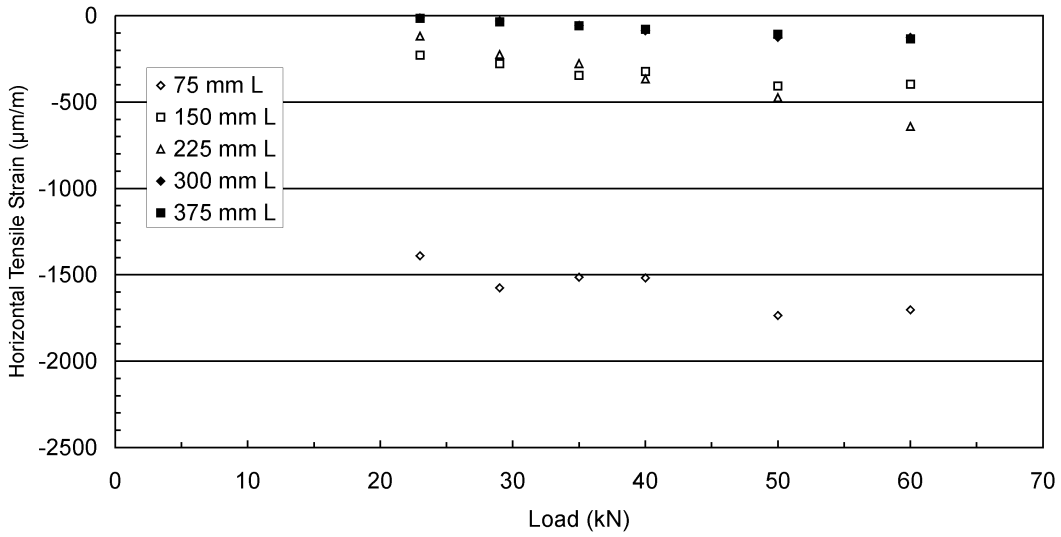

Figure A.16 Horizontal longitudinal strain versus load for various depths at station 29, ram 153 cm, PR3-0610 pavement.

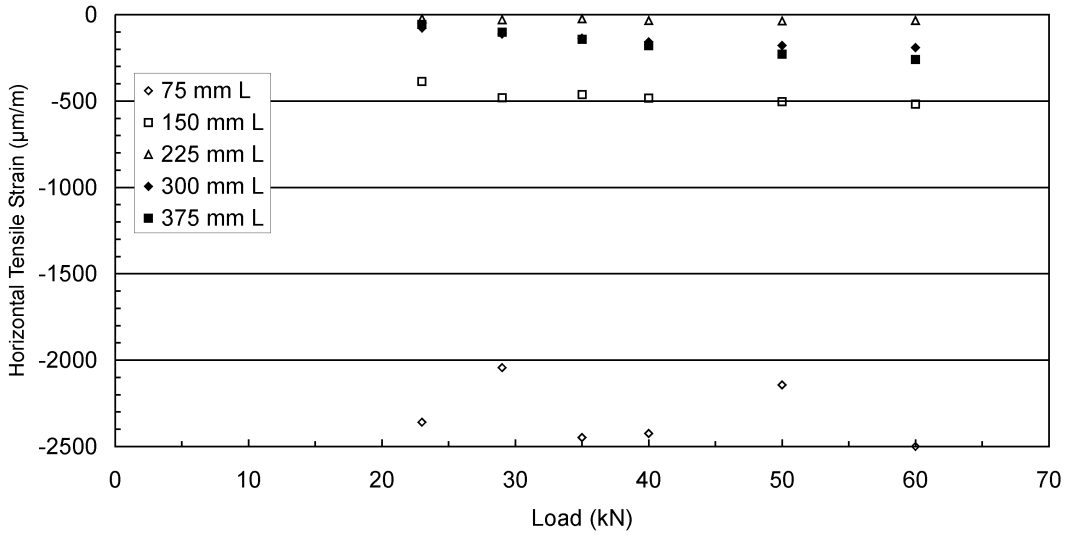

Figure A.17 Horizontal longitudinal strain versus load for various depths at station 38, ram 153 cm, PR3-0610 pavement.

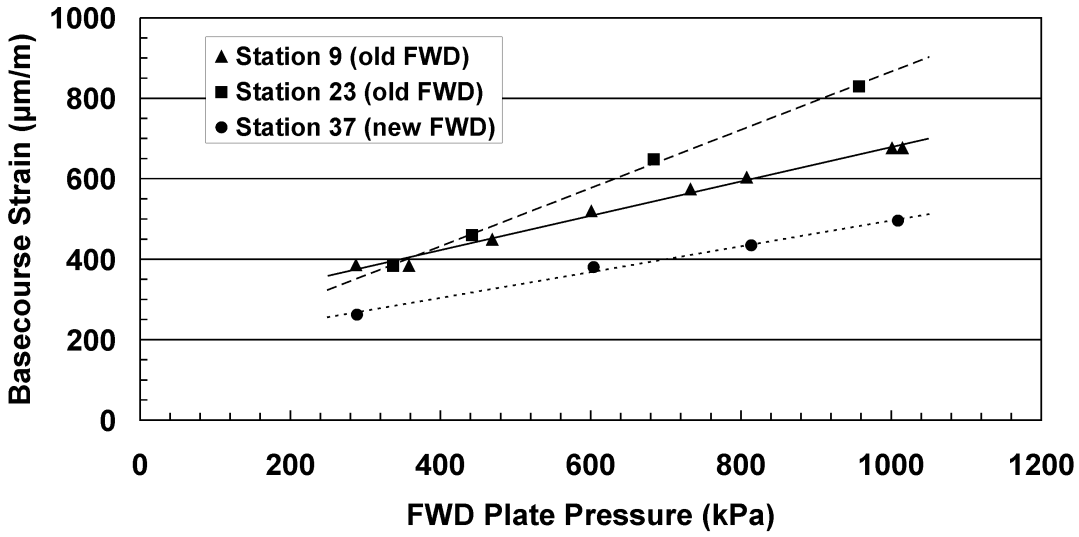

Figure A.18 Measured strains at a depth of 112.5 mm induced by various FWD load levels.

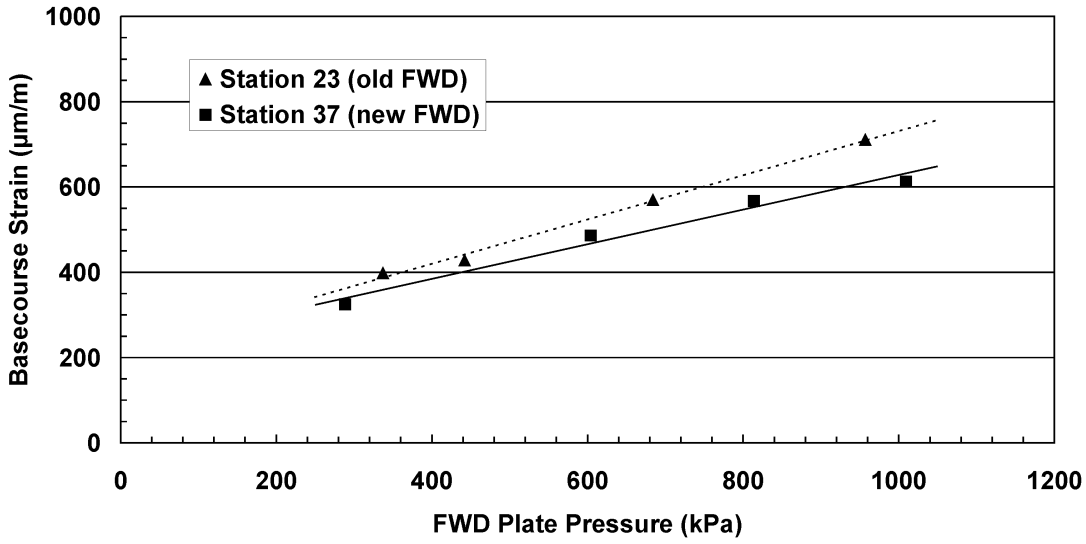

Figure A.19 Measured strains at a depth of 187.5 mm induced by various FWD load levels.

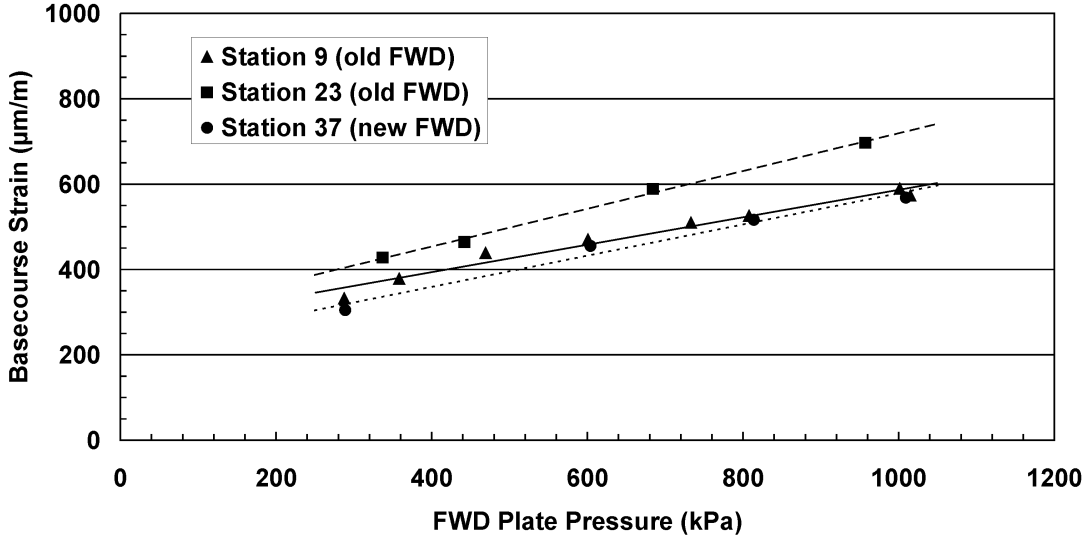

Figure A.20 Measured strains at a depth of 262.5 mm induced by various FWD load levels.

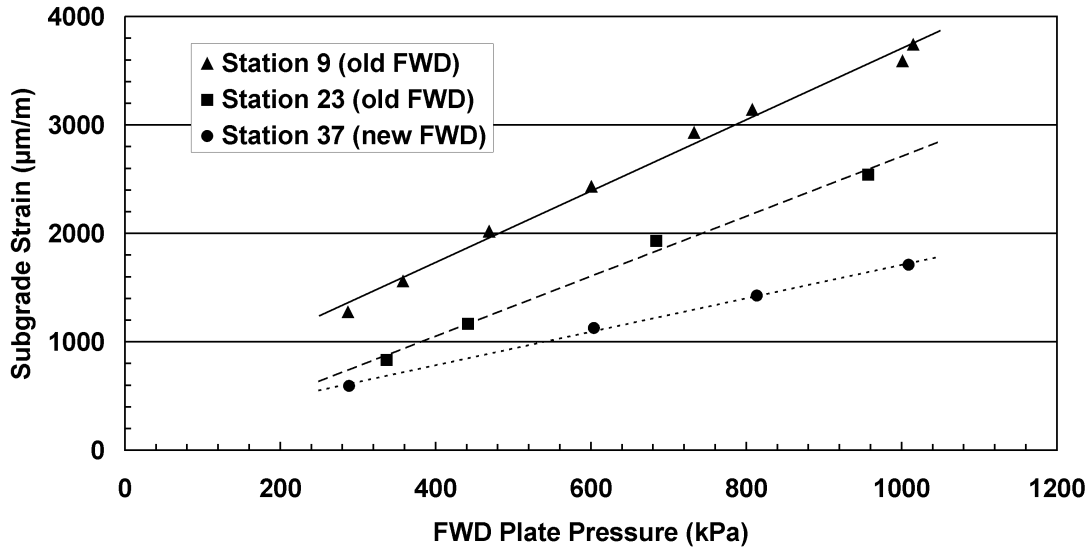

Figure A.21 Measured strains at a depth of 412.5 mm induced by various FWD load levels.

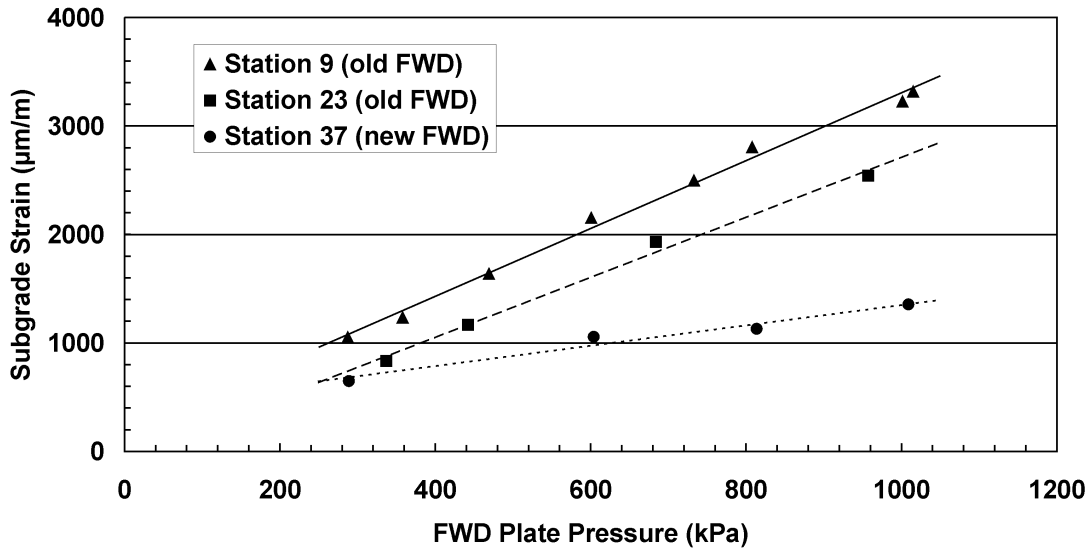

Figure A.22 Measured strains at a depth of 487.5 mm induced by various FWD load levels.

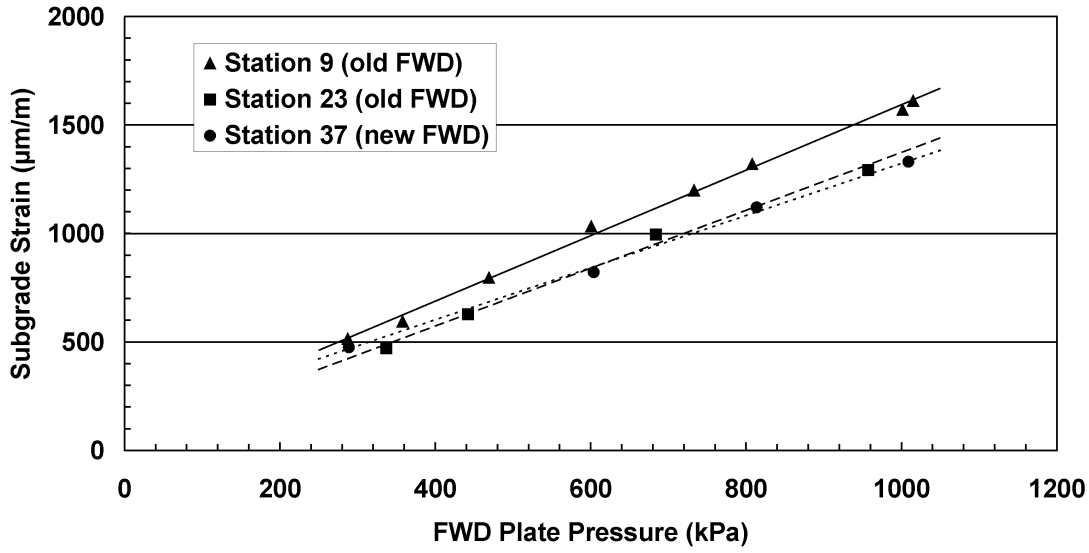

Figure A.23 Measured strains at a depth of 562.5 mm induced by various FWD load levels.

This page is intentionally left blank.

Appendix B UMAT Source Code

```
SUBROUTINE UMAT(STRESS,STATEV,DDSDDE,SSE,SPD,SCD,&
 RPL,DDSDDT,DRPLDE,DRPLDT,&
 STRAN,DSTRAN,TIME,DTIME,TEMP,DTEMP,PREDEF,DPRED,CMNAME,&
 NDI,NSHR,NTENS,NSTATV,PROPS,NPROPS,COORDS,DROT,PNEWDT,&
 CELENT,DFGRD0,DFGRD1,NOEL,NPT,LAYER,KSPT,KSTEP,KINC)
!
 INCLUDE 'ABA_PARAM.INC'
!
 CHARACTER*80 CMNAME
 DIMENSION STRESS(NTENS),STATEV(NSTATV),&
  DDSDDE(NTENS,NTENS),DDSDDT(NTENS),DRPLDE(NTENS),&
  STRAN(NTENS),DSTRAN(NTENS),TIME(2),PREDEF(1),DPRED(1),&
  PROPS(NPROPS),COORDS(3),DROT(3,3),DFGRD0(3,3),DFGRD1(3,3)
!
! Programmer defined variables below
!
 REAL*8:: oct_shear,EMOD,mm,nn
 REAL*8:: dd,uu,vv,tt
 REAL*8:: TAU, THETA=0.D0
 REAL*8,    DIMENSION(3) :: PS=0
 REAL*8,    DIMENSION(3,3) :: AN=0
 REAL*8,    DIMENSION(3) :: PSTEST=0
 REAL*8,    DIMENSION(3,3) :: ANTEST=0
 REAL*8,    DIMENSION(NTENS) :: MODSTRESS
 REAL*8,    DIMENSION(6) :: MODSTRESSTEST
 REAL*8,    DIMENSION(NTENS) :: SIGMASTRESS
 INTEGER::LSTR
 PARAMETER(ZERO=0.D0, ONE=1.D0, TWO=2.D0, THREE=3.D0, SIX=6.D0, &
  ENUMAX=.4999D0, NEWTON=10, TOLER=1.0D-6, GRAVITY=0.981E-05)
!------------------------------------------------------------------------
!   UMAT FOR ANISOTROPIC ELASTICITY
!      with principal stresses
!   CANNOT BE USED FOR PLANE STRESS
!------------------------------------------------------------------------
! This source code is copyright 2003 - Bruce Steven
!------------------------------------------------------------------------
!   PROPS(1) - Material model
!   PROPS(2) - NU
!   PROPS(3) - K1
!   PROPS(4) - K2
!   PROPS(5) - K3
!   PROPS(6) - Eh/Ev
!   PROPS(7) - 1 for principal stress / 0 for S11/S22/S33 to calculate EMOD
!   PROPS(8) - K0 for horizontal overburden stress
!   PROPS(9) - density for overburden stress (t/m^3)
!   PROPS(10) - Minimum EMOD (MPa)
!   PROPS(11) - EMOD for first increment (zero applied stress) (MPa)
!
!   DEPVAR order(9)
!   SDV(1) - sig1
!   SDV(2) - sig2
!   SDV(3) - sig3
!   SDV(4) - oct shear stress
!   SDV(5) - Horizontal stress due to overburden
!   SDV(6) - Vertical stress due to overburden
!   SDV(7) - Theta
!   SDV(8) - EMOD(Calc),
!   SDV(9) - EMOD(THETA),
!------------------------------------------------------------------------
!
    IF (NDI/=3) THEN
        WRITE (7, *) 'THIS UMAT MAY ONLY BE USED FOR 3D and AXISYMMETRIC &
            ELEMENTS WITH THREE DIRECT STRESS COMPONENTS'
        CALL XIT
    END IF
!
! Change sign on stress values to reflect geomech principal of
! compression = positive
! set stress to 1 kPa if zero or tensile. These values are used in the EMOD
! calcs only
! Units of stress are in MPa
! Modified values stored in SIGMASTRESS array which has the same dimension
! as STRESS
!
!*********************************************************************
!*********************************************************************
! Loop for 3D
```

```
!*********************************************************************
!*********************************************************************
 IF (NSHR==3) THEN
!Calculate principal stresses if PROPS(7)=1
    SIGMASTRESS=STRESS*-1
    MODSTRESS=STRESS*-1
    MODSTRESSTEST=STRESS*-1
    IF(TIME(1)>0) THEN
        SIGMASTRESS=SIGMASTRESS/TIME(1)
        MODSTRESS=MODSTRESS/TIME(1)
        MODSTRESSTEST=MODSTRESSTEST/TIME(1)
    END IF
    MODSTRESS(1)=MODSTRESS(1)+abs(COORDS(3)*PROPS(8)*PROPS(9)*GRAVITY)
    MODSTRESS(2)=MODSTRESS(2)+abs(COORDS(3)*PROPS(8)*PROPS(9)*GRAVITY)
    MODSTRESS(3)=MODSTRESS(3)+abs(COORDS(3)*PROPS(9)*GRAVITY)
    SIGMASTRESS(1)=SIGMASTRESS(1)+abs(COORDS(3)*PROPS(8)*PROPS(9)*GRAVITY)
    SIGMASTRESS(2)=SIGMASTRESS(2)+abs(COORDS(3)*PROPS(8)*PROPS(9)*GRAVITY)
    SIGMASTRESS(3)=SIGMASTRESS(3)+abs(COORDS(3)*PROPS(9)*GRAVITY)
    DO K1=1, NTENS
        IF (SIGMASTRESS(K1)<0) THEN
            SIGMASTRESS(K1)=0.001
        END IF
    END DO
    IF (PROPS(7)==1) THEN
        LSTR=1
        CALL SPRIND(MODSTRESSTEST,PSTEST,ANTEST,LSTR,3,3)
        IF (PSTEST(1)==ZERO .AND. PSTEST(2)==ZERO .AND. PSTEST(3)==ZERO) THEN
            K2=0
        ELSE IF (PSTEST(1)>=PSTEST(2) .AND. PSTEST(1)>=PSTEST(3)) THEN
            K2=1
        ELSE IF (PSTEST(2)>=PSTEST(1) .AND. PSTEST(2)>=PSTEST(3)) THEN
            K2=2
        ELSE IF (PSTEST(3)>=PSTEST(1) .AND. PSTEST(3)>=PSTEST(2)) THEN
            K2=3
        ELSE
            K2=0
        END IF
        IF (K2/=0) THEN
            THETA=ACOS(ANTEST(K2,3))
        END IF
        PSTEST=ZERO
        ANTEST=ZERO
        CALL SPRIND(MODSTRESS,PSTEST,ANTEST,LSTR,3,3)
        DO K1=1, NDI
            IF (PSTEST(K1)<0) THEN
                SIGMASTRESS(K1)=0.001
            ELSE
                SIGMASTRESS(K1)=PSTEST(K1)
            END IF
        END DO
        oct_shear=SQRT(((SIGMASTRESS(1)-SIGMASTRESS(2))*(SIGMASTRESS(1) &
            -SIGMASTRESS(2))+(SIGMASTRESS(2)-SIGMASTRESS(3))*(SIGMASTRESS(2) &
            -SIGMASTRESS(3))+(SIGMASTRESS(1)-SIGMASTRESS(3))*(SIGMASTRESS(1) &
            -SIGMASTRESS(3)))/9)
!   end of principal stress loop
    END IF
    IF (PROPS(7)==0) THEN
        oct_shear=SQRT(((SIGMASTRESS(1)-SIGMASTRESS(2))*(SIGMASTRESS(1) &
            -SIGMASTRESS(2))+(SIGMASTRESS(2)-SIGMASTRESS(3))*(SIGMASTRESS(2) &
            -SIGMASTRESS(3))+(SIGMASTRESS(1)-SIGMASTRESS(3))*(SIGMASTRESS(1) &
            -SIGMASTRESS(3)))/9+2/3*(SIGMASTRESS(4)*SIGMASTRESS(4)+ &
            SIGMASTRESS(5)*SIGMASTRESS(5)+SIGMASTRESS(6)*SIGMASTRESS(6)))
    END IF
    IF (PROPS(6)==ONE) THEN
        THETA=ZERO
    END IF
    IF (abs(STRESS(3))<=0.005*TIME(1)) THEN
        IF (PROPS(1)==1) THEN
            oct_shear=ZERO
        END IF
        THETA=ZERO
    END IF
    STATEV(1)=SIGMASTRESS(1)
    STATEV(2)=SIGMASTRESS(2)
    STATEV(3)=SIGMASTRESS(3)
    IF (oct_shear<=0.001) THEN
        oct_shear=0.001
```

```
    END IF
    IF ((STATEV(5)-STATEV(6))>(-1*STRESS(3)/TIME(1))) THEN
        THETA=ZERO
        IF (PROPS(1)==1) THEN
            oct_shear=ZERO
        END IF
    END IF
    STATEV(4)=oct_shear
    STATEV(5)=abs(COORDS(3)*PROPS(8)*PROPS(9)*GRAVITY)
    STATEV(6)=abs(COORDS(3)*PROPS(9)*GRAVITY)
 IF (PROPS(1)==1) THEN
    ! Uzan Model for Granular material
    ! stresses are defined by abaqus in MPa, formula based on kPa
    ! orig formula as declared by Uzan, second formula adj for stress magnitude
    !EMOD=k1*100*(((sig1+2*sig2)/100)**k2)*(((sig2-sig1)/100)*(2**0.5)/3)**k3
    EMOD=PROPS(3)*100*(((SIGMASTRESS(1)+SIGMASTRESS(2)+SIGMASTRESS(3))*10) &
        **PROPS(4))*((oct_shear*10+ONE)**PROPS(5))
    STATEV(8)=EMOD
    EMOD=EMOD/(1+(SIN(THETA)*SIN(THETA)-0.25*SIN(2*THETA))*(PROPS(6)-1))
    IF (TIME(1)==0) THEN
        EMOD=PROPS(11)
    END IF
    IF (EMOD<PROPS(10)) THEN
        EMOD=PROPS(10)
    END IF
 END IF
 STATEV(9)=EMOD
!
!   ELASTIC PROPERTIES
!
    nn=PROPS(6)
    vv=PROPS(2)
    uu=PROPS(2)*nn
    tt=1/(1-vv*vv-2*uu*vv-2*vv*vv*uu)
!
!   ELASTIC STIFFNESS
!
    DDSDDE=0
    DDSDDE(1,1)=EMOD*nn*(1-uu*vv)*tt
    DDSDDE(2,2)=DDSDDE(1,1)
    DDSDDE(3,3)=EMOD*(1-vv*vv)*tt
    DDSDDE(4,4)=EMOD*nn/(2*(1+vv))
    DDSDDE(5,5)=EMOD/(2*(1+vv))
    DDSDDE(6,6)=DDSDDE(5,5)
    DDSDDE(1,2)=EMOD*nn*(vv+uu*vv)*tt
    DDSDDE(2,1)=DDSDDE(1,2)
    DDSDDE(1,3)=EMOD*nn*(vv+vv*vv)*tt
    DDSDDE(2,3)=DDSDDE(1,3)
    DDSDDE(3,1)=DDSDDE(1,3)
    DDSDDE(3,2)=DDSDDE(1,3)
!
!   CALCULATE STRESS
!
  DO K1=1, NTENS
   DO K2=1, NTENS
    STRESS(K2)=STRESS(K2)+DDSDDE(K2, K1)*DSTRAN(K1)
   END DO
  END DO
 END IF
!*********************************************************************
! end of 3D loop
!*********************************************************************
!*********************************************************************
!
!*********************************************************************
! start of axi-symm loop
!*********************************************************************
!*********************************************************************
IF (NSHR==1) THEN
    SIGMASTRESS=STRESS*-1
    MODSTRESS=STRESS*-1
    IF (TIME(1)>0) THEN
        SIGMASTRESS=SIGMASTRESS/TIME(1)
        MODSTRESS=MODSTRESS/TIME(1)
    END IF
        MODSTRESSTEST(1)=MODSTRESS(1)
        MODSTRESSTEST(2)=MODSTRESS(3)
```

```
        MODSTRESSTEST(3)=MODSTRESS(2)
        MODSTRESSTEST(4)=ZERO
        MODSTRESSTEST(5)=MODSTRESS(4)
        MODSTRESSTEST(6)=ZERO
    MODSTRESS(1)=MODSTRESS(1)+abs(COORDS(2)*PROPS(8)*PROPS(9)*GRAVITY)
    MODSTRESS(2)=MODSTRESS(2)+abs(COORDS(2)*PROPS(9)*GRAVITY)
    MODSTRESS(3)=MODSTRESS(3)+abs(COORDS(2)*PROPS(8)*PROPS(9)*GRAVITY)
    SIGMASTRESS(1)=SIGMASTRESS(1)+abs(COORDS(2)*PROPS(8)*PROPS(9)*GRAVITY)
    SIGMASTRESS(2)=SIGMASTRESS(2)+abs(COORDS(2)*PROPS(9)*GRAVITY)
    SIGMASTRESS(3)=SIGMASTRESS(3)+abs(COORDS(2)*PROPS(8)*PROPS(9)*GRAVITY)
    DO K1=1, NTENS
        IF (SIGMASTRESS(K1)<0) THEN
            SIGMASTRESS(K1)=0.001
        END IF
    END DO
    IF (PROPS(7)==1) THEN
        LSTR=1
        CALL SPRIND(MODSTRESSTEST,PSTEST,ANTEST,LSTR,3,3)
        IF (PSTEST(1)==ZERO .AND. PSTEST(2)==ZERO .AND. PSTEST(3)==ZERO) THEN
            K2=0
        ELSE IF (PSTEST(1)>=PSTEST(2) .AND. PSTEST(1)>=PSTEST(3)) THEN
            K2=1
        ELSE IF (PSTEST(2)>=PSTEST(1) .AND. PSTEST(2)>=PSTEST(3)) THEN
            K2=2
        ELSE IF (PSTEST(3)>=PSTEST(1) .AND. PSTEST(3)>=PSTEST(2)) THEN
            K2=3
        ELSE
            K2=0
        END IF
        IF (K2/=0) THEN
            THETA=ACOS(ANTEST(K2,3))
        END IF
        MODSTRESSTEST(1)=MODSTRESS(1)
        MODSTRESSTEST(2)=MODSTRESS(3)
        MODSTRESSTEST(3)=MODSTRESS(2)
        MODSTRESSTEST(4)=ZERO
        MODSTRESSTEST(5)=MODSTRESS(4)
        MODSTRESSTEST(6)=ZERO
        PSTEST=ZERO
        ANTEST=ZERO
        CALL SPRIND(MODSTRESSTEST,PSTEST,ANTEST,LSTR,3,3)
        DO K1=1, NDI
            IF (PSTEST(K1)<0) THEN
                SIGMASTRESS(K1)=0.001
            ELSE
                SIGMASTRESS(K1)=PSTEST(K1)
            END IF
        END DO
        oct_shear=SQRT(((SIGMASTRESS(1)-SIGMASTRESS(2))*(SIGMASTRESS(1) &
            -SIGMASTRESS(2))+(SIGMASTRESS(2)-SIGMASTRESS(3))*(SIGMASTRESS(2) &
            -SIGMASTRESS(3))+(SIGMASTRESS(1)-SIGMASTRESS(3))*(SIGMASTRESS(1) &
            -SIGMASTRESS(3)))/9)
!end of principal strain loop
    END IF
    IF (PROPS(7)==0) THEN
        oct_shear=SQRT(((SIGMASTRESS(1)-SIGMASTRESS(2))*(SIGMASTRESS(1) &
            -SIGMASTRESS(2))+(SIGMASTRESS(2)-SIGMASTRESS(3))*(SIGMASTRESS(2) &
            -SIGMASTRESS(3))+(SIGMASTRESS(1)-SIGMASTRESS(3))*(SIGMASTRESS(1) &
            -SIGMASTRESS(3)))/9+2/3*SIGMASTRESS(4)*SIGMASTRESS(4))
    END IF
    IF (PROPS(6)==ONE) THEN
        THETA=ZERO
    END IF
    IF (abs(STRESS(2))<=0.005*TIME(1)) THEN
        IF (PROPS(1)==1) THEN
            oct_shear=ZERO
        END IF
        THETA=ZERO
    END IF
    STATEV(1)=SIGMASTRESS(1)
    STATEV(2)=SIGMASTRESS(2)
    STATEV(3)=SIGMASTRESS(3)
    STATEV(5)=abs(COORDS(2)*PROPS(8)*PROPS(9)*GRAVITY)
    STATEV(6)=abs(COORDS(2)*PROPS(9)*GRAVITY)
    IF ((STATEV(5)-STATEV(6))>(-1*STRESS(2)/TIME(1))) THEN
        THETA=ZERO
        IF (PROPS(1)==1) THEN
```

```
            oct_shear=ZERO
        END IF
    END IF
    STATEV(4)=oct_shear
    IF (PROPS(1)==1) THEN
    ! Uzan Model for Granular material
    ! stresses are defined by abaqus in MPa, formula based on kPa
    ! orig formula as declared by Uzan, second formula adj for stress magnitude
    !EMOD=k1*100*(((sig1+2*sig2)/100)**k2)*(((sig2-sig1)/100)*(2**0.5)/3)**k3
        EMOD=PROPS(3)*100*(((SIGMASTRESS(1)+SIGMASTRESS(2)+SIGMASTRESS(3))*10) &
            **PROPS(4))*((oct_shear*10+ONE)**PROPS(5))
        STATEV(8)=EMOD
        EMOD=EMOD/(1+(SIN(THETA)*SIN(THETA)-0.25*SIN(2*THETA))*(PROPS(6)-1))
        IF (EMOD<PROPS(10)) THEN
            EMOD=PROPS(10)
        END IF
        IF (TIME(1)==0) THEN
            EMOD=PROPS(11)
        END IF
    END IF
    STATEV(9)=EMOD
    !
    !   ELASTIC PROPERTIES
    !
    nn=PROPS(6)
    vv=PROPS(2)
    uu=PROPS(2)*nn
    tt=1/(1-vv*vv-2*uu*vv-2*uu*vv*vv)
    !
    !   ELASTIC STIFFNESS
    !
    DDSDDE=0
    DDSDDE(1,1)=EMOD*nn*(1-vv*uu)*tt
    DDSDDE(2,2)=EMOD*(1-vv*vv)*tt
    DDSDDE(3,3)=EMOD*nn*(1-uu*vv)*tt
    DDSDDE(4,4)=EMOD/(2*(1+vv))
    DDSDDE(1,2)=EMOD*nn*(vv+uu*vv)*tt
    DDSDDE(2,1)=DDSDDE(1,2)
    DDSDDE(2,3)=EMOD*(uu+uu*uu)*tt
    DDSDDE(3,2)=DDSDDE(2,3)
    DDSDDE(1,3)=EMOD*nn*(vv+vv*uu)*tt
    DDSDDE(3,1)=DDSDDE(1,3)
    !
    !   CALCULATE STRESS
    !
    DO K1=1, NTENS
        DO K2=1, NTENS
            STRESS(K2)=STRESS(K2)+DDSDDE(K2, K1)*DSTRAN(K1)
        END DO
    END DO
!*********************************************************************
! end of axi-symm loop
!*********************************************************************
    END IF
 IF (TIME(1)>0) THEN
    PNEWDT=(ONE-TIME(1)-DTIME)/DTIME
    IF (PNEWDT<ONE) THEN
        PNEWDT=ONE
    END IF
 END IF
 STATEV(7)=THETA
 RETURN
 END SUBROUTINE UMAT
```

Appendix C FEM Model Results

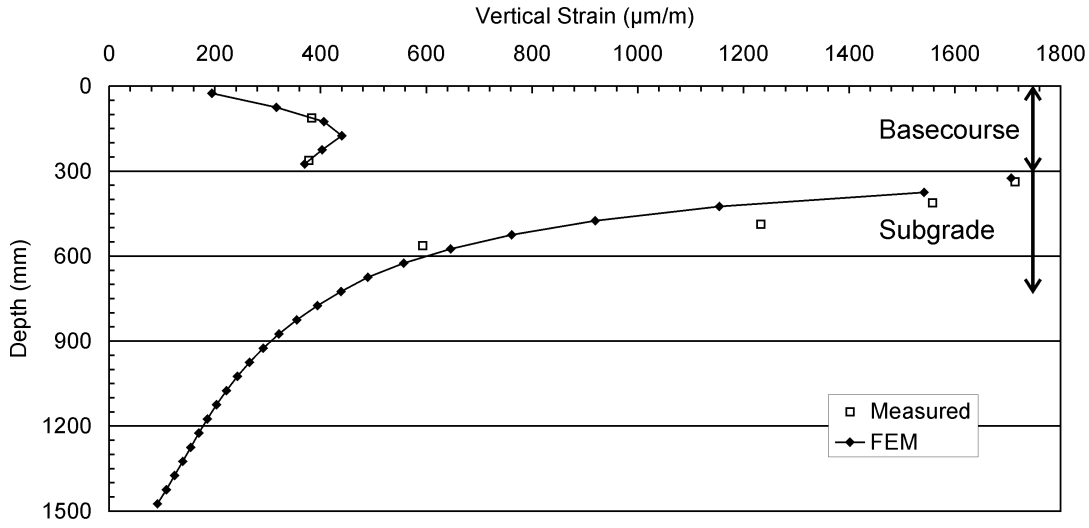

Figure C.1 Measured and computed vertical strain values for a FWD load of 25.3 kN

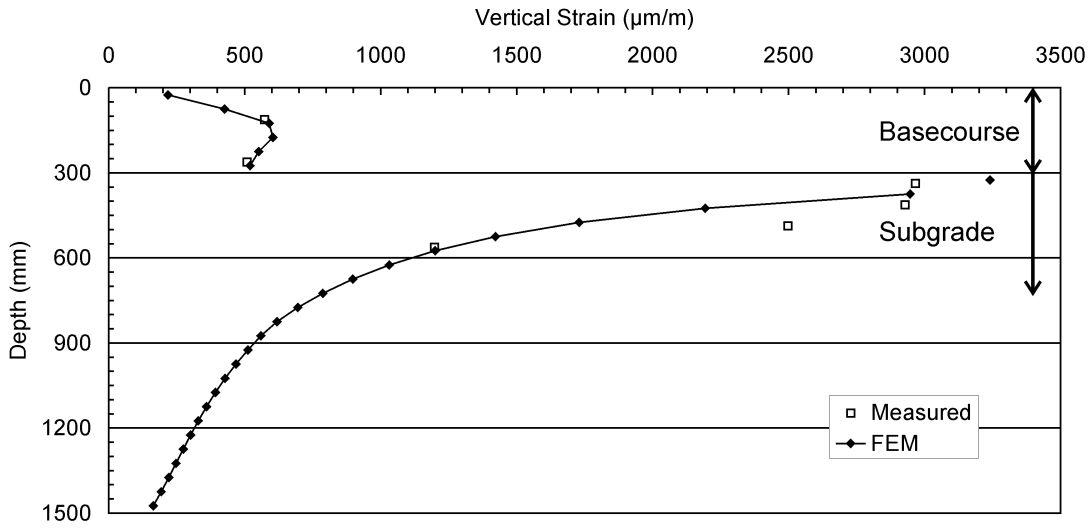

Figure C.2 Measured and computed vertical strain values for a FWD load of 51.8 kN

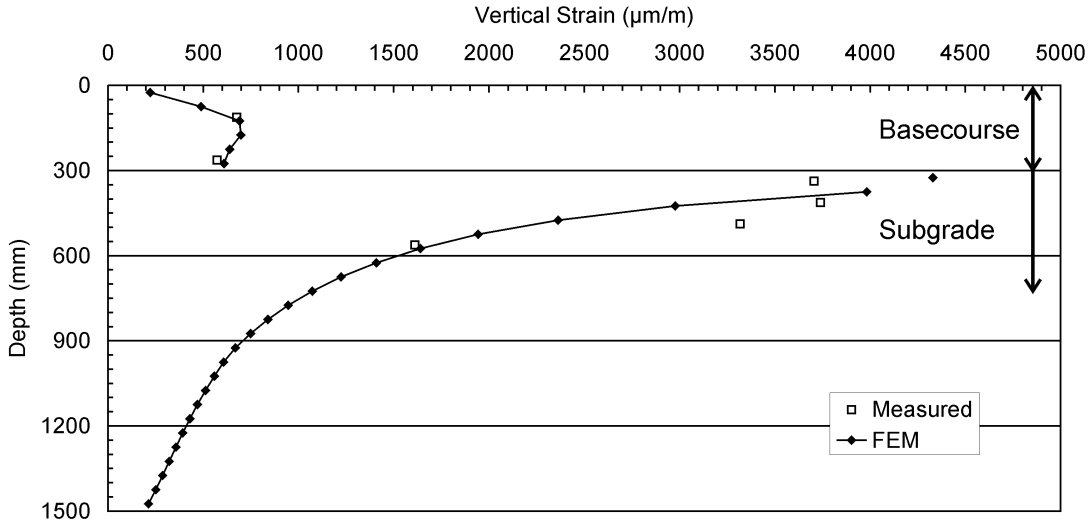

Figure C.3 Measured and computed vertical strain values for a FWD load of 71.7 kN

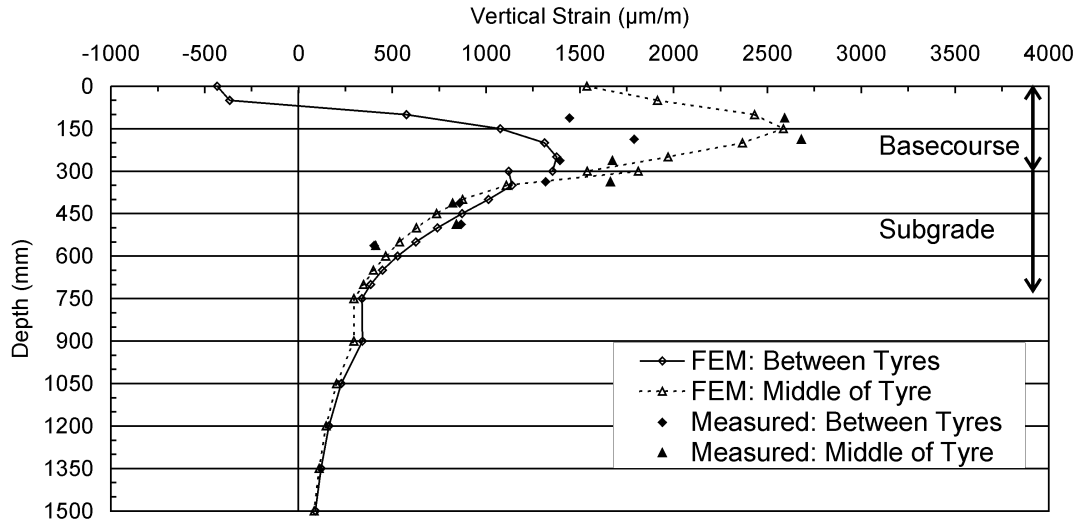

Figure C.4 Measured and computed vertical strains for a 23 kN dual wheel load, Station 38, outer wheelpath, PR3-0610 pavement, 1447k laps.

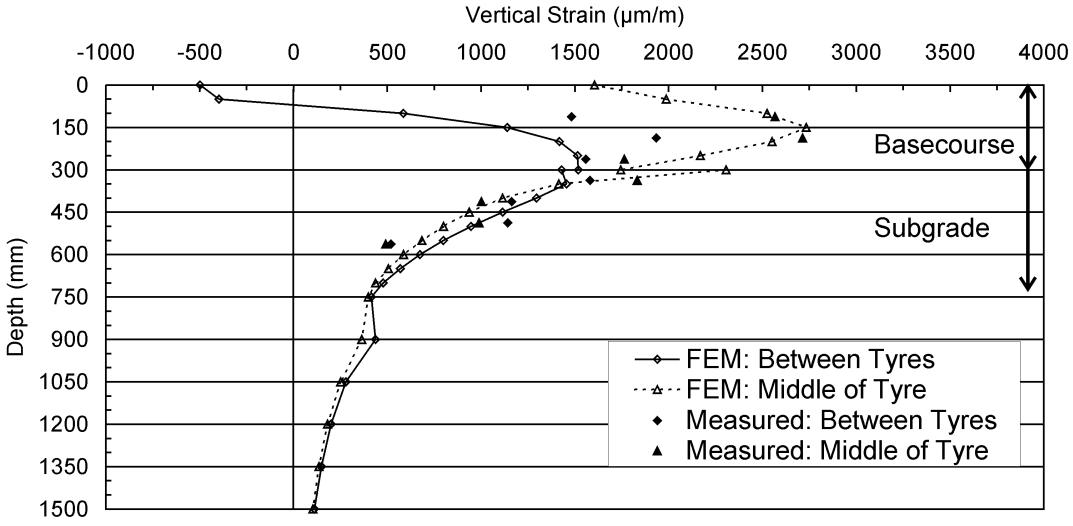

Figure C.5 Measured and computed vertical strains for a 29 kN dual wheel load, Station 38, outer wheelpath, PR3-0610 pavement, 1447k laps.

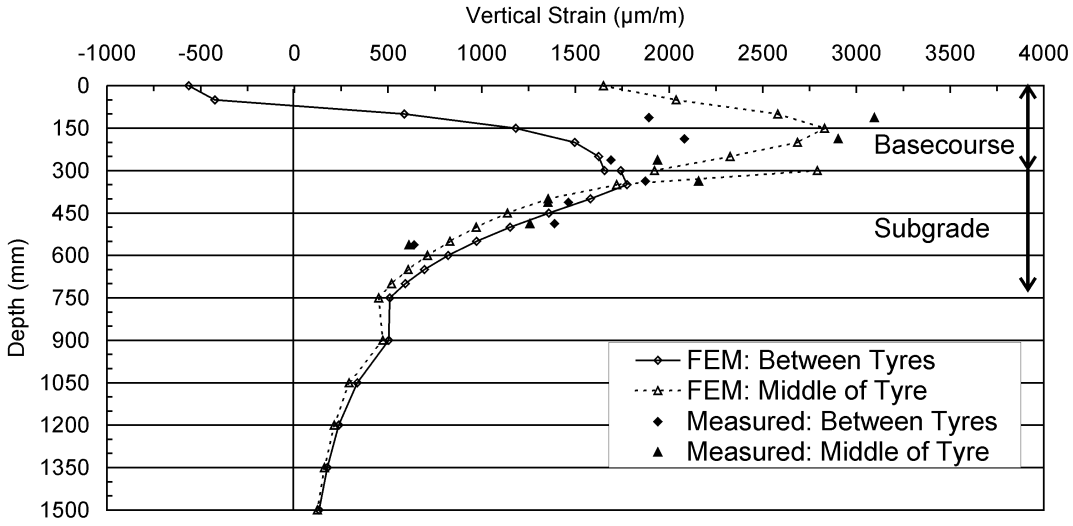

Figure C.6 Measured and computed vertical strains for a 35 kN dual wheel load, Station 38, outer wheelpath, PR3-0610 pavement, 1447k laps.

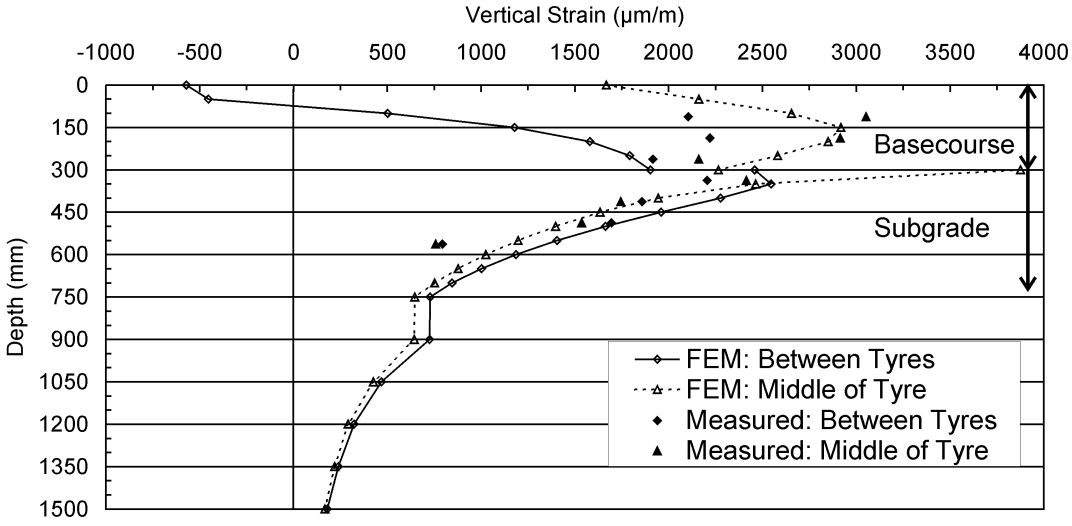

Figure C.7 Measured and computed vertical strains for a 50 kN dual wheel load, Station 38, outer wheelpath, PR3-0610 pavement, 1447k laps.

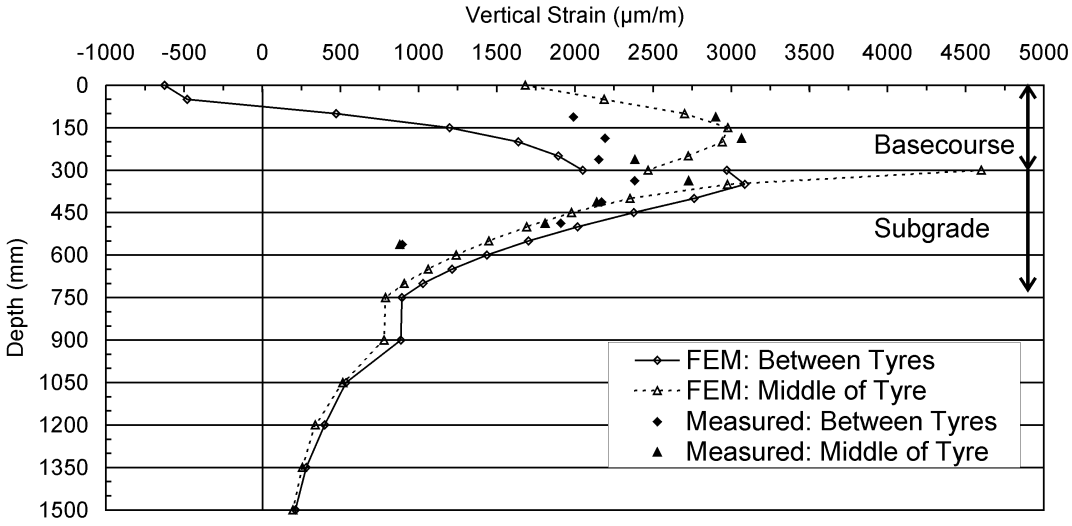

Figure C.8 Measured and computed vertical strains for a 60 kN dual wheel load, Station 38, outer wheelpath, PR3-0610 pavement, 1447k laps.

This page is intentionally left blank.

Appendix D Pavement Performance Modelling

Table D.1 PD calculations for Station 9, inner wheelpath, PR3-0404 pavement (300 mm / 40 kN).

Model I, Station 9, inner wheelpath (300 mm / 40 kN), PR3-0404 pavement h=50 mm N=900,000		$\dot{\varepsilon}_p = 0.4908 \times 10^{-3} \cdot e^{3.9479 \times 10^{-3} \cdot \varepsilon_r}$, $\Delta\varepsilon_p = \dot{\varepsilon}_p \times h \times N$				
Depth to midheight of sublayer (mm)	Between tyres			Beneath tyre		
	ε_r (μm/m)	$\dot{\varepsilon}_p$ (μm/m/cycle)	$\Delta\varepsilon_p$ (mm)	ε_r (μm/m)	$\dot{\varepsilon}_p$ (μm/m/cycle)	$\Delta\varepsilon_p$ (mm)
25	-236	0.0[1]	0.0	531	0.004003	0.2
75	-31	0.0[1]	0.0	762	0.009953	0.4
125	227	0.001205	0.1	953	0.021110	0.9
175	454	0.002944	0.1	1007	0.026154	1.2
225	598	0.005196	0.2	965	0.022138	1.0
275	696	0.007656	0.3	887	0.016304	0.7
PD in basecourse layer (mm)			0.7			4.4

[1]Value set to zero because of tensile vertical strain

Table D.2 PD calculations for Station 29, outer wheelpath, PR3-0610 pavement (225 mm / 40 kN).

Model III, Station 29, outer wheelpath (225 mm / 40 kN), PR3-0610 pavement h=56.25 mm N=900,000		$\dot{\varepsilon}_p = 0.4908 \times 10^{-3} \cdot e^{3.9479 \times 10^{-3} \cdot \varepsilon_r}$, $\Delta\varepsilon_p = \dot{\varepsilon}_p \times h \times N$				
Depth to midheight of sublayer (mm)	Between tyres			Beneath tyre		
	ε_r (μm/m)	$\dot{\varepsilon}_p$ (μm/m/cycle)	$\Delta\varepsilon_p$ (mm)	ε_r (μm/m)	$\dot{\varepsilon}_p$ (μm/m/cycle)	$\Delta\varepsilon_p$ (mm)
28	-31	0.0[1]	0.0	823	0.012660	0.6
84	92	0.000707	0.0	1116	0.040285	2.0
141	481	0.003285	0.2	1338	0.096553	4.9
197	775	0.010449	0.5	1358	0.104777	5.3
PD in basecourse layer (mm)			0.7			12.8

[1]Value set to zero because of tensile vertical strain

Table D.3 PD calculations for Station 38, inner wheelpath, PR3-0610 pavement (300 mm / 60 kN).

Model IV, Station 38, inner wheelpath (300 mm / 60 kN), PR3-0610 pavement
h=50 mm
N=900,000
$\dot{\varepsilon}_p = 0.4908 \times 10^{-3} \cdot e^{3.9479 \times 10^{-3} \cdot \varepsilon_r}$, $\Delta\varepsilon_p = \dot{\varepsilon}_p \times h \times N$

Depth to midheight of sublayer (mm)	Between tyres			Beneath tyre		
	ε_r (μm/m)	$\dot{\varepsilon}_p$ (μm/m/cycle)	$\Delta\varepsilon_p$ (mm)	ε_r (μm/m)	$\dot{\varepsilon}_p$ (μm/m/cycle)	$\Delta\varepsilon_p$ (mm)
25	-219	0.0[1]	0.0	733	0.008869	0.4
75	-66	0.0[1]	0.0	1067	0.033207	1.5
125	245	0.001291	0.1	1319	0.089797	4.0
175	620	0.005680	0.3	1433	0.140638	6.3
225	873	0.015417	0.7	1421	0.134197	6.0
275	1052	0.031233	1.4	1332	0.094315	4.2
PD in basecourse layer (mm)			2.5			22.4

[1]Value set to zero because of tensile vertical strain